Imperial College London

Experimental study of smouldering wildfire mitigation: spread, suppression and transition to flaming

A thesis submitted in partial fulfilment of the

requirements for the degree of

Doctor of Philosophy

in

Mechanical Engineering

by

Muhammad Agung Santoso

2020

Supervised by Prof. Guillermo Rein

Declaration of Originality

I declare that this thesis and the work described within have been completed solely by myself under the supervision of Prof. Guillermo Rein. Where others have contributed or other sources are quoted, full references are given.

Muhammad Agung Santoso

2020

Copyright Declaration

To my family,

for all the love and patience.

ABSTRACT

Experimental study of smouldering wildfire mitigation: spread, suppression and transition to flaming

by

Muhammad Agung Santoso

Doctor of Philosophy in Mechanical Engineering

Imperial College London, 2020

Supervised by Prof. Guillermo Rein

Smouldering and flaming combustion are both important in wildfires, and one can lead to the other. Although the characteristic temperature, spread rate and power of smouldering are low compared to flaming combustion, smouldering is far more persistent. Peatland wildfires are dominated by smouldering combustion and have been reported to be some of the largest wildfires in terms of fuel consumption and pollutant emissions. Unfortunately, current fundamental understanding of smouldering wildfire is limited, resulting in ineffective mitigation strategies. In this thesis, novel experiments were developed to study three phenomena: smouldering peat fire, its suppression, and the transition from smouldering to flaming combustion. To understand the behaviour of smouldering under real conditions, the largest to-date peat wildfire experiment was conducted in Sumatra, Indonesia, investigating ignition, spread, emission and suppression. The fire was observed continuously for the first time propagating for 10 days during day and night times, and despite major rainfalls. Lab-scale experiments were conducted to study the suppression under variable flow rate and wetting agents. The minimum suppression column height at the lab-scale agrees with the field-scale experiment. The required volume of suppressant per mass of peat was constant, therefore suggesting a fundamental property, at around 5.7 L/kg-peat despite changes in flow rate and wetting agent concentration. To further understand the transition from smouldering to flaming combustion, a novel experimental rig was designed to investigate the role of wind. Compared to continuous wind exposure, transition from smouldering to flaming occurred earlier under pulse wind and depended less on sample size. The results in this thesis can help to improve prevention and mitigation efforts.

ACKNOWLEDGEMENTS

I would like to thank my supervisor, Prof. Guillermo Rein, for his guidance, expertise, and generosity during my PhD study at Imperial College London. It has been a pleasure and luxury to have the chance to work with him, with all the supports and encouragements.

Thank you very much, Imperial Hazelab. It has been a great honour to be part of a wonderful group of people with excellent professionalism and characters. Thank you to Fahd, Eirik, Yuqi, and Wuquan for being my lab mates, mentors, and system of supports during my time of working in the lab. Immeasurable gratitude to all Hazelab members and alumni, Francesco, Egle, Nieves, Iza, Nils, Franz, Han, Matt, Ben, Francesca, Dwi, Xuanze, Zhenwen, Guoxiang, Harry, Simona, Tatenda. It has been so full of learning and experiences to be around you, enabling me to grow both professionally and as a person.

This journey will be less bearable without all the supports and love from Indri, Kasih, Laras, and Zia. You all have been so supportive and patience during all the fun and challenging times we had. No amount of words can express my gratitude to all of you. Thank you to Pak Doddy, Uki, Achi, Ansel, Rashid, Wulan, for making UK feels so much like home, and for being always there ready to help each other. Thank you to Prof. Yulianto Nugroho and all my teachers and colleagues at UI for the wise advices, supports, and friendships I am so lucky to have.

Thank you to LDPD, European Research Council, and Imperial College London to provide the financial supports for my research study in the UK, to Serena and Asanka for all the administrative and technical supports in the college, and to Pak Pither from UNCEN for being a mentor and a friend especially on how to be adventurous and fun during our peatland field explorations.

To my parents and family, my deepest thanks to all of you for all the love, supports, and understanding. It is truly a blessing to have you all in my life.

Muhammad Agung Santoso
London, UK
December 2020

TABLE OF CONTENTS

NOMENCLATURE

m	Mass (g or kg)
m_{sp}	Mass of dry peat and residue at the start of suppression (g)
$\hat{m}_{sp}$	Normalized mass of peat at the start of suppression (based on initial mass, -)
ρ_b	Peat bulk density (kg m^{-3})
ρ_w	Density of water (kg m^{-3})
ρ_{sp}	Density of suppressant (kg m^{-3})
T_a	Wind temperature (^oC)
V_a	Wind speed (m/s)
$V_{a,t}$	Maximum wind speed (m/s)
t	Time (s, min, or h)
t_{sp}	Time at the start of suppression (min)
$\dot{V}_s$	Suppression flow rate (L/h)
Δt_s	Suppression time (min or h)
A_f	Fire area (m^2)
A_s	Coverage area of the suppression method (m^2)
A_r	Reactor area (m^2)
H_s	Suppression column height (mm)
S_l	Horizontal Spread rate (cm/h)
S_d	In-depth spread rate (cm/h)
h_b	Depth of burn (cm or m)
h_o	Depth of fuel (cm or m)
V_o	Volume of suppression run-off (L)
V_t	Total volume of suppressant (L)
$V_{w,sp}$	The original moisture content left at the start of suppression (L)
L_{sp}	Smouldering front location at the start of suppression (cm)
L_r	Length of the reactor (cm)
X_{sp}	Volume fraction of the unburnt sample at the start of suppression (-)
$m_{w,sp}$	Mass of the water at the start of suppression (g or kg)
k	Thermal conductivity (w/m-K)
c_p	Specific heat at constant pressure (J/kg-K)
D	Day

Abbreviation

DOB	Depth of burn
MLR	Mass Loss Rate (g/min)
IPCC	Intergovernmental Panel on Climate Change
IPS	International Peat Society
ISO	International Organization of Standardization

IC	Inorganic Content (ratio of inorganic mass to dry fuel mass, %)
OC	Organic Content (ratio of organic mass to dry fuel mass, %)
MC	Moisture Content (ratio of mass of water to dry fuel mass, %)
VMC	Volumetric Moisture Content (ratio of water volume to soil volume, %)
LIDAR	Light detection and ranging
PSF	Peat Swamp Forest
T or TC	Thermocouple
SNB	Slash-and-burn ignition
CI	Charcoal ignition
IR	Infra Red
WIT	Western Indonesia Time
PFAS	Per and poly-fluoroalkyl substances
AFFF	Aqueous Film Forming Foam
PFOA	Perfluorooctanoic acid
FAP	Fatty Acid-based foaming agent from Palm oil
P1N	Plot 1 North
P2N	Plot 2 North
P3N	Plot 2 North
P1S	Plot 1 South
P2S	Plot 2 South
P3C	Plot 3 Centre
OM	Organic Matter
PM	Particulate Matter
LC	Low Concentration wetting agent (ratio of mass of wetting agent to mass of water, %)
HC	High Concentrtion wetting agent (ratio of mass of wetting agent to mass of water, %)
pH	potential of hydrogen
CO	Carbon monoxide
CO_2	Carbon dioxide
O_2	Oxygen
H_2O	Water
$CaCO_3$	Calcium Carbonate
CH_4	Methane

PREFACE

This thesis starts with **Chapter 1** discussing about smouldering fire and peat fires behaviour. This chapter generally outlines the behaviour of peat fire smouldering under real conditions, its suppression difficulty, and smouldering-to-flaming transition in wildfire as topics with currently limited understanding. This chapter is based on:

> Santoso MA, Huang X, Prat-Guitart N, Christensen E, Hu Y, Rein G (2019). Smouldering fires and soils. In 'Fire Effects on Soil Properties'. (Eds P Pereira, J Mataix-Solera, X Ubeda, G Rein, A Cerdà) pp. 203–216. (CSIRO Publishing: Melbourne) https://doi.org/10.1071/9781486308149

Chapter 2 presents field experiment on peat fires conducted in tropical peatland in Indonesia in 2018. This chapter outlines the experimental evidence in the field regarding the persistency of smouldering peat fire, surviving for 10 days during day and night and despite rainfall events, until controlled suppression attempts were conducted. This chapter is based on:

> Muhammad A. Santoso, Eirik G. Christensen, Hafiz M. F. Amin, Pither Palamba, Yuqi Hu, Dwi M. J. Purnomo, Wuquan Cui, Agus Pamitran, Franz Richter, Thomas E. L. Smith, Yulianto S. Nugroho, and Guillermo Rein. GAMBUT field experiments on tropical peat fires in Sumatra: from ignition to spread and suppression. (to be submitted)

Chapter 3 presents lab-scale experiment on the suppression of smouldering peat fire by varying suppression flow rate and wetting agent concentration. This chapter confirms the suppression dynamics of peat fires observed during the field experiments presented in **Chapter 2**. Chapter 3 is based on:

> Santoso MA, Cui W, Amin HMF, Christensen EG, Nugroho YSN, and Rein G. Laboratory study on the suppression of smouldering peat wildfires: effects of flow rate and wetting agent. International Journal of Wildland Fires. https://doi.org/10.1071/WF20117

Chapter 4 presents literature review on smouldering-to-flaming transition in wildfires, identifying the governing underlying mechanisms, i.e. oxygen supply and heat loss. This chapter is based on:

> Santoso MA, Christensen EG, Yang J and Rein G (2019) Review of the Transition From Smouldering to Flaming Combustion in Wildfires. Front. Mech. Eng. 5:49. doi: 10.3389/fmech.2019.00049

Chapter 5 presents the lab-scale experiment investigating the effect of wind on smouldering-to-flaming transition, following the literature review in **Chapter 4**. This chapter is based on:

> Muhammad A. Santoso[CO], Eirik G. Christensen[CO], Guillermo Rein. The effects of pulse and continuous wind on the transition from smouldering to flaming combustion on wood. (to be submitted)

Chapter 6 outlines the general conclusions of the thesis.

Other Publications

Book chapter:

> E. Christensen, H. Y., F. Restuccia, M. A. Santoso, X. Huang, and G. Rein, "Experimental methods and scales in smouldering wildfires," in *Fire Effects on Soil Properties*, P. M.-S. Pereira Jorge Ubeda, Xavier Rein, Guillermo Cerdà, Artemi, Ed. CSIRO Publishing, 2019, pp. 267–280.

Journal article:

> Hu, Y., Smith, T.E.L., Santoso, M. A., Amin, H.M.F., Christensen E., Cui, W., Purnomo, D.M.J., Nugroho, Y.S. and Rein, G., GAMBUT field measurement of emissions from a tropical peatland fire experiment: from ignition to spread to suppression" (to be submitted)

Conference oral presentation:

> Santoso MA, Jiuling Y, Christensen E, Rein G, Literature Review on the Transition from Smouldering to Flaming Fires and Peat fires. **8th International Conference on forest Fire Research**, November 9-16, 2018, Coimbra, Portugal.
> Santoso MA, Rein G, Transition from Smouldering to Flaming: Review of Literature, **1st UK Postgrad Fire Discussions (Fired-UP)**, May 17-18, 2018, University of Edinburgh, Edinburgh, UK

> Muhammad A. Santoso, Eirik G. Christensen, Hafiz M. F. Amin, Pither Palamba, Yuqi Hu, Dwi M. J. Purnomo, Wuquan Cui, Agus Pamitran, Franz Richter, Thomas E. L. Smith, Yulianto S. Nugroho, and Guillermo Rein,

GAMBUT Field experiment on tropical peat fires in sumatra, indonesia : from ignition to spread and suppression, **The Great Fired-UP of London**, May 16-19, 2019, London, UK.

Conference poster presentation:

Muhammad Agung Santoso, Jiuling Yang, and Guillermo Rein, Transition from Smoldering to Flaming Combustion: a Literature Review, **12th International Symposium on Fire Safety Science (IAFSS)**, June 12–16, 2017, Lund University, Sweden.

Muhammad Agung Santoso, Francesco Restuccia, Yuqi Hu, Eirik Christensen, Yuan Han, and Guillermo Rein, Smouldering Megafires: Laboratory to Earth scale Research at Imperial Hazelab, **DTP Conference 2017: Frontiers in Natural Environmental Research**, August 24 – 25, 2017, Imperial College London, UK.

Chapter 1

Smouldering fires and soils

1.1. Smouldering of organic soils[1]

Smouldering is the slow, low temperature, flameless burning of porous fuels [1]. Smouldering is a form of combustion causing long-lasting fires in natural fuels, such as coal deposits and peatlands, that is persistent despite firefighting measures and extensive rains. Once an organic soil is ignited either by flames or lightning strike, smouldering fires can be sustained for months, and spread over both the surface and deep layers of the fuels. Smouldering fires in organic soils, especially peat, have received increased attention from the geoscience community in recent years due to the extensive scale of ecosystem damage, pollution and climate effects.

Smouldering fires in organic soils consume a massive amount of mass due to their persistent nature and the possible spread deep into the soil. Davies et al. [2] surveyed an afforested peatland in the Scottish Highlands after a severe wildfire during the summer of 2006. Fires continued for more than a month and engulfed an area of 4.1 ha. The reported value of organic matter consumption was 773 ± 120 t. Recent experiments showed that the carbon emission rate from organic soil fires is ~200 t day^{-1} ha^{-1} [3]. Given the massive carbon emission from smouldering fires, its inclusion in the Intergovernmental Panel on Climate Change (IPCC) global carbon budget needs to be considered. Differing from flaming wildfires over the surface vegetation and tree crown, which are faster and release more heat [1,4], the smouldering of organic soil poses a greater threat in terms of the fuel consumption, emissions and effects on the soil system.

Soil is a natural system composed of solids, liquids and gases that occurs on a land surface [5]. The amount of organic matter in a soil determines its classification as mineral or organic. Organic soils formed where the rate of organic matter accumulation exceeds the decomposition rate; such conditions are met in cold climates or regions with high level of precipitation [6]. There are several classification systems for soil types. Hence, different definitions of organic soil can be found, i.e. histosol, peat or muck, based on the organic content of the soil. Huang

[1] This chapter is based on "Santoso MA, Huang X, Prat-Guitart N, Christensen E, Hu Y, Rein G (2019). Smouldering fires and soils. In 'Fire Effects on Soil Properties'. (Eds P Pereira, J Mataix-Solera, X Ubeda, G Rein, A Cerdà) pp. 203–216. (CSIRO Publishing: Melbourne) https://doi.org/10.1071/9781486308149."

et al. [7] summarised the soils classification as shown in Figure 1.1. Three classification systems agree that soils primarily containing organic carbon are defined as peat. For this reason, this chapter focuses attention on peat as the best representative of organic soils.

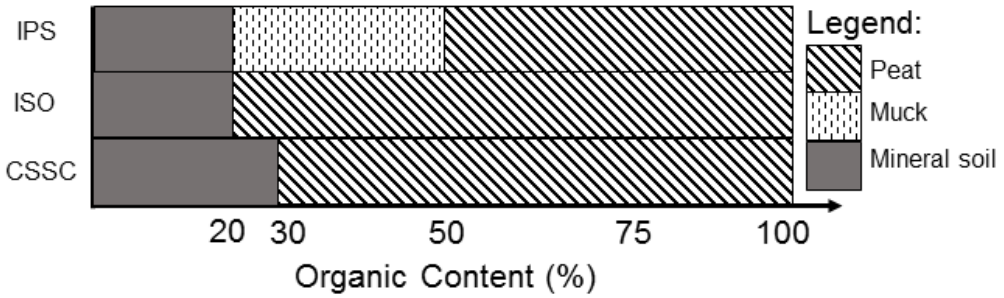

Figure 1.1. Summary of classification systems for soils using organic content for the determination of peat, muck or mineral soil according to the International Peat Society (IPS), Canada Soil Survey Committee (CSSC) and International Organization of Standardization (ISO). Example interpretation: in IPS classification, if soil has organic content of 0–20%, 20–50%, or more than 50%, the soil is mineral soil, muck, or peat, respectively. Based on data from Huang et al. [7].

Worldwide, peatlands cover around 3% of the Earth's land surface, while storing one-third of the world's soil carbon [8,9]. Peatlands can be found in Europe, North America, Siberia, Africa and South-East Asia. This makes the carbon stored, which is the result of thousands of years of natural accumulation of biomass, equal in size to the atmospheric carbon pool, and exceeds the carbon in the global surface vegetation [10].

Large smouldering fires are rare events on the local scale but occur regularly on a global scale [11]. A major threat from large smouldering fires is the massive release of carbon into the atmosphere. Carbon emissions of peatland fires have been reported in various studies with respect to their global impacts on climate change, health effects, air pollution and carbon deposits [2,12–16].

Page et al. [12] studied smouldering peat fires in Indonesia during the 1997 El Nino event. The estimated extent of these fires was ~20 million ha of peatland. The peat mass loss caused by prolonged smouldering fire was estimated to be between 1.123 and 1.367 Gt. This estimation was made with the assumption that the peat bulk density was 100 kg/m^3. In the same climatic region, Ballhorn et al. [13] estimated depth of burn with LIDAR aerial remote sensing in Kalimantan, Indonesia, after the 2006 severe peatland fires. They reported an average mass loss of 0.439 Gt from ~1 million ha of burned peatland.

In flaming wildfire, fireline intensity can be estimated by using Byram's fireline intensity equation [17–20]. This equation considers the fuel low heat of combustion, quantity of fuel consumption, and linear fire spread rate [17,19]. Intensity of smouldering peat fire can also be estimated by using this equation and

might show comparable intensity to flaming wildfire fireline intensity due to the significantly massive fuel consumption in peat fire. Though, it can be argued that this approach may not capture the overall intensity of peat fire which also well known for its massive carbon emission which is the result of thousands of years accumulation (having higher chance of being irreversible), pollution effect in the form of regional haze episode, deep underground fire spread, and subsidence and flooding effect. Even if peat fire identified with lower spread rate and temperature than flaming wildfire, peat fire intensity might require more variables than flaming wildfire to be well estimated. Another variable that can be considered is thermal residence time which will be discussed in the following subsection of *Chapter 1.3. Thermal Severity on Soils*.

Peatlands around the world play an important role in the global carbon balance [21] and their role as carbon sinks is becoming even more important under the current climate change projections. However, after large smouldering fire events, peatlands act as carbon sources and this effect can last for up to about a decade until the ecosystems once again become carbon sinks [22,23]. In undisturbed pristine condition, peatland is protected from fire because of the wet condition (very high moisture content (MC) that can be up to ~300% in dry basis [10,24]) or because of the cold climate such as in arctic region. The peatland then acts as a carbon sink by sequestering the carbon from the dead organic material with minimum carbon emission due to the fire-protected conditions and slow decomposition rate [10]. However, due to global warming and land-use change, the occurrence of fire in peatland can disturb the pristine conditions of peatland by lowering the water table and/or decreasing the average soil MC. As a result, the peatland will be more susceptible to fire, easily burning in the following fire season, and releasing the massive amount of carbon that has been stored for millennial [9,12,25]. This massive emissions from smouldering fires [12,14] and its widespread occurrences could lead to the acceleration of climate change. The release of ancient carbon creates a positive feedback mechanism in the climate system: a self-accelerating process [25] as illustrated in Figure 1.2. Warmer global climates would result in more frequent and more extensive smouldering fires from areas where warmer and drier soils are induced by climate change [26].

In conditions where long severe droughts persist, such as during El Nino events, smouldering peatland fires can lead to regional haze episodes [12,14]. Haze is defined as the large-scale accumulation of smoke at low altitudes in the atmosphere [27]. Haze results in poorer air quality, transportation disruption, impaired visibility and vast economic losses. It also carries broad health effects, predominantly to the respiratory and cardiovascular systems [28–30].

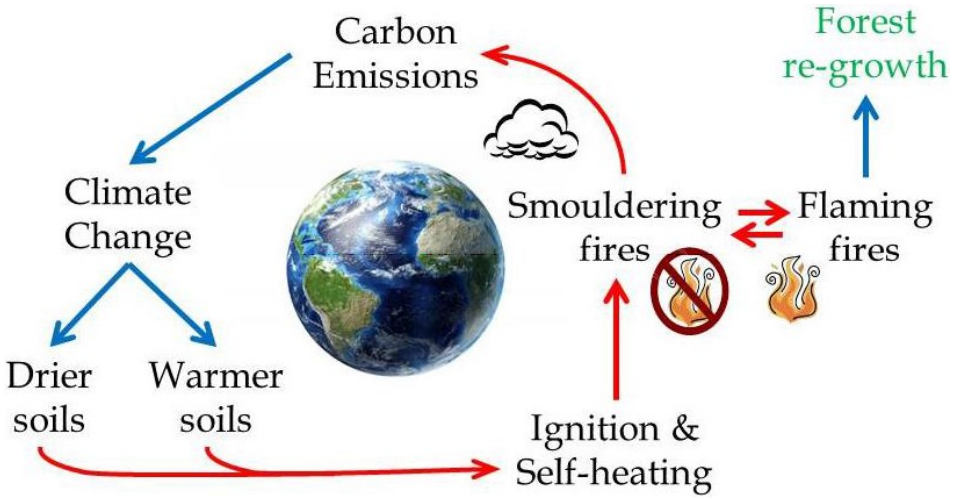

Figure 1.2. Schematic of the feedback loop between smouldering fires and climate change. Image from Rein [25], CC BY.

Degraded peatlands are the most vulnerable to smouldering fires [10]. This degradation is often due to drought, climate change, drainage or land-use change. The water content of wildland fuels such as peat varies naturally over a wide range (from dry to flooded in water) and, because water represents a significant energy sink, MC is the single most important property governing the ignition and spread of smouldering wildfires [1]. During the degradation process (a process that takes years), the water table is lowered and peatlands are exposed to the atmosphere with a subsequent reduction in MC and loss of organic matter. The current high degradation rate of several peatlands worldwide is expected to lead to an increase of smouldering peat fires in all climate regions [22,31–35].

Smouldering of organic soil can be represented by a multi-step process: drying (Eq. 1.1), pyrolysis (Eq. 1.2), and the oxidation of char produced from pyrolysis (Eq. 1.3). Figure 1.3 shows the generalised chemical reaction paths and the main species involved. Four condensed-phase species (water, organic soils, char, and ash) and one gas-phase species (pyrolysate) are shown. To start the process, heat is required for drying and pyrolysis. Pyrolysis is the thermal degradation of the organic matter, resulting in a porous char, pyrolysates and ash. If the oxygen is consumed in char oxidation (Eq. 1.3, Path I) by directly attacking the surface of the porous char matrix, the combustion process is smouldering. On the other hand, flaming fires involve the oxidation of the pyrolysates released in pyrolysis (Eq. 1.4) [1]. Thus, depending on the oxygen supply and heat transfer process, either smouldering or flaming could dominate the combustion process. Nevertheless, both paths produce heat required to maintain the drying and pyrolysis in adjacent organic soil.

Soil drying:

$$\text{Organic Soils (s)} \cdot \text{Water (l)} \xrightarrow{heat} \text{Organic Soils (s)} + \text{Water vapour (g)} \quad (1.1)$$

Organic soil pyrolysis:

$$\text{Organic Soils (s)} \xrightarrow{heat} \text{Char (s)} + \text{Pyrolysate (g)} + \text{Ash (s)} \quad (1.2)$$

Char oxidation (as 'smouldering' in Figure 1.3):

$$\text{Char (s)} + O_2\text{ (g)} \rightarrow \text{Heat} + CO_2 + H_2O + \text{Other emission gases} + \text{PMs} + \text{Ash (s)} \quad (1.3)$$

Pyrolysate oxidation (as 'flaming' in Figure 1.3):

$$\text{Pyrolysate (g)} + O_2\text{ (g)} \rightarrow \text{Heat} + CO_2 + H_2O + \text{Other emission gases} + \text{PMs} \quad (1.4)$$

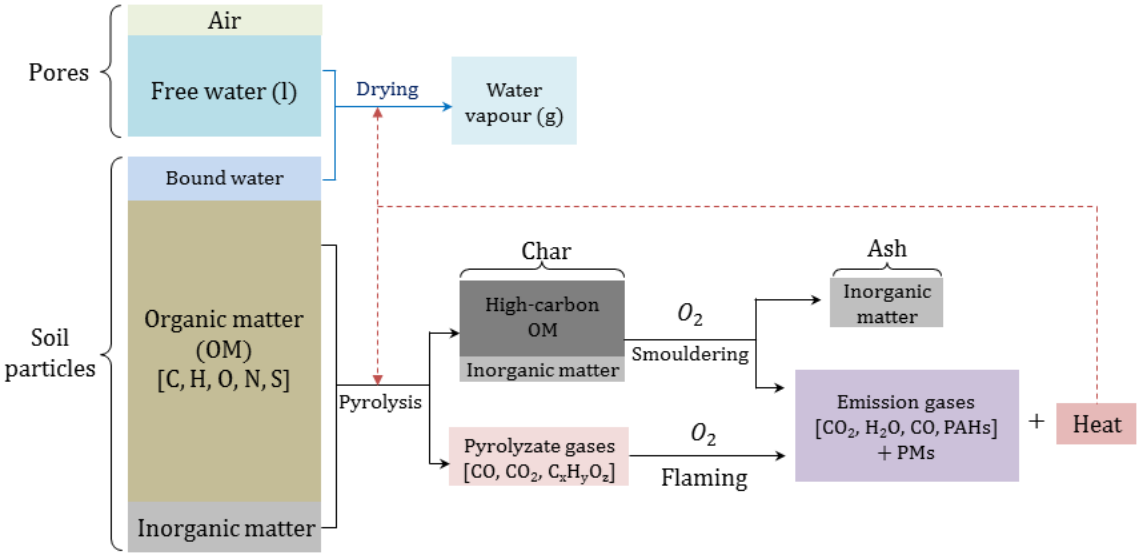

Figure 1.3. Possible reaction paths and main species of organic soils combustion in wildfires. Source: X Huang, CC BY.

The two controlling mechanisms of smouldering spread are the oxygen supply and heat losses from the reaction zone [36]. Atmospheric oxygen feeds smouldering wildfires in all cases. However, this supply decreases with soil depth (or distance to air channels) but increases with greater soil permeability. On the other hand, heat losses hinder smouldering and increase with environmental wind speed because of convective cooling. However, heat losses decrease with soil depth because of the insulating effect of the ground [25].

Smouldering and flaming are closely related, and one can lead to the other. The persistent smouldering of thick fuels (i.e. tree branches, trunks) typically observed for days after a flaming wildfire has passed by has been called residual smouldering combustion and has received some attention in the literature (e.g. Bertschi et al. [37]). The reverse, transition from smouldering to flaming, is less often observed or archived in wildfires, even though transition to flaming is more important since smouldering is more readily to be ignited than flaming [38].

Transition to flaming is a spontaneous gas-phase ignition supported by the smouldering reaction, which acts both as the source of gaseous fuel and of heat to ignite the flame [39]. This transition has received very little attention and the current understanding of the process is still limited. Recently, attention on transition to flaming in wildfire has been increased due to the community started to investigate wildfire spread via embers deposition [40–44]. Beside investigating transition to flaming through embers deposition, which is already a complex process, there is also a need to fundamentally understand transition to flaming in wildfire due to simpler thermodynamic conditions, such as under enhanced oxygen supply (i.e. strong winds).

1.2. Peat Fire Behaviour

The MC (presented in dry weight basis) is an important factor governing smouldering ignition, spread and extinction [45–48]. A peatland during the wet season can consistently hold ~300% of MC, thus difficult to ignite [10]. However, during drought events, peatlands dry out and become prone to fires. The threshold to ignition depends on the inorganic content and MC of organic-rich soil [47,49]. This relationship was further explored via numerical simulation by Huang et al. [48], as summarised in Figure 1.4.

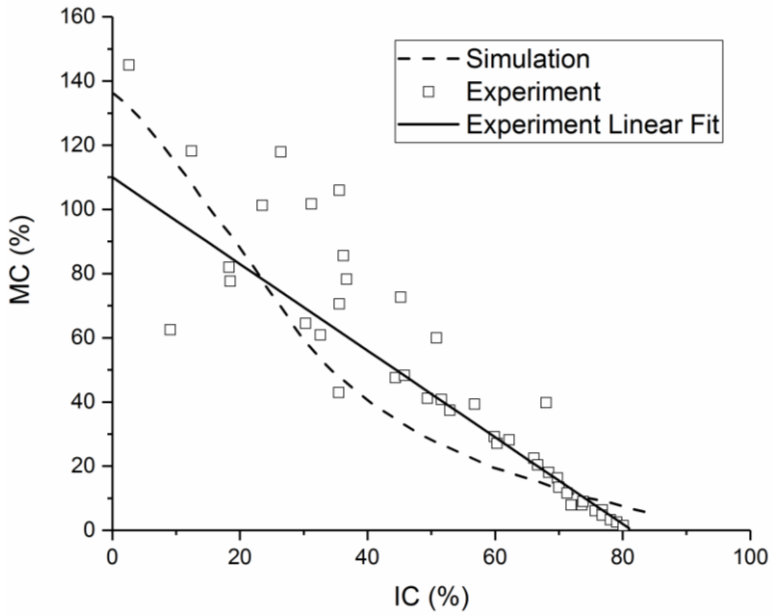

Figure 1.4. Critical ignition limit of peat as a function of moisture content (MC) and inorganic content (IC). The black line is the linear fit from experimental data (square symbol) [47,49]. The dashed black line are computational simulations by Huang et al. [48]. Source: Figure from Huang et al. [48], CC BY.

Once peat is ignited on the free surface (below the critical line in Figure 1.4), smouldering propagation develops in two dimensions: the lateral (horizontal) and

in-depth spread (vertical), as shown in Figure 1.5. Readily available oxygen makes the lateral fire spread faster than the in-depth spread. For the latter, the oxygen has to diffuse through the ash layer accumulated on top of the smouldering front [50]. Thus, the surface extent of smouldering peat fires will be governed by the rate of lateral spread and the existence of flaming spread. As mentioned earlier, the most important property in smouldering peat fires is soil MC, because the heat required to evaporate MC reduces the heat available to sustain smouldering [1]. In field measurements, it has been reported that the MC could be as high as ~220% at a depth of 50 cm [51] and even at 268% at a depth of 11–20 cm [52] limiting the extent of in-depth spread.

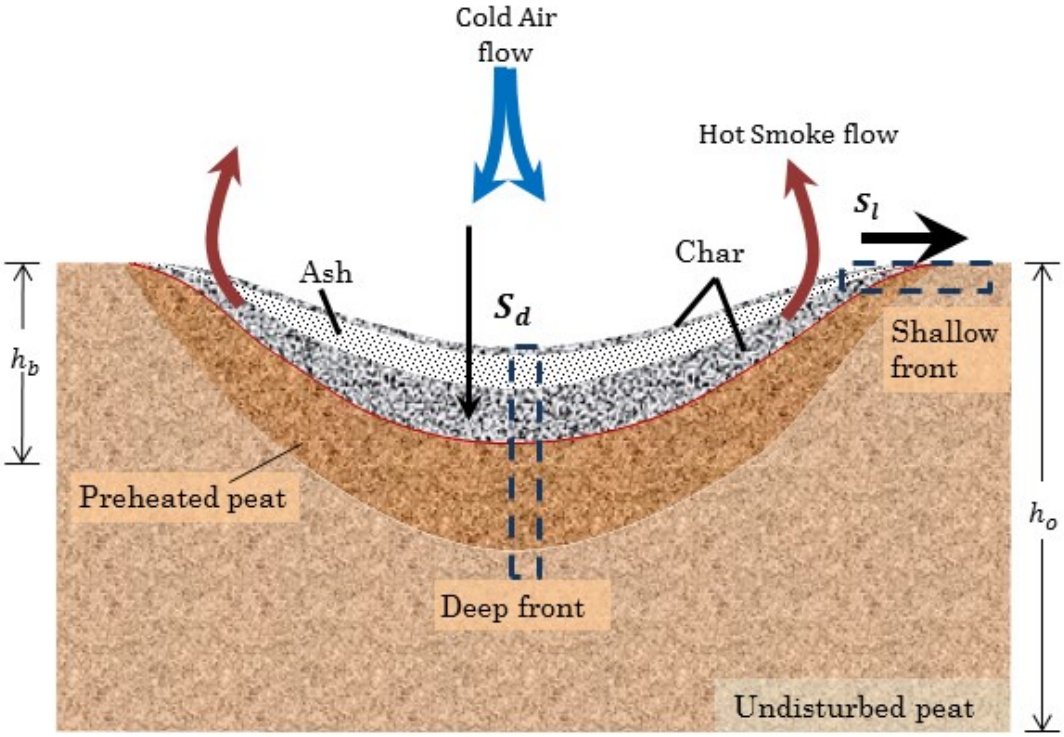

Figure 1.5. Schematic of smouldering front in lateral and in-depth spread in peat fires. Source: Huang and Rein [50], CC BY.

Because the large convective heat losses on the free surface caused by wind can limit the local smouldering process, the lateral spread rate next to the free surface becomes slower or even ceases. The difference in the lateral spread rate with depth eventually leads to the formation of overhang, because the peak spread rate is located where heat losses and oxygen supply are optimally balanced below the surface, as explained by Huang et al. [53].

Table 1.1 summarises the available data on lateral smouldering spread rate gathered from different sources found in the literature. The soil samples originated from boreal and tropical climate regions. The boreal peat soil is formed from low growing vegetation (mosses, herbs, shrubs and small trees) and the tropical peat soil is formed from the remains of the highly productive rainforest

trees (branches, leaves, roots and trunks) [54]. However, the different origins do not have a significant effect on the spread rate, probably because they have a similar organic content. Table 1.1 also shows that the lateral spread rate strongly depends on the MC, especially for MC less than 20%. The pattern of this behaviour can be seen in Figure 1.6. In general, the influence of soil depth on the lateral spread is found to be small, compared with the drastic decrease of smouldering spread as MC increases up to 20%. By considering the wide range of possible MC in peatlands, from 10% under drought conditions to well in excess of 300% under flooded conditions, the results show a generally slow lateral spread of peat fires (3.1 ± 1.1 cm h^{-1} on average) unless MC is extremely low.

Table 1.1. Data on lateral spread rate of smouldering taken from literatures.

MC (wt% in dry base)	Density (kg m^{-3})	Depth (cm)	Sample origin	Study scale	Lateral spread rate (cm h^{-1})	Source
5–10	136	0–8	Boreal	Laboratory measurement	21.5 ± 1.9	[53]
5–10		2.5–10			16.6 ± 1.2	[55]
25	116 ± 9	0–5			4.3 ± 0.9	[56]
50 ± 5	163	0–8			3.6 ± 0.4	[53]
100 ± 5	171	0–8			3.6 ± 0.3	[53]
100	80 ± 7	0–5			2.6 ± 1.1	[56]
150	62 ± 5	0–5			2.1 ± 0.6	[56]
90–150		0–20	Tropical	Field observation	3.8 ± 1.4	[51]
130–150		20–50			1.3 ± 0.6	[51]
Average of all spread rates					3.1 ± 1.1	

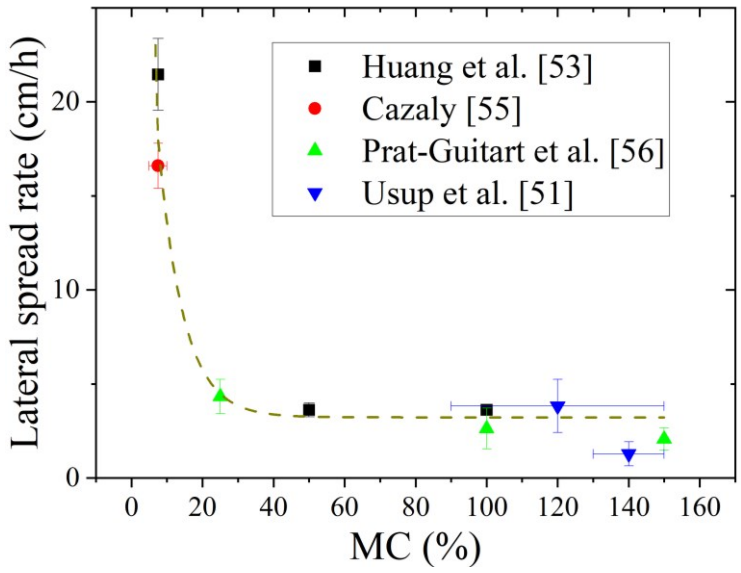

Figure 1.6. Data of lateral spread rate of smouldering as a function of moisture content (MC) for the values in Table 1.1.

The other mode of spread, namely the in-depth spread, ranges from 0.5 to 2 cm h^{-1} [3]. The accumulation of ash on top of the smouldering front limits the oxygen supply and slows down the spread. Huang and Rein [3] studied the in-depth smouldering spread using boreal peat with MC up to 70% using both experimental and computational approaches. It was found that the in-depth spread rate decreases significantly with both depth and density. However, it was reported for the first time the counterintuitive fact that the downward spread rate increases substantially with moisture. This goes against previously observed trends for the lateral spread of the same peat [53] and other peat types [56]. The in-depth spread rate is fundamentally a rate of fuel consumption (or burning), and it increases with MC because of the volume expansion of the peat when it absorbs water, which reduces the density of organic matter. Numerical simulations further confirmed that if the peat MC was well below the critical MC of extinction (up to 250%), the in-depth spread rate is controlled by the oxygen supply and the rate of burning. When the peat MC approaches this critical value of extinction, the in-depth spread becomes slower [48]. The in-depth spread process and the extinction limit are particularly important to predict the depth of burn (DOB), which controls the total carbon emission per unit area from a peatland fire. DOB from peatland fires has been reported to be between 1 and 51 cm on average (Table 1.2). However, field observations revealed small number of cases where DOB can be as deep as 1.1 m, which can be caused by ignition of tree trunks and roots that enabled fires to propagate deeper into the peat layer [13].

In peatland fires, the high degree of heterogeneity affects the multidimensionality of the spread pattern. The vegetation and microtopography of the peatland's surface play an important role in the lateral propagation patterns, as has been suggested by several post-fire studies on burn patterns [2,57,58]. Overall, the fire behaviour is governed by the spatial variation of organic soil properties at fine and large scales. Figure 1.7 shows a high spatial variability of surface peat MC in a blanket bog in Ireland. This high variability is linked to the distribution of vegetation [59].

The surface spatial variation of peat conditions affects the fire spread behaviour in a lateral direction, and has a range of local impacts on the soil and the ecosystem. Studies in boreal and temperate peatlands have reported the irregular distribution of surface peat consumption following smouldering fires [60] (Figure 1.8).

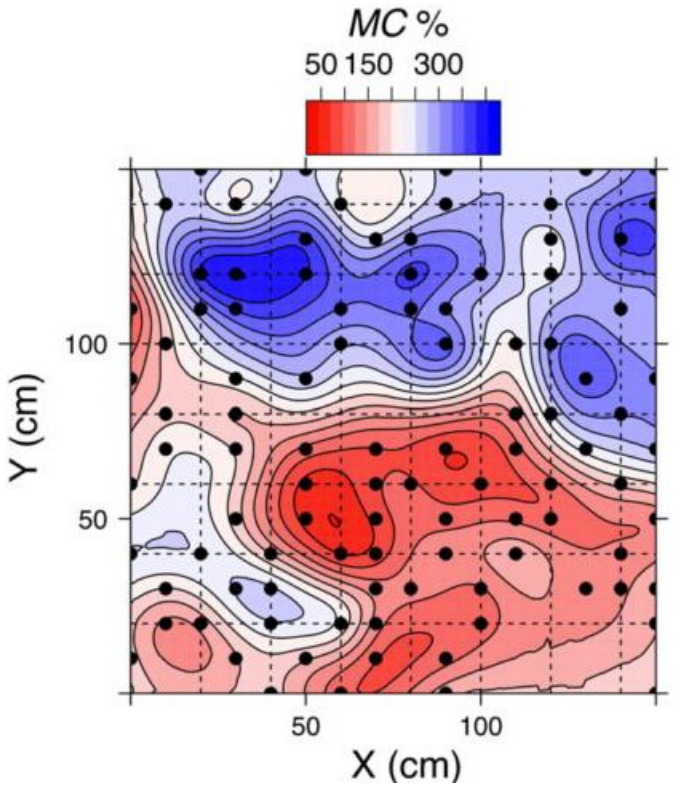

Figure 1.7. An example of the spatial distribution of peat moisture content (MC) in a quadrat of 150 × 150 cm of a surface of a drained blanket bog from Ireland. The contour line interval is 50% MC. Contour lines nearby indicate sharp gradients of MC. Black points indicate data points where MC was measured with a moisture sensor. Measurements were taken during a drought season. Source: Prat-Guitart et al. [59].

Figure 1.8. Soil surface 24 h after a smouldering fire event: the 2015 Wicklow Mountains National Park Wildfire, Ireland. Surface consumption (charred areas) is irregularly distributed. Photo: Ecological Modelling Group, University College Dublin.

Figure 1.9. Photographs of adjacent forest stands from the July 2006 Rothiemurchus peat fire in Scotland, UK. (Left) Stand not affected by the fire showing the trees and the peat layer. (Right) Stand of trees trunks charred by the flames and the soil consumed by smouldering fire to a peat depth of 0.5 m. Photos: G Rein, CC BY licence, also found in Rein et al. [11].

Figure 1.9 shows field observation after smouldering fires during the July 2006 Rothiemurchus peat fire in Scotland [11]. It was observed that many smouldering pan-shape voids were formed around forest stands and single trees all over the burned area. These were formed by the consumption of large masses of soil in approximately circular areas 0.5 to 3 m around the tree bases, exposing the mineral soil layer beneath. It was observed that soil consumption decreased with distance from the tree bases [2]. This dependence of soil consumption on distance has been observed in other smouldering fires [60,61]. The most plausible explanation for this is that of moisture distribution. Near the bases of trees, the crown cover intercepts the rainfall, preventing some of the water reaching the ground, and roots are actively drawing up water, ultimately resulting in decreased soil moisture and faster lateral smouldering spread. When an approaching smouldering front reaches the outer edge of a root system, the fire spreads faster along the direction of the roots towards drier soils. Upon reaching the tree base, it then spreads radially from it creating the circular pattern illustrated in Figure 1.9. When trees and roots are close together as part of a stand, the resulting pan-shape voids join and form a continuous void pattern.

Table 1.2 summarises the burnt area, depth of burn, carbon emission flux and total carbon emitted from different peat fires reported in the literature between 1983 and 2015. In general, boreal peat fires have a lower carbon emission flux compared with tropical peat fires, represented as well by the lower average burnt area and depth of burn of boreal peat fires than tropical. Averaging the data from all the peat fires, the burnt area, depth of burn, carbon emission flux, and total carbon emitted are 2122 km^2, 39 cm, 14.3 kg-C m^{-2} and 841.7 Mt-C, respectively. The maximum values for those four variables are 24 410 km^2, 51 cm, 44 kg-C m^{-2}, and 2570 Mt-C. The highest values are from an Indonesian peat fire

event in 1997 [12], except for the highest carbon emission flux, which resulted from the Lateral West fire in the USA in 2011 [62].

1.3. Thermal Severity on Soils

Peatland fires have a much higher impact on soils than flaming fires which mainly consume the surface vegetation (i.e. litter, tree branches, forest canopies and grass) and only heat up the soil superficially. Even though the flame temperature and heat release rate are quite high, the residence time of the flames is short (~15 min max) and only at the surface level. This causes a minimal heating of the soil up to a few centimetres below the surface. Peak temperatures reach 300°C at very superficial layers (<10 mm) and less than 80°C at depths below 40 mm [63]. Figure 1.10 shows the comparison of temperature residence time between smouldering and flaming fires. For example, in flaming fires, temperatures of around 100°C in soils only persist for no more than around 30 min, while in smouldering the same temperature could last for ~2 h. Flaming surface heating therefore has relatively small impacts on the soil and its flora and fauna [64–73].

Beside the thermal residence time, the ability of fire to spread underground and affecting wider soil mass significantly influence the thermal severity on soil, such as the case in peatland fire where the fire can spread up to ~51 cm depth mainly due to the extent of the natural fuel bed deposit. A lesser soil thermal severity than peatland fire can be expected in smouldering fire of surface fuel vegetations that survive after flaming wildfire (residual smouldering), logging slash leftover, or surface fuel collapse after a blowdown or avalanche. Smouldering on this kind of fuels might resulted in longer thermal residence time than flaming fire, but can also be expected to be shorter than organic soil smouldering. The shorter thermal residence than smouldering organic soil might be due to the exposure of convective heat loss to the surface fuel piles.

Table 1.2. Data available in the literature of peat fire events and their footprints.

Peat type	Fire location & year	Burnt area (km^2)	Depth of burn (cm)	Carbon emission flux ($kg\text{-}C\ m^{-2}$)	Total carbon release (Mt-C)	Source
Tundra	Anaktuvuk River, Alaska, USA, 2007	1039	6 ± 1	2 ± 0.4	2.1	[74]
Boreal	Rosie Creek, Alaska, USA, 1983	28	13	4.3	0.1	[75]
	Granite Creek, Alaska, USA, 1987	200	9	1.5	0.3	[75]
	Porcupine, Alaska, USA, 1990	117	11	1.3	0.2	[75]
	Tok River, Alaska, USA, 1990	400	10	2.5	1	[75]
	Dry Creek, Alaska, USA, 1993	1	12	2	0.01	[75]
	Hajduko Vich Creek, Alaska, USA 1994	89	26	7.6	0.7	[75]

	Western Canada, Canada, 1980 to 1995	1470±59	N/A	3.2 ± 0.4	4.7 ± 0.6	[76]
	Tetlin, Alaska, USA, 1996	27	26	2.8	0.1	[75]
	Russia (71%) & North America (29%), 1998	17900	N/A	0.1 to 1.2	290 to 383	[77]
	Patuanak forest fire, Western Canada, Canada, 1999	N/A	5 to 10	2.2 ± 0.5	N/A	[78]
	Frostfire, Alaska, USA, 1999	9	9	0.9 ± 0.9	0.01	[75]
	Donnelly Flats, Alaska, USA, 1999	76	3	1.8 ± 1	0.1	[75]
	Unnamed, Saskatchewan, Canada, 1999	2	N/A	2.2 ± 0.5	0.01	[75]
	Southeast Slave Lake wildfire (Pristine), Alberta, Canada, 2001	1050	7 ± 1	2 ± 0.5	N/A	[79]
	Southeast Slave Lake wildfire (Drained), Alberta, Canada, 2001		19 ± 3	16.8 ± 0.2	N/A	
	Chisholm, Alberta, Canada, 2001	1160	N/A	2.1 ± 0.4	2.4	[75]
	Burntwood River, Manitoba, Canada, 2003	26	6	1	0.03	[75]
	Kasabonika, Ontario, Canada, 2003	820	9	1.6	1.3	[75]
	Thompson, Manitoba, Canada, 2004	426	11	2.2	0.9	[75]
	Dawson City, Yukon, Canada, 2004	174	11	2.2	0.4	[75]
	Wood Buffalo National Park, Northwest Territories, Canada, 2004	520	5	1.3	0.7	[75]
	Utikuma Complex forest fire (peatland margins area), Canada, 2011	0.05	42 ± 2	19.9 ± 2	0.01	[80]
	Experimental study. Sample collected from boreal bogs	N/A	1 to 17	N/A	N/A	[81]
Temperate	Pocosin Lakes Wildfire, North Carolina, USA, 1985	346	1 to 10	0.2 to 11	1 to 3.8	[82]
	Caringorms National Park afforested peatland, Scottish Highlands, UK, 2006	0.041	18 ± 2	9.6 ± 1.5	0.01	[2]
	Lateral West fire in the Great Dismal Swamp National Wildlife Refuge, Virginia, USA. 2011	25	46 ± 18	44	1.1	[62]
Tropical	Indonesia, 1997	24410	51 ± 5	26 to 31.5	810 to 2570	[12]
	Indonesia, Malaysia, and Papua New Guinea, 2000–2006	N/A	N/A	N/A	128 ± 51 yr^{-1}	[83]
	Kapuas, Central Kalimantan, Indonesia, 2009 and 2011	1100	2	1.3	14.3	[84]

Indonesian Peat Fire, southern Sumatra and southern Kalimantan, Indonesia, 2015	8000	26	N/A	227 ± 67	[14]
Jambi province, Indonesia, 2015	0.052	23 ± 19	13.4 ± 2.9	0.01	[85]
Average of boreal fire events	1225	12	1.7	257.4	
Average of temperate fire events	124	8	8.2	1.9	
Average of tropical fire events	8378	43	28	1286	
Average of all fire events	2122	39	14.3	841.7	
Maximum value for all fire events	24410	51	44	2570	

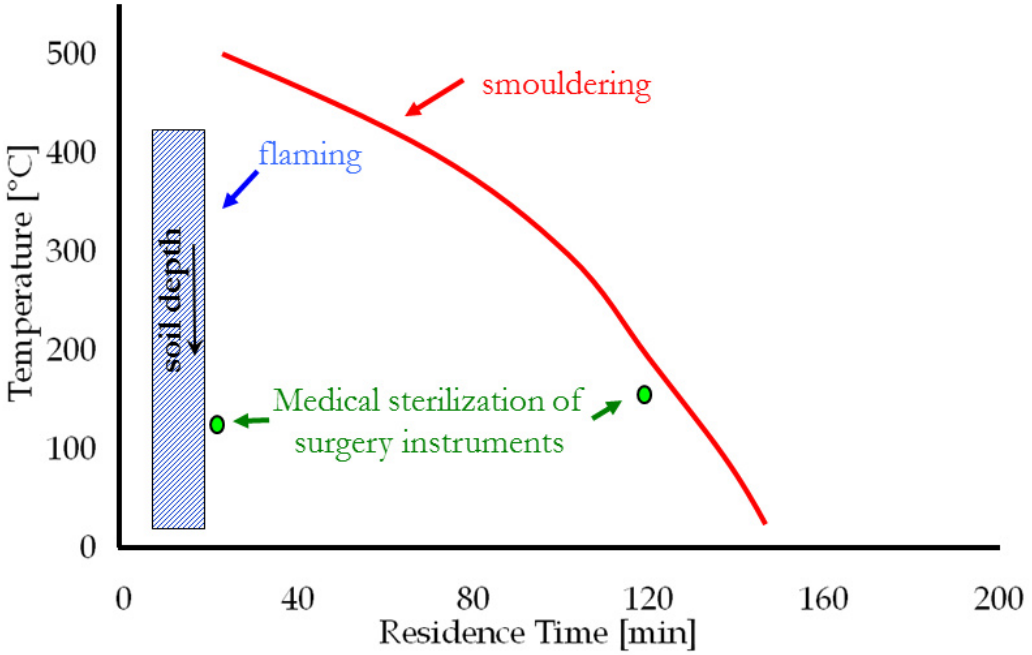

Figure 1.10. Thermal fire severity of smouldering v. flaming fires measured as the average residence times above a given temperature threshold. The severity used in medical sterilisation for autoclave and dry heat are included for reference. Data from Rein et al.[11]. In Rein [25], CC BY.

Compared with flaming wildfires in natural fuels, smouldering fires have a much more significant effect on soils. These effects cause a range of effects on the carbon stocks, biodiversity, and flora and fauna habitat. The changes to the soil produced by smouldering fires are driven by two factors: the residence time of high temperature and mass loss [25]. The thermal severity can be described by the temperatures reached in the soil and the residence time of this heating. This was quantified by Rein et al. [11] (Figure 1.10), where smouldering fires could result in temperature in the soils as high as 200°C for as long as 1–2 h. Figure 1.10 shows that smouldering fires lead to enhanced heat transfer to the soil for much longer durations (i.e. in the order of 1 h) than flaming fires and could exhibit peak temperatures as high as 500°C [11]. These thermal conditions are more severe than in medical sterilisation treatments, meaning that the soil is exposed to

conditions that are lethal to biological systems [11,86]. This concept of thermal severity from smouldering fires to soil is illustrated in Figure 1.11. This thermal condition could then affect deeper soil layers, involving loss of root systems and stability, flora and fauna habitat, and soil integrity.

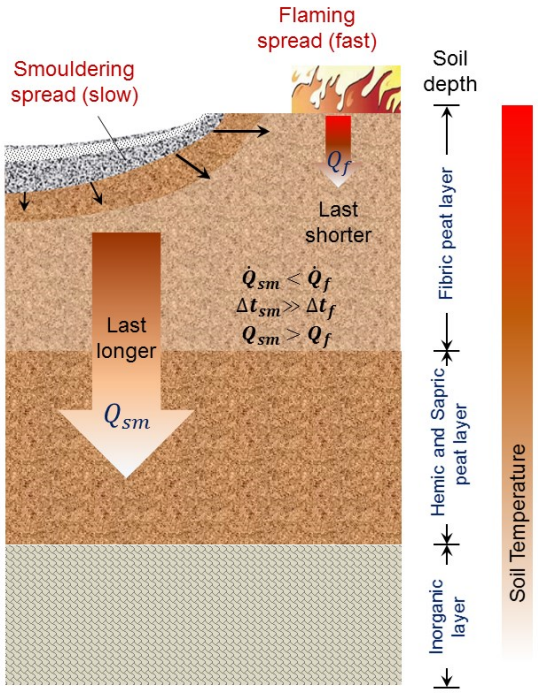

Figure 1.11. Thermal severity comparison between flaming and smouldering wildfires. Δt is residence time. Fibric, hemic, and sapric are terms used to define approximate decomposition degree of organic material (fibric is lowest, hemic is intermediate, and sapric is highest. Subscript sm and f refer to smouldering and flaming, respectively. Q refers to heat transferred to the soil. Modified from X. Huang, CC BY licence.

1.4. Effects on soil properties

Another important issue is the effect of smouldering fires on soil properties and constituents. Certini [87] reviewed the literature on the effects of flaming fire on forest soils, classifying the affected properties as physical, chemical or biological. In relation to smouldering fires, the most relevant physical properties are bulk density, stability and water repellency [67,68]. The changes in the bulk density of the soil left behind after a fire are due to the increase in porosity caused by the burning of organic particles in the soil. The changes in the structural stability are due to the decrease of soil compaction and the loss of cementing agents in the soil that can be in the form of organic and mineral components. The loss of structural stability is larger in smouldering fires than in flaming fires because the larger amount of soil mass lost and the deeper heating [67]. The removal of organic soil layers at the surface can lead to structural collapse and potential erosion of ashes and soil particles. Overhangs, holes in the ground and pan-shape voids around tree bases are commonly produced during smouldering fires and can lead to local

subsidence, threatening tree stability and disturbing hydrology dynamics [11]. Root systems in contact with smouldering peat can also be damaged, sometimes causing the death of the plant. These require a long-term recovery and severe soil subsidence. Without considering fires, subsidence in peat by drainage alone was typically around 2.5 m in 25 years and could be more than 5 m in 100 years [88].

The increase of water repellency is due to the formation of a continuous water – repellent layer a few centimetres beneath the surface. This water – repellent layer could be thicker in smouldering fires than in flaming fires because the organic layer is thicker in soils such as peat. The depth of the water-repellent layer is a function of heating, soil moisture and particle size [87]. Chistjakov et al. [89] briefly discussed the mechanism of water repellency in peat after fires based on the bitumen content, arguing that during smouldering combustion, bitumen condensed in the upper layer forming a water – repellent film. However, more recent studies of smouldering peat in Spain did not detected water repellency in the samples [24]. Whether or not water repellency takes place should be considered when restoring fire – disturbed peat via rewetting [90].

Dikici and Yilmaz [91] have reported that the alteration of soils properties by peat fires (i.e. density, pH, amounts of soluble salts, $CaCO_3$, etc.) do not recover in the long term. On the other hand, Smith et al. [92] reported that peat fires resulted in a decrease of total carbon, nitrogen and organic phosphorus, but an increase in the concentration of phosphorus and total calcium content of the soil. In term of after-effects on soil constituents, the impacts of peat fire were reported to be more significant than surface fires.

Generally, microbial and invertebrate biomass both decrease after fire [87]. The recovery of both soil organism and plant recolonisation are interdependent. The heat affects the recovery of soil organisms through the reduction of organic matter which is the source of organic residue, while the plants need soil organisms as biofertilizer which releasing required nutrients for plant growth [87]. Among the soil organisms, invertebrates recover more quickly than microbes because they are more mobile. The effect of MC on microbial biomass was investigated by Choromanska and Deluca [93]. The highest decline of microbial biomass was found to be after fires with the highest MC [71]. This is thought to be due to the faster heat transmission than in drier soil because water is a better heat conductor than air. The mosaic consumption of surface layers has an overall negative impact on the ecosystem. Fire reduces the accumulation of organic material, but some vegetation species (e.g. Sphagnum mosses in northern and temperate peatlands) can recolonize peatland by accessing water table and become less dependent on external water inputs [94]. Severe fire occurrence, though, can interfere with this recovery process, disturb peatland hydrologic self-regulation, and causing further drying; making peatland to be less protected from deep-burning smouldering fires [10].

1.5. Conclusion

Smouldering is the main driving combustion phenomenon for wildfires in organic soil. Organic soils, such as peat, store terrestrial carbon sequestered over millennia. Despite only covering 3% of the Earth's surface, peatlands store 25% of world soil carbon. This is more carbon than that stored in global vegetation and may be equal to the atmospheric carbon pool. Thus, fires in organic soils release an enormous amount of carbon emissions, leading to a positive feedback mechanism driving climate change. Compared with flaming wildfires, smouldering wildfires pose more significant threats in terms of fuel consumed, gas emissions and their effects on the soil system.

Smouldering fires reach deep into the soil system, making them difficult to detect and extinguish. This leads to a longer recovery time than flaming fires in terms of the overall soil system, causes severe soil subsidence, and has a negative impact on soil stability and hydrophobicity. The overall soil system includes microbial biomass, invertebrate biomass, and includes soil properties and constituents. From a thermal severity point of view, the slow spread rate and persistency of smouldering fires in peatlands leads to long retention times of hazardous temperatures in the soil system, resulting in soil sterilisation. The increased hydrophobicity of peatlands during and after fires also needs to be considered more carefully, because this knowledge could lead to more effective fires mitigation and peatland restoration strategies. Currently few literature investigated peat fires in the real scale and methods to effectively mitigate this fire.

Furthermore, smouldering has been known to transition to flaming, causing a drastic increase in fire hazard and might contribute to wildfire reignition. Currently, the understanding of this phenomena is limited that the mechanisms and variables leading to this transition are unclear. Thus, fundamental understanding of this phenomena is needed and can be obtained by investigating the important variable that can facilitate this understanding. A review of literatures is needed to determine this important variable which then can be systematically studied in the laboratory.

1.6. Thesis outline

In this chapter, three problems on the mitigation of smouldering wildfires are identified: 1) the lack of understand of peat fire behaviour in field scale, 2) behaviour of smouldering peat fire under suppression, and 3) transition from smouldering to flaming in wildfires. Currently, most studies investigated smouldering peat fire at laboratory scale and small number of field studies are of forensics nature in which actual peat fires were observed with minimum systematic investigation [95]. Due to the limited systematic field-scale study [96], the behaviour of peat fire under real conditions and the identification of

prospective effective mitigation strategy are unclear. Thus, systematic field experiments of peat fire are of high value to better understand an effective mitigation strategy. In **Chapter 2** of this thesis, GAMBUT: the largest to-date field experiments of peat fire conducted in Sumatra is reported. The fires in this study persistently survived during day and night, and despite two major rainfall events. Comparison between rainfall events that failed to suppress the fire and the successful controlled suppressions that were conducted to terminate the experiments allowed for the identification of variables that can be used as a guideline for successful suppression efforts. This variable is suppression column height.

In **Chapter 3** of this thesis, lab-scale suppression experiments were conducted to further systematically investigate the suppression of smouldering peat fire under different flow rate and wetting agent concentration.

In **Chapter 4** of this thesis, a literature review on the transition from smouldering to flaming combustion is presented. This chapter discusses the controlling mechanisms of transition to flaming.

In **Chapter 5** of this thesis, lab-scale experiments on the StF transition due to continuous and pulse wind are presented. This chapter discusses the fundamental mechanisms on the effect of wind on StF transition.

In **Chapter 6** of this thesis, conclusions on the context of mitigation of smouldering wildfire are presented.

Chapter 2

GAMBUT field experiments on tropical peat fires in Sumatra: from ignition to spread and suppression

Summary[2]

Peat fires can sustain for long periods of time (weeks or months) and spread over a massive area (~10^4 to 10^6 m^2), releasing large amounts of stored ancient carbon to the atmosphere, contributing to global warming self-acceleration, causing environmental damage and haze pollution episodes of regional scale. Peat is a plant material that accumulated and degrades over millennia and takes the same amount of time to be fully restored after consumed in a fire. Currently, fire mitigation strategies are hindered by fragments of literature on burning peatlands. Literatures on peatland fires are either of forensic nature at the field scale or of controlled nature at laboratory scale. This chapter presents GAMBUT, the largest to-date smouldering peat fire experiments on a degraded peatland with an area of 374 m^2. This work allows us to identify multi-scale signatures of the fire behaviour, which are key for novel suppression technologies, early detection systems, and modern forecasting technologies. Over 11 days, the temperature, spread rate, thermal residence, and visual and infrared signatures of smouldering peat were recorded. The peat was ignited by two methods, the application of burning charcoal, and slash-and-burn. The fires persistently spread over 4 to 10 days during day and night, and despite two major rainfalls with a water column height of 2.5 to 4.8 mm. Slash-and-burn ignition resulted in strong ignition at shallow layer indicated by maximum temperature of 700^{o}C and smouldering residence time of 8.2 ± 7.8 h, while charcoal ignition resulted with strong ignition at deep layer with maximum temperature of 550^{o}C and residence time of 16.8 ± 12.2 h. The horizontal spread rate is 0.7 ± 0.1 cm/h and the depth of burn is 25 cm in average. Comparison of failed suppression due to rainfall events to the controlled suppression indicate the existence of a critical suppression column height below which suppression is not possible. A minimum suppression column height in this study was measured to be 26.5 ± 9.2 mm, agrees with results from lab-scale study ranged from 13 to 36.5 mm, thus demonstrating the applicability of results from small-scale experiments in the literature to burning peatlands at field-scale. GAMBUT explores the smouldering of peat fire in real environmental conditions, scales, and precipitation, providing a unique understanding of these wildfires.

---

[2] This chapter is based on "Muhammad A. Santoso, Eirik G. Christensen, Hafiz M. F. Amin, Pither Palamba, Yuqi Hu, Dwi M. J. Purnomo, Wuquan Cui, Agus Pamitran, Franz Richter, Thomas E. L. Smith, Yulianto S. Nugroho, and Guillermo Rein. GAMBUT field experiments on tropical peat fires in Sumatra: from ignition to spread and suppression. (to be submitted)"

2.1. Introduction

Different scale of experiment reveals different information about peat fire behaviours [95]. In micro scale, at the order of milligram sample, the fundamental chemistry of peat fires has been identified, revealing peat fire exothermic and endothermic reaction schemes [97,98]. In meso scale, at the order of gram to kilogram samples, the outputs are the fundamental dynamics of peat fire such as critical moisture content (MC) and inorganic content (IC) for ignition [47–49], horizontal and in-depth spread [3,53,56,99–101], gaseous emission [102–104], and suppression [105,106]. Currently the maximum characteristic length of laboratory meso scale investigation in the literature is 40 cm [81,99,100]. Although these investigations in the micro and meso scale provide fundamental understanding of peat fire behaviors, they were conducted in a simplified condition and constant laboratory environments compared to natural scenario where MC, IC, density, and environmental conditions changes over time. Thus, experimental evidence in the field scale are needed to link between understanding in the meso scale to the real peat fire events.

Forensic field scale studies of peat fires have been previously conducted [12,14,51,85,107,108], investigating actual field scale peatland fires with minimum systematic in situ measurements. Only Pastor et al. [96] attempted to conduct systematic experiments in real peat land in Peruvian Andes, with each experimental area of 50 × 50 cm^2. Even though the experimental location is in the field, the experimental size is as small as in the lab scale and only 3 out of 18 tests was registering temperature above 100^oC in which only 1 recorded temperature up to 400^oC. This indicates that the smouldering was weakly self-sustained and many were not successfully ignited. Thus, the required information to understand the actual behavior of real peat fire, surviving despite rainfalls and firefighting response, is still minimum.

This paper reports GAMBUT, the experimental campaign of field scale tropical peat fires in which the largest to-date peat fire experiments were conducted to measure field scale peat fire behavior signatures in terms of smouldering temperature, spread rate, thermal residence time, fire area and perimeter, and critical column height for successful suppression. The location is in a secondary peat swamp forest (PSF) in Indonesia where the largest share of peat carbon in Southeast Asia is contained (65%, 57.4 Gt) and widespread peatland fires have been reported to occurred annually [109–112]. Secondary or degraded PSF is the result of disturbed pristine PSF by fire or human activities [113]. The experimental area is ranged from 0.2 × 0.5 m to 8 × 10 m area. The shortest and longest fires observed in this study were 4 to 10 days, respectively, up to controlled suppression. GAMBUT is the first to fill the gap to understand peat fires dynamics between lab and field scale. These experimental evidences can also provide peat fire behavior signatures in field scale such as spread rate and residence time to

predict peat fire propagation, surface signature of peat propagation under changing environmental conditions to enable early detection, and successful suppression criteria such as suppression column height to enable effective firefighting response.

2.2. Experimental Method

2.2.1. Field sites and experimental plots

The site of the experimental work was in Rokan Hilir regency, Sumatra, Indonesia. The site in this study is a secondary/degraded PSF mostly covered by palm trees, ferns, and sedges, and closely located with an artificial pond (Figure 2.1). While some work has focused on the increase rates of methane and CO_2 emission from a degraded peatland, little is known about its fire behavior [114,115]. This work aims to fill the gap on the soil properties and fire behavior of a field-scale degraded PSF.

The experiments were conducted from 19 August to 29 August 2018. The location of this site generally has a tropical wet climate with mean annual rainfall at 2080 mm [116]. Drought season occurs in June and July with monthly rainfall at ~85 mm, and started to increase in August then peaked in November at about 300 mm [116]. From the climate data in the last five years, from 2013 to 2017, the mean daily rainfall in August is 6.5 mm which started to increase during the last of August with maximum at 117.2 mm [117]. These rainfall data allowed the approximate determination of the experimental dates to intersect with the start of rain season, enabling the investigation of the effect of rainfall on smouldering peat fire. The average temperature in August is 27.4 ^{o}C with minimum at 23.4^{o}C and maximum at 33 ^{o}C, in the last 5 years [117].

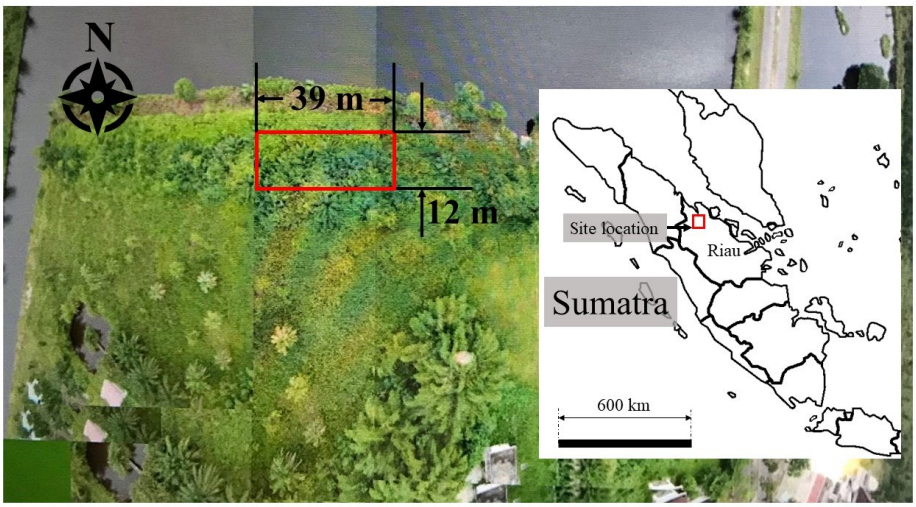

Figure 2.1. Site and experiment plot area location showing top view of the site taken by drone and the plot area location inside the red rectangle in the secondary peat swamp forest in Rokan Hilir, Sumatra, Indonesia (1°36'17.1"N 100°58'30.5"E) (Image from YS Nugroho, CC BY). Inset shows site location in Sumatra island (public domain license, source: republikseo.net).

Peat fire experiments were conducted in three 10 by 10 m experimental plots (Figure 2.2A). Fire breaks were made by digging a trench of 50 cm wide and 50 cm deep which were filled with sand, around the perimeter of each plot. This fire break prevented fires spread outside the experimental plot. Plot surfaces were cleaned from palm trees, ferns, sedges, and surface litter vegetation, except plot 1 where surface litter vegetation was kept intact to study the effect of surface litter vegetation on the fire spread (Figure 2.2B). The topography of the experimental plots shows a significant elevation difference of ~1 m between south and north sides. This topography difference influences the decision on pre-experiment sampling location to investigate the peat properties (black circles in Figure 2.2A) and on the location of ignition attempts. See also Figure A 2.1 in Appendices.

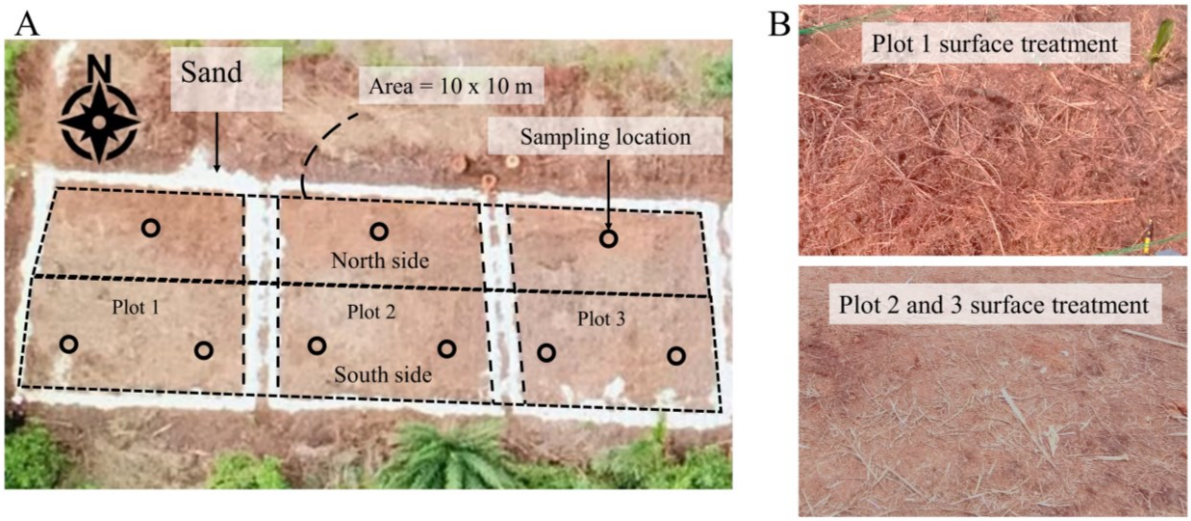

Figure 2.2. (A) Top view of the three 10 by 10 m of experiment plot area after surface treatment to cut and clean surface vegetation (palm trees, reeds, sedges, and grasses) (Image from YS Nugroho, CC BY). Black circles represent sampling locations for bulk density, MC, IC, and C/H/N measurements, taken at four different depths, 0 to 10 cm, 10 to 20 cm, 20 to 30 cm, and 30 to 40 cm. Horizontal dashed line at the middle of the plots is an imaginary line to divide between north and south sides of the plots (B) The difference of surface treatment between plot 1 where surface litters vegetations kept intact and other plots (plot 2 and 3) where surface litters vegetations were also removed.

2.2.2. Peat properties

Pre-experiment peat sampling was conducted to measure bulk density, moisture content (MC), elemental content (C/H/N), and inorganic content (IC). The locations of the sampling are shown in Figure 2.2A and were chosen based on the topography difference between north and south sides of the plots (Figure A 2.1B to D). Thus, sampling locations were determined to investigate peat properties variations due to topography difference. Samples were taken at four depths, i.e. 0 to 10 cm, 10 to 20 cm, 20 to 30 cm, and 30 to 40 cm, by using a cylindrical container with dimension of 2.54 cm diameter and 10 cm long. These depths were chosen based on the average depth of burn of peat fire events recorded in the literature from 1983 to 2015 [118]. The samples were immediately weighed to measure the

wet bulk density ($\rho_{b,wet}$). Volumetric moisture content (VMC) was measured by Delta-T SM150T soil moisture sensor probe with an accuracy of ±3%. Using the measured bulk density, then the dry-mass-based moisture content (MC) is calculated by using Eq. 2.1 where ρ_w is water density of 1 kg/m^3. After the bulk density was measured, another small sample of ~10 g was taken and sent to Exeter Analytical (UK) Ltd. to measure the C/H/N content using CE440 Elementa Analyzer. The rest of the sample was then used for the measurement of IC by means of Loss on Ignition (LoI) method by burning the sample in a furnace with temperature set at 1000^{o}C. Prior to the LoI test, the sample was dried in an 80^{o}C oven for 48 h. The dry sample then heated in the furnace until no mass loss was detected, obtaining IC in dry mass basis.

$$MC = \frac{1}{\frac{\rho_{b,wet}}{VMC.\rho_w} - 1} \tag{2.1}$$

2.2.3. Fire area and ignition methods

During this work, smouldering of peat was measured for 11 days across different diurnal weather patterns and precipitation. Six peat fire experiments were conducted with different ignition methods, surface treatment of the plots, and topography. Figure 2.3 shows the six fire experiment areas, noted as plot 1 north (P1N), plot 1 south (P1S), plot 2 north (P2N), plot 2 south (P2S), plot 3 north (P3N), and plot 3 center (P3C). In this experiment, fire in north and south sides of the plots were well separated and did not spread into each other. Ignition methods are charcoal ignition and slash-and-burn. Charcoal ignition was attempted by putting burning charcoal, which had been ignited using gasoline and left to burn for 10 min, into an ignition pit. This ignition attempt was conducted in P1S, P2S, and P3C fire area to observe smouldering behavior under strong ignition in deep layer. There are three ignition pits in P1S each with dimension of 0.5 × 0.2 m^2 and 0.2 m deep, while ignition pits in P2S and P3C were 6 × 0.2 m^2 and 0.2 m deep and 0.5 × 0.5 m^2 and 0.4 m deep, respectively. A total of 9.3 kg, 70 kg, and 16 kg of activated charcoal were put in ignition pits in P1S, P2S, and P3C, respectively. In P3C, the charcoal ignition was aided by additionally burning 500 mL of gasoline in the ignition pit, resulted in strong flaming combustion with about 1.5 m flame height for ~15 min. The longest self-sustained smouldering peat fires is charcoal-ignited peat fires on the south side of plot 1 (P1S, Figure 2.3) which lasted for ten days. Figure 2.4 shows the chronology of peat fires test in this study.

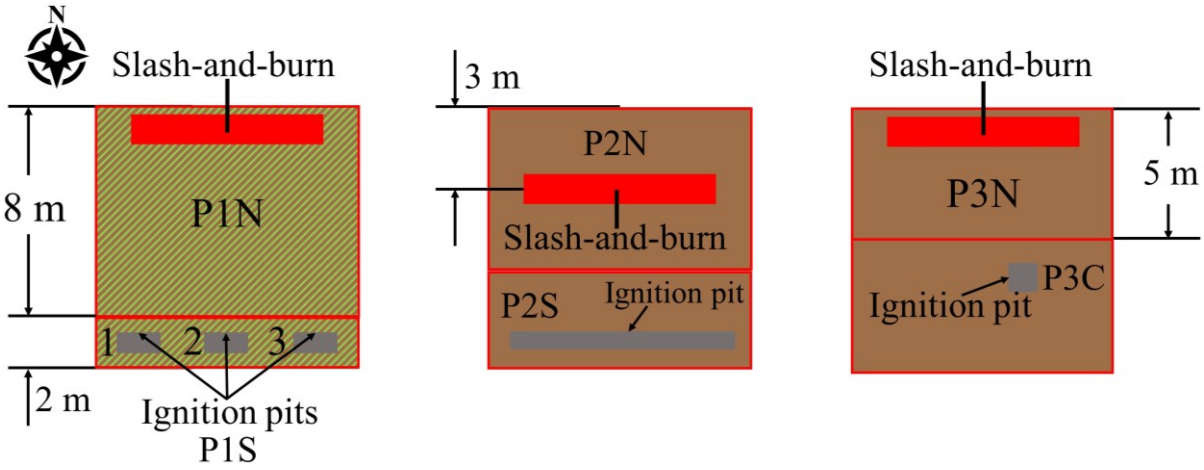

Figure 2.3. Schematic of fire area and different ignition methods conducted in this study. The experimental area were designed to study different ignition methods, surface treatment, MC, and bulk density on smouldering peat fire.

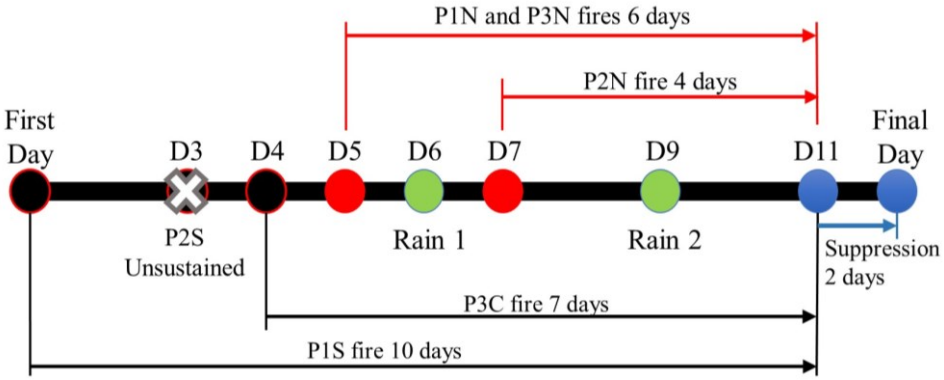

Figure 2.4. Chronology of peat fires experiments from ignition to suppression attempts (D = day). Black, red, green, and blue circles represent peat fires ignited by charcoal combustion, peat fires ignited by slash-and-burn, incident of rain event, and suppression, respectively.

Figure 2.5 and Figure 2.6 show charcoal-ignited smouldering peat in P1S and P3C two days after their ignition. On D3, the smouldering area of each three pits in P1S were increased significantly from 0.1 m^2 of pit area before ignition to 0.42 m^2, 0.6 m^2, and 0.5 m^2 for pit 1, 2, and 3, respectively. While in P3C, the area increased from 0.25 to 0.46 m^2 in two days. The smouldering area is estimated by analyzing infrared image which will be discussed in a later section. These increases in smouldering area indicate self-sustaining smouldering. The charcoal ignition in P2S resulted in unsustained smouldering propagation shown by the absence of increase in smouldering area (Figure 2.7B). Further, during digging on D12 prior to experiment termination, no hotspot was found under the layer of ash. Thus, both horizontal and in-depth smouldering spread were unsustained. Possible explanation to this unsuccessful ignition is heat loss in P2S was higher than P1S and P2C due to larger ignition pit area in P2S. The larger ignition pit area in P2S resulted in the open top area of P2S to be as high as 5 to 12 times than of P3C and P1S, causing higher convective heat loss to the ambient air.

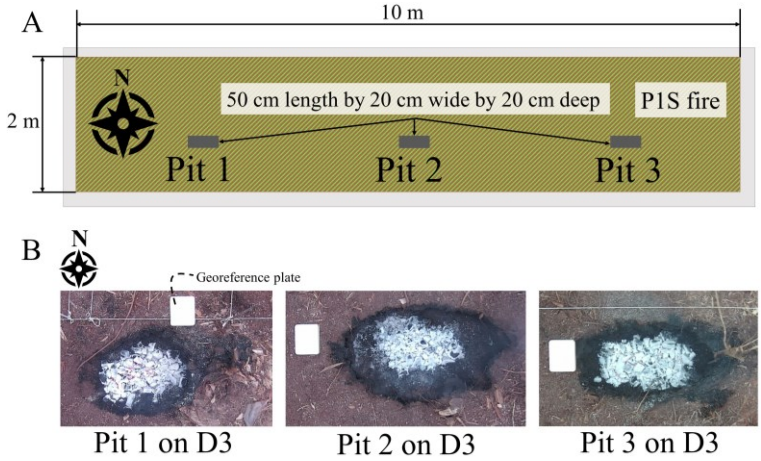

Figure 2.5. Charcoal – ignition pits in P1S fires area. Refer to Figure 2.3 for the full schematic of the experiment locations. (A) The schematic of location and dimension of ignition pits in P1S fires area. (B) Ignition pits top view image on D3. In each image, a geo-reference plate with known dimension (17 cm by 14 cm) is included for geo-referencing and to calibrate the IR images to estimate the increase of smouldering spread area.

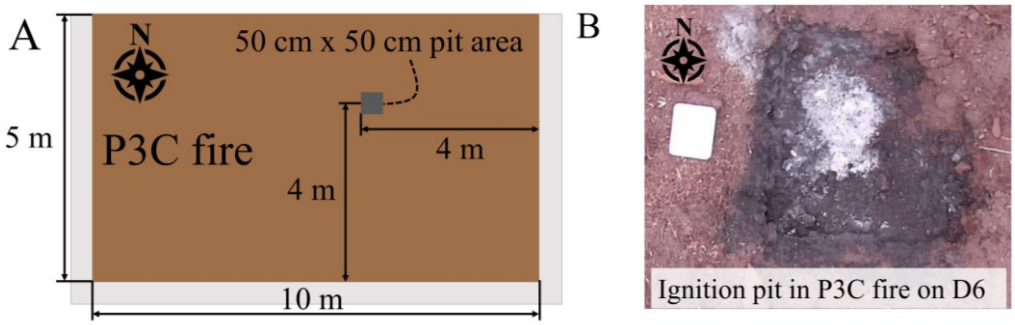

Figure 2.6. Charcoal – ignition pit in P3C fires area. Refer to Figure 2.3 for the full schematic of the experiment locations. (A) The schematic of location and dimension of ignition pit in P3C fire area. (B) Top view of ignition pit on D6.

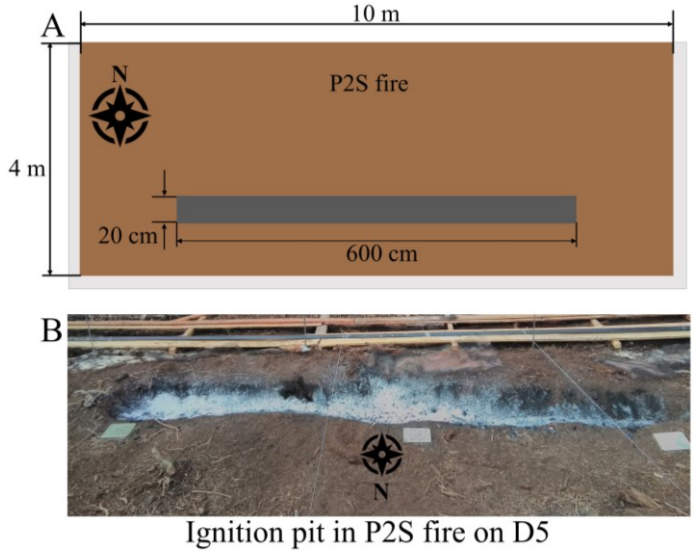

Figure 2.7. Charcoal – ignition pit in P2S fires area. Refer to Figure 2.3 for the full schematic of the experiment locations. (A) The schematic of location and dimension of ignition pit in P2S fires area. (B) Perspective view of ignition pit on D5.

Slash-and-burn ignition was conducted in P1N, P2N, and P3N by burning slashed dried tree branches, palm tree leaves, sedges, and litters put together in a pile with dimension of 8 m length, 1 m wide, and 50 cm high. Most of the occurrences of smouldering megafires in peatland were due to uncontrolled smouldering spread during the attempt to convert peatland for agricultural purpose [9]. During this land-use change process, the peatland was cleaned by cutting down and burning the native vegetations, hence the name slash-and-burn, as the cheapest way to prepare the land for a more economically beneficial plantation. Around every couple years, e.g. ~three years, this land conversion activity resulted in regional scale pollution called haze driven by smouldering peat fires made worse by a longer and warmer drought season due to El Nino [12,14,27]. The purpose of slash-and-burn ignition conducted in this experiment is to observe the spread of smouldering peat fires due to the ignition method that has been recorded to cause uncontrolled widespread of peat fires. The pile of slashed vegetations were put at the north-side edge of P1N and P3N, and at ~3 m from the north-side edge of the P2N (Figure 2.3). Slash-and-burn was conducted on the north side of the plots to ignite smouldering by means of a strong ignition source since the MC and bulk density of the north side of the plot was found to be significantly higher than the south side (Table 2.1). All slash-and-burn ignitions resulted in self-sustained smouldering propagation (Figure 2.4). Figure 2.8 shows the slash-and-burn ignition in P1N on D5.

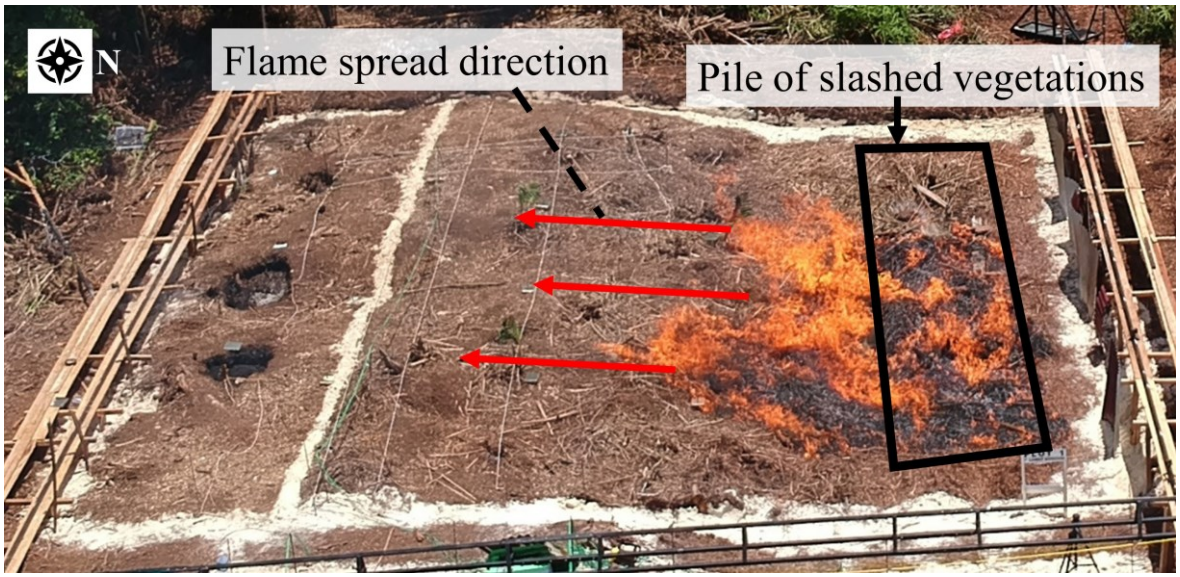

Figure 2.8. Slash-and-burn ignition in P1N on D5 (Photo by YS Nugroho, CC BY license). The surface vegetation was not removed which resulting in flame spread beyond the biomass pile and ignited the peat. The sand line between P1N and P1S was put to ensure that the strong slash-and-burn ignition in P1N not spreading into P1S. Such line was not introduced in plot 2 and plot 3 since the slash-and-burn ignition in P2N and P3N were not as intense and wide as P1N.

2.2.4. Diagnostics methods

Thermocouples were used to measure smouldering temperature and spread rate. Due to the uncertain smouldering propagation direction, thermocouples were placed on certain points based on visual observation and the likelihood of propagation direction. To obtain spread rate data, two thermocouple points were located at known distance, i.e. 15 cm. Each thermocouple point contains two thermocouples at 10 cm (shallow layer) and 30 cm depth (deep layer). See Figure A 2.2 in Appendices for thermocouples placement. As smouldering progressed and passed a thermocouple point, the thermocouples were then moved to a new location, if the thermocouples were not burnt. The thermocouple points shown in Figure 2.11 are the total points of thermocouple placements at the end of the experiment.

Infrared images were recorded using FLIR Duo-R camera, mounted on a crane with angle-adjustable hand in order to adjust the field of view of the camera. This crane was mounted on a rail to allow convenient IR signature measurement along plot 1, 2, and 3 (Figure 2.9A), on both the north and south sides of the plot. Figure 2.9B shows IR camera attached to the crane for IR image acquisition during the experiments. A geo-reference plate with known size (17 × 14 cm) was used to analyse smouldering area and perimeter from infrared image. Furthermore, depth of burnt (DOB) was measured by burying a metal pole (diameter of 2.5 mm) with geo-reference plate on top at several locations in the plot before ignition was conducted (Figure 2.11). The burial of the pole was up to the point that the plate at the level of surface layer of the plot. The diameter of the metal pole was chosen to be small, 2.5 mm, to not significantly disturb the density of the peat. The measurement of DOB was taken on D12 and found to be 25 cm in average.

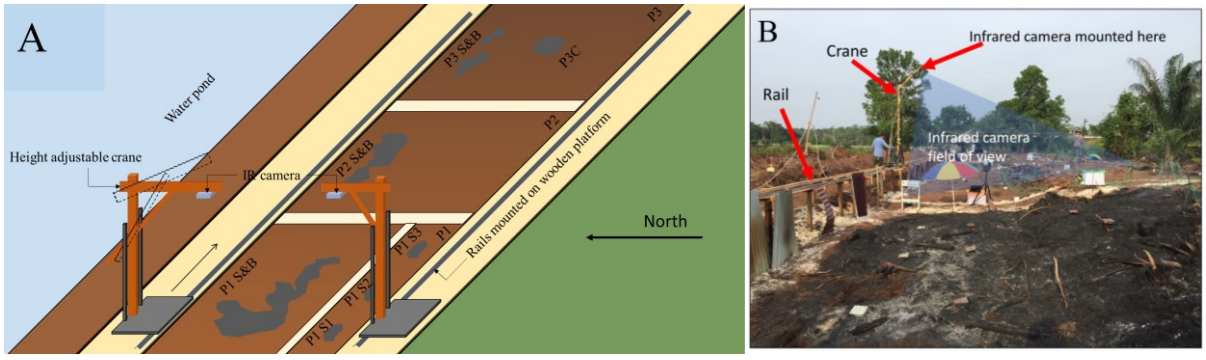

Figure 2.9. Methodology for acquisition of infrared signature from smouldering area in the plots (A) schematic showing the method of IR image acquisition across plot 1, 2, and 3 (B) photo during experiment showing the crane and rail in the field during the experiments.

A weather station was installed near the plots to measure ambient temperature, humidity, precipitation, and wind direction and magnitude. Figure 2.10 shows the precipitation and summary of ambient temperature and humidity during the experiment. Five self-sustained smouldering peat fires in this

experiment were recorded to survive the two rainfall events on D6 and D9 (Figure 2.4). Figure 2.10A shows the recorded rainfall events in term of rainfall rate on D6 and D9. The maximum and minimum ambient temperatures were 35.9 and 21.6 ^{o}C, respectively. The maximum and minimum ambient relative humidity were 98 and 38 %. Considering that the difference between maximum and minimum temperature, and of ambient relative humidity, was 14.3 ^{o}C and 60 %, we have recorded smouldering peat fires propagation against relatively significant diurnal changes of environmental conditions, i.e. dry and hot (peak at ~14:00 western Indonesian time (WIT)) and wet and cold (peak at ~05:00 WIT).

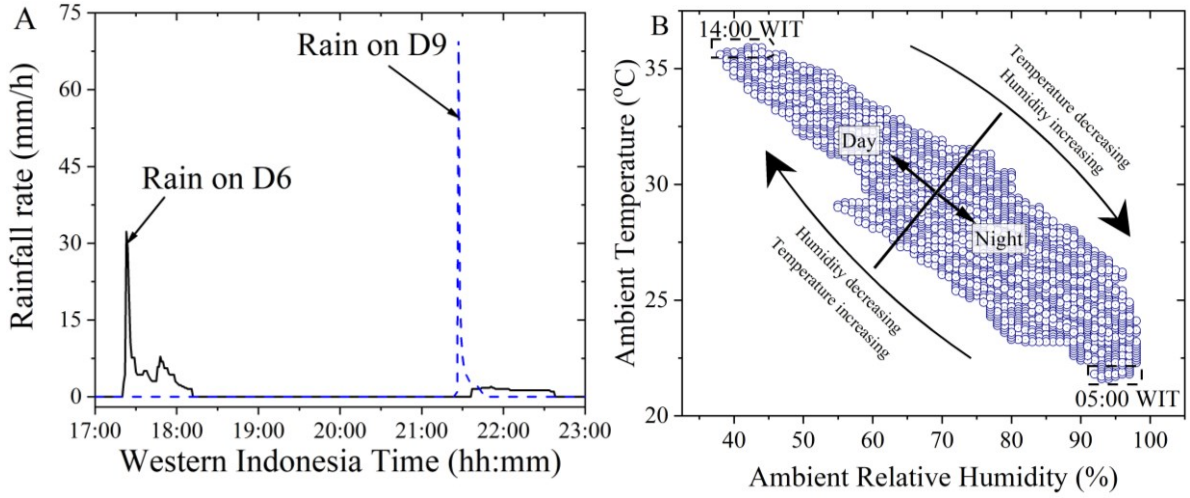

Figure 2.10. Weather condition during the experiments. (A) Two recorded rainfall events on D6 and D9 (B) Recorded ambient temperature and relative humidity from D1 to D12. WIT is Western Indonesia Time (GMT + 7 h). Day time is from 09:00 to 18:00 WIT and Night time is from 18:00 to 09:00 WIT.

2.3. Results and discussion

2.3.1. Peat properties

The mass fraction of C/H/N of the north and south side of the plots are 29.2±5.9%/6.8±4.9%/1.1±0.4% and 20.7±5.6%/2.7±1.3%/0.6±0.2%, respectively. Both sides have lower Carbon content than what is typically expected of pristine or degraded tropical peat forest which is ~55 to 60% [119]. IC of peat in this site is also considerably high, i.e. 52.7 ± 11.6 %, while IC of tropical peatland has been measured to be 3 ± 1.96 % [105]. This means that the peatland in our site has been considerably degraded. However, based on three established peat classification systems of International Peat Society (IPS), Canada Soil Survey Committee (CSSC), and International Organization of Standardization (ISO), the soil in this study can still be classified as peat because the IC is less than 70% and the organic content (OC) is more than 30% [7] (see also Figure 1.1). The average IC in this study is 52.1±11.9% in dry basis. Table 2.1 shows MC, wet bulk density, elemental analysis, and inorganic content measurements of the peat in this study, based on the sampling locations in Figure 2.2A and fire location index in Figure 2.3 (see also Figure A 2.3 for graphical illustration).

Table 2.1. Physical and chemical properties of peat in this study. Sampling location is referring to Figure 2.2A.

Measurement Locations	Measurement depth (cm)	$\rho_{b,wet}$ (kg/m^3)	Moisture Content (% dry mass basis)	Elemental analysis			Inorganic content (%)
				C (%)	H (%)	N (%)	
P1N	0 to 10	1136	150.9	33.73	3.2	0.88	44.8
	10 to 20	1230	191.2	30.73	16.46	0.82	23.6
	20 to 30	1458	153.3	25.97	10.21	0.62	
	30 to 40	1483	200.3				
P1S	0 to 10	656	32.3	21.94	2.43	0.57	63.5
	10 to 20	766	39	23.81	2.48	0.55	57.6
	20 to 30	793	64.6	26.05	2.11	2.51	54.9
	30 to 40	879	78.2				
P2N	0 to 10	921	77.5	22.56	3.86	0.69	49.5
	10 to 20	934	231.8	34.77	6.34	1.69	
	20 to 30	1243	292.1	36.56	6.67	1.53	38.4
	30 to 40	1389	458.0				
P2S	0 to 10	714	24.1	22.37	2.66	0.63	53.2
	10 to 20	776	41.0	17.89	3.46	0.5	
	20 to 30	890	55.6	24.76	5.39	0.74	53.5
	30 to 40	1037	54.7				
P3N	0 to 10	737	91.9	23.22	2.66	1.09	49.8
	10 to 20	905	189.8	32.92	3.38	1.57	
	20 to 30	1455	126.1	22.21	8.34	0.61	55
	30 to 40	1478	197.0				
P3C	0 to 10	806	18.9	17.19	1.81	0.49	71.2
	10 to 20	925	27.3	14.2	1.53	0.4	
	20 to 30	991	35.3	17.98	1.96	0.46	62.3
	30 to 40	988	50.9				

2.3.2. Temperature

2.3.2.1. Temperature profile

Figure 2.11 shows smouldering propagation sketch at the surface of plot 1 on D5, plot 2 on D8, and plot 3 on D7. The sketch was made based on visual observation after slash-and-burn ignition. Widest and longest flaming spread was evident in P1N due to intact surface vegetations, causing flaming to spread farther than the initial piles of slashed vegetations. This caused the flaming to ignite wider smouldering than initial ignition location. Contrary to P1N, smouldering in P2N and P3N only ignited and propagated around the location of the initial slash-and-burn location, even after 6 days of propagation. This also partly caused by the slow smouldering spread rate which will be discussed later.

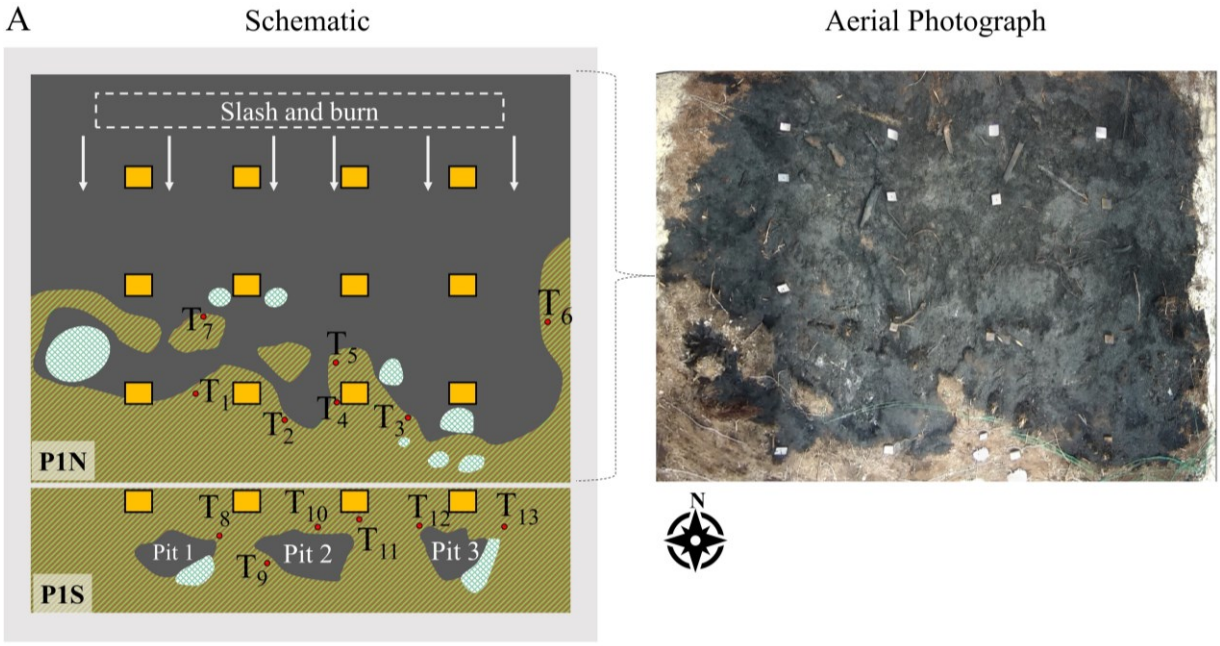

Plot 1, Day 5, after flaming from slash-and-burn extinguished

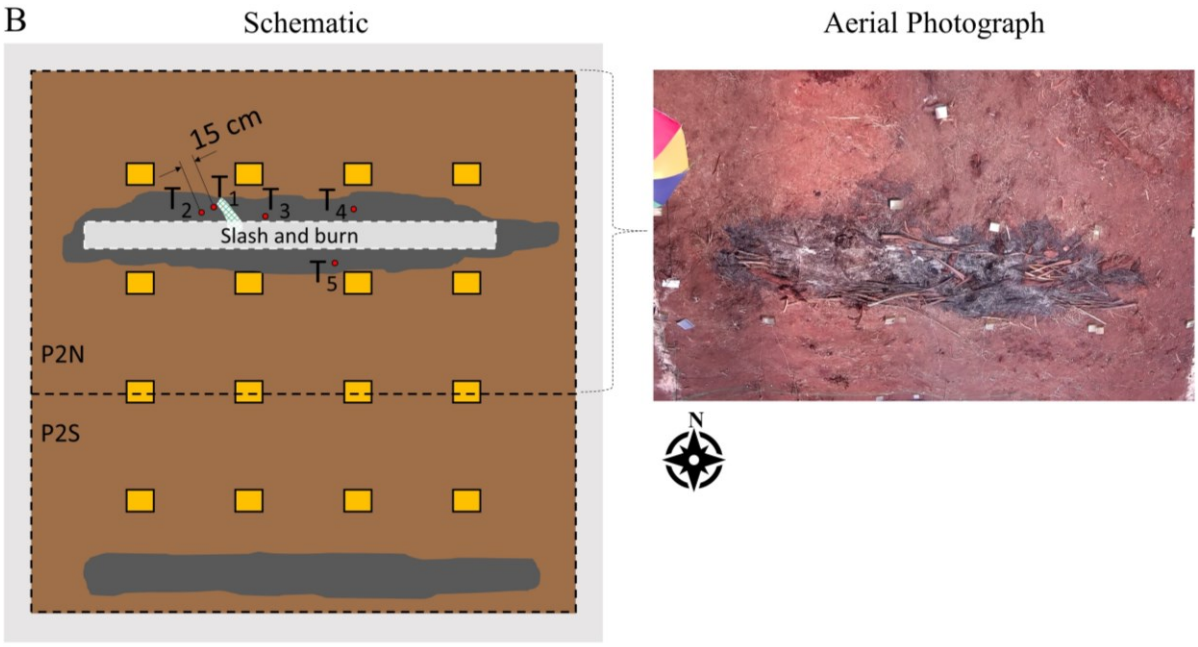

Plot 2, Day 8, after flaming from slash-and-burn extinguished

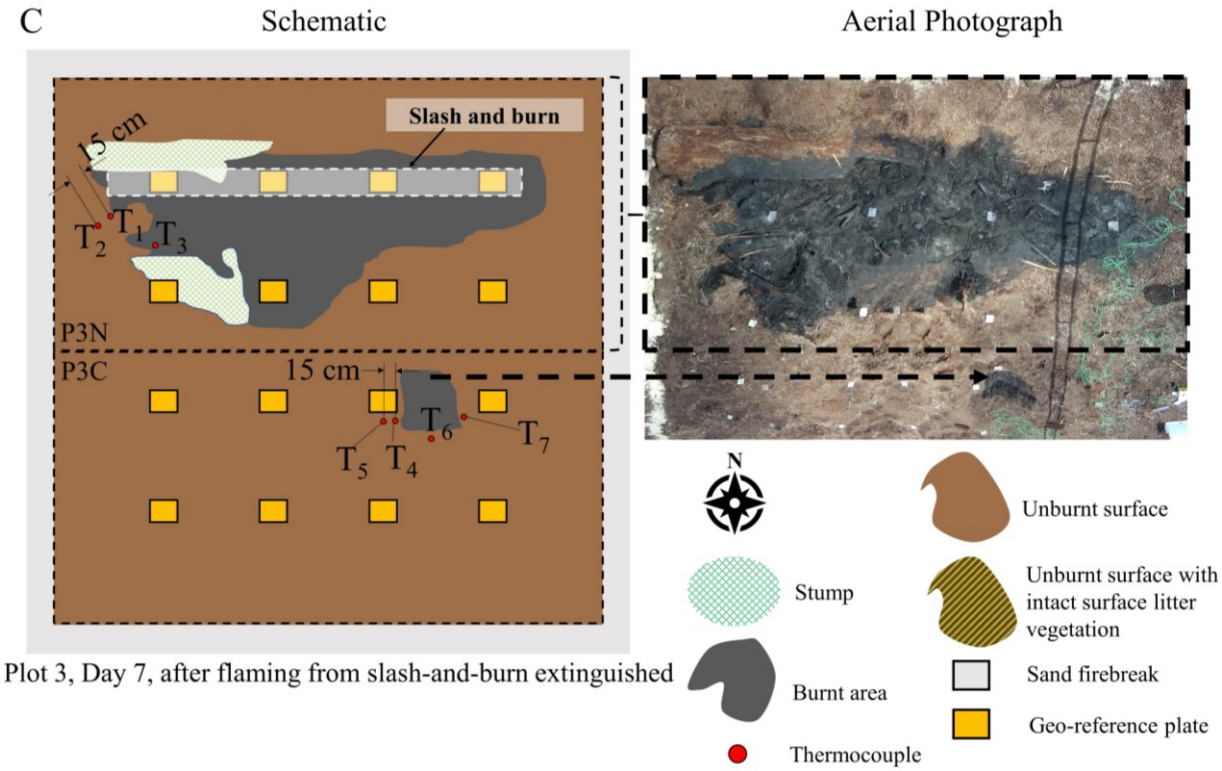

Figure 2.11. Sketch of thermocouples placement and smouldering area after slash-and-burn and charcoal ignition attempts. The picture on the right-hand side of the sketch is the aerial photograph of the fire area. (A) Plot 1 on D5 where slash-and-burn was conducted on P1N and charcoal ignition on P1S. Aerial photograph of P1N was taken on D7 (B) Plot 2 on D8 where slash-and-burn was conducted on P2N and charcoal ignition on P2S. Aerial photograph of P2N was taken on D8 (C) Plot 3 on D7 where slash-and-burn was conducted on P3N and charcoal ignition on P3C. Aerial photograph of plot 3 was taken on D7. For photo of smouldering area in P1S, P2S, and P3C fires area, refer to Figure 2.5B, Figure 2.7B, and Figure 2.6B, respectively.

Thermocouples were placed on points that prospectively, based on visual observation, would capture smouldering spread, (Figure 2.11). Due to the high level of peat properties heterogeneity in lateral and in-depth orientations, e.g. MC and ρ_b (Table 2.1 and Figure A 2.3), not all thermocouples captured smouldering spread. Figure 2.12 shows temperature in P1N from the day when slash-and-burn was conducted (D5) to the end of D8, with t = 0 h indicating 00:00:00 am of D5. This figure shows temperature at T3 and T6 where smouldering spread was relatively well recorded, represented by clear temperature growth, peak, and the start of decay. Smouldering in P1N was self-sustained until D11, however temperatures after D8 are not reported in this figure due to unclear smouldering propagation because of power cut on the night of D8 to the early morning of D9 due to technical issue and on the night of D9 to the early morning of D11 due to heavy rain on the night of D9 (Figure 2.4 and Figure 2.10) causing the tent protecting the electrical sources to the measurement devices to collapsed, cutting off power supply to data loggers. Figure A 2.4 in appendices shows the

temperature in P1N up to D11 where technical issue and power cut are indicated by blank temperature data. These occurrences represent the difficulty of conducting smouldering field experiment in peatland forest where harsh environment and logistics management can be challenging.

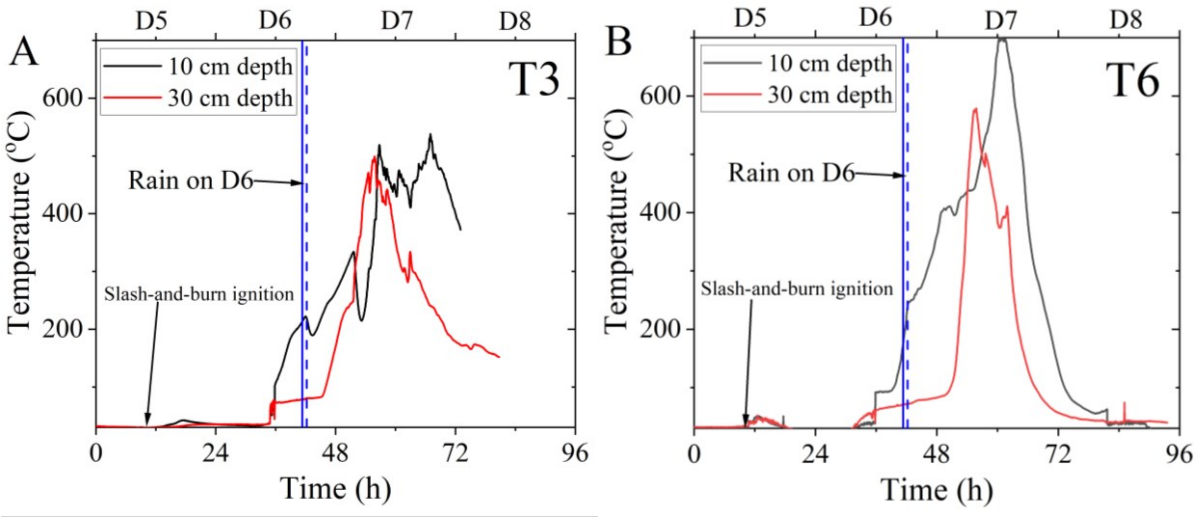

Figure 2.12. Example of temperature profiles in P1N, at (A) T3 and (B) T6 showing clear temperature growth, peak, and the start of decay, indicating smouldering propagation. See Figure A 2.4 for temperature profile of all TCs in P1N. Time at 0 h indicates 00:00:00 am in D5. Slash-and-burn ignition was conducted on D5 at ~11:27:00.

Overall, the measurement depths in this study, i.e. 10 cm (shallow layer) and 30 cm depth (deep layer), well represents smouldering propagation, demonstrating peak at a typical strong smouldering in peat (~700°C) (Huang & Rein, 2019). Smouldering can be seen to propagate from shallow to deep layer represented by higher temperature at 10 cm depth than 30 cm depth (Figure 2.12 and see also T4 and T5 in Figure A 2.4), except at T7 where stronger deep layer smouldering than at the shallow layer can be observed (Figure A 2.4).

Overhang formation and collapse were mostly visible in this study (Figure A 2.9A). Overhang formed due to slower smouldering propagation at the shallow layer than at deep layer of the peat (Huang et al., 2016). In this study the formation of overhang was compounded by surface vegetation at the shallow layer. The surface vegetation layer provided temporary stability on the soil due to its network of fibers. Because ignition was conducted on the surface layer, i.e. slash-and-burn, the peat in this overhang was already burning as well (Figure 2.12). As smouldering continues to propagate deep below the surface, the surface vegetation was intact up to the point that it loses its stability and the burning peat in this overhang collapse onto the soil around the TCs, represented by abrupt temperature increase (see T7 at 10 cm depth at noon of D8 in Figure A 2.4). Close to overhang location, few occurrences of transition from smouldering to flaming were observed. The transition occurred once overhang cracked and releasing some of the pyrolyzate from deep layer. The flaming might be sustained for a time if

there was a surface vegetation or twigs on the overhang that was ignited by the transition. However, currently it was not possible to systematically investigate this occurrence in this field experiments since the key variables leading to transition are not yet identified. In Chapter 4, the key variables leading to transition that have been reported in the literature are identified, followed by systematic investigation of one of these key variables in Chapter 5. See also Figure A 2.9 for short discussion of overhang collapse and transition to flaming encountered during these field experiments.

Rainfalls occurred twice during the experiments, on D6 and D9 (Figure 2.10A). The average rainfall rate (rainfall depth) on D6 and D9 was 5.6 mm/h (4.8 mm) and 8.3 mm/h (2.5 mm), respectively. Both rainfalls were not enough to extinguish the smouldering in this study as can be seen in Figure 2.12 for D6 rain. The smouldering was still propagated downward (at T3 and T6 in Figure 2.12) or vigorously survived at in-depth layer (T7 in Figure A 2.4). In average, the temperature in both P1N (Figure A 2.4) and P1S (Figure A 2.7) decreased for only 1.7^{o}C during this rainfall, while the temperature during this rainfall in P3N and P3C were not recorded because the TCs located as shown in Figure 2.11 were not captured smouldering spread, yet. Meanwhile, P2S was unsustained and P2N was not ignited yet. The effect of the second rainfall (on D9) on temperature, as has been mentioned previously, was unable to be recorded due to power cut. The effect of both rainfalls, including rain on D9, on smouldering will be discussed during the analysis of infrared image in the next section. Lin et al. [106] reported that the critical rainfall rate to extinguish peat fire is 4 mm/h, well below rainfall rate recorded here. However, successful suppression with 4 mm/h requires ~5 h of suppression, much longer than the rainfall durations reported here which are 50 and 17 min for D6 and D9 rainfall, respectively. This implies a critical intensity (or flow rate) and duration for a successful suppression. Figure 2.12 shows that the smouldering peat fires in this study survived for about 1 to 2 days at one measurement point, indicating both a slow spread rate and a very persistent fire despite rain event and diurnal weather variation.

Smouldering due to slash-and-burn ignition mostly propagated from shallow to in-depth layer (from 10 to 30 cm depth), except in P3N (Figure A 2.6). However, smouldering at T2 at 30 cm deep in P3N was weakly propagating, indicated by periodical increase up to 400^{o}C followed by sharp decrease below 200^{o}C (Figure A 2.6). Thermocouple at T2 was located 15 cm from T1 (Figure 2.11C). A possible explanation is that smouldering was weakly propagating from T1 from T2. This weak smouldering propagation implied by shallow smouldering at T1 (10 cm depth) creeping to deep layer first at T2 (30 cm depth) before propagating to shallow layer at T2 (10 cm depth). This might be due to a less effective slash-and-burn since the surface vegetation litters were removed and relatively high MC in the north side of the P3N, ~200% initial MC at 10 and 30 cm depth (Table 2.1). Comparing MC between P1N, P2N, and P3N, also explains the weak smouldering propagation in

P2N (Figure A 2.5) in which the MC ranged from 230 to 460% at 10 to 40 cm depth (Table 2.1). In P1N, smouldering propagated relatively well showing peak temperature at ~700°C with initial MC ranged from 100 to 200%.

Contrary to smouldering due to slash-and-burn, smouldering due to charcoal ignition was mostly stronger at deep layer compared to at shallow layer (Figure A 2.7). Smouldering at T4 → T5 in P3C (Figure A 2.8) demonstrating a similar propagation to T1 → T2 in P3N (Figure A 2.6) where smouldering was creeping from shallow to deep layer at the adjacent location and then propagating upward to the shallow layer. The peak temperature in charcoal-ignited fire was at deep layer at ~550°C.

2.3.2.2. Spread rate

From both T1 → T2 (10 cm depth) in P3N and T4 to T5 (10 cm depth) in P3C (see Figure 2.11), horizontal smouldering spread rate was calculated to be 0.6 and 0.8 cm/h, at isotherm of 300°C which is well above smouldering temperature (230°C [97]). The slight difference between these horizontal spread rate despite wide difference of initial MC, 135.9 ± 40.6% in P3N and 27.2 ± 6.7% in P3C (Table 2.1), might be due to compounding effects of the degradation level of the peatland in this study (relatively low carbon content/high inorganic content) and high bulk density of the peat (Figure A 2.3B). These spread rates are in the lower range of values reported in the literature i.e. ~0.5 to 19.5 cm/h [56,120,121].

2.3.2.3. Smouldering Thermal Residence Time

Thermal residence time is duration in which a location recorded temperature equal to or greater than a specified temperature. [11]. In this study, the threshold was varied from 200°C up to the peak temperature at a certain point, thus investigating smouldering residence time. This minimum temperature threshold is above peat pyrolysis temperature, i.e. 150°C, but below peat char oxidation temperature, i.e. 230°C [97]. The points included in thermal residence time analysis are the points in which temperature was demonstrating a clear temperature growth, peak, and decay at least to 200°C.

Figure 2.13 shows thermal residence time of plot 1 and plot 3. Overall, the smouldering in this study sustained from a few hours up to 40 h at a single location. On average, smouldering from slash-and-burn ignition in P1N (Figure 2.13A), where the surface vegetation was not cleared, resulted in relatively stronger smouldering at the shallow layer than at deep layer. In contrast, smouldering in P3N (Figure 2.13B), where surface vegetation was cleared, demonstrated a weaker smouldering at shallow than at deep layer. This might be due to a less intense ignition on the surface than in P1N. However, the smouldering residence time at deep layer in P3N is relatively similar to the average of deep layer in P1N. This indicates that despite the less intense ignition on the surface, smouldering at deep layer can still have a relatively high severity once self-sustained.

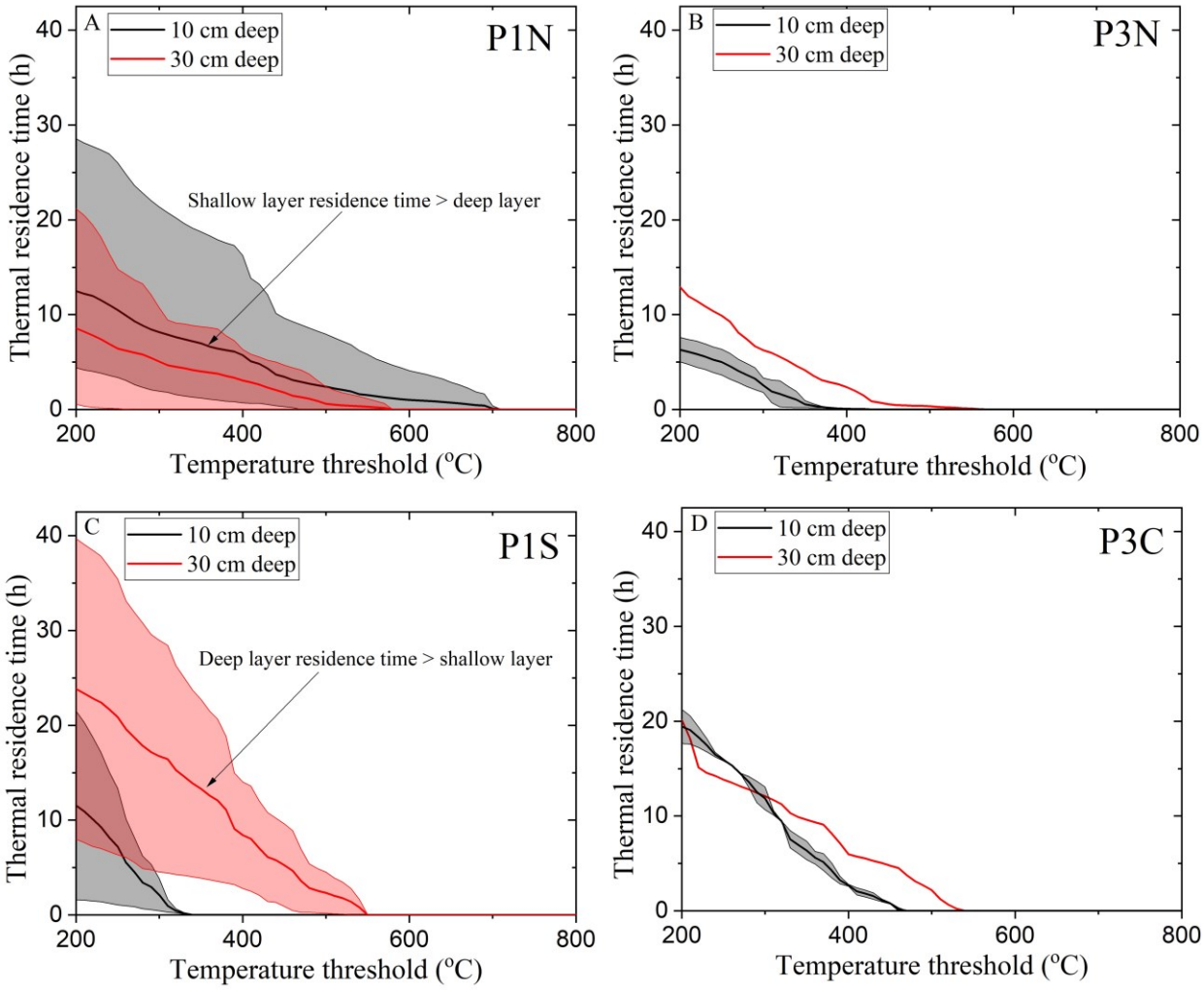

Figure 2.13. Smouldering thermal residence time for slash-and-burn in A) P1N and B) P3N, and charcoal ignited fires in C) P1S and D) P3C. Clouds represent minimum and maximum range of the residence time.

Smouldering due to charcoal ignition demonstrated stronger propagation at deep layer than at the shallow layer (Figure 2.13C). This might be due to the ignition method in which the burning charcoal was put in a 20 cm deep hole in P1S and a 40 cm deep hole in P3C, thus directly igniting the peat deep below the surface. The most severe smouldering was indicated to be in P1S where 200°C residence time was recorded to be as long as 40 h at maximum. This fire is also the longest self-sustained smouldering in this study (Figure 2.4). The surface smouldering propagation in this fire (Figure 2.13C) is also to be in the same order as those in P3N (Figure 2.13B) where weak slash-and-burn ignition was conducted. In contrast, the smouldering in P3C at shallow layer (Figure 2.13D) seems to be stronger that in P1S (Figure 2.13C), indicated by the higher residence time at higher temperature threshold. This might be due to the additional burning of gasoline aided the charcoal ignition.

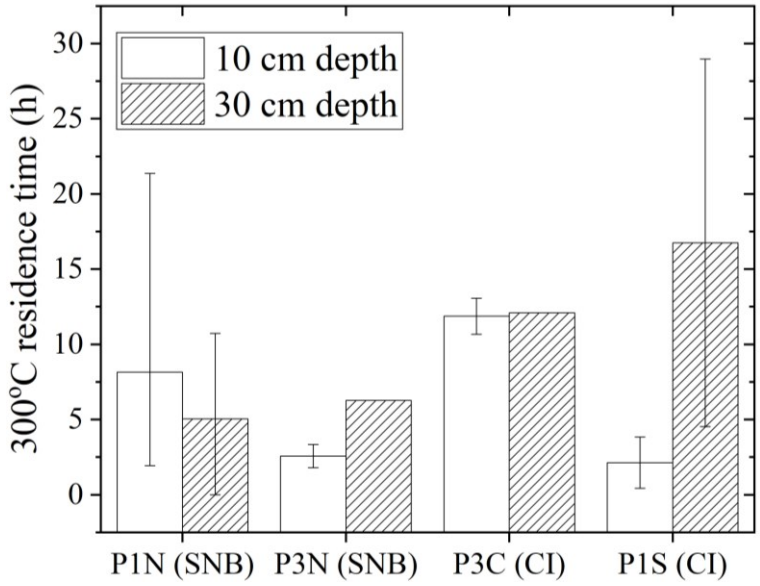

Figure 2.14. Smouldering residence time, at 300°C, for fires in in P1N, P3N, P1S, and P3C. SNB and CI stand for slash-and-burn and charcoal ignition. Residence time in P2N is not possible to analyze because no thermocouple points captured clear temperature growth, peak, and decay (Figure A 2.5); while fire in P2S was not self-sustained.

Figure 2.14 shows thermal residence time at 300°C temperature threshold indicating smouldering residence time. This figure shows that the most severe smouldering propagation occurred in P1S at deep layer due to in-depth ignition location of charcoal, resulting in average of ~17 h of smouldering at deep layer at 1 point of measurement. The most severe smouldering at shallow layer occurred in P1N, with average residence time of ~7 h and maximum of ~21 h at 1 measurement point. As surface vegetation was cleaned or ignition was conducted in-depth, smouldering at shallow layer was less severe (P3N and P1S). However, as the charcoal ignition was aided by burning gasoline, smouldering at shallow layer could be as strong as deep layer such as the case in P3C.

2.3.3. Infrared signature

Active fire area on the surface was calculated through infrared image analysis. The infrared image was converted to greyscale and the pixel location where the normalized intensity increases above an intensity threshold of 0.1 was marked (Figure 2.15). The area inside the marked perimeter line was then calculated to be the active fire area. The scaling from pixel to physical length was possible through the use of a steel plate with a known dimension (0.17×0.14 m^2). Intensity threshold of 0.1 was chosen to identify the first pixel location where the pixel intensity started to steeply increased [99].

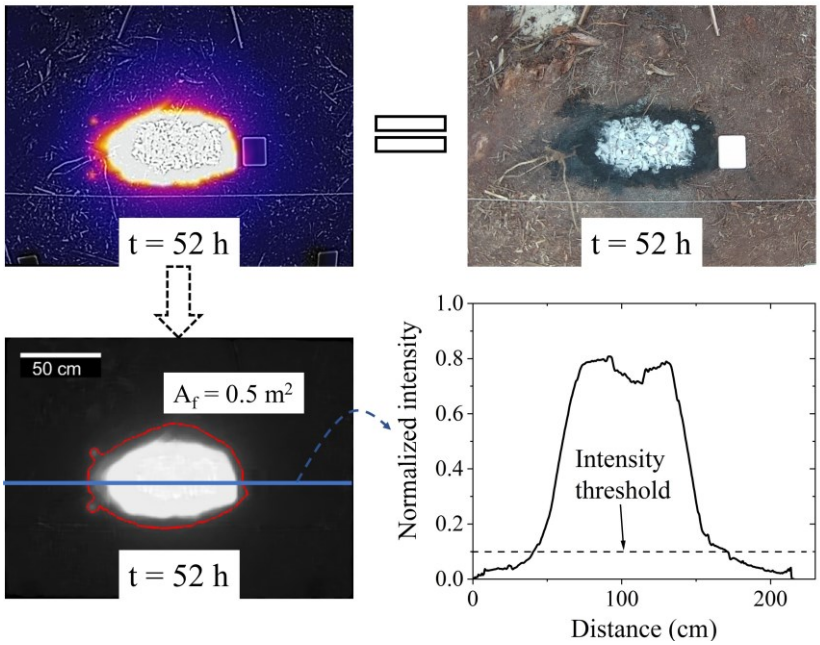

Figure 2.15. Infrared image analysis to measure smouldering area and perimeter. Normalized pixel intensity threshold is chosen to be 0.1 to represent the point at which the intensity started to steeply increase, indicating the outer perimeter of smouldering area.

Figure 2.16 shows the area changes on fires in P1S and P3C. In experiments ignited by slash-and-burn, i.e. P1N, P2N, and P3N, the active surface fire area changes are highly uncertain since the smouldering ignited on separate spot locations. Figure A 2.10 shows these spot locations and its propagation during the experiment.

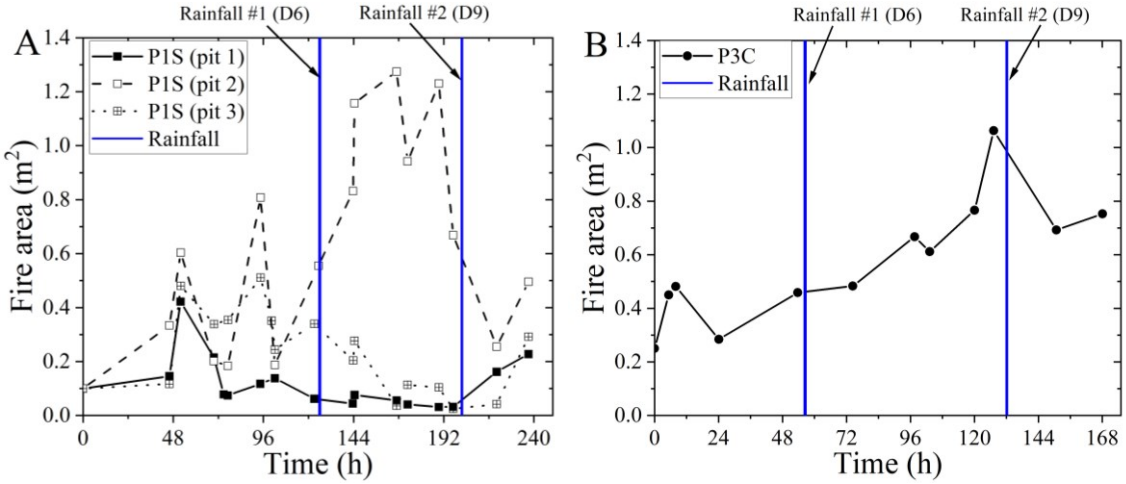

Figure 2.16. Smouldering area in P1S and P3C from infrared image analysis. Smouldering area in slash-and-burn fires resulted in patched smouldering spots as shown in Figure A10 for fires in P1N. The x-axis scale in time between P1S and P3C are different due to different time of ignition (Figure 2.4). Time at 0 h in each plots represent the time of ignition and the last data point represent infrared measurement before controlled suppression in D11 was conducted.

The active surface fire area in this study spread up to 1.4 m^2 area and with perimeter up to 9 m (see also Figure A 2.11). The steadiest increase of the area is demonstrated in P3C since the charcoal ignition in this fire was aided by burning gasoline resulting in strong smouldering at the shallow layer, as previously discussed. In P1S, the area of the three ignition pits were fluctuating. These fluctuations were due to overhang collapse or extinguished char layer on the top surface layer covering smouldering char in deeper layer [50,53]. These extinguished char layer and overhang collapse cause the shape of the surface smouldering front to radically change, seemingly indicating decrease of the active fire area while the deep layer was still burning. This can be seen in Figure 2.17 from t = 94.5 to 100.4 to 123.1 h when smouldering continuously propagated but the active surface fire area seems to be decreasing in some patches of the fire. In case of peat fire in a larger scale and with higher spread rate (~3 cm/h), the characteristic of spread on the surface can also be measured by means of metal poles grid, such as conducted by Usup et al [51] to measure spread rate of an actual peat fire event.

After the first rainfall occurred on D6 (Figure 2.4), active fire area and perimeter in P1S decrease, except the area in ignition pit 2 of P1S. Despite these decreases, smouldering was not extinguished and still progressing well indicated by the detectable fire area and perimeter in the following days after the first rainfall event (Figure 2.16A). The area and perimeter in pit 1 and 3 of P1S seemingly stayed at 0.05 to 0.1 m^2 and ~1 m (perimeter is in Figure A 2.11), respectively, which might be due to MC increase on the shallow layer. Ignition pit 2 of P1S and P3C, however, seems to be the least affected by the rainfall. In the case of ignition pit 2 of P1S, it might be because pit 2 was relatively the most intense smouldering, in term of spread rate, compared to pit 1 and 3 as can be seen by the fire area comparison prior to rainfall. Thus, the low rate and short duration of rainfall was unable to affect the smouldering in pit 2. In the case of P3C, it might also be due to the burning gasoline in the ignition stage.

The effect of rainfall on the extinction of smouldering at the shallow layer can be seen in Figure 2.17 showing drastic decrease of fire perimeter in pit 3 of P1S from t = 123.1 to 143.8 h. Further smouldering propagation can be seen from t = 143.8 to 197 h, showing that smouldering at the surface was weakly self-sustained. This, however, is not implying that the smouldering at deep layer was also weakly survived since a self-sustained smouldering at the shallow layer with higher MC after rainfall should be supported by a strong smouldering in deeper layer, as also shown by Figure 2.13C in which smouldering residence time at 30 cm depth in P1S was significantly longer than at 10 cm depth.

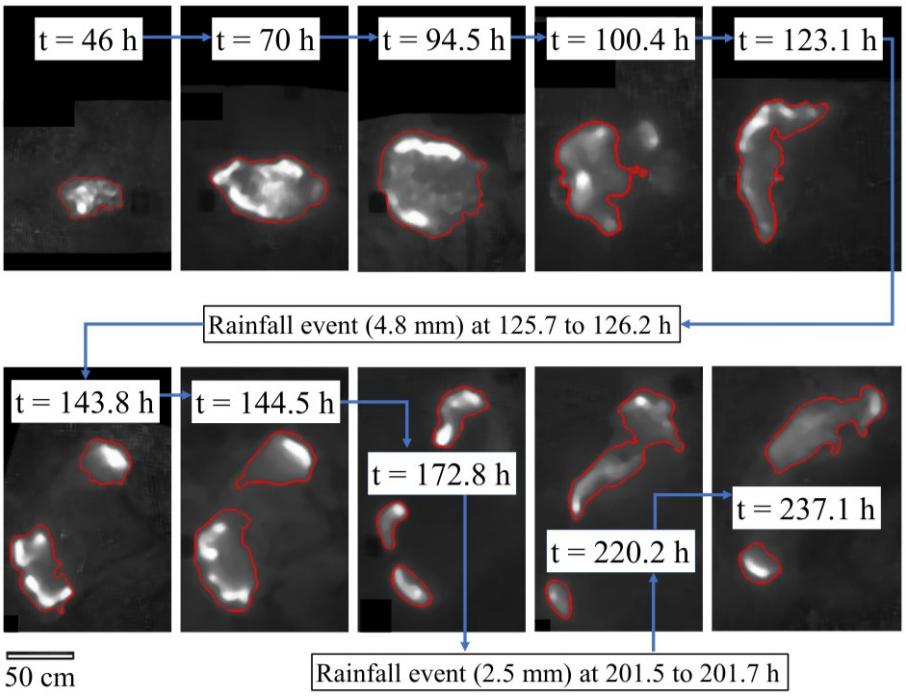

Figure 2.17. Smouldering spread propagation at the surface as can be detected by infrared camera on pit 3 of P1S from t = 46 to 237.1 h. Both rainfalls occurred at t = 125.7 h and t = 201.5 h, respectively. Controlled suppression attempt on this fire was conducted at t = 244 h.

The second rainfall occurred on D9 and with a higher rainfall intensity than the first (Figure 2.10A). This rainfall affected smouldering more than the first as can be seen by the decrease of fire area in P1S and P3C (Figure 2.16). Fire area and perimeter of pit 1 in P1S can be seen to be weakly increasing after this second rainfall. This increase, however, up to the range of fire area in pit 2 and pit 3, indicating that these three pits had the same intensity of deep layer smouldering. Thus, the two rainfall events occurred in this study, with rainfall depth (intensity) in the range of 2.5 mm (8.3 mm/h) to 4.8 mm (5.6 mm/h) for 17 to 50 min, are insufficient to suppress smouldering at deep layer but seem to have a more substantial effect on shallow smouldering spread.

2.3.4. Suppression

Suppression was conducted on D11 (Figure 2.4) with water spray and lance injection methods. Water spray suppression was conducted on P1N, P2N, P3N, and P3C, while lance injection method was conducted on the three ignition pits in P1S. Flow rate for water spray on P1N, P2N and P3N was 3,024 ± 18 L/h and on P3C was 4,878 ± 120 L/h, while for lance injection the flow rate was 1,669 L/h. The suppression was conducted by means of a fire hose and a fire pump. In case of lance injection suppression, the fire hose is connected to a lance injection device. The flow rate was measured by filling a container with known volume and noting the duration needed for the container to be fully filled at specified pump discharge pressure. Suppression was conducted for 1 h in P1N, P2N and P3N, and for 25 min

in pit 1 of P1S, 35 min in pit 2 of P1S, and 13 min in pit 3 of P1S. During suppression, a portable thermocouple was used to survey temperatures in the fire area, different to the fixed TC in Figure 2.11. After suppression, none of the surveyed points shown temperature above 50°C. The exact suppression duration was then estimated by the time since the suppression started to the point that temperature recorded by TCs in Figure 2.11 decreased below 50°C. Temperature of 50°C was chosen as a conservative threshold and has been detected to be low enough to avoid reignition [122,123].

Figure 2.18A shows that the successful suppression with water spray and injection agree with the critical suppression threshold obtained from a laboratory scale peat fire with reactor dimension of 20 × 20 cm and 10 cm depth reported in Chapter 3 of this thesis. The two rainfall events that were unsuccessful to suppress peat fires were below the critical threshold, indicating that the rainfall intensity and duration were too low and too short, respectively. The rainfall intensity of these rainfall was 5.6 and 8.3 mm/h, which is greater than the 4 mm/h indicated by Lin et al. [106] for successful suppression of smouldering peat fire in a reactor of 10 cm diameter and 15 cm depth. However, this minimum rainfall intensity needs to last for ~5 h, which much longer than rainfall events in this study and typical rainfall.

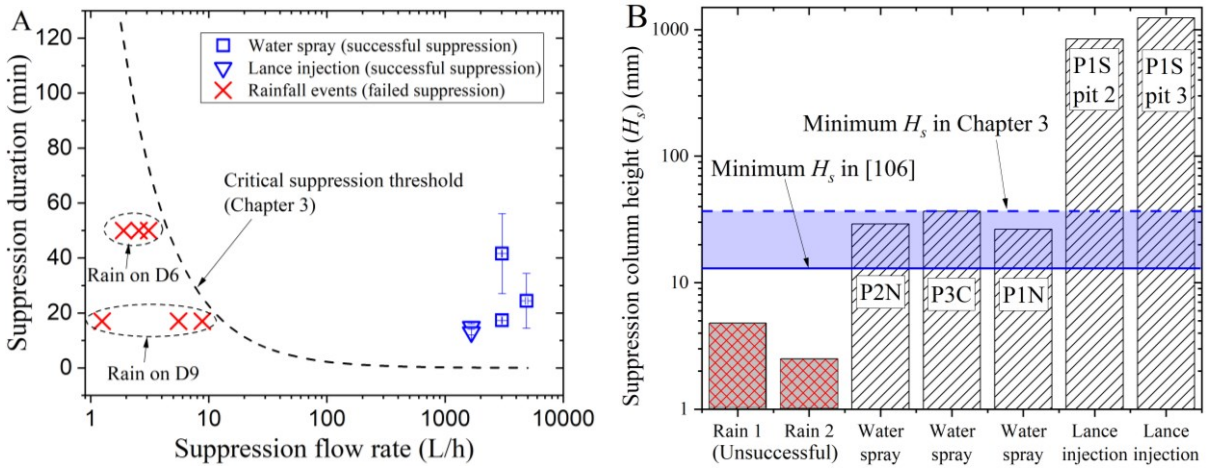

Figure 2.18. Suppression duration and column height in this study. (A) Suppression duration and flow rate of water spray, lance injection, and rainfall events in this study. The dashed line represents critical suppression threshold from lab-scale experiment of smouldering peat fire suppression reported in chapter 3 of this thesis. (B) Suppression column height across the two suppression attempts, i.e. water spray and lance injection, and rainfall events. Dashed and solid blue lines represents the minimum suppression column height in Chapter 3 of this thesis and in Lin et al. [106].

Beside suppression time, the efficacy of suppression can also be expressed by suppression column height. It represents the flux of the suppression over a fire area. Suppression column height is calculated with Eq. 2.2, where $\dot{V}_S$ is the

suppression flow rate (L/h), Δt_s is the suppression time (h), A_f is the fire area (m^2), and A_s is the coverage area of the suppression method (m^2). Values for these variables are shown in Table A 2.1. Since lance injection locally suppresses a smouldering hot spot, the suppression was conducted with an aid of an infrared camera to detect a local hot spot at which the lance was injected. As soon as the infrared camera did not detect any hot spot and portable thermocouple measurements shown no temperature more than 50°C, the suppression was stopped.

$$H_s = \frac{\dot{V}_s \Delta t_s}{\max(A_f, A_s)} \tag{2.2}$$

Figure 2.18B implies that successful suppression occurred at a certain threshold of suppression column height, below which the suppression is not successful. In this study, the minimum column height resulted in successful suppression is 26.5 ± 9.2 mm from water spray suppression in P1N. This value is in the range of the minimum column height reported in literature, 13 ± 1.9 mm in [106] (10 cm diameter and 15 cm depth peat fire) and 36 ± 5 mm in Chapter 3 of this thesis (20 × 20 cm and 10 cm depth peat fire). Far below this range is the column height due to rainfall events resulted in unsuccessful suppression, i.e. 4.8 and 2.5 mm. Suppression by lance injection method appears to be an inefficient method due to the high column height, indicating an excess use of water in order to obtain the suppression durations that are not far shorter than water spray. This low efficiency of lance injection has been implied previously in the suppression of smouldering coal by using pipe injection in [122] due to high run-off percentage. Considering the low efficiency of this method but the merit of attacking a local and in-depth hot spot, this method might be more suitable for mopping up residual in-depth and patched smouldering spots after a large peat fire to avoid fire regrowth, with an aid of infrared visual.

After controlled suppression methods were conducted on D11, a detailed survey of the plots was conducted on D12 to ensure that the smouldering in all fire areas were totally extinguished. This survey was conducted by digging the fire area to find any surviving char smouldering in-depth. The digging of the fire area was conducted up to the depth of the virgin peat layer. A small number of survived hot spots in deep layer was found and was covered by wet layers of ash and extinguished char. No gaseous emission and strong smouldering were found during this survey. After digging, the fire area was sprayed with water again to ensure no reignition will occur after the experiment was terminated. However, if the experiment was not terminated, the probability of that small number of hot spots to cause peat fires reignition is currently unknown. Thus, in the future, longer field experiment time is needed to confirm that the minimum suppression column height reported in Figure 2.18B resulted in no reignition probability.

2.4. Conclusion

In this chapter, GAMBUT, the largest to-date peat fire experiments in Sumatra, Indonesia, is reported. The field experiments were conducted on a degraded peatland in which the smouldering fire survived from 4 to 10 days despite the diurnal environmental condition variations and rainfall events with intensity of 5.6 mm/h for 50 min and 8.3 mm/h for 17 min. Even though the inorganic content in the peatland was high, i.e. 36.3 ± 11% to 66.7 ± 6.7%, indicating an already high degree of decomposition, the risk of a persistent self-sustain smouldering peat fire still exist. Smouldering propagation in this study was self-sustained despite initial MC of up to 200%. Horizontal spread rate was measured to be 0.6 to 0.8 cm/h at initial MC of 135.9 ± 40.6% and 27.2 ± 6.7%, respectively. This spread rate is in the lower range of values reported in the literature i.e. ~0.5 to 19.5 cm/h [56,120,121], that might be due to the level of the peatland degradation.

Smouldering was found to propagate stronger at shallow than deep layer when a strong slash-and-burn ignition was conducted, with temperature up to ~700^{o}C. Without surface vegetation, smouldering spread in an area not far from the initial location of slash-and-burn, at least over the duration of experiment in this study. Smouldering was stronger in deep than shallow layer in fire area where ignition was conducted by filling pit with burning charcoals, with temperature up to ~550^{o}C. Smouldering residence time in P1N following a strong slash-and-burn ignition was found to be 8.2 ± 7.8 h and 5.1 ± 5.07 h at 10 and 30 cm depth, respectively. At P1S, where the most severe smouldering was identified (due to charcoal ignition), the smoudering residence time was 2.1 ± 1.7 h at 10 cm depth and 16.8 ± 12.2 h at 30 cm depth.

After rainfalls, infrared image analysis shows that the burning area was reduced by these rainfall events, as the water locally extinguished the fire. Following the decrease, however, the area and perimeter of the fire at the surface sustained until the controlled suppression attempts were conducted. This indicates that rainfall events might suppress the smouldering at the shallow but not at deep layer, implying that a successful suppression can be identified by a certain amount of column height in order for the water to reach smouldering at deep layer. In this study, the minimum column height resulted in successful suppression is 26.5 ± 9.2 mm, which is far above the column height of the two rainfall events, i.e. 4.8 and 2.5 mm. Agreement of suppression column height between field-scale conducted here and laboratory-scale in the literature implies that suppression dynamics studied in the lab-scale are valuable to provide ideas for better mitigation strategies. Relatively well agreement of minimum suppression column height between field and lab-scale experiments despite the large difference of the flow rate, thousands vs. tens L/h, respectively, suggesting

that the minimum column height is weakly influenced by flow rate, though further detailed study might be needed for validation.

Results in this study represent quantified signatures of peat fires smouldering dynamics in the field in term of smouldering temperature, spread rate, thermal residence time, fire area and perimeter, and critical column height for successful suppression. These results can be used to develop effective detection and mitigation plans of peat fire response, and also raising new questions to be explored and understood at smaller scales such as smouldering propagation at various IC and MC due to slash-and-burn ignition, the effect of duration and depth of ignition on the self-sustain propagation of peat with high MC and IC, smouldering propagation in peat with variable IC in in-depth direction, the influence of fibrous fuel at the shallow layer on smouldering propagation and overhang formation, and different regimes of suppression column height that can result in failed, reignition, and successful suppression.

Chapter 3

Laboratory study on the suppression of smouldering peat wildfires: effects of flow rate and wetting agent

Summary[3]

The application of water, or a mix of suppressant and water, to combat wildfires is one of the most common firefighting methods but is rarely studied for smouldering fires which are among the largest worldwide. Suppression experiments presented in this chapter were conducted by spraying suppressant to the top of a burning peat sample inside a reactor with 20×20 cm^2 cross-section area and 10 cm depth. A plant-based wetting agent as a suppressant was mixed with water at three concentrations, 0% (pure water), 1% (low concentration), and 5% (high concentration), and delivered with varying flow (0.3 to 18 L/h). The results showed that suppression time decreased non-linearly with flow rate. The average suppression time for low-concentration solution was 39% lower than that with just water, while high-concentration solution reduced suppression time by 26%. The volume of fluid that contributes to the suppression of peat in these experiments is relatively constant at 5.7±2.1 L/kg-peat, despite the change in flow rate and suppressant concentration. This constant volume suggests that suppression time is the duration needed to flood the peat layer and that the suppressant acts thermally and not chemically. The minimum suppression column height identified in this study agrees well with previous field experiment, confirming that the column height due to rainfalls were not deep enough to reach deep layer of smouldering peat. The results provide a better understanding of the suppression mechanism of peat fires and can improve firefighting and mitigation strategies.

[3] This chapter is based on "Santoso MA, Cui W, Amin HMF, Christensen EG, Nugroho YSN, and Rein G. Laboratory study on the suppression of smouldering peat wildfires: effects of flow rate and wetting agent. International Journal of Wildland Fire. https://doi.org/10.1071/WF20117"

3.1. Introduction

In order to further systematically study peat fire suppression, lab-scale experiments on the effect of suppression flow rate and wetting agent concentration on the smouldering peat were conducted. Large-scale peatland fires are subject to suppression efforts but typically only stop when the rainy season arrives, i.e. haze episode in 1997 and 2015 [12,14]. This illustrates the persistency of smouldering and the difficulty in suppressing such fires [25,105,106]. In pristine conditions, peatlands are naturally protected from burning because of their high moisture content, which can be up to 300% of dry-base mass in flooded condition [10,24]. Due to climate change and human activities, peatlands are drying in many places which increases the susceptibility of peatlands to fire [10,12].

3.2. Suppression efforts during peat fires

Flaming wildfires spread fast [1,36], and pose a direct harm to lives and properties [124,125], thus are perceived to be more common in term of public and media attentions compared to smouldering wildfires. Hence, most firefighting techniques are developed for flaming wildfires. The same techniques are also employed to fight smouldering wildfires, incorrectly assuming that both fire types are similar. Techniques commonly used to suppress flaming wildfires include aerial attack by air tanker or helicopter, land attack by water with a hose either for flanking the flame front or mopping up residual smouldering fuel, removing vegetation for firebreaks, and backburn [126]. Land attack by water, aerial attack, and firebreak are commonly employed to fight smouldering peat fires as well. Different to flaming wildfires, firebreaks in smouldering fires can be done by removing the peat layer (not only the surface vegetation) by digging a ditch along the fire perimeter [2,11], or by reflooding the fire area by diverting water from nearest sources [127,128]. However, unique techniques have also been developed specifically to fight peatland fires. These techniques include soil compaction to reduce oxygen ingress underground [24] and water injection to directly attack the fire [122]. Another novel method developed to fight smouldering is by burying a cooling pipe [129]. Figure 3.1 illustrates several methods employed in the suppression of peatland fires, where a natural occurrence, i.e. heavy rain, is also included since it has been recorded to successfully suppress large peat fire [12,14]. The investigation of the suppression of smouldering peat fire due to rainfall has been investigated by Lin et al. [106]. They conducted laboratory scale experiments and varying the rainfall intensity, indicating that rainfall intensity of 4 mm/h for at least 5 h is needed to successfully extinguish peat fire. Another prospective method is by artificially inducing rain fall by seeding clouds with aerosol of dry ice, calcium chloride, calcium oxide, and kitchen salt, or by sending salt flares into the clouds [130]. These techniques increase the water density and make water particle in clouds to freeze. Recently, this technique has been adopted to fight peatland

wildfires in Indonesia [131]. This method might help in reducing hotspots and improving the air quality in the affected areas.

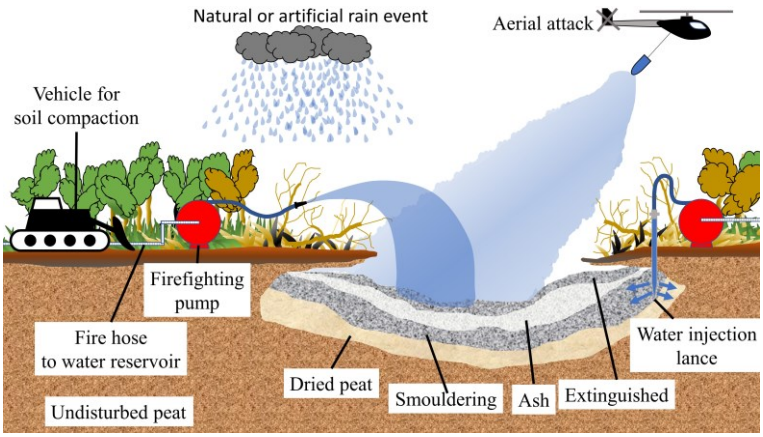

Figure 3.1. Direct firefighting methods during peatland fires, including cooling and smothering. Cooling methods shown in this illustration are ground spray, aerial attack, and injection lance. Smothering method shown here is through soil compaction to remove the natural oxygen pipe network in the peatland soil. In addition, rain event, both naturally or artificially, is also illustrated.

Due to the subsurface nature of smouldering fires, it is much harder to detect and to access the underground hotspots. As a result, an intuitive suppression approach might prove effective by directly channelling water into the subsurface hotspot with a water injection lance (Figure 3.1). This method allows a targeted attack of smouldering hot spots. The efficiency of this method has been investigated in the lab for smouldering coal fires [122] and in smouldering peat field experiments (Chapter 2), showing lower efficiency (more water required) than spray methods.

Reflooding the peatlands by temporally diverting water stream or the municipal supply is generally effective by increasing the moisture content (MC) of the peat above the critical MC of smouldering [48,49], thus preventing further spread. Even though flooding requires large volumes of water, up to billions L of water, it has been shown to effectively suppress peat fires. Two examples are during the 2008 Evans Road Fire in North Carolina, USA, and the 2018 Lake Cobrico Peat Fire in Victoria, Australia. In the 2008 Evans Road Fire, up to ~7.5 billion L of water were pumped from nearby lakes to reflood the peatland [132–134]. This fire was declared to be extinguished 7 months after the fire started by a lightning strike [135]. In the 2018 Lake Cobrico peat fire, 4 km pipeline connected to the nearest municipal water connection was laid supplying ~65 million L of water enabling the flooding of the fire perimeter [128]. This fire was extinguished after 2 months [127].

Beside firebreak by flooding the fire perimeter, fire breaks by fuel removal can also be considered in controlling peatland fire spread. However, this effort might not be effective if the peatland water table is very low [51,136] since the

peat layer can be very deep and the trench would need to be more than 5 m deep [9], causing this effort to be a tedious task.

The deep subsurface spread of peatland fires is possible and is fed by oxygen diffusion deep below the ground due to porosity of peat [1]. Removal of the oxygen supply by compacting the soil has been suggested as an effective firefighting method, according to the investigation conducted during the 2009 smouldering peat fire in Las Tablas de Daimiel National Park, Spain [24]. However, this method requires heavy machinery and the access of such vehicles might be unavailable to peatlands due to their geographic location. In summary, compared to soil compaction and fuel removal, cooling methods are the most feasible to suppress peatland fires, including water spray, aerial attack, perimeter area reflooding, and injection method, but the question is how much water is required for a successful suppression.

3.3. Suppressant agents to fight wildfires

The suppression efficiency varies with the suppressant agents. The most utilized suppressants are water, firefighting foam, or mix of water and other suppressant. Sand can also be considered as a suppressant because it is inert and highly dense but is more difficult to transport. In field conditions, the suppressant agent can be applied through the use of handheld firefighting equipment, firetruck, or aerial fleets [126]. In utilizing firefighting agents, environmental safety is an important criterion. The development of environmentally friendly firefighting foams and agents and their effectiveness on both building and wildland fires have been investigated by several authors [137–142].

Foam suppression acts by smothering the smouldering by covering the surface of the fuel with the foam layer that prevents oxygen from accessing to the fuel. In addition to the smothering effect, foam layer is also cooling the surface of the fuel due to the water content of the foam solution. Ratnasari et al. [143] and Subekti et al. [142] investigated the suppression time of peat fires by using class A fluorine-based foam and palm oil fatty acid-based foaming agent (FAP) foam, respectively. Suppression time decreases with foam layer height while FAP foam performed poorer than fluorine-based foam. In another report, Rivai et al. [141] reported suppression times by applying various foam formulations derived from palm oil fat on 10 cm deep smouldering peat. Foam stability can be an issue because the foam will quickly disappear during the suppression effort. Since foam suppression relies on depriving smouldering of oxygen, once the foam disappears, it is no longer effective. This implies another difficult aspect of suppressing peat fires with foam since the required smothering holding time for smouldering can be days, weeks, or months. This is in contrast to flaming wildfires which might need hours [1] and flaming liquid fires which might only need minutes [140].

The use of fluorine-based foam to suppress wildfires is currently controversial due to the environmental issues of per and poly-fluoroalkyl substances (PFAS) which are the main component of current commercial aqueous film forming foam (AFFF) [144–147]. There is also an indication that a long-chain PFAS, such as Perfluorooctanoic acid (PFOA), can increase hydrophobicity [148] which by itself is a problem after peat fires [149]. If peat becomes hydrophobic after suppression with fluorine-based foam, the restoration effort by rewetting might become ineffective, leaving the peatland vulnerable again to fires in the next drought. Due to the environmental issue of fluorine, alternative fluorine-free surfactants have been developed, including hydrocarbon-based foam [140], FAP foam [142], and fluorine-free wetting agent [139].

Smouldering peat fire suppression by means of water has been investigated by Ramadhan et al. [105] in 10 cm deep peat and Lin et al. [106] in 15 cm deep peat. Ramadhan et al. [105] reported a suppression time of ~65 min with ~12 L/h of water spray, while Lin et al. [106] investigated water spray suppression at variable flow rate in term of rainfall rate (mm/h). The critical rainfall rate required to suppress peat fires reported by Lin et al. [106] is 4 mm/h for at least 5 h.

Wetting agents are substances that can reduce the surface tension of solid particles in a solid-liquid type suspension [150]. Contrary to foam that stays on the surface of the fuel, wetting agent can penetrate deep into the fuel. Due to their lower liquid surface tension, wetting agent solutions penetrate better into the soil than water, up to 68 times faster than water through forest ground surface fuel [139]. Peat fires can propagate in the shallow and deep layer of peat, leading to the subsurface spread. Thus, surfactant ability to access shallow layer and quickly reach deeper peat layer is an important property for suppression efficiency. While the effectiveness of foam on peat fire suppression have been investigated before, but no study has been conducted on the effectiveness of wetting agents on peat fires. In this study, we aim to fill this gap by performing laboratory scale experiments of peat fire suppression with both variable flow rate and environmental-friendly (fluorine-free) wetting agents.

3.4. Experimental method

In this study, sample preparation protocol followed that in [95,104]. A commercially available peat was used (Shamrock Irish Moss Peat, Bord na Mona Horticulture Ltd.) due to its homogeneous properties and batch consistency in the long term. The elemental content of the peat in dry-mass-basis was C/H/N/S of 54.1/5.1/1.3/0.5%, with an inorganic content (IC) of 2.5 ± 0.6% [99]. In this experiment, MC of peat is around 100% (mass of water content over mass of dried peat). This MC is below the critical value for ignition of boreal peat when IC < 10% [48,49] and would represent drought peatlands [51]. Samples were prepared by oven drying peat at 80^{o}C before adding water. The sample was mixed to ensure

homogenization and stored inside a sealed container for 24 h. Prior to the start of experiment, the sample was mixed well again. A subsample of 100 g was put inside an oven at 90°C for 7 h to measure the final MC [95]. The MC obtained in these experiments is 103 ± 6.8% which corresponds to 204.4 ± 8.90 kg/m^3 of wet bulk density. A total of 19 kg of dry peat were used in all 49 experiments in this study.

An open-top reactor with internal dimensions of 20 × 20 × 10 cm was used [53] where conditioned peat was deposited up to the rim. The reactor was built using ceramic insulation boards (k = 0.7 w/m-K, ρ = 310 kg/m^3, c_p = 1090 J/kg-K). The ignition protocol consisted of supplying 100 W for 30 min through an 18 cm coil heater mounted on one side of the reactor, which was 5 cm below the free surface. This ignition protocol is strong enough to initiate self-sustained smouldering in peat with MC < 160% and IC < 10% [104]. Figure 3.2a shows the schematic of the experimental setup. Measurements included in this experiment are mass loss (Mettler Toledo balance, resolution 0.01 g), visual and infrared (IR) imaging of the surface spread (GoPro and FLIR camera) and temperature-time histories using thermocouples (twelve K-type thermocouples (TCs) array, 3 rows × 4 columns [Figure 3.2b]). To avoid fluid built-up inside the reactor and to imitate suppression on deeper soils, holes were made at the bottom face of the reactor to allow fluid flow into a basin connected to a container (Figure 3.2a). At the end of each experiment, the volume of fluid in this container was measured and denoted as run-off volume (V_o). The basin also prevented the access of air into the peat sample through the holes at the bottom face of the reactor, thus the smouldering depth was similar to the case without holes [53].

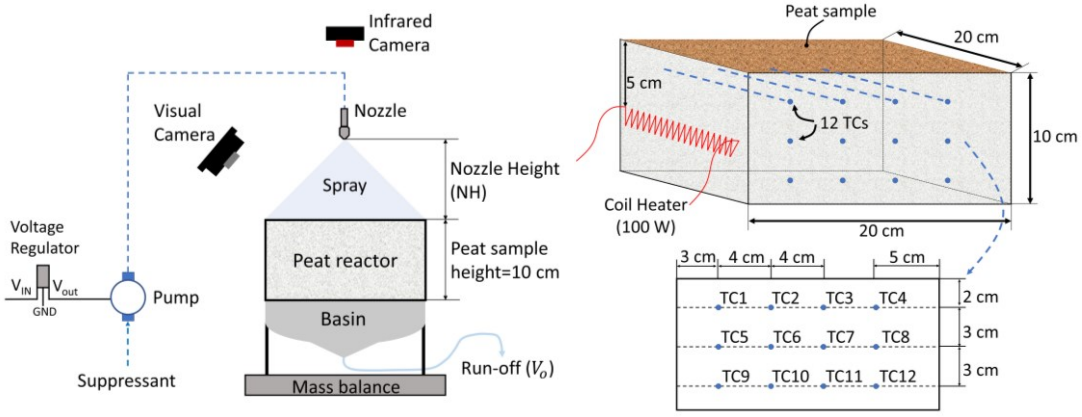

(a) (b)

Figure 3.2. (a) Schematic of the suppression experimental setup showing the diagnostics using infrared and visual camera, mass balance, and measurement of run-off volume; and the voltage regulation of the diaphragm pump to adjust suppression flow rate, along with nozzle height. (b) Schematic of the reactor showing ignitor coil and thermocouple placement. Thermocouples are placed at the centre plane of the reactor. Smouldering spreads from left to right. Dimensions are internal and do not include the thickness of the insulation board.

An infrared camera was used to determine the timing for initiation of suppression. This was when the smouldering front arrived at the centre of the reactor such that the front was directly below the spray nozzle. Since infrared image only represents surface smouldering, the addition of mass loss measurements provides comprehensive monitoring to ensure the initiation of suppression was consistent across all experiments. Figure 3.3 shows that the average mass fraction at the initiation of suppression, i.e. to the arrival of smouldering front to the centre of the reactor, is 59.6 ± 1.66%. This is equivalent to peat mass loss of 40.4%. Average time at the start of suppression (t_{sp}) is 303.6 ± 49.3 min, across all 49 set of conducted experiments. At the time that these two criteria are met, i.e. front below the nozzle and 40% mass loss, resulting temperature of TC9 and TC10 were 400 to 550°C. This will be discussed further in Chapter 3.5. Smouldering was considered extinguished when all temperatures decreased below 50°C. This temperature criterion to identify extinguishment is a conservative value and has been used before in studies on smouldering coal [122]. Once this was achieved suppression was terminated and the suppression time was recorded.

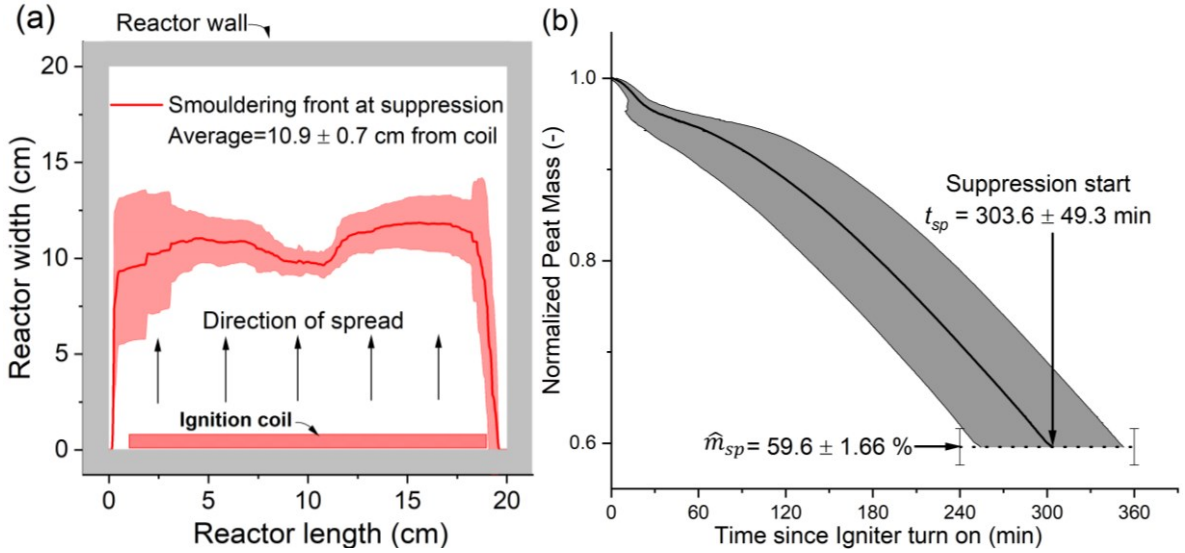

Figure 3.3. (a) Top view of smouldering front location at the initiation of suppression. Red line indicates average front location at the start of suppression from IR footage, i.e. 10.9 cm, with standard deviation indicated by shade, i.e. ± 0.7 cm. (b) Average peat mass (normalized to initial value) (line) and standard deviation (shade).

Three different suppressant mixtures were studied: 0% (only water), 1% (low concentration [LC]), and 5% (high concentration [HC]) concentration of fluorine-free wetting agent by weight in water. The wetting agent is ColdFire, produced by FireFreeze Worldwide, Inc. (N.J., US). This wetting agent is a proprietary environmentally friendly formulation consisting of biodegradable anionic and nonionic surfactants, organic compounds and minerals that have been tested to be free of Perfluoroalkyl and polyfluoroalkyl substances (PFAS) [151]. This wetting

agent has liquid-to-air surface tension of 29.7±2.36 mN/m [139], ~2.5 times lower than water which has liquid-to-air surface tension of 72.02 mN/m [152]. Complete physicochemical properties of the wetting agent can be found in Rakowska et al. [139]. Due to the lower surface tension, the water that mixed with a surfactant has a better ability to wet or smeared over a surface, rather than stayed in a spherical shape of a water particle.

Suppression flow rates ($\dot{V}_s$) were varied by adjusting both the height of the nozzle and the voltage supply to the pump (Figure 3.4). Parameters controlling the flow rate were measured using an empty reactor on a mass balance. The flow rate was the rate of mass gained by the empty reactor. The flow rate decreased both with nozzle height and voltage supply (Figure 3.4a). The increase of voltage supply increased pump pressure which increased both volumetric flow rate and spray angle. Despite the increase in the volumetric flow rate, the increase in spray angle decreased the amount of water entering the reactor because the spray was wider than the reactor top area. The nozzle height and pump voltage were set prior to each experiment to obtain the desirable flow rate based on the result shown in Figure 3.4a. Suppression flow rate values were confirmed by data analysis averaging mass gain rate into the reactor, from the start of the suppression to ~50 to 60% of the suppression time. Figure 3.4b shows an example of mass gain rate from the start of suppression over the next 29 min, which is ~60% of the suppression time, in which the average of this mass gain rate corresponds to a suppression flow rate of 3.96±0.47 L/h. Because the mass loss from smouldering was negligibly small compared with the mass gain from suppression (~2 orders smaller than mass gain) and the decreasing burning rate due to smouldering being suppressed, mass loss from smouldering at this stage of suppression can be neglected. The rate of suppressant evaporation can also be assumed to be negligibly small, of the same order of sample mass loss due to smouldering. Table 3.1 shows the summary of variables investigated in this study.

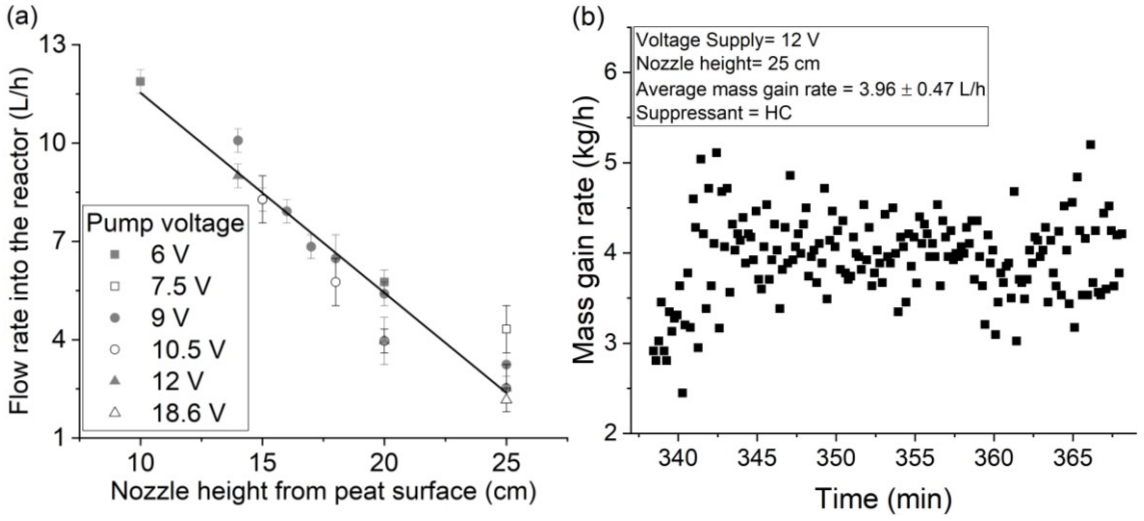

Figure 3.4. Suppression flow rate resulting from changes to nozzle height and pump voltage (a) Measurement of flow rate vs nozzle height and voltage supply (b) Example of mass gain rate during suppression to confirm flow rate values. This shows that the average suppression flow rate is 3.96 ± 0.47 L/h, since the density of the wetting agent ≈ ρ_w = 1 kg/L [139].

Table 3.1. Experiment variables investigated in this study. The flow rate range is obtained by setting the pump voltage and nozzle height as shown in Figure 3.4a to target a desired flow rate and then clarified by averaging the mass gain rate during the early stage of suppression (Figure 3.4b).

Wetting agent concentration (% by weight)	Flow rate range (L/h)	MC (% in dry basis)	Wet bulk density (kg/m^3)	Number of experiments
0	3.6 to 16.6	103 ± 6.8	204.4 ± 8.90	21
1	0.3 to 16.6			17
5	1.2 to 7.7			11

3.5. Results and discussions

3.5.1. Results on smouldering spread

3.5.1.1. Temperature profiles

Before suppression was initiated, horizontal spread was faster at 8 cm below surface, leaving a layer of peat on top, as evidenced by the low temperatures measured by the top thermocouples in Figure 3.5. This unburnt surface layer stayed intact for some time, forming an overhang, which collapsed later on. This was observed previously by Huang et al. [53].

Figure 3.5 shows temperature profiles without suppression as a baseline behaviour for comparison (red lines) and average temperature profiles from 21 experiments of water suppression (black lines) in which flow rate was varied between 3.6 to 16.6 L/h. The ignition procedure is evidenced by the sharp increase in temperature measured by TC5 and TC9, followed by also a sharp decrease when ignition procedure was stopped. Smouldering started at 5 cm depth from the top surface. From this point, i.e. TC5, smouldering then spread at a depth of ~8 cm, indicated by trend of temperature increase from TC5 → TC9 → TC10 → TC11 → TC12 (red lines in Figure 3.5).

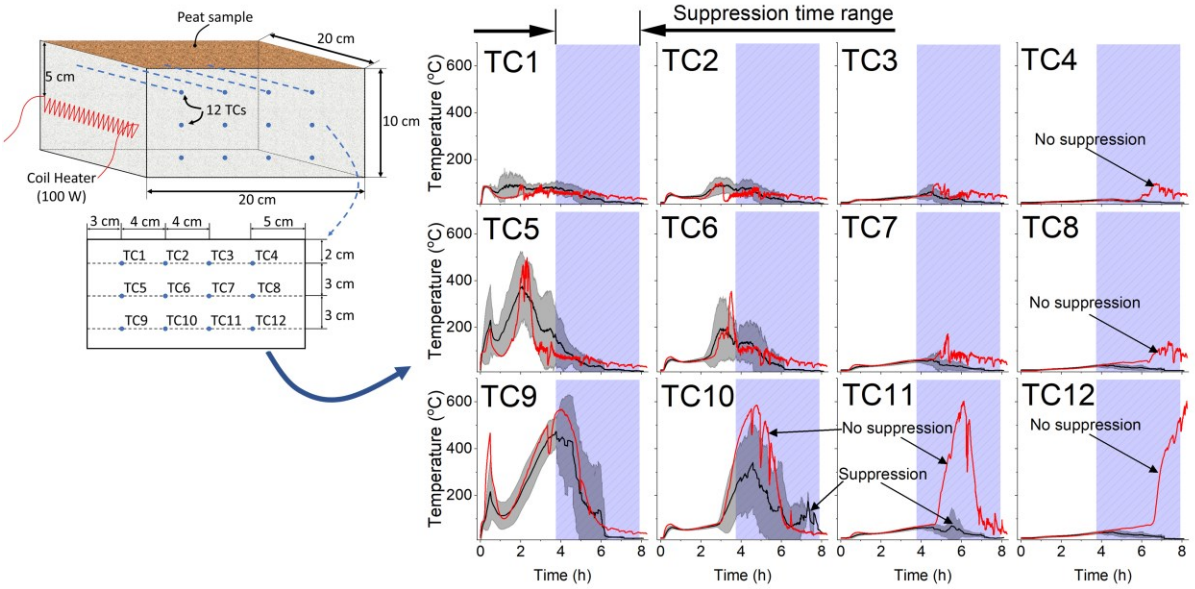

Figure 3.5. Temperature profiles in experiments with and without water suppression. Red line is temperature in experiment without suppression; black lines are the average temperature profiles from 21 experiments of water suppression (without wetting agent) in which flow rate was varied between 3.6 to 16.6 L/h; gray shade is data range for temperature in experiments with suppression; blue shade is the time range from start to finish of suppression.

In experiment with water suppression (black lines in Figure 3.5), only TC9 and TC10 were measuring temperatures above 400°C when suppression started (the left side of rectangular blue shade in Figure 3.5). Thus, at the start of suppression, the smouldering front was around TC9 and TC10 (up to 7 cm away from the ignition wall). Figure 3.5 also shows that smouldering propagation at this time was also well beyond into the steady state which can also be seen in mass data in Figure 3.3b. A small bump of temperature increase at TC11 in experiments with suppression indicates that leading edge of drying front was probably located between TC10 and TC11, ~9 cm away from ignition wall. As can be seen in Figure 3.5, smouldering spread beyond TC10 was successfully prevented after water suppression across all 21 experiments.

The dynamics of smouldering fires can be studied by the temperatures reached and the thermal residence time [11,63,87]. Thermal residence time is the amount of time that a point in the sample is above a certain temperature threshold, e.g. 60 min of thermal residence time for 100°C means that a point in the sample was at 100°C or above for 60 min [11]. Figure 3.6 shows thermal residence time of TC10. It shows that suppression decreases thermal residence time across the temperature range from 100 to 650°C, compared to no suppression. It can be seen that compared to the effect of suppressant concentration, flow rate has stronger effect on decreasing residence time. By increasing flow rate from 0.6 to 7.6 L/h, thermal residence time decreases by ~1 h, at 100 to 550°C (Figure 3.6a). Considering the effect of the suppressant concentration, it can be seen that the LC

affects thermal residence time about the same as water and further decreases residence time by 0.5 h only at temperature above 300°C (Figure 3.6b). HC has a stronger effect than LC in which the residence time decreases by ~0.5 h across all temperature, in comparison to water. In Figure 3.6a, the standard deviations of LC thermal residence time are 0.6 h at low flow rate, 0.2 h at intermediate flow rate, and 0.12 h at high flow rate; while in Figure 3.6b, the standard deviations of thermal residence time are 0.35 h for water, 0.2 h for LC, and 0.03 h for HC.

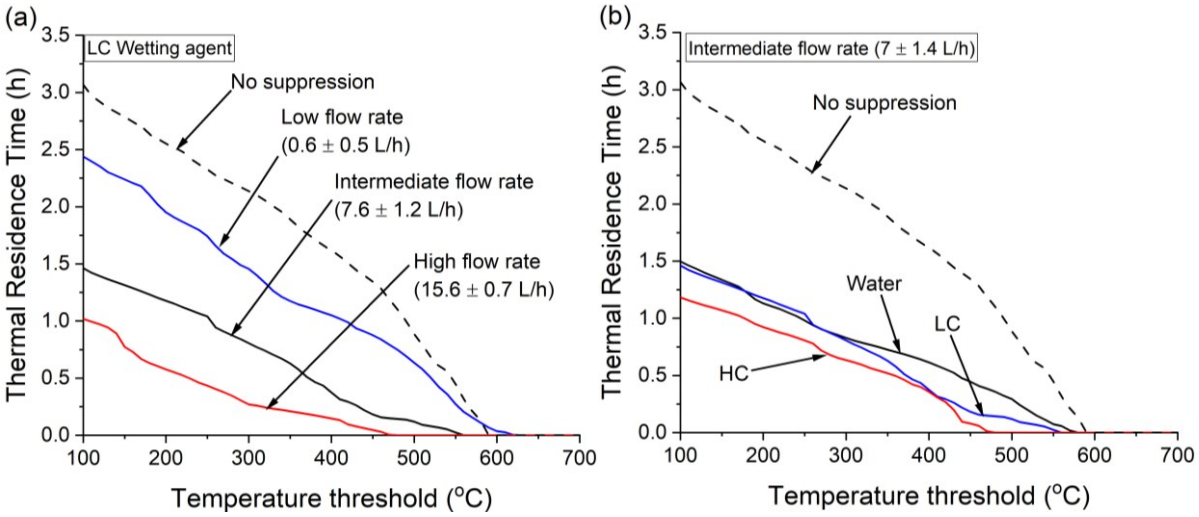

Figure 3.6. Average thermal residence time vs temperature threshold with (a) LC suppressant at increasing flow rates, and (b) intermediate flow rate at increasing suppressant concentrations. The thermal residence time is time from the start of ignition until termination.

3.5.1.2. Persistent smouldering

Figure 3.7 shows a side-view schematic of the smouldering propagation in this study based on temperature in Figure 3.5 and visual observation of the experiments (Figure A 3.1) and illustrating the location of TC10 close to smouldering leading edge at the initiation of suppression. In [105], temperature threshold of 80°C anywhere in the sample was the suppression criteria. However, 14 experiments out of 49 show the occurrences of persistent smouldering, represented by a temperature increase and continuation of spread during suppression. During this persistent smouldering, the temperature at TC10 was seen to increase up to ~220°C (approximately peat smouldering temperature [97]) and this increase occurred after this temperature had decreased to as low as ~66°C (Figure 3.8a). In other cases, smouldering continuously spread despite ongoing suppression as indicated by a temperature increase at TC11 (Figure 3.8b). Both cases show a potential of reignition if suppression was stopped at a temperature above 50°C. In another study, Lin et al. [106] reported a reignition of peat at temperature of ~60°C. Temperature of 50°C is chosen as a conservative threshold for successful extinction since no reignition was observed when 50°C was the

criteria. Successful suppression can also be identified by surface infrared radiation; however, IR was unable to detect the occurrence of persistent smouldering (Figure A 3.2 and Figure A 3.3 in Appendices).

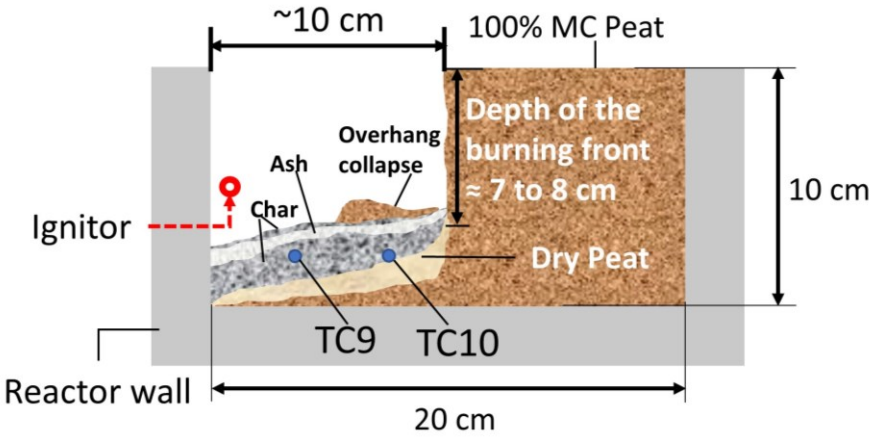

Figure 3.7. The side-view schematic of the smouldering front at the start of suppression. TC9 and TC10 roughly indicate the trailing and leading edges of char oxidation front.

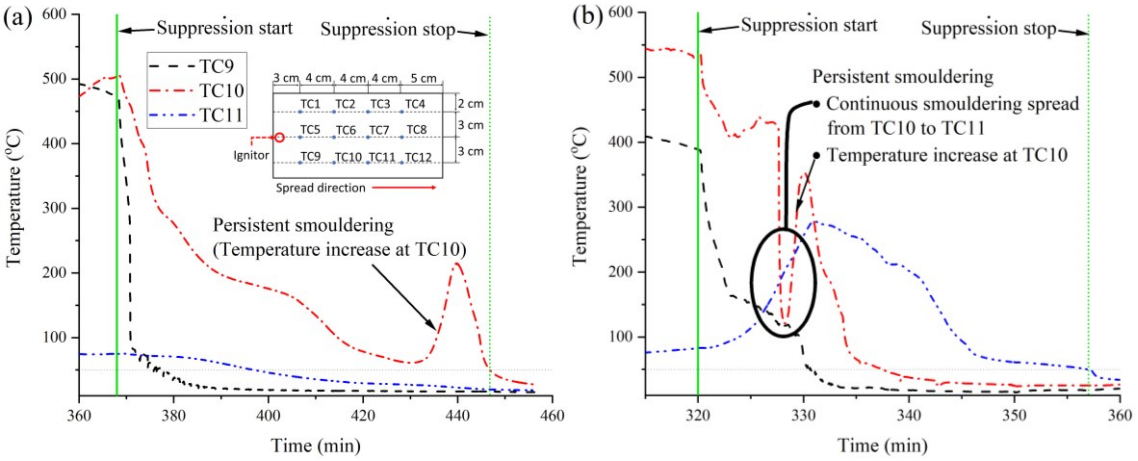

Figure 3.8. Examples of persistent smouldering during suppression indicated by temperature profiles at deep layer, i.e. TC9, TC10, and TC11. (a) Water at 4.3 L/h flow rate, suppression time is 78.8 min. (b) Water at 7.2 L/h flow rate, suppression time is 36 min.

Temperature anomalies in Figure 3.8a can also be caused by thermocouple tip being enveloped by the solution for a while, thus causing a temperature decrease, followed by a temperature increase once the enveloping solution has dried. Another possible cause for the increase in temperature is the collapse of an overhang that burned near a thermocouple (Figure 3.7), causing a perturbation in the temperature curve, which is thus not as smooth as if there was no collapse. Figure 3.9 shows the summary of the occurrences of persistent smouldering (temperature increase at TC10 and continuation of spread to TC11) during the ongoing suppression, showing a clear indication that these occurrences are less frequent with increasing flow rate and wetting agent concentration, with flow rate

having the greater effect. Uncertainty can be caused by the TC being enveloped by the solution and overhang collapse.

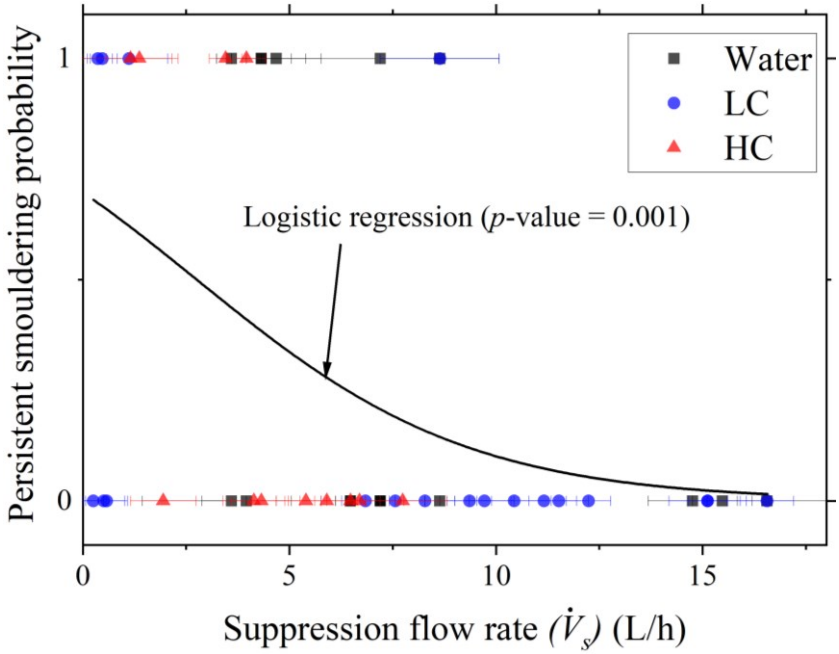

Figure 3.9. Occurrences of persistent smouldering. A value of 1 on the y axis indicates that persistent smouldering was observed in the experiments conducted at a particular flow rate, while 0 means that persistent smouldering was not observed.

3.5.2. Results on suppression dynamics

3.5.2.1. Suppression time

As seen in Figure 3.10, suppression time decreased with flow rate for all suppressant concentrations. The best fit lines in Figure 3.10 can be assumed to be a critical suppression limit for suppression flow rate and time, below which suppression is unsuccessful. In the range from 5 to 9 L/h, the average suppression time with LC was 39% lower than water, while with HC the suppression time was 26% lower than water. Even though LC on average was faster than HC, the standard deviation of LC times was ~20 min, significantly greater than the 6 min standard deviation for HC. This means HC is statistically more reliable in reducing suppression time than LC. For example, the data shows that a suppression time of around 70 min can be achieved by HC with a flow rate of 1.5 L/h or a flow of 4.1 L/h with water. In high flow rates (9 to 18 L/h), LC suppressant and water resulted in similar suppression times (< 40 min). However, to achieve ~60 min suppression time, HC suppressant required lower flow rate compared to water, resulting in 63% lower pump power (pump power is proportional to flow rate [153]) which is a crucial consideration for the field conditions where remote locations make power supply challenging. The range and trend of suppression time reported here agrees with previous studies for water [105,106], while the study here includes wetting agents. Longer suppression time in [105] can be due to the much lower MC in their samples, i.e. 15%. With Netherlands peat samples at 50%

MC, Lin et al. [96] reported that 0.16 L/h water spray was the minimum flow rate for successful suppression, thus in agreement with the study here, even if there is 50% difference in the MC between [96] and this study.

3.5.2.2. Suppression column height and run-off

Figure 3.11a shows the amount of run-off measured for the three fluids (water, LC, and HC). Run-off ratio is between the run-off (V_o) volume and the total suppressant volume (V_t). Run-off can be caused by uniform penetration of the suppressant or by channel formation. Uniform penetration is aided by the low surface tension enabling the suppressant to seep through the pores between soil particles. In this study, the wetting agent surface tension is ~2.5 times smaller than water surface tension, i.e. 29.7±2.36 mN/m for the wetting agent [139] and 72.02 mN/m [152] for water. Higher run-off due to uniform penetration can aid suppression of deeper hotspots. In the event run-off is due to channel formation, most of the suppressant flows through the same path, causing poor heat transfer and less contact surface between the suppressant and the particle [122], thus decreasing suppression performance. The channels are formed when the surface tension is high and the suppressant finds more resistance to seep through the pores.

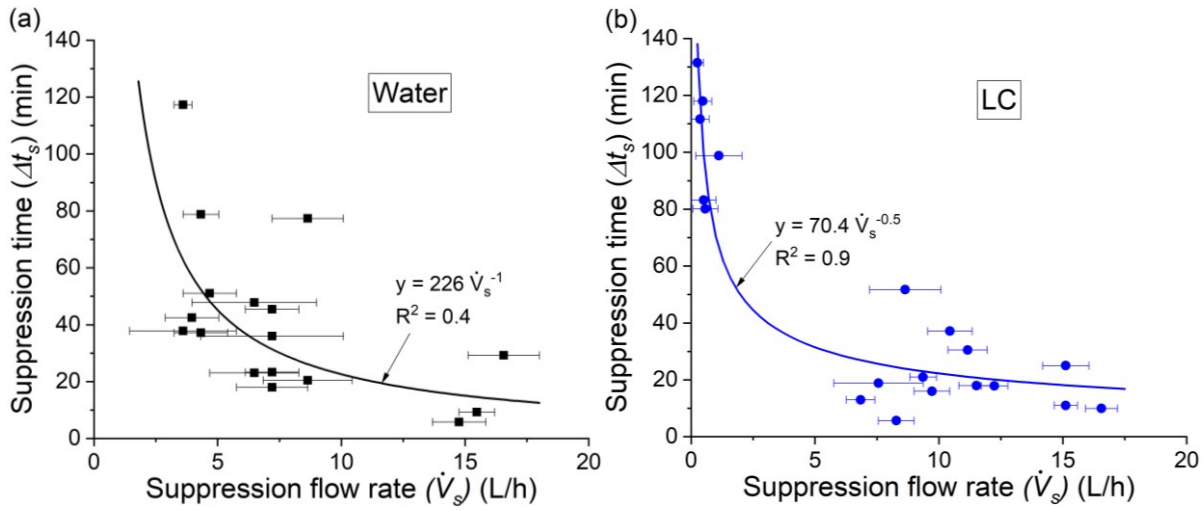

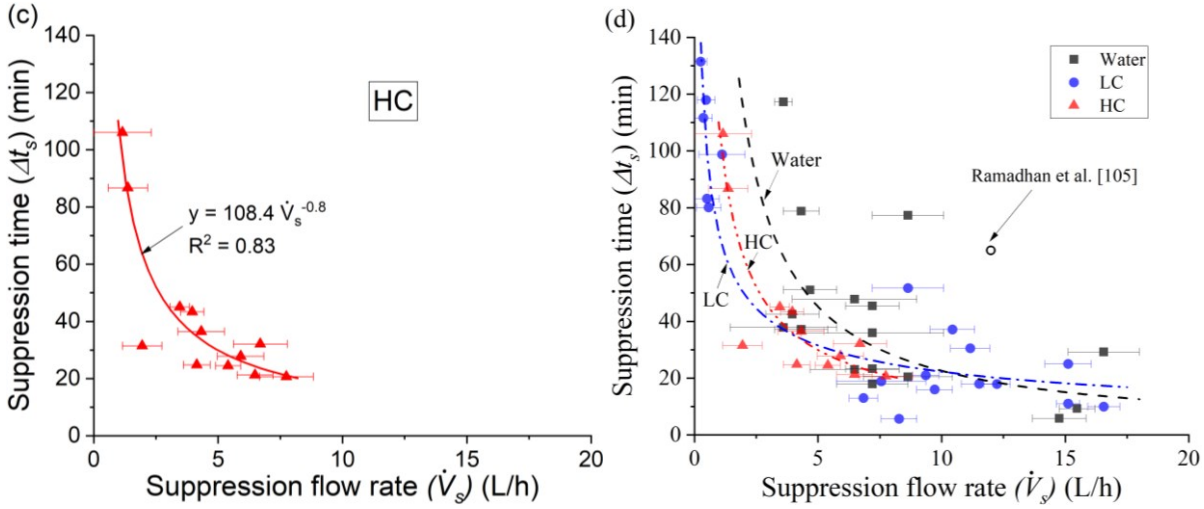

Figure 3.10. Suppression time vs suppression flow rate. The best fit lines represent a critical suppression limit for flow rate and suppression time, below which suppression is not successful. (a) Water suppression (b) LC suppression (c) HC suppression (d) all suppressants, and with comparison to data point of suppression time from Ramadhan et al. [105]. Standard deviation for suppression time is too small to be included in the graph (±10 s).

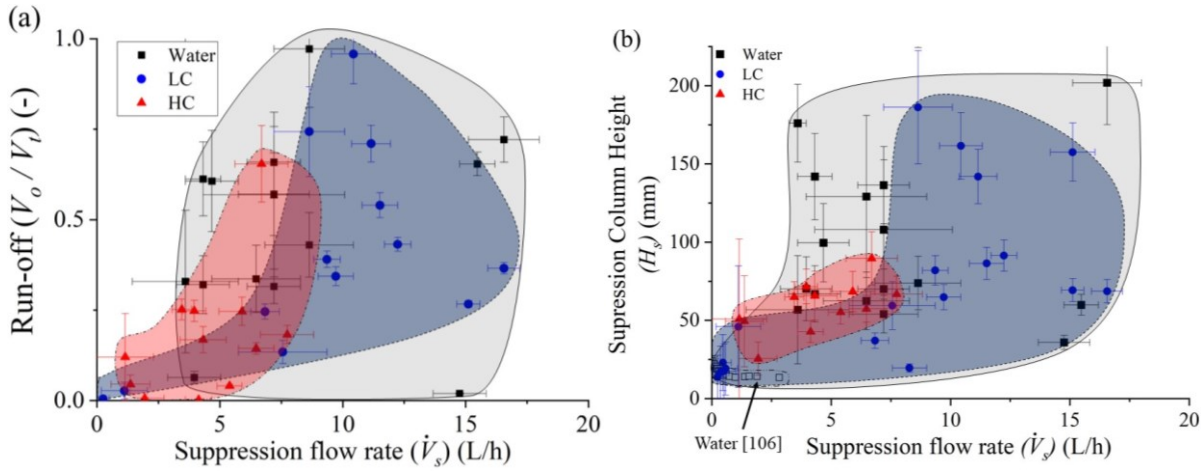

Figure 3.11. Run-off and suppression column height (a) The ratio of suppression run-off to the total volume of suppressant applied, (b) Suppression column height, the product of flow rate and suppression time divided by the reactor area (Eq. 3.1). The clouds for each suppressant agent are rough estimation to assist visual observation.

Figure 3.11a shows run-off data for water, which are widely scattered and demonstrating no clear trend. Comparing with Figure 3.10d, shows water has a higher run-off than wetting agent suppressants (both LC and HC) and it is not accompanied by a shorter suppression, especially at low flow rate. This means that at low flow rates, water travels through the sample faster than wetting agent suppressants because of channelling and thus the longer suppression time. With wetting agent suppressants, run-off increases with flow rate. Comparing Figure 3.11a with Figure 3.10d, it can be seen that the increase of run-off in wetting agent is accompanied by significant decrease of suppression time. As flow rate increases

beyond ~7 L/h, run-off of wetting agent increases to the level of water, and results in shorter suppression time than water. This means that run-off in wetting agent is mainly caused by uniform penetration and that higher run-off is equivalent to better wetting over the whole sample.

Suppression column height or suppressant fluid per unit area can be calculated by using Eq. 3.1 where H_s is the suppression column height, $\dot{V}_s$ is the flow rate, Δt_s is the suppression time, and A_r is the reactor area (0.2 m x 0.2 m). By looking into the lower suppression column height and shorter suppression time (at flow rates below 7 L/h) of LC and HC compared to water (Figure 3.10d and Figure 3.11b), it can be seen that wetting agents increase suppression efficiency. Comparing Figure 3.10d and Figure 3.11b, the decrease of suppression time with flow rate is followed by increasing suppression column height, which can have positive effect on suppression performance if the run-off is caused by uniform solution penetration.

$$H_s = \frac{\dot{V}_s \Delta t_s}{A_r} \tag{3.1}$$

3.5.2.3. Fluid volume per mass of peat

The required volume of fluid to successfully suppress one kg of peat (V_{sp}/m_{sp}) is calculated by using Eq. 3.2 where V_{sp} is the total fluid volume, including the volume of suppressant applied ($\dot{V}_s \Delta t_s$) and the original moisture content left when suppression was initiated ($V_{w,sp}$), but excluding run-off (V_o); and m_{sp} is the mass of the dry peat and residue (char and ash) when suppression was initiated, i.e. 299.3 ± 18.5 g (equivalent to 40.4 ± 1.66% mass loss). m_{sp} was calculated by estimating the amount of water content at the start of the suppression ($m_{w,sp}$). By observing the average location of the front at suppression (L_{sp}), i.e. 10.9 ± 0.7 cm (Figure 3.3a), the volume fraction of the unburnt sample (X_{sp}) can be estimated to be 0.46 ± 0.04 (Eq. 3.3, where L_r is the length of the reactor which is 20 cm). Multiplying this volume fraction with the initial moisture content of the peat sample before ignition results in $m_{w,sp}$ (Eq. 3.4, where m_b is the bulk mass of the sample before ignition). $m_{w,sp}$ was obtained by subtracting $m_{w,sp}$ from the mass data at the start of the suppression. The volume of water at the start of the suppression ($V_{w,sp}$) is obtained from the mass of the water ($m_{w,sp}$) and $\rho_w = 1\ kg/L$ (in Eq. 3.2). Run-off is excluded in this calculation because it escapes the sample and therefore is not absorbed. As a note, the estimation of the volume fraction of the unburnt sample by using Eq. 3.3 and Figure 3.3a is made easier since the shape of the smouldering front was as shown in Figure 3.7. With different MC, the smouldering front will be in a different shape [53] and the estimation of the unburnt volume fraction conducted here cannot be used.

$$\frac{V_{sp}}{m_{sp}} = \frac{\dot{V}_s \Delta t_s + \rho_w m_{w,sp} - V_o}{m_{sp}} \quad (3.2)$$

$$X_{sp} = \frac{L_r - L_{sp}}{L_r} \quad (3.3)$$

$$m_{w,sp} = X_{sp} \frac{MC.m_b}{1+MC} \quad (3.4)$$

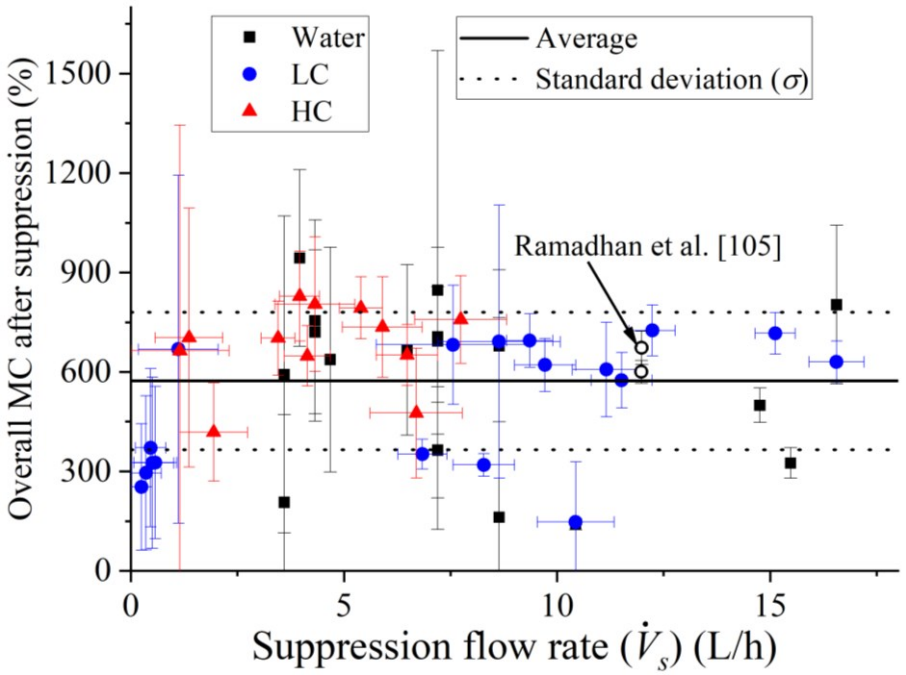

Figure 3.12. Overall MC of peat after successful suppression according to Eq. 3.2, assuming $\rho_{sp} = 1\ kg/L$. The density of the wetting agent is similar to water [139], thus $\rho_{sp} = \rho_w$. The average value is 572.9 ± 207.8 % of MC in dry-mass-base.

This total fluid volume per mass of peat is rather constant despite wide range of flow rates and suppressant fluids. In other words, with increasing flow rate, run-off increases, and the volume of suppressant that is actively suppressing the fire is of 5.7 ± 2.1 L/kg-peat. This value of 5.7 ± 2.1 L/kg-peat can be understood as a critical flooding point, demonstrating the amount of water required to flood the peat fires for successful suppression. Figure 3.12 reports the critical flooding point in term of MC percentage (conversion of V_{sp}/m_{sp} by dividing it to ρ_w and times 100% where wetting agent density (ρ_{sp}) is the same as $\rho_w = 1\ kg/L$ [139]), showing a value of 572.9 ± 207.8 %MC required to suppress the peat fire. This is almost twice the typical value of peatland at flooded pristine conditions, i.e. about ~300% MC [10,24].

This critical value suggests that the suppression time is the duration needed to flood the peat. In other words, suppression time is the time needed for the suppressant at a specified flow rate and concentration to flood the peat to that level of critical flooding point. This value is also affected to a certain degree by run – off as well, since a higher run-off causes a longer time needed to flood the peat.

This means suppression is a thermofluids phenomenon in absorbing media, and that the suppressant acts thermally and not chemically. Thus, the effect of both suppressant concentration and flow rate is to accelerate fluid transport through porous media over the depth of the sample. The low surface tension of the wetting agent probably helps avoiding channel formation. This critical flooding point could be a soil property and the value found here is valid for the peat type used in the study. Compared with literature, this critical value generally agrees in the order of magnitude with value reported by Ramadhan et al. [105], i.e. ~6.4 L/kg-peat. Slightly different average than Ramadhan et al. [105] might be due to the value reported in that study was based on the mass of the peat before ignition, differs from the value reported in this study which is based on the mass of the peat and residue before suppression started.

Even though higher run-off can indicate deeper suppressant penetration, the formation of channels especially for water is a concern causing less fluid participating in suppression. The constant critical flooding point confirms the two possible run-off mechanisms, i.e. channelling and uniform penetration. At low flow rate, the low run-off of LC and HC caused by uniform penetration resulted in shorter suppression time than water due to faster flooding of the peat by LC and HC (Figure 3.11a and Figure 3.10d). While in case of water, the higher run-off at low flow rate is accompanied by a longer suppression time than LC and HC because the run-off was mainly caused by channel formation, causing most of the water not contributing to the peat flooding.

Here, the critical flooding point of 5.7 ± 2.1 L/kg-peat can be considered as a theoretical value in which run-off is not included. In practical application, however, run-off cannot be avoided. Thus, including the run-off into this critical flooding point can provide a practical guidance and resulted in 14.4±9.2, 9.3±6.6, and 8.5±1.9 L/kg-peat with water, LC, and HC, respectively.

3.5.3. Upscaling to field conditions

3.5.3.1. Peat fire field experiments

In 2018, field-scale experiments of peat fire were conducted in Indonesia during which five peat fires burned for 4 to 10 days (Chapter 2). Two rain events occurred during this time but the fires survived. The rainfall heights, equivalent to the suppression column height shown in Eq. 3.1, were 2.5±0.1 mm and 4.8±0.2 mm (Table 3.2). These values agree with data in this chapter because less than 36±5 mm of water suppression would not suppress a peat fire. This value of 36±5 mm was taken from the minimum suppression column height shown in Figure 3.11b. After 10 days, the five peat fires were suppressed in a controlled manner by means of water spray. The suppression times ranged from 17 to 42 min, and flow rate from 3,000 to 4,900 L/h, resulted in column height from 26.5 to 36.7 mm. This range of suppression times agree well with the lab measurements even though the flow rate were far higher. The suppression column height can also be seen as the

amount of water that needed to be supplied in an area of a fire. Thus, 26.5 mm is 26.5 L of water per m^2 of the fire area, and a higher flow rate can quickly supply this required amount of water. Considering the significantly higher flow rate than in the lab-scale, the suppression time in field-scale though is not significantly shorter. This can be due to the significantly larger fire area in the field, up to 0.3 to 80 m^2.

The two rainfall events correspond to 1.9 to 2.6 L/h for 50 min and 1.3 to 8.8 L/h for 17 min, and both fall below the below the critical suppression limit of Figure 3.10a (see also Figure 2.18a), thus too quick for successful suppression. Lin et al. [106] reported that the minimum column rate to suppress peat fires is 4 mm/h, which is less than rain events recorded in our field experiments, i.e. 5.6 and 8.3 mm/h. However, the minimum column rate should last for more than 5 h in order to successfully suppress peat fires [106], which is much longer than typical rainfall but agrees relatively well with minimum suppression column height reported both in this chapter (36±5 mm) and chapter 2 (26.5±9.2 mm), i.e. 4 mm/h × 5 h = 20 mm.

Table 3.2 shows the summary of suppression column height and run-off data for all currently available literature of peat fire suppression. It can be seen that the minimum suppression column height ranges from 13 to 36 mm, except for the two extremely high column height values from [105] of 579±30.8 mm and from lance injection in GAMBUT (Chapter 2) which is 842.5±57.7 mm.

Table 3.2. Data of minimum suppression height (mm) and run-off (%) from this study and available literature of peat fire suppression.

Fluid	Minimum Suppression column height (mm)	Run-off (%)
This work – laboratory experiment *(spray)*		
Water	36±5	2±0.15
Low concentration wetting agent (1% weight in water)	14±14	0.5±0.45
High concentration wetting agent (5% weight in water)	26±11	0.6±0.2
Literature		
Water [105] – laboratory experiment *(Spray)*	579±30.8	*N/A*
Water [106] – laboratory experiment *(Spray)*	13±1.9	*N/A*
Water (Chapter 2) - field experiment:		
Successful suppression (Spray)	26.5±9.2	*N/A*
Successful suppression (Lance injection)	842.5±57.7	*N/A*
Unsuccessful suppression (Rain 1)	2.5±0.1	*N/A*
Unsuccessful suppression (Rain 2)	4.8±0.2	*N/A*

3.5.3.2. Upscaling of laboratory results

Upscaling from laboratory data to the field can give an idea of the challenges of peat fire suppression in terms of flow rate and suppression time. Based on the data presented here, the amount of suppressant fluid required to extinguish an hypothetical peat fires in the field can be estimated by Eq. 3.5. It basically upscales

the amount of required suppressant fluid from laboratory data ($\dot{V}_s \Delta t_s$) to a hypothetical field scale through ratio of the fire area in the field to fire area in the lab. This equation assumes a uniform flow rate over an extended area of the wildfire, thus can be used to approximate the required volume of suppressant fluid for relatively small peat fire area.

$$V_s = \dot{V}_s \Delta t_s \frac{A_f}{A_r} \tag{3.5}$$

Where V_s as the required volume of suppression agent (L) (which is shown to be about 5.7 ± 2.1 L/kg-peat in Figure 3.12, and if including run-off can be up to 14.4±9.2, 9.3±6.6, and 8.5±1.9 L/kg-peat with water, LC, and HC, respectively), $\dot{V}_s$ as suppression flow rate (L/h), Δt_s as required suppression time (h), A_f as fire area (m^2), and A_r as reactor area used in this study, i.e. 0.04 m^2 (at the start of suppression, half of the reactor had already burnt).

For example, the average suppression time for water at a flow rate of 4 L/h in the laboratory reactor is ~63 min. Using Eq. 3.5, the amount of water required to extinguish, say, a 1 ha. (1×10^4 m^2) peat fire can be estimated to be in the order of 1 million L. In case HC suppressant is used at the same flow rate, the average suppression time was 35 min, resulting in ~580,000 L of suppressant, about half of the required volume with water.

Volumetric consideration can also be made in the upscaling by including the depth of burn in Eq. 3.5, done by multiplying both fire area in the field and in the lab scale with their respective depth of burn. Taking the average depth of burn in peat fires from boreal and tropical regions, i.e. 39 cm [118], and the laboratory-scale depth of burn in this study, i.e. ~3 cm, results in ~13 fold increase of the amount of solution required to extinguish the hypothetical peat fire in the example above. The upscaling conducted here was done simply by assuming a linear scaling of smouldering and suppression dynamics. By considering the relatively well agreement of minimum suppression column height (Table 3.2), and suppression time and flow rate, between lab and field-scale (Figure 2.18a), linear scaling can be assumed to be acceptable. At least, to give a general idea on the difficulties and the very high required suppressant volume peat fire firefighting, as also reported from real peat fires incidents [128,132,133,135].

3.6. Conclusion

This chapter presents suppression experiments on smouldering peat fires exploring the effect of three different concentrations of suppressant and variable flow rate. Suppression data is represented by suppression time, run-off volume, column height, and fluid volume per mass of peat. Flow rates decrease suppression time for all solutions explored. By using higher concentration of wetting agent as suppressant, 26 to 39% decrease in suppression time can be achieved with HC

performed more reliable in reducing suppression time. The use of wetting agent could decrease the required flow rate by 63%, thus also reducing the required pump power by the same order, and significantly decrease required volume of suppressant agent. Upscaling demonstration of the results in this study to the field, an example case of a small peat fire, shows that a 50% decrease in the required suppressant volume per hectare fire could be achieved with wetting agents as suppressant.

The decrease of suppression time with flow rate is at the expense of higher run-off. The run-off is caused by channelling in water or uniform penetration by wetting agent. The uniform penetration by wetting agent is because it has ~2.5 times lower surface tension than water. Run-off by uniform penetration is good to suppress deep fires.

The actual volume of suppressant that actively extinguishes the fires is found to be rather constant across different flow rates and suppressant agents. This value is coined as critical flooding point, which is 5.7±2.1 L/kg. This value being constant suggests that the wetting agent as suppressant acts thermally and not chemically. The minimum suppression column height in water suppression in this lab-scale study agrees with the field experiment presented in Chapter 2, i.e. 36±5 and 26.5±9.2 mm, respectively. This suggests that suppression efforts or rainfall events with column height below this minimum value results in water not reaching the in-depth smouldering, thus resulting in unsuccessful suppression.

The experiments presented here were conducted at constant setup of MC, bulk density, and sample depth. Previous studies found that smouldering spreads deeper with MC and that spread rate decreases with bulk density [3,121]. More studies are needed to clarify the correlation between suppression and smouldering dynamics across these soil properties. As with sample depth, its influence on suppression can be expected to be closely related to MC which has been known to govern smouldering front width [121]. Thus, different sample depth might result in minimum effect on suppression if the MC is constant, hence constant smouldering front width.

This chapter presents the occurrences of persistent smouldering despite ongoing suppression. The possibility of persistent smouldering decreased with increasing flow rate and suppressant concentration. The results presented here contribute to a better understanding on the mechanism of peat fires suppression, the role of flow rate and suppressant fluids, and the amount of resources needed to successfully stop peat wildfires.

Chapter 4

Review of the Transition from Smouldering to Flaming Combustion in Wildfires

Summary[4]

Wildfires are uncontrolled combustion events occurring in the natural environment (forest, grassland, or peatland). The frequency and size of these fires are expected to increase globally due to changes in climate, land use, and population movements, posing a significant threat to people, property, resources, and the environment. Wildfires can be broadly divided into two types: smouldering (heterogeneous combustion) and flaming (homogeneous combustion). Both are important in wildfires, and despite being fundamentally different, one can lead to the other. The smouldering-to-flaming (StF) transition is a quick initiation of homogeneous gas-phase ignition preceded by smouldering combustion and is considered a threat because the following sudden increase in spread rate, power, and hazard. StF transition needs sufficient oxygen supply, heat generation, and pyrolysis gases. The unpredictable nature of the StF transition, both temporally and spatially, poses a challenge in wildfire prevention and mitigation. For example, a flaming fire may rekindle through the StF transition of an undetected smouldering fire or glowing embers. The current understanding of the mechanisms leading to the transition is poor and mostly limited to experiments with samples smaller than 1.2 m. Broadly, the literature has identified the two variables that govern this transition, i.e., oxygen supply and heat flux. Wind has competing effects by increasing the oxygen supply, but simultaneously increasing cooling. The permeability of a fuel and its ability to remain consolidated during burning has also been found to influence the transition. Permeability controls oxygen penetration into the fuel, and consolidation allows the formation of internal pores where StF can take place. Considering the high complexity of the StF transition problem, more studies are needed on different types of fuel, especially on wildland fuels because most studied materials are synthetic polymers. This chapter synthesises the research, presents the various StF transition characteristics already in the literature, and identifies specific topics in need of further research.

[4] This chapter is based on "Santoso MA, Christensen EG, Yang J and Rein G (2019) Review of the Transition From Smouldering to Flaming Combustion in Wildfires. Front. Mech. Eng. 5:49. doi: 10.3389/fmech.2019.00049"

4.1. Introduction to smouldering-to-flaming transition in wildfires

This chapter reviews the transition from smouldering to flaming in the literatures, identifying the mechanisms and important variable that can be further investigated to understand the fundamental of transition. A wide range of materials can undergo smouldering, such as cellulosic insulation, coal, polyurethane (PU) foam, cotton, wood, and peat, making smouldering a serious hazard in both residential and wildland areas. In particular, the hazard of wildfire increases at the wildland urban interface (WUI), where wildfire fronts meet houses and urban sites. In such an event, two types of fuels are involved, i.e. WUI and wildland fuels. WUI fuels are found in the built environment (e.g., polymers and timber), where the smouldering-to-flaming (StF) transition has been investigated in more studies than wildland fuels (e.g., leaves, twigs, and organic soils), which are rarely discussed in the literature. In solid fuel with charring capability, both smouldering and flaming can occur, and one can lead to the other [1].

The chemical pathways of solid fuel combustion can be broadly simplified and has been discussed in Chapter 1 (Eq. 1.1 to 1.4). Although flaming is characteristically different from smouldering; smouldering is the heterogeneous reaction of solid fuel with an oxidiser (Eq. 1.3), whereas flaming is the homogeneous reaction of gaseous fuel with an oxidiser (Eq. 1.4), which releases more heat (Table 4.1); the two fires have their genesis from the same process, namely, pyrolysis (Eq. 1.2).

Table 4.1. Smouldering and flaming combustion characteristics [1,38]

Characteristics	Smouldering	Flaming
Peak temperature (^oC)	450–700	1,500–1,800
Typical spread rate (mm/min)	1	100
Effective heat of combustion (kJ/kg)	6–12	16–30
Ignition source (kW/m^2)	8	30

The commonality of pyrolysis (Eq. 1.2) prior to both smouldering and flaming combustion allows the transition between them. In one case, a flaming fire can extinguish, and a smouldering fire can proceed in a flaming-to-smouldering transition. This transition may have significant effects on soil consumption during wildfires, as flaming fires quickly spread over the surface of the forest floor and consume shallow layers of ground fuels, while smouldering occurs both above- and belowground, slowly releasing massive amounts of carbon, and can be far more detrimental to the ecosystem. For example, during peat fires in Indonesia in 1997, it was found that smouldering combustion consumed organic soils as deep as 51 ± 5 cm and released approximately 2.57 Gt of carbon [12]. At the global scale estimate, the average annual greenhouse gas emissions from smouldering fires

are equivalent to 15% of manmade emissions [25]. Owing to its low temperature, propensity to travel belowground, and flameless characteristics, smouldering of organic soils is difficult to detect [1,11,12]. Additionally, when detected, smouldering is notoriously difficult to extinguish, requiring vastly greater quantities of water [1,105,122,143].

In Southeast Asia, this flaming-to-smouldering transition is common, as it is frequently used in agricultural practices to clean the land and return nutrients for use in plantations—this practice is typically referred to as slash and burn (Figure 4.1). These practices can lead to widespread peat fires during prolonged dry spells, such as El Nino, and are often the cause of dramatic haze episodes, such as those regularly recorded in Indonesia [12,14]. Additionally, smouldering wildfire produces more toxic compounds per kilogram of fuel compounds than flaming [1,103], and due to the low temperature causing weakly buoyant plumes, smoke can be blown into nearby cities, causing severe degradation of air quality and significant adverse health effects [1,27,154]. In 2015, the haze episode caused an economic loss of 16 billion US$ to Indonesia, not including economic losses to the other affected countries, such as Malaysia, Singapore, and Brunei Darussalam[5].

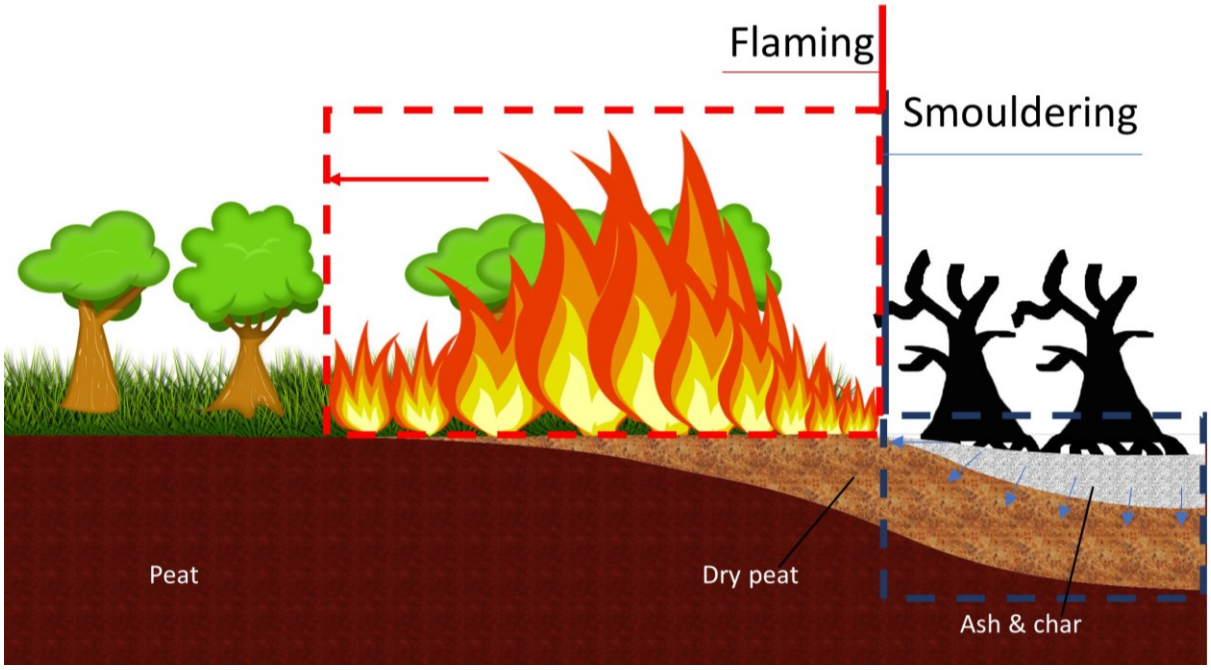

Figure 4.1. Simultaneous occurrence of smouldering and flaming in peatland forest fires. Flaming wildfire consumes surface fuel vegetation and tree crowns. Smouldering combustion consumes organic soil, dominantly spreading on and below the ground.

However, the more dramatic transition is StF, as it represents a sudden increase in spread rate, power, and hazard (Table 4.1). Smouldering ignition requires less energy than flaming ignition, and as such, the StF transition

[5] Haze fires cost Indonesia S$ 22 b, twice the tsunami bill: World Bank, The Straits Times, Singapore, 16 December 2015.

provides a path to flaming via heat sources too weak to directly ignite a flame [38]. In addition, based on the review of research of fire spread in WUI fires, Caton et al. [155] identify StF transition as one of the pathways of building fire spread in the WUI fires. There is a rather informal technical term used to express the reignition of fire that previously has been extinguished, i.e., rekindle [156]. StF transition can be one of the mechanisms leading to rekindling in wildfire. This is further discussed in Chapter 4.6 (*Embers and StF Transition in Wildfires*).

In addition to heat flux from the flame, embers generated by wildfires are a major cause of wildfires spread and ignition in WUI building [157]. Embers (also called as firebrands or firedrops) are pieces of hot or burning fuel lofted by the plume of the fire [40] (Figure 4.2). Once accumulated, embers can cause WUI structures such as roofing material, decks, and vents to smoulder and, in some cases, transition to flaming. The generation of embers, its transport and the vulnerability of ignition of WUI fuels due to flaming and smouldering embers have been widely investigated [41,42,44,158–164]. Embers also provide an alternative mode of fire spread during wildfires through spotting, whereby embers land and locally ignite dry fuels, often transitioning from StF and thus advancing the flame (Figure 4.2). This particular behaviour can be highly hazardous to firefighters who may quickly find themselves surrounded by flames. Moreover, the current codes and standards of WUI represent a lack of understanding of how WUI structure can ignite during wildfire, one of which is the WUI structural vulnerability to ember showers [165,166].

Figure 4.2. Ember shower during the 2018 Delta Fire in the Shasta – Trinity National Forest, California, USA. Photo courtesy of Noah Berger / Associated Press (noahbergerphoto.com). Photo shows flaming fires of grass due to embers, representing a smouldering-to-flaming transition from embers.

Despite the significant risks associated with the transition from StF, limited research is available on the topic, and a fundamental theory of the phenomena has yet to be found. Current research has identified a few key mechanisms but has also found that the transition is inherently difficult to predict. This unpredictable nature of the StF transition both temporally and spatially poses an additional challenge in wildfire prevention and mitigation. This paper aims to synthesise findings in the literature of the StF transition and identify the leading mechanisms and key influencing variables for both wildland and WUI fuels to identify further research required to fully understand the StF transition.

4.2. Role of oxygen supply and heat transfer

Airflow has been frequently found to be a factor that influences the StF transition, as it increases the oxygen supply into the reaction zone, increasing the smouldering spread rate. The StF transition is likely to occur with increasing smouldering spread rate as the intensity of combustion and rate of pyrolysis increase, resulting in a greater mass flux of pyrolyzates. Palmer [167] particularly described that the StF transition was preceded by glowing, which is the visual indication of a high local temperature due to strong smouldering [1]. Notably, the wind direction relative to the spread is also markedly important to the spread dynamics of smouldering. Forward smouldering propagates in the same direction as the airflow, whereas opposed smouldering propagates against the flow of air [1]. Forward and opposed smouldering propagations represent different heat transfer mechanisms that influence the heating process of the fuel [1,36,168,169], thus affecting the occurrence of the StF transition. In opposed smouldering, airflow carries the heat from the smouldering zone away to the ash layer, diminishing the heat supplied for heating the fuel. In forward smouldering, the airflow transfers heat from the smouldering zone to the unreacted fuel, resulting in a more efficient fuel heating process. The smouldering front is also narrower in opposed smouldering than in forward smouldering, representing the lower amount of heat produced in opposed smouldering [168]. Due to the stronger influence of airflow on the smouldering spread rate in forward smouldering than in opposed smouldering, forward smouldering has a greater propensity for the StF transition [167,170,171].

StF transitions can also occur under opposed smouldering [171–173] but with a lower propensity than those under forward smouldering because of the heat transfer direction previously discussed. Basically, the increase in airflow velocity plays two roles in smouldering. Airflow increases both oxygen supply to the smouldering front and convective heat loss. Increased oxygen supply increases the rate of the exothermic reaction needed to sustain smouldering, while increased convective heat losses decrease heat transfer into the unreacted fuel. The latter

role is more significant in opposed smouldering propagation than in forward smouldering propagation.

Two types of StF transitions were identified by [171]: trailing- and leading-edge transitions (Figure 4.3a). Figure 4.3a illustrates smouldering fronts and the location of the leading-edge and trailing-edge StF transitions. The trailing-edge StF transition occurred at the char layer at the trailing edge of the smouldering front. The flame caused by this transition was blue, lasted up to 2 min, and spread up to 10 cm on the residual char. The blue colour of the flame was probably due to a lean mix of gaseous fuel with air prior to ignition. In addition to the mixture concentration, the fuel (i.e., hydrocarbon such as CO or pyrolyzate [171]) is known to affect the colour of the flame, along with the tendency to produce soot. The leading-edge StF transition occurred at the leading edge of the smouldering front, spread downstream onto the unburnt layer of cellulosic insulation, and lasted up to 5 min. Figure 4.3b shows that both leading-edge and trailing-edge StF transitions occurred in forward smouldering, while only the trailing-edge StF transition occurred in opposed smouldering under an airflow of up to 5 m/s. Considering the slower smouldering spread in opposed smouldering, it can be seen that a slower smouldering spread rate results in a lower StF transition propensity.

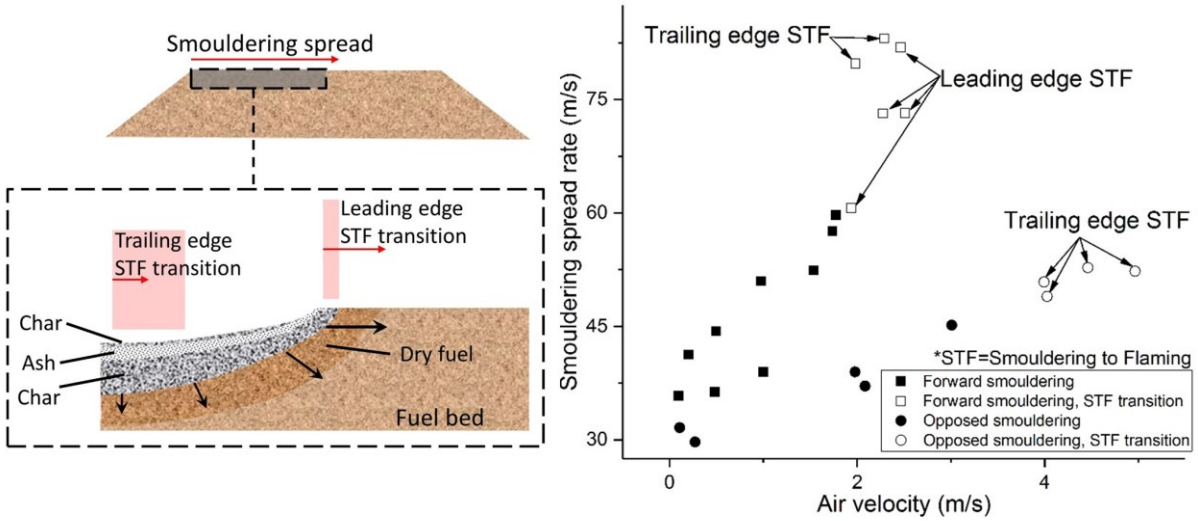

Figure 4.3. (a) Smouldering front diagram showing leading and trailing edges of the StF transition. No significant difference in the smouldering front structures between forward and opposed smouldering in [171] other than the relative thickness of each layer, i.e., drying, char, and ash layers. The detailed smouldering front diagram is a modification from X. Huang (CC BY license) in [50]. The shaded red area represents the rough estimation of the possible location for the StF transition. Red arrow indicates the duration length of the StF transition. (b) Smouldering spread rate of cellulosic insulation under forward and opposed smouldering propagation modes. Data from [171].

Building on this fundamental concept of the rate of oxidation being crucial in the transition phenomena, the increase in ambient oxygen concentration has been investigated and found to have a profound effect on the StF transition. StF

transitions of smouldering PU foam with no external airflow occurred at oxygen concentrations ranging from 17 to 37 vol%, depending on the ambient pressure, and only for large samples (50 × 120 × 450 mm; [174]). The samples in the form of small cylinders (18 mm in diameter) did not experience a transition. The dimensions of the sample govern the self-sustainability of smouldering since smaller samples lead to higher heat losses [175]. By increasing ambient pressure, the oxygen concentration at which the StF transition occurred (critical oxygen concentration) decreased. This result implies that increased oxygen diffusion penetration into smouldering fuel under increased ambient pressure leads to lower critical oxygen concentration. However, when the ambient oxygen concentration is further increased to 35–54 vol% with assistive heating (4.5–55 kW/m^2), the StF transition can occur in samples with characteristic lengths as small as 10–12.5 cm [176–181].

It is important to note that in wildfires, the oxygen concentration will not become higher than the atmospheric oxygen concentration. In fact, the oxygen concentration can be lower. Thus, the effect of airflow velocity and particle diameter in terms of oxygen supply is the most prominent in the StF transition in wildfires. Other important parameters in wildland fuel are moisture content (MC) and inorganic content (IC). MC and IC reduce the propensity to ignition and decrease the lateral fire spread rate of wildland fuel due to their roles as heat sinks [1,47,49,53,95,118]. MC absorbs heat for water vaporisation, and IC absorbs heat and does not contribute to further exothermic reactions due to its inert nature, contributing to increased heat losses. Interestingly, it has been recently reported that the in-depth spread rate increases with MC, which is counterintuitive to the widely assumed decrease in spread rate with MC [3]. Thus, the lateral and in-depth spread rates in smouldering fires respond differently to MC. As MC increases, the density of organic matter per unit volume decreases and porosity increases due to volumetric expansion. The spread rates, i.e., lateral and in-depth, are limited and pre-dominantly governed by two different processes of heat loss and oxygen diffusion. However, the mechanism causing these different responses still needs further investigation. Increased propensity of the StF transition with decreased MC has been shown in both WUI and wildland fuels [43,182–184].

The critical velocity of the StF transition occurred as the velocity ranged from 1 to 5 m/s for studies at atmospheric oxygen concentration and without assistive heating, such as radiant heating, deposited embers, and deposited hot particle (Table 4.2). With external heat flux and increased ambient oxygen concentration, the critical velocity decreased because the convective cooling effect was minimised [178]. In turn, the decreasing convective cooling effect decreased the required heat needed to induce the StF transition. In the case of the deposition of embers at atmospheric oxygen concentration, the StF transition was found to occur at velocities as low as 1 m/s [183,184] or even with no airflow velocity when the assistive heating was from a hot steel particle at a temperature of ~1,200^{o}C [43].

Table 4.2. Studies of the smouldering-to-flaming transition in the literature.

Consolidation/ fuel category	Sample material	Sample shape and orientation (characteristic length [m])	Ignition source (size and duration)	Smouldering spread mode	Critical velocity [m/s]	Oxygen concentration [Vol%]		External heat flux [kW/m^2]		Location of transition	Time to StF transition [mm:ss]	Reference
						Range	Critical	Range	Critical			
Unconsolidated/ Wildland fuel	Pine straw mulch, Shredded hardwood mulch, Cut grass, Pine needles	Thin rectangular block/horizontal (0.23)	Smouldering embers (Four 50 mm (diam.) by 6 mm (thick), 1.5 g)	Forward and opposed (simultaneously)	1	21	21	N/A (ember deposition)	N/A (ember deposition)	Free surface	N/A	[183,184]
	Pine needles	Thin rectangular block/horizontal (0.31)	Spherical metal particle (Diam. 6, 8, 10, 12, 14 mm and temperature 680 to 1190 °C)	Forward	0 to 4	21	21	None	From the hot steel particle under high temperatures	Free surface	~01:40 to 10:20	[43]
	Pine needles	Thin rectangular block/horizontal (0.6)	Flaming wood stick (4x4x130 mm) on dry pine needle bed (150×20×40 mm)	Forward	1.1	21	21	None	None	Free surface	N/A	[185]
Unconsolidated/ WUI fuel	Filter paper & Cardboard	Cylindrical/vertical (0.1)[#1]	Small flame (N/A)	Opposed	1.52±0.82 (Filter paper)	18 to 62	52±2 (Filter paper)	N/A	N/A	N/A	N/A	[176]

					1.73±0.81 (Cardboard)		44±4 (Cardboard)					
	Cork dust & deal sawdust[¶]	Rectangular block/horizontal (0.15 to 0.2)	Small flame (N/A)	Forward	1.8±0.8	21	21	N/A	N/A	Free surface	N/A	[167]
	Cellulosic insulation	Flat rectangular with wedge ends/horizontal (0.46)	Electrical heater (375°C and 60 min)	Forward and opposed	2.2±0.22 (forward) 4.4±0.4 (opposed)	21	21	N/A	N/A	Free surface	N/A (50:00[ł])	[171]
	Wood shavings, shredded papers, beeswings*	Rectangular block/horizontal (0.61)[#1]	Electrical coil (80 volts and N/A)	Forward and opposed (simultaneously)	2.23±0.63 (wood shaving) 0 (Shredded paper)	21	21	N/A	N/A	N/A	02:00 to 76:00	[170]
Consolidated/WUI fuel	*Pinus Pinaster*	Thin slab/horizontal (0.11)	Spontaneous, Propane-air flame (piloted, no airflow, 10 mm flame length), Electrical spark (piloted, with airflow)	N/A	2.4±1.4	21	21	10 to 55	35.48±9.61	N/A	00:09 to 12:17 (spontaneous) 00:10 to 13:10 (Piloted)	[177]
	Fibre insulated board	Hollow rectangular block/vertical (0.15)	Bunsen flame	Forward	0.18±0.06	21	21	N/A	N/A	Free surface	10:12 to 23:36	[186]

	Fire-retarded (FR) and Non-fire-retarded (NFR) polyurethane (PU) foam	Rectangular block/horizontal (0.1 to 0.4)	Electrical heater (40 to 200 W)	Lateral in natural convection	N/A	21	21	N/A	N/A	Free surface	60:00 to 138:05	[182]
	NFR PU foam	Rectangular block/vertical (0.125)	Electrical heater (23.25 W and until self-sustained smouldering identified)	Forward	0.82±0.5	30 to 40	37.5±2	7.25 to 8.75	8±0.6	Within the sample	17:34	[178]
	FR PU foam	Rectangular block/vertical (0.125)	Electrical heater (115 W and 250 to 300 s)	Forward	0.15	30 to 60	42.5±7.5	4.5 or 5.5	5±0.5	Within the sample	09:12	[179]
	NFR PU foam	Rectangular block/vertical (0.125)	Electrical heater (23.25 W and 11.7 min)	Forward	0.5	25 and 40	35 and 40	8 and 8.75	8 and 8.75	Within the sample	17:00 (~16:00[ŧ])	[180]
	PU foam (NFR and FR)	Rectangular block/vertical (0.125)	Smouldering: Electrical heater (23 W for NFR foam and 115 W for FR foam)	Forward	0.5 (NFR)	15 to 35	0.2±0.02 (NFR foam)	7.25 to 8.75 (NFR)	5±0.5 (NFR foam)	Within the sample	~18:00 (NFR foam at 21 Vol% O_2 and 8 kW/m^2)	[181]
			Pilot ignition: resistance wire (8.8 A for NFR foam and 10 A for FR foam)		0.15 (FR)		0.28±0.05 (FR foam)	4.5 and 5.5 (FR)	8±0.61 (FR foam)			
	NFR PU foam	Rectangular block/horizontal (0.23)[#3]	Cigarette ignition	Lateral in natural convection	N/A	21	21	None	None	N/A	~50:00	[187]

	NFR PU foam lined with cotton fabric	Rectangular block/vertical (0.3)	Electrical heater rod (Diam. 0.64 cm, 11 W DC)	Upward natural convection	N/A	21	21	None	None	Free surface	14:00 to 60:00	[188]
	NFR PU foam	Rectangular block/vertical (0.381)	Electrical heater (70 W and 50 min)	Forward	0.78±0.48	21	21	N/A	N/A	Within the sample	56:54 to 127:36	[189]
	NFR PU foam	Rectangular block/vertical (0.406)	Electrical heater (70 W and 50 min)	Forward	0.25 and 0.75	21	21	N/A	N/A	Within the sample	96:00 to 113:00	[39]
	NFR PU foam	Rectangular block/horizontal (0.45)	Heating element (N/A)	Lateral in natural convection	N/A	17 to 62	27.7±8.1	N/A	N/A	N/A	N/A	[174]
	Red oak & White pine	U-shaped rectangular block/horizontal (0.74)	Electrical heater (N/A and 60 min)	Forward, opposed, and mixed	0.23±0.03	21	21	N/A	N/A	Free surface	N/A	[172]
	Upholstered furniture	Upholstered shapes and orientations (N/A)	Cigarette and electrical ignition (N/A)	N/A	N/A	21	21	N/A	N/A	In the crevice between two cushions	18:00 to 306:00	[190–192]
	Cedar, Douglas-fir, Redwood	Slab/horizontal (1.2)	Firebrand showers (17.1±1.7 g/m^{2}s)	Forward and opposed (simultaneously)	6	21	21	N/A (ember(s) shower)	N/A (ember(s) shower)	Free surface	05:56 to 19:40	[162]

	oriented strand board (OSB); roofing assembly (OSB, tar paper, and shingles); and dried pine needles and leaves	Valley configuration of OSB; and flat configuration of roofing assembly with attached gutter filled by dried pine needles and leaves/angled position (1.22)	Firebrand showers (up to 0.4 g and 6 min)	Forward and opposed (simultaneously)	7	21	21	N/A (ember(s) shower)	N/A (ember(s) shower)	In the crevice§ and in the gutter8	N/A	[41]
	Cotton	Cuboid/vertical (0.15)	Electrical heater (12.8 kW/m^2 and 24 min)	Upward natural convection#4	N/A	21	21	None	None	Within the sample	117:00, 118:00, 133:00	[193]
	OSB	Slab/horizontal (0.18)	Fire brand (L 25.4 mm x Ø 6.35, 9.52, 12.7 mm x piles (1 brand, 20 g, 50 g, and 100 g))	Forward and opposed (simultaneously)	1.84	21	21	N/A (ember(s) deposition)	N/A (ember(s) deposition)	Free surface	~01:30	[44]

¶ No transition to flaming in samples with particle diameters less than 0.1 cm
ɬ Computationally predicted by Yang et al. 2018
ǂ Computationally predicted by Dodd et al. 2012
* Transition to flaming only occurred once in thin filmy pieces of bran
§ For material construction of valley configuration with only base material (oriented strand board)
8 For the flat configuration of roofing assembly attached with gutters filled by dried pine needles and leaves
#1 Diameter varied from 0.0027 to 0.0054 m
#2 Depth varied from 0.1 to 0.2 m
#3 Width varied from 0.08 to 0.16 m
#4 Sample was in a cube shape and ignited at the bottom

In all investigated consolidated WUI fuels (Table 4.2), the StF transition occurred only if the smouldering sample was assisted with heat insulation, heated boundaries, and increased ambient oxygen concentration [39,174,178–181,187,189]. However, this finding is not the case when there is a radiation exchange between smouldering char surfaces [172,186,188]. In this case, the critical airflow velocity of the StF transition can be lower than 1 m/s, even without assistive external heating and elevated ambient oxygen concentration. Ohlemiller [172] found that the StF transition consistently occurred in both forward and opposed smouldering for airflows between 0.2 and 0.25 m/s with a smouldering sample in a U-shaped geometry. The U-shaped geometry increased the radiation heat exchange between the smouldering surfaces of a wood sample. The increased radiation exchange is also the prominent factor in the StF transition mechanism hypothesised from a series of upholstered furniture fire tests [190–192], as discussed further in the next section.

4.3. The chimney effects

Many StF transition investigations, especially for upholstered furniture, were conducted during the 1970s and 1980s due to the concern of residential fires in which cigarettes were considered to be the major cause of ignition [190,194]. From a series of tests with assorted sofas, chairs, mattresses, and box springs as test materials, the time to StF transition occurred from 20 to 132 min [194–197]. It was not until the fire tests conducted by Ogle and Schumacher [192] that the mechanism leading to the StF transition was proposed. The proposed mechanism emphasised the role of oxygen supply and air current in inducing the StF transition. Ogle and Schumacher [192] performed 11 fire tests on 10 upholstered furniture items, where seven tests were ignited by a smouldering cigarette and four using a flaming liquid fuel. The StF transition was preceded by a "burn-through" of the smouldering cigarette at a crevice location of upholstered furniture (Figure 4.4). This "burn-through" is downward smouldering cigarette propagation through the crevice of cushions forming a narrow vertical channel due to smouldering consumption of the cushion material. The formation of this narrow vertical channel enhances the air entrainment to the smouldering zone from below due to the chimney effect. The greater air entrainment increases both oxygen supply to smouldering reaction and convective heat losses. However, the convective heat losses are compensated for by the radiation exchange between the two smouldering surfaces facing each other, which are also more exothermic due to the enhancement air entrainment. This leads to vigorous smouldering which is favourable for the StF transition.

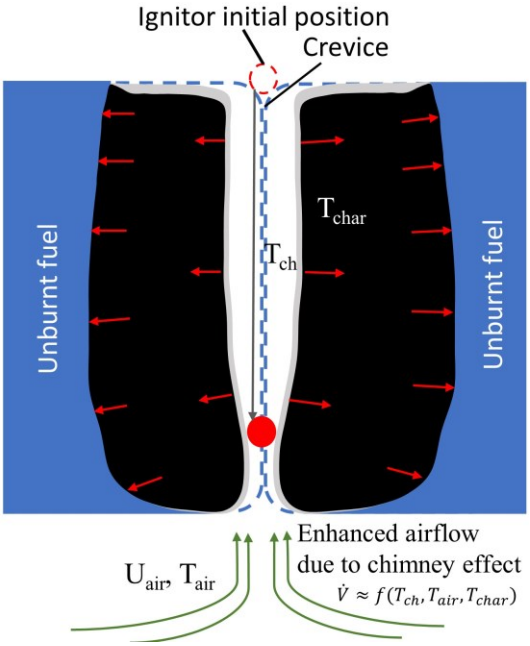

Figure 4.4. Enhanced oxygen supply in the channel formed by downward smouldering propagation of an ignitor at the crevice location of two adjacent solid fuels. The enhanced airflow increases the oxygen supply to the smouldering fuel, leading to a more exothermic smouldering reaction. This figure is an adaptation from [192].

The radiation exchange between the two smouldering char surfaces in a vertical channel influences the StF transition and induces a StF transition even at low airflow velocities, i.e., 0.1–0.27 m/s [172,186]. In experiments of chimneys with different shapes, i.e., square, rectangular, and slot shaped, conducted by Alexopoulos and Drysdale [186] (Figure 4.5a), the time to StF transition was found to be independent of airflow and shortest in the chimney shape with the narrowest vertical channel space, i.e. the slot-shaped chimney (Figure 4.5b). The temperatures inside the vertical channel, i.e., T1 and T2 (Figure 4.5a), were higher in the slot-shaped chimney than in the square and rectangular chimneys. This temperature trend and independence of the StF transition time to airflow imply that conservation of heat governs the StF transition mechanism along with oxygen supply. This result is in agreement with recent findings by Stoliarov et al. [188], who performed a series of experiments of smouldering PU foam under natural convection with an adjustable vertical channel gap between the front face of the PU foam and a thermal insulation plate (Figure 4.6A). With a large gap, the oxygen supply was adequate, and smouldering was the dominant reaction (Figure 4.6B). With a smaller gap, smouldering was not the dominant reaction due to insufficient oxygen supply (Figure 4.6C). With the availability of heat from smouldering and a deficient oxygen supply, pyrolysis was more intense in the smaller gap configuration than in the larger channel gap configuration, leading to more pyrolyzates being produced. Moreover, a smaller gap might result in a higher concentration of pyrolyzates inside the channel (Figure 4.6B). The StF transition then occurred when the pyrolyzates were heated by char oxidation up to the point

where the pyrolyzate temperature and concentration were above the lower flammability limit. In this case, the StF transition was a piloted ignition of pyrolyzate by char oxidation. This finding was also observed by Alexopoulos and Drysdale [186], who found that the StF transition time was longer in wider vertical channel gaps. In another study of StF transitions in small Pinus pinaster wood samples with dimensions of 11 by 11 by 1.9 cm, Bilbao et al. [177] found that the radiative heat flux affected the time to StF transition more than convection. A previous ignition study of polyurethane foam found that the critical radiation heat flux to ignite smouldering is lower than that to ignite flaming combustion and decreases with sample size [38]. This result represents the important role of radiation heat transfer in smouldering and the following possible StF transition.

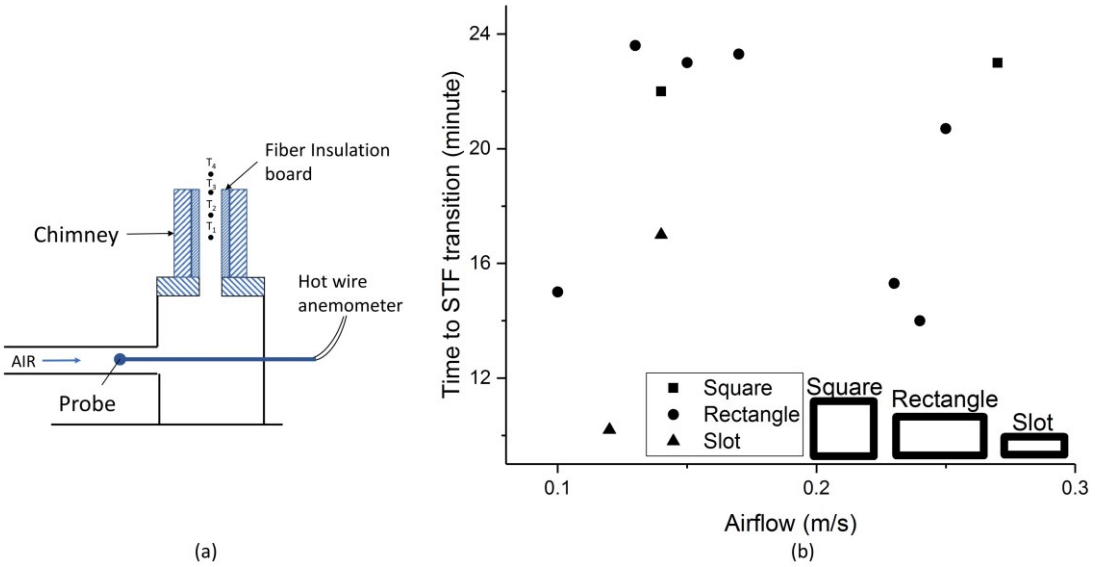

Figure 4.5. StF transition experiments in a chimney of fiber insulation board [186]. (a) Experimental setup of chimney configuration. (b) Time to StF transition vs. airflow. Data from [186].

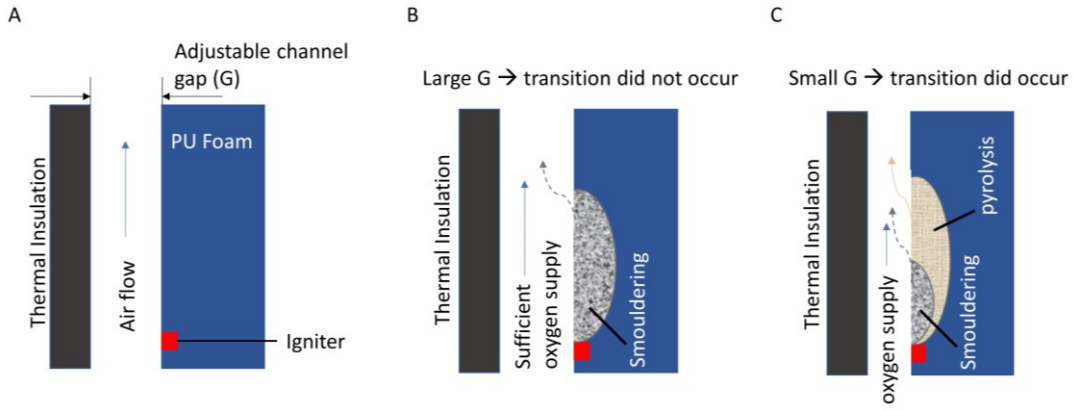

Figure 4.6. StF transition experiment by Stoliarov et al. [188]. (A) Experimental setup. (B) Experiment in which the StF transition did not occur due to a large channel gap. (C) Experiment in which the StF transition occurred due to a small channel gap. Solid blue, dotted black, and solid beige arrows indicate oxygen supply, gases and aerosol products from char oxidation, and pyrolyzates, respectively.

The mechanism of the StF transition at a crevice location is particularly important in WUI fires, i.e., where two or more fuels abut each other such as in wood decks and house roofing. The deposition of embers in a crevice of these fuels has been experimentally investigated as a favourable location for ember accumulation that leads to a StF transition [41,162]. Fundamentally, this follows the same mechanism as that shown in Figure 4.4. In addition, wood was found to crack during smouldering. This cracking leads to local crevice formation on the wood surface, leading to a StF transition without heating support from embers [172].

4.4. Secondary char oxidation

The mechanism of the StF transition due to strong secondary char oxidation (SCO) was first proposed by Torero and Fernandez-Pello [175], who conducted an experimental study of upward smouldering combustion of polyurethane foam in natural convection (Figure 4.7a). In this experiment, the StF transition was preceded by a second oxidation of char, which was more exothermic than the first. This mechanism is best discussed by referring to Figure 4.7b. Upward smouldering propagation was initiated from t_1 to t_2. At time t_2, the ignitor was turned off. By this time, smouldering had propagated up to the P_5 position. Temperatures at P_1 to P_4 can be observed to decrease, with the temperature at P_1 decreasing the most. The smouldering spread rate decreased, as indicated by a slower temperature increase in downstream positions, i.e., P_6 and P_7. P_5 and P_6 reached a plateau of the pyrolysis temperature (T_p) by the time the experiment approached time t_3. Thus, smouldering fronts propagated to these positions. SCO occurred between times t_3 and t_4. In this time period, the large temperature increase at P_1 indicates a strong char oxidation in the char layer upstream of the smouldering fronts, which is the second char oxidation in that layer. Hence, the name secondary char oxidation is assigned to this process.

Extinguishment of char oxidation at P_1 is not observed prior to SCO since temperatures were still relatively high (~500 – 600°C). However, its rate of exothermic reaction decreased, as indicated by the temperature decreases, most likely because of the absence of heating from the ignitor. It can be hypothesised that as the smouldering leading edge moved downstream to P_6, the smouldering trailing edge was still around P_1. This process resulted in increases in the smouldering front thickness as smouldering propagated. The term SCO then represents a sudden increase in the exothermic reaction rate at the smouldering trailing edge.

Due to oxygen consumption by secondary char oxidation (SCO), the oxygen concentration was depleted and unable to sustain further oxidation. During this time, t_4 to t_5, endothermic pyrolysis reactions induced by heat provided by previous SCO took place and produced flammable pyrolyzates, as indicated by the

decreasing temperature. Whether char or unreacted PU foam undergoes pyrolysis remains to be determined. Computationally, the pyrolysis of char is one of the key reactions leading to the StF transition [198].

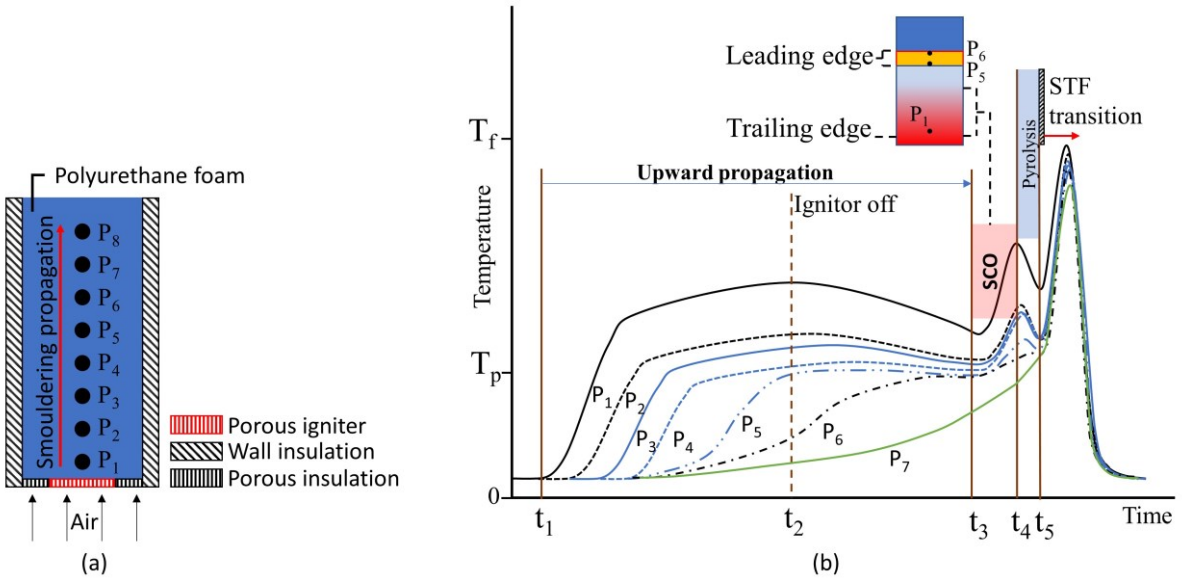

Figure 4.7. (a) Experimental setup by Torero and Fernandez-Pello [175]. (b) Schematic of the temperature distribution in the experiment that led to the StF transition. Figures are redrawn and simplified from the original in [175]. T_p and T_f are the temperatures at which PU foam undergoes pyrolysis (300°C) and the approximate flaming temperature of PU foam (900–1,000°C).

Once the oxygen concentration naturally increased again and mixed with the pyrolyzate gases bringing the mixture to within the flammability limits, StF transition occurred (t_5 in Figure 4.7b). This mechanism is consistent with the smouldering of cotton under asymmetric boundary conditions [193]. The asymmetric boundary condition was when one face of the cotton sample was closed by a concrete wall. Under this condition, the StF transition occurred due to the slower smouldering spread rate at the closed face than at the open face. One would argue that at the closed face, pyrolysis was more dominant than smouldering due to the insufficient oxygen supply because of the closure by the concrete wall. Pyrolysis provided pyrolyzates that were then ignited by heat provided by smouldering at the open face.

Figure 4.8a shows a visual observation of the StF transition in a 40-cm-long PU foam slab during upward propagation. In this experiment, one lateral face of the PU foam was exposed to radiant heat flux, the bottom face was in contact with a heater, and the top face as well as the three remaining lateral faces were insulated [1,169]. Chao and Wang [182] experimentally investigated the StF transition in PU foam in horizontal propagation under natural convection and found SCO prior to the StF transition. The probability of transition increased with the length of the PU foam.

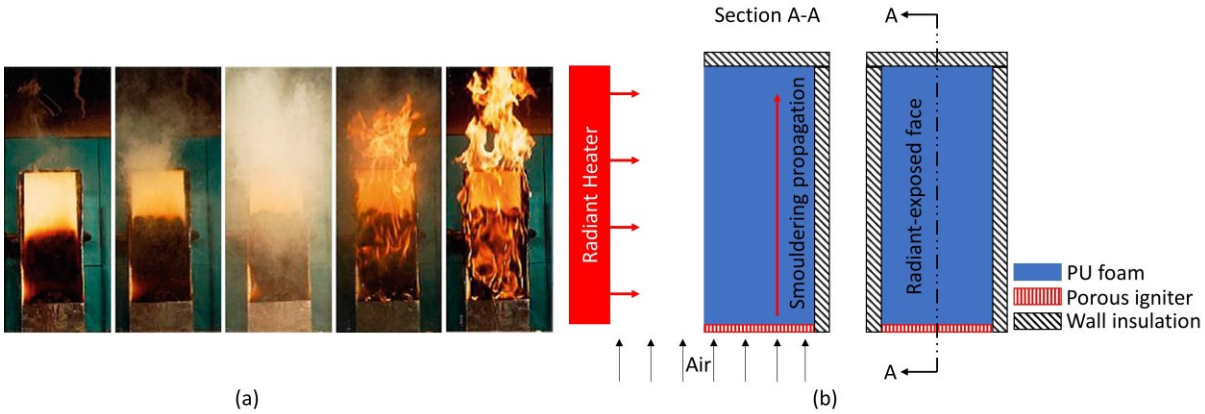

Figure 4.8. (a) Series of photographs of a combustion experiment illustrating the transition to flaming in a smouldering polyurethane slab 40 cm high under external forced flow (photo by the group of Prof. Carlos Fernandez-Pello, University of California at Berkeley). After 1 h of burning, only half of the sample smouldered (photo 1, far left). When the transition took place (photos 2 and 3), the whole sample was engulfed in flames in a few seconds (photos 4 and 5, far right). (B) Experimental setup of a series of works by Prof. Fernandez-Pello at the University of California at Berkeley, USA [39,178,180,181,198]. Figure is redrawn from the original version in [180]. Figure on the left shows radiant-exposed face of the figure on the right.

Recent findings on secondary char oxidation (SCO) were derived from collective works of smouldering PU foam with variable oxidiser supply and radiant heat flux, as shown in Figure 4.8b [39,178,180,181,198]. The location of the strong char oxidation upward from the smouldering front, thus located in the char layer upstream of the smouldering leading edge, was confirmed by Tse et al. [39], who measured the evolution of permeability inside the PU foam with ultrasonic imaging. The permeability substantially increased as char continued to react. This reaction leads to the formation of voids that provide favourable locations for combustible gas accumulation, thus favouring the StF transition. The SCO, which is more exothermic once reacted, acted as the ignition source for the accumulated gas in the void.

Putzeys et al. [180] measured the intensity of SCO and concluded that the direction of SCO was downward, while the primary smouldering front was upward. This SCO propagation direction was computationally proven by Dodd et al. [198], who developed a two-dimensional numerical transport model to predict the StF transition of PU foam in the study by Putzeys et al. [180]. In Dodd et al. [198] model, there are seven heterogeneous reactions with one global homogeneous gas-phase reaction. Four reactions were important in the model for the StF transition to occur. These reactions are the pyrolysis of thermal char, oxidation of α-char, oxidation of char that produces α-char, and flaming combustion of gaseous fuel. In this scheme, SCO is the oxidation of α-char. The results by Dodd et al. [198] for temperature and transition time agreed well with the experimental results by Putzeys et al. [180].

In the kinetic model in [198], secondary char oxidation (SCO) is important in providing gaseous fuel and heat required to ignite flaming combustion. This gaseous fuel is produced from SCO and thermal char pyrolysis. Thus, SCO provides gaseous fuel and heat. In addition to sustaining the thermal char pyrolysis which provides the pyrolyzates, heat also acts as the ignitor of the produced gaseous fuel/air mixture once it is above its lower flammability limit. This finding is related to the mechanism proposed by Torero and Fernandez-Pello [175]. To computationally reproduce the experimental work of smouldering cellulosic insulation in [171], Yang et al. [199] found that char oxidation and pyrolysis of cellulose provide gaseous fuel, while the ignitor is the hot char at the surface of the cellulosic insulation (Figure 4.9). There is no SCO in this model. In conclusion, gaseous fuel is simultaneously produced by char oxidation and pyrolysis reaction (Figure 4.9). Whether the prominent pyrolysis reaction takes place on unreacted fuel or char still needs to be determined.

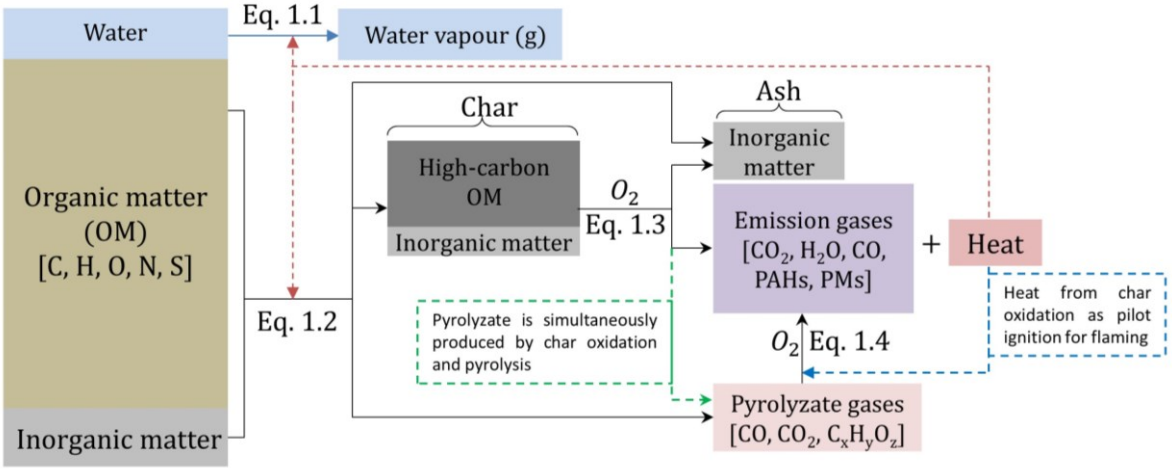

Figure 4.9. Reaction schematics of organic matter undergoing pyrolysis (Eq. 1.2), smouldering (Eq. 1.3), and flaming (Eq. 1.4). StF transition occurs when oxidation reaction of pyrolyate (Eq. 1.4) occurs alongside oxidation reaction of char (Eq 1.3). Solid black lines indicate reaction representing Eq. 1.2–1.4) in this paper; dotted red line indicates heat feedback from exothermic reaction; blue line indicates evaporation of MC in the fuel (Eq. 1.1); dotted green line indicates pyrolyzate gases production from char oxidation as concluded in [180,198,199], and dotted blue line indicates heat feedback from char oxidation that ignite flaming reaction as concluded in [39,175,180,198,199]. Figure after diagram in Lin et al. [200].

4.5. Permeability and consolidation

Two material properties that particularly seem to control the location of the transition are permeability and consolidation. Permeability is a property of a porous material that represents the ability of fluid to flow through that material [201]. This review proposes a material property, namely, consolidation, that represents a material's ability to not collapse during burning and thus remain

consolidated. For example, consolidated materials are synthetic polymers and solid wood (embers, timber, and tree trunks), and unconsolidated materials are peat soils and the litter layer made of loose materials such as peat grains, leaves, and needle vegetation. In organic soils, the degree of consolidation depends on the degree of decomposition of parent materials. For example, the presence of partially decomposed hardwood, natural fibers, and tree roots can make organic soils remain consolidated during burning, and once these parent materials are consumed, the organic soils become unconsolidated.

For consolidated materials with high permeability (e.g., PU foam) (Figure 4.10a), the location of the StF transition tends to be initiated within the material [39,178,180,181,198]. The high permeability of a material allows oxygen to flow inside the fuel bed. Consolidation of the fuel bed allows the fuel to remain intact as smouldering propagates within the material and forms void spaces. The formation of void spaces is confirmed by the increasing internal permeability of the fuel during smouldering prior to the StF transition [39,180]. This void then becomes the favourable space for gaseous fuel to accumulate. The heat produced from the more exothermic char oxidation will ignite the gaseous fuel in the void spaces (Figure 4.10a).

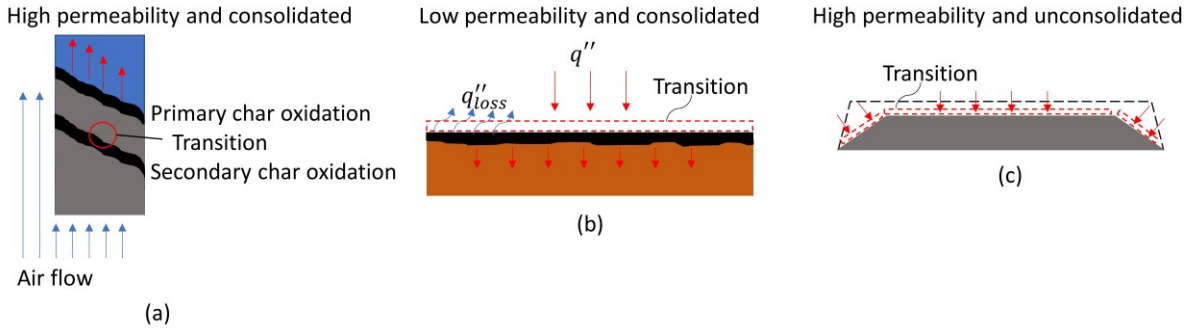

Figure 4.10. Smouldering-to-flaming transition location with respect to permeability and consolidation of the material. (a) High permeability and consolidated material, i.e., polyurethane foam, cotton cladding, upholstery material. (b) Low permeability and consolidated material, i.e. wood. (c) High permeability and unconsolidated material, i.e. dust layer, cellulosic insulation, and organic soil.

For low permeability and consolidated material (Figure 4.10b). Smouldering propagates at the surface of the material since the oxygen diffusion inside the material is limited. At the surface, the smouldering front also undergoes high convective heat losses. To be self-sustained, smouldering needed to be assisted with decreasing heat loss or external heat flux, i.e., a U-shaped fuel geometry to maximise radiation heat exchange between the smouldering surfaces or deposited embers on fuel bed surface [41,44,158,159,162,163,172,184]. Under this condition, the transition tends to occur at the surface of the material. Bilbao et al. [177] conducted an experiment with small *P. pinaster* wood, i.e., dimensions of 11 by 11 by 1.9 cm, under radiative heat flux and forced convection. They found that

radiative heat flux affected the time to StF transition more than convection did, implying that the low permeability of the material made the smouldering less dependent on airflow and that minimising convective heat losses by assisting smouldering with radiative heat flux governs the StF transition.

In high permeability and unconsolidated materials (Figure 4.10c), the fuel is not able to maintain its structural integrity during burning and thus immediately collapses during fuel consumption. The fuel in this category includes fuel beds made of dusts, cellulosic insulation, vegetation (grasses and pine needles), and organic soils. Most wildland fuels fall in this category, except wood, which is a consolidated fuel with low permeability. In the smouldering of this fuel category, the transition tends to occur at the surface of the fuel bed [43,167,171,183–185,199].

For solid fuels that have high permeability and an intermediate degree of consolidation during smouldering, such as peat, an overhang can form and collapse during fire spread [53]. An overhang is a temporary hanging surface of burning organic soil, where its intermediate layer below has been consumed (Figure 4.11). An overhang is formed because of the faster horizontal spread rate a few centimeters below the surface due to the reduced convective heat losses compared to the free surface of the organic soil fuel bed [1,53]. The collapse of the peat overhang is because the char layer is gradually consumed and can no longer support the weight of the above soil. Currently, in the literature, there is no mention of StF transition during overhang formation. However, the possible influence of intermediate consolidation of peat represented by overhang formation and collapse on the StF transition could still be explored since overhang formation and collapse are also recent findings, and their scope of influence on fire dynamics has not yet been identified.

One of the difficulties in mitigating peat fires is its propensity to spread deep below the ground [1,11,12], hence the deep penetration of oxygen diffusion to the smouldering peat. Considering permeability alone, subsurface smouldering propagation can lead to resurfacing of smouldering that can lead to a StF transition. The resurfacing of an underground smouldering front is made possible because of the consolidation of the char layer left behind by oxygen – limited smouldering propagation [100].

Another parameter found to affect the StF transition, in relation to permeability, is the particle diameter of the fuel bed. For natural fuel beds filled with particles, the permeability is proportional to the square of the particle diameter ($K \sim d_p^2$) [202]. The particle diameter also affects the heat exchange and mass transfer between the solid matrix and porous pores, thus influencing the chemical reactivity. With increasing particle diameter, the StF transition occurred at a lower critical velocity, which is the velocity at which the StF transition occurs. In smouldering dust beds, the StF transition did not occur when dust particles were < 0.1 cm [167]. An increase in particle diameter leads to an increase in the

total pore surface area and a decrease in the specific surface area (SSA: total surface area of the fuel bed per unit volume or mass) of the fuel bed. Song et al. [203] investigated the particle diameter effect on the reaction rate of a heterogeneous coal reaction. Knudsen (intra-particle) diffusion, which is the diffusion of a gas, in this case oxygen, into the interior of particles decreases with increasing particle diameter due to increasing pore surface area or permeability. The decrease in Knudsen diffusion decreases the overall reaction rate of coal oxidation by up to 50%. This finding is contrary to that by Palmer [167], where increasing particle diameter leads to an increasing tendency for the StF transition. The effects of particle diameter on the Knudsen oxidation rate and StF transition need to be investigated further. Currently, the influence of specific surface area to StF transition cannot be assessed at this point because there are no data available in the literature.

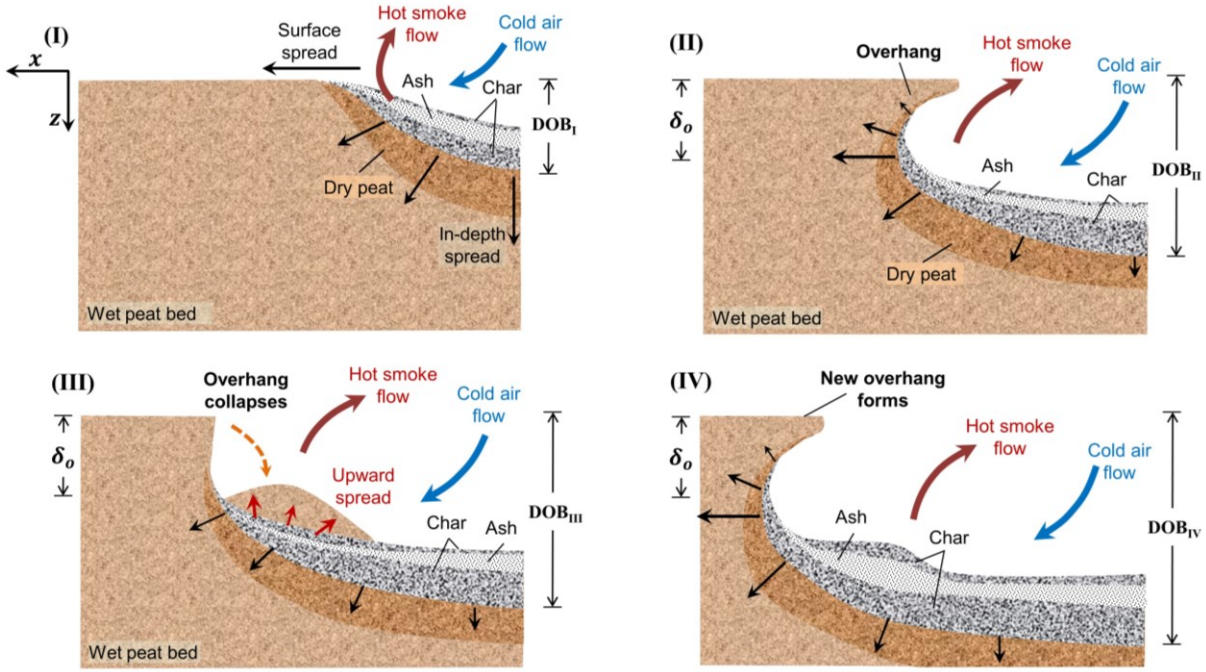

Figure 4.11. Schematic diagram for the periodic formation and collapse of overhang in smouldering spread over wet peat: (I) soon after ignition, (II) formation of the overhang, (III) collapse and consumption of the overhang, and (IV) formation of a new overhang. Illustration from [53] (X. Huang, CC BY license).

4.6. Embers and StF transition in wildfires

Embers contribute to the devastating spread of wildfires by being lofted in the fire plume and carried vast distances by strong winds [40,204,205]. Embers, commonly called firebrands and different from hot metal fragments, are combustible and rich in carbon. The accumulation of these embers can start local smouldering and, in some cases, exhibit StF transitions that result in fire spread far beyond the original fire front. This behaviour is also known as spotting (Figure 4.2). Field observations of StF are hard to find in the scientific literature, but a

few exist. Pagni [204] qualitatively described the 1991 Oakland Hills wildfire in California, USA, during which embers landed on a downwind region of high fuel load and led to a massive fires conflagration. The report mentions "flaming debris," but we can infer that this term represents a broad range of burning embers, including smouldering embers. This wildfire burned 600 ha, caused 25 fatalities and damaged 2,334 structures [204]. The wind was dry and of high velocity (~10 m/s), with a strong inversion layer of 600 m, and on a complex hill topography. Field observations of the role of smouldering ember were also recorded in the 1994 South Canyon Fire in Colorado, USA. This fire suddenly shifted from a slow surface fire to a fast crown fire, causing the deaths of 14 firefighters. The surface fire included flaming grass and smouldering litter, with occasional torching of individual trees, which when combined produced flying smouldering embers. This result could imply that the shift from low – to high – intensity fire could have involved the StF transition of smouldering embers. From the survey conducted after the January 1994 wildland fires in Sydney, Australia, 52 of the WUI materials were ignited by embers while the rest, i.e., 18, were ignited by radiation [206]. In another investigation, Maranghides and Mell [207] concluded that 55 of 74 destroyed homes were ignited by embers, 80 min before the arrival of the fire front. This is in agreement with Bell [208], concluding that radiation alone is rarely the cause of house to be lost.

Manzello et al. [183] investigated the ignition of pine straw mulch, shredded hardwood mulch, and cut grass by embers. Fuel MC was either dry or 11% MC and placed inside an aluminium foil pan with dimensions of 23 by 23 by 5.1 cm. The StF transition occurred when four smouldering firebrands 50 mm in diameter were deposited on the samples and exposed to an airflow of 1 m/s. This airflow was lower than the critical velocity of 2 m/s for the StF transition in cellulosic insulation [171], which may be due to the difference in material or the enhanced radiation feedback between the sample and the firebrands, resulting in more intense smouldering.

To focus the investigation on the ignition of fuel beds, embers can be represented as hot metal particles [43,209]. This approach eliminates the complexity of the ember reaction process, its variable heat release, and coupled heat transfer interaction between the fuel bed and embers. In addition to these conveniences in investigating fuel bed ignition by hot metal particles, real wildfires are often initiated and accelerated by hot metal particles from clashing power lines and machine processes, such as grinding and welding [40]. A smaller particle size leads to a higher temperature required for the flaming ignition of cellulosic fuel beds [209]. Particles as small as 19.1 mm with a temperature of 650°C can initiate flaming combustion. Embers with sizes ranging from 25 to 50 mm have been found in studies investigating StF transitions [41,44,183,184]. In pine needle beds, the time to StF transition was ~2.5–5 min at particle temperatures within the range of smouldering temperatures, ~630–700°C [43].

For drier fuel, the StF transition propensity increases, represented by the decreased StF transition time to as short as ~2 min in fuel with ~6% MC. In all cases, a larger particle size requires a lower particle temperature to initiate the StF transition in pine needles at higher MC. In comparison, an increasing particle size from 8 to 14 mm at a particle temperature of 925°C placed on a fuel bed at 25% MC can lead from no ignition to the occurrence of a StF transition in pine needle beds. Another interesting finding related to hot metal particle ignition is the effect of the melting process of the metal. It was found that the melting of hot metal particles increases the propensity of smouldering ignition [210].

Considering the fire hazard of embers to WUI fuels, Manzello et al. [41] investigated the showering of firebrands on roofing assemblies. Roofing assemblies were varied into three configurations: (1) valley configuration of only base material, i.e., oriented strand board (OSB); (2) valley configuration of full roofing assembly, i.e., OSB, tar paper, and shingles; and (3) flat configuration of the roofing assembly with gutters filled with dried pine needles and leaves. A StF transition occurred on the (1) valley configuration of only base material and on the (3) flat configuration of the roofing assembly with gutters filled with dried pine needles and leaves. In configuration 1, the StF transition only occurred when the valley configuration was set at a 60◦ angle. The StF transition occurred due to the accumulation of firebrands in the crevice. The onset of the StF transition was on the back side of the OSB. In this case, the StF transition was due to the chimney effect, as discussed in the section The Chimney Effects. The chimney effects was more significant in this case than in the case of upholstered furniture fire due to a smouldering cigarette because the embers continuously accumulated in the crevice. In configuration 3, the StF transition was inside the gutter in the dried pine needles and leaves. The flame did not spread up to the roofing assembly. However, it was able to melt the shingles. It is not discussed whether flaming was preceded by smouldering of the dried pine needles and leaves or went directly to flaming. The time to StF transition was not recorded; however, the experiment was carried out in 6 min, and the StF transition occurred within that time frame. This StF transition time was significantly shorter than the recorded time of the StF transition in the upholstered furniture fire tests due to a smouldering cigarette, i.e., between 20 and 132 min [194–197]. Extrapolating the scenario of flaming from accumulated vegetation in the gutter, the melted shingles can lead to exposed wood roofing structures. With consistent ember showers lasting longer than 6 min and pre-heated and aged shingles, WUI fires can spread substantially through this mechanism.

The short time to the StF transition in wildland and WUI fuels due to embers certainly shows the scale of wildfire threat, representing sudden fire spread in distant locations. More focused studies closely investigating the mechanism leading to the StF transition of the fuel due to embers are needed. Currently, in the literature, it is not clear whether the StF transition of the fuel is preceded by

sustained smouldering of the fuel or only by pyrolysis of the fuel. In the former case, smouldering or flaming embers ignite smouldering of the fuel up to the point where the fuel is self-sustained and spread is uninfluenced by heat from the embers. This self-sustained smouldering later transitions to flaming. In the latter case, the StF transition was piloted ignition of pyrolyzate from the fuel by smouldering embers. Thus, pyrolysis is supported by heat from smouldering embers, and flaming ignition of the fuel occurs in the vicinity of embers where heat is most available. In this case, the StF transition of the embers could also precede flaming ignition of the fuel, where flaming embers act as a heat source for the fuel pyrolysis reaction and pilot ignition of the pyrolyzates from the fuel [44]. The comparison of these two cases shows that the embers enhance flaming ignition of the fuel more in the latter case than in the former case, assuming that self-sustained smouldering can take a long time to establish and has equal probability to extinguish as to transition from StF.

Valdivieso and Rivera [185] investigated the StF transition in self-sustained smouldering of pine needle fuel beds with dimensions of 60 by 15 by 4 cm and, interestingly, they observed that the StF transition is a cyclic transition from smouldering to flaming to smouldering up to the point at which the whole fuel bed is consumed. This cycle occurred with a wind velocity of 1.1 m/s and a fuel MC of 69% (dry mass basis). This cycle was also found in the StF transition of a cellulose fuel bed by Ohlemiller [171], and was argued to be caused by smouldering fronts that provide heat and pre-heated gaseous fuel. Because the smouldering process is at a lower rate than flaming, the gaseous fuel supply from smouldering fronts soon becomes insufficient to provide self-sustained flaming. In other words, self-sustained flaming could be established if the heat feedback from flaming is sufficient to increase the smouldering rate at a required level of gaseous fuel production. Another way to interpret this cycle is that gaseous fuel is provided by in – depth pyrolysis of fuel. As smouldering progresses, the char layer forms and becomes thick enough to insulate the fuel, decreasing the pyrolyzate diffusion rate to flow outside the fuel bed to mix with oxygen. As smouldering progresses further, the char layer is consumed and becomes thinner. Under this condition, the pyrolyzate diffusion rate increases again and mixes with oxygen. The StF transition occurs once the pyrolyzate/oxygen concentration is above the lower flammability limit. However, whether the StF transition depends on the pyrolysis of unreacted fuel/char or the oxidation of char remains to be determined and could be fuel and experimental – setup – dependent.

In general, currently there is insufficient statistics and observations of StF transition in field – scale wildfire. These statistics and observations are much – needed data to identify the large gap in the understanding of StF transition and wildfire spread. Largely, rekindle can be initiated by residual smouldering fuel, i.e., wood log, embers, and duff layer, transitioned to flaming, thus starting a new fire front. During the Portugal wildfire in the summer of 2010, rekindle accounted

for an additional 2,497 fires [211]. This put a massive burden to firefighters as they need to revisit a reignited fire while under immense pressure to suppress other untreated fires. Pacheco et al. [211] discussed the importance of mop – up operation to avoid rekindle. A recent example of rekindle was Canyon Fire 2 in California in October 2017, in which the fire was likely to be started by strong winds pushing smouldering embers from previous fires in late September in the same area [212]. Rekindle is also an issue when fires survive winter and reignited once weather is warming. This is especially a concern when fires could spread onto organic soils, which is essentially providing a massive amount of fuel supply [213]. Fires in organic soils have been known to survive under sub-atmospheric oxygen concentration and very wet conditions [1]. An example of this is the October 1997 fire in Yeodene peat swamp, Australia. Three weeks after suppression, the fire was thought to be fully extinguished by means of visual observation and infrared signature from aerial operation. However, in March 1998, the fire reignited and burnt 680 ha of the peat swamp area [214]. Due to the unknown cause of the fire, Gunning [214] also mentioned the possible rekindle of fire in 1881, 1886, 2006, and 2010, emphasising that rekindle possibility can span across years.

4.7. Conclusion

In this chapter, 28 studies of StF transition reported in English published from 1957 to 2019 have been reviewed. As shown in Table 4.2, wildland fuels need more attention in terms of their combustion behaviour and StF transition, as only three of the 28 studies observed StF transitions in wildland fuels. By critically reviewing findings in the literature, oxygen supply and heat flux are identified as the primary variables governing the StF transition. Specifically, these two parameters govern the StF transition in fuel subject to external airflow, fuel in a narrow vertical channel configuration, and fuel that undergoes more exothermic SCO. Afterwards, a fuel classification based on the permeability of the fuel and the ability of the fuel to remain consolidated during burning is proposed. These two properties of the fuel affect the oxygen supply and heat transfer during fuel combustion, thus affecting the StF transition.

In essence, the StF transition is a spontaneous gas-phase ignition supported by the heat and reaction from smouldering [39,169,178,180,181,199]. Mechanisms leading to StF transition are governed by complex interactions of heat transfer and chemistry. From studies of widely different experimental setups on samples ranging from 0.1 to 1.2 m (Table 4.2), two variables are found to govern the StF transition, i.e., oxygen supply and heat flux. Airflow has a dual effect on smouldering. Airflow increases the oxygen supply to the fuel, thus increasing the reaction rate of an oxygen-limited spread, which favours the occurrence of the StF transition, but it also increases convective heat losses from the smouldering front, thus decreasing the tendency of the StF transition. The external supply of heat

flux minimises heat loss and assists the fuel heating required for self-sustained smouldering progress and pyrolyzate production. Assistive fuel heating can be in the form of external heat flux such as embers in the case of WUI fires or from pertinent features of the fuel configuration such as when heat loss is minimised by the possible presence of radiation exchange between smouldering surfaces, i.e., smouldering at the fuel crevice or smouldering in U-shaped fuels [41,44,158,159,163,172,186,188,192].

Vertical channel formation in smouldering at a crevice leads to radiation exchange between smouldering char surfaces and the chimney effect, increasing airflow from the buoyant flow [41,188,192]. The radiation exchange between smouldering surfaces leads to more effective heating, while buoyant flow increases the oxygen supply to smouldering fronts. The radiation exchange between surfaces minimises the convective cooling effect from the increased buoyant airflow. This mechanism is most relevant to WUI fires [41]. The StF transition is favourable at crevice locations in between smouldering fuels, i.e., embers at crevices of wood decks or house roofing, leading to increased buoyant flow through a vertical channel insulated by the char layer, thus minimising heat losses.

Strong char oxidation triggers a StF transition, as it provides heat to accelerate gaseous fuel production from pyrolysis and to ignite gaseous fuel [39,175,178,180,181,198,199]. Whether pyrolysis takes place in unreacted fuel or char remains to be determined. SCO represents a sudden increase in the exothermic reaction rate at the smouldering trailing edge and releases more heat than the previous char oxidation at the same location. The role of this strong char oxidation in providing the required gaseous fuel, and regarding its sequentially secondary nature, needs to be further explored in different types of fuel and experimental setups.

Permeability and consolidation of the fuel bed control the location of the StF transition. Both parameters control the propagation of smouldering fronts, ultimately dictating the location of the StF transition [39,180,198]. Permeability controls the diffusion of oxygen penetration into the fuel bed, while consolidation controls the availability of space for smouldering to propagate within the fuel bed. Consolidated fuel with high permeability, such as open-celled polyurethane foam, tends to have a transition initiated close to the surface but within the fuel bed. Consolidated fuels with low permeability such as wood and unconsolidated fuels with high permeability such as cellulosic insulation tend to undergo transition at the surface. In a fuel bed such as peat, which is highly permeable and unconsolidated, overhang formation and collapse could alter the StF occurrence due to intermediate production of a char layer that has a tendency to hold its structural integrity but lose it once undergoing further smouldering, leaving only ash.

Deposited embers on a fuel bed increase the propensity of StF due to the embers' role in assisting the fuel heating process. In wildfire propagation, embers

contribute to spotting and the quick initiation of new flaming sites [40,155,157]. The recorded StF transition time from studies of embers deposited on WUI and wildland fuels is < 10 min and decreases with drier fuel [41,201]. With the predicted drier climate in the future, faster and more widespread propagation of WUI fires is to be expected. Considering that population movement contributes to the increase in WUI fire frequency [26,215–217] and that current WUI fuels are vulnerable to StF transitions due to embers [162], more studies should investigate the design of smouldering – resistant material in the WUI area. Fundamentally, this calls for a better understanding of the StF transition mechanism.

This chapter synthesises the research, identifies regions for further research, and provides information on various StF transition mechanisms in the literature. These mechanisms converge on two fundamental aspects, heat transfer and chemistry. As airflow has a chemical effect (providing oxygen for the exothermic reaction) and a heat transfer effect (convective cooling), vertical channel formation also similarly provides more oxygen (chemistry) from the buoyant effect and a more effective heating process from radiation exchange between smouldering char surfaces (heat transfer). A better understanding of heat transfer and the chemical reactions of the StF transition mechanism can lead to prospective opportunities to better mitigate wildfires and protect the WUI. In Chapter 5, a laboratory study conducted to study the effects of wind, thus oxygen supply and heat loss, on StF transition is presented.

Chapter 5

The effects of pulse and continuous wind on the transition from smouldering to flaming combustion on wood

Summary[6]

Two combustion types, flaming and smouldering, are present in fires and one can led to the other. The transition from smouldering to flaming (StF) represents a drastic increase of fire hazards in terms of temperature, spread rate, and thermal power. Currently, the understanding of the mechanism of StF transition is limited to a small number of studies in the literature implying the role of air supply in providing competing effects on StF transition: positively by providing more oxygen, and negatively by taking heat via convective heat loss. Furthermore, the literature has only studied continuous wind while variation of wind speed occurs naturally especially in wildland environment. In this study, StF transition on a wood sample has been investigated in a rig designed to study the role of pulse wind. The rig designed in this study is characterized with wind temperature and speed errors of up to 4 and 11%, respectively, providing repeatable and reliable times for StF transition. With surface dimension of 10 × 10 cm2 and above the critical wind speed value of 3.1 m/s, the time to StF transition decreased with wind speed. Smouldering was not self-sustained with wind speed below 1.9 m/s, and no StF transition with wind speed between 1.9 to 3.1 m/s. The role of wind on oxygen supply on the StF transition is identified to be significant up to 9.1 m/s, above which the effect of oxygen supply is balanced by convective heat loss. With pulse wind, StF transition can take place up to ~5 min earlier. This indicates that pulse wind enhances the StF transition by first providing oxygen supply; and then once wind stopped, increasing the flow time and the concentration of pyrolyzates. The results from this study contribute to the understanding of StF transition mechanism.

[6] This chapter is based on "Muhammad A. Santoso[CO], Eirik G. Christensen[CO], Guillermo Rein. The effects of pulse and continuous wind on the transition from smouldering to flaming combustion on wood. (to be submitted)"

5.1. Introduction

The literature review of StF transition in Chapter 4 reveals that transition is governed by two processes, i.e. chemistry and heat transfer. Specifically, wind speed has been identified to influence StF transition occurrence [43,170–172,178,185], and fundamentally has two competing effects on combustion process, i.e. oxygen supply and convective heat loss. In this chapter, the systematic investigation of wind effects on StF transition is presented. To focus on the fundamental influence of wind on StF transition, a solid fuel (wood slab) was chosen as the sample in this study. It is because this type of fuel has been observed to undergo transition to flaming during field experiments in Chapter 2 (Figure A 2.9B), is easier to handle than peat and the mechanical disturbance effect of wind to particulate sample such as peat can be avoided. This chapter provides findings on the fundamental mechanisms on the effect of wind on StF transition in terms of transition time, transition probability, and the competing effects of chemistry and heat loss.

5.2. Experimental method

In this study, the StF transition was investigated on untreated *pine* sample. The sample was 10 × 10 cm^2 and 2.7 cm depth. Prior to an experiment, the sample was dried for 48 hours in 80^oC oven. Thus, the sample in this experiment can be assumed to be 0% MC, enabling this study to solely focus on the effect of airflow on StF transition, without disturbance from natural variation of wood MC. In addition, the typical range of wood MC of 10 to 20% has been reported to only contribute to 18% variation in charring rate [218]. However, this is not claiming that MC is not significant to StF transition, rather that the full understanding of StF transition is yet to be obtained. In another study, [219] found that the ignition time and critical mass flux (CMF) for sustained flaming of *poplar* wood increase with MC (ranged from 0 to 18% MC), indicating that MC might also affect StF transition occurrence. However, this MC effect is not currently investigated in this study which solely focus on the effect of airflow velocity on StF transition.

Figure 5.1 shows the experimental rig in this study designed to investigate the effect of wind on the StF transition of a burning wood. The wind supplied by a blower (no. 6 in Figure 5.1) connected to a control unit (no. 7 in Figure 5.1) to maintain the airflow velocity. A heating coil was placed in the blower and the temperature was regulated using a thermocouple mounted near the outlet of the blower connected to a PID controller. In this study, the wind temperature was maintained at 30.5 ± 1.3^oC. Measurements made in this study were mass loss (Mettler Toledo balance, resolution 0.01 g), visual and infrared (IR) imaging of the surface spread (GoPro and FLIR camera) and temperature-time histories using thermocouples (K-type thermocouples, 3 on the sample surface and 1 at the centre – 1.35 cm depth of the sample). Due to the wind exposure, the mass data was noisy

and filtered by Fast Fourier Transform – Moving Average (FFT-MA) across 30 s window.

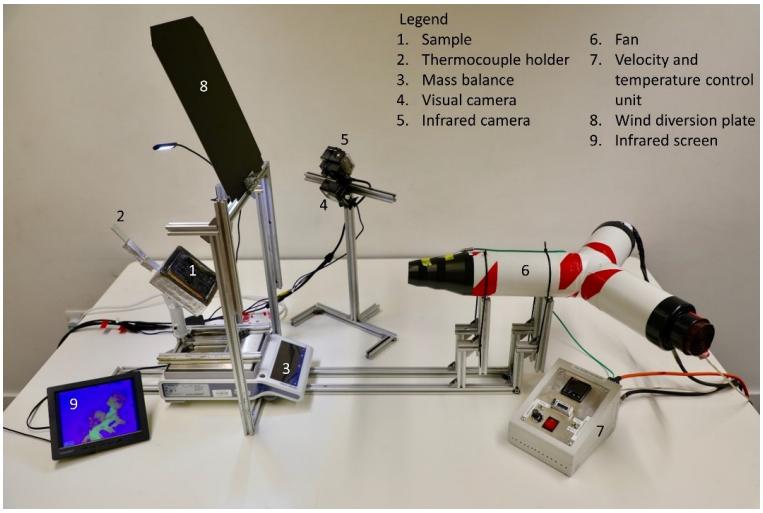

Figure 5.1. Diablo experimental rig. The name of the experimental rig refers to the hot and dry wind that occurs in the San Francisco Bay Area, contributing to the ignition and rapid fire spread in Northern California, USA [220]. The experimental rig aims to study the effect of wind on the StF transition of a burning wood by regulating both the wind velocity and temperature. (Photograph credit to Wuquan Cui).

Smouldering was ignited by exposing the samples to an incident heat flux of 25 kW/m^2 from a cone heater for 10 min. During the ignition, the sample was already placed inside the reactor, with thermocouples placed on the sample surface and in 1.35 cm depth through the bottom face of the sample. This irradiation level was sufficient to establish smouldering combustion but low enough to avoid flaming ignition of the sample [221–223]. Ignition procedure in this study also agrees with [224] in which white pine sustained smouldering under incident heat flux of 25 to 69 kW/m^2 for 12 to 15 min. Figure 5.2 shows a typical surface temperature of the sample in this study during ignition. The surface temperature increases rapidly at the early stage of ignition and then slowing down due to char layer formation. The steady state temperature reached after about 6 min of ignition and stayed at about 500^{o}C. This temperature well above the onset of wood smouldering identified in [221], i.e. 422^{o}C, and well below flaming ignition temperature of 754^{o}C [221], which obtained after 20 min exposure of 40 kW/m^2 heat flux. In another study with 10 × 10 cm and 3.8 cm depth of Canadian white spruce [225], the surface temperature after exposed to transient heat flux increasing linearly to 25 kW/m^2 at 10 min was constant at ~400^{o}C with no flaming ignition. Thus, the ignition procedure conducted in this study agrees well with the heat flux and exposure time in the literature to obtain smouldering ignition but well below conditions to incite flaming ignition.

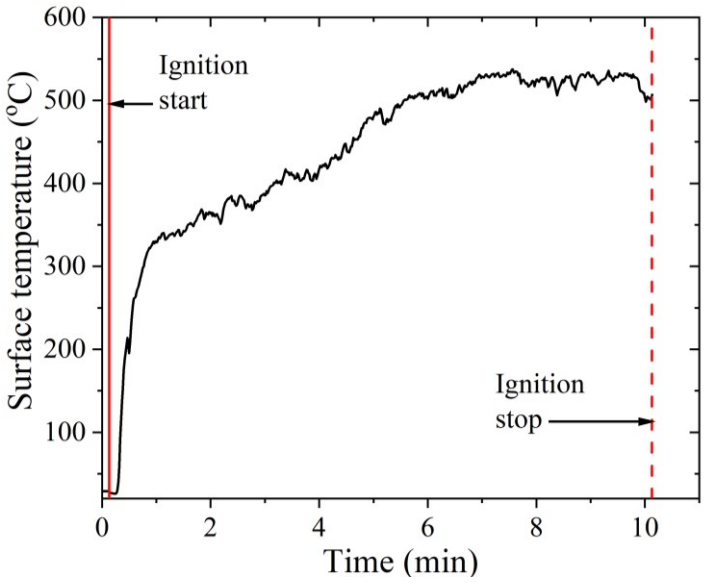

Figure 5.2. Typical surface temperature of a sample during ignition protocol. The ignition protocol was exposing the sample with irradiation of 25 kW/m^2 for 10 min to obtain smouldering ignition but low enough to avoid flaming ignition.

After ignition conducted, the sample then immediately placed to the experimental rig, inside a reactor on top of a holder plate (no. 1 in Figure 5.1). The reactor was built using ceramic insulation boards (k = 0.7 w/m-K, ρ = 310 kg/m^3, c_p = 1090 J/kg-K), with internal dimension of 10 × 10 cm and 2.7 cm depth, to fit the sample with the same size. The reactor then placed on top of a holder plate with adjustable angle. In this study the angle of the reactor was set constant at 45^o (Figure 5.1). This angle enables the exposure of stagnation flow from the fan but with clear visual observation when flaming occurs. The effect of angle, thus resulting in a different wind profile when reaching on the sample surface, on the occurrence of StF transition was not investigated in this study.

The sample was exposed to 6 different wind conditions, 1.9, 2.6, 3.1, 6, 9.1, and 11.8 m/s. The flow profile was characterized for each of these wind speeds by measuring the wind velocity at several points at the rim height (xy plane) of an empty reactor using a hot wire at several measurement points (Figure 5.3B). Figure 5.4 shows the characterized wind velocity on the six settings, obtaining tip velocity ($V_{a,t}$) at the center of the sample at 1.9±0.2, 2.6±0.1, 3.1±0.02, 6±0.1, 9.1±0.1, and 11.8±0.1 m/s. These tip velocities correlate to the average of the velocity profile at 0.81, 0.95, 1.18, 2.14, 3.14, 3.96 m/s, respectively. Due to the orientation of the sample relative to the wind direction, the wind profile upon arrival to the sample surface will behave relatively similar to a stagnation flow. Thus, the reporting of the velocity variable in the subsequent discussion will be made based on the tip velocity rather than the average of the wind profile since the latter is not representing the boundary condition likely to be made when the characterized flow meet the sample surface.

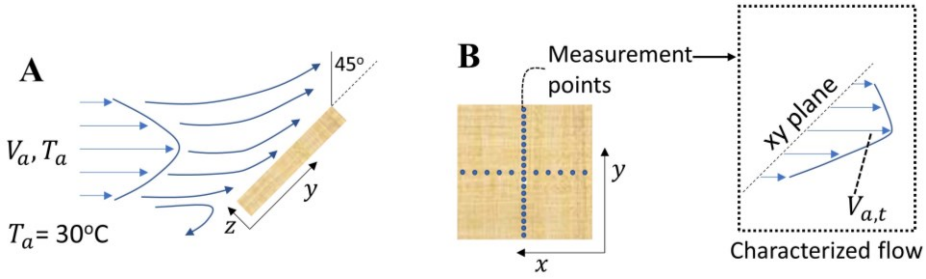

Figure 5.3. Schematic of sample orientation to the wind direction. (A) Side view schematic of the sample placement showing the 45° orientation of the sample to the flow direction and (B) measurement points of the flow profiles characterization.

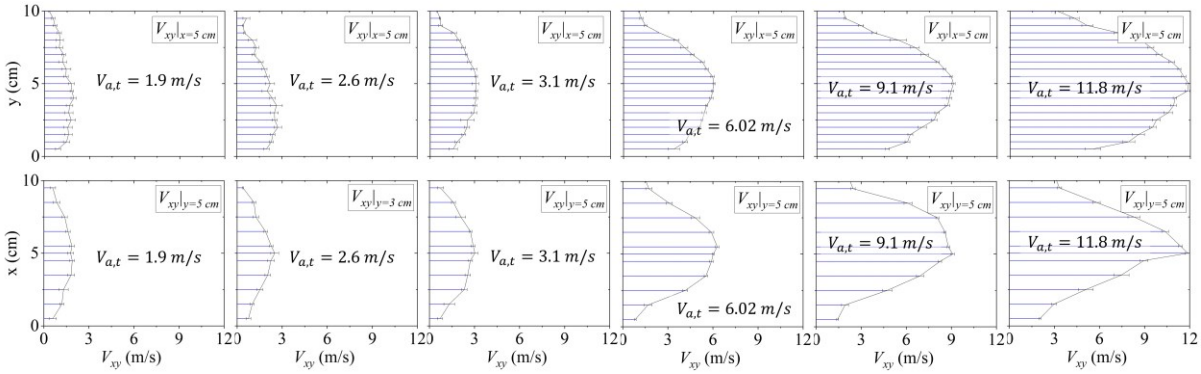

Figure 5.4. Characterized flow at the six settings resulting in six different flow velocity profiles with tip velocity of 1.9, 2.6, 3.1, 6, 9.1, and 11.8 m/s, at the center of the sample surface. The flow characterization was made at the rim height of the reactor (xy plane in Figure 5.3B). Above figures are V_{xy} at x = 5 cm and bottom figures are V_{xy} at y = 5 cm, except for $V_{a,t}$ = 2.6 m/s where the bottom figure is V_{xy} at x = 3 cm.

Two series of experiments were conducted in this study, i.e. continuous wind and pulse wind. In continuous wind experiment, the wind was continuously exposed to the sample surface until either the sample completely consumed or extinguished. In this experiment series, the StF transition may occur during the wind exposure. The sample was deemed to be extinguished when the in-depth TC in the sample decreased below 100°C, no elevated temperature from surface TC, and there was no visible glowing char on the sample surface. Figure 5.5 shows an example of mass and temperature data of a sample which extinguished with no wind exposure. Without wind exposure, the sample burning rate, indicated by the mass loss rate, was decreased significantly in the first 5 min and then slowly extinguished at ~20 min, indicated by the decreasing in-depth temperature below 100°C. Thus, the sample in this experiment, i.e. untreated pine wood with dimension 10 × 10 cm^2 and 2.7 cm depth, will not self-sustain smouldering without the assistances of irradiation or wind to provide heat and oxygen supply. This figure also shows that at the start of the experiment, after the sample removed from the cone heater and immediately placed at the sample holder, the mass loss rate (MLR) was at ~1.8 g/min. This indicates that the sample was still smouldering

[219] and the time gap between the removal of the sample from the cone heater to the start of the wind exposure was not significant to the burning of the sample and the results presented in this study.

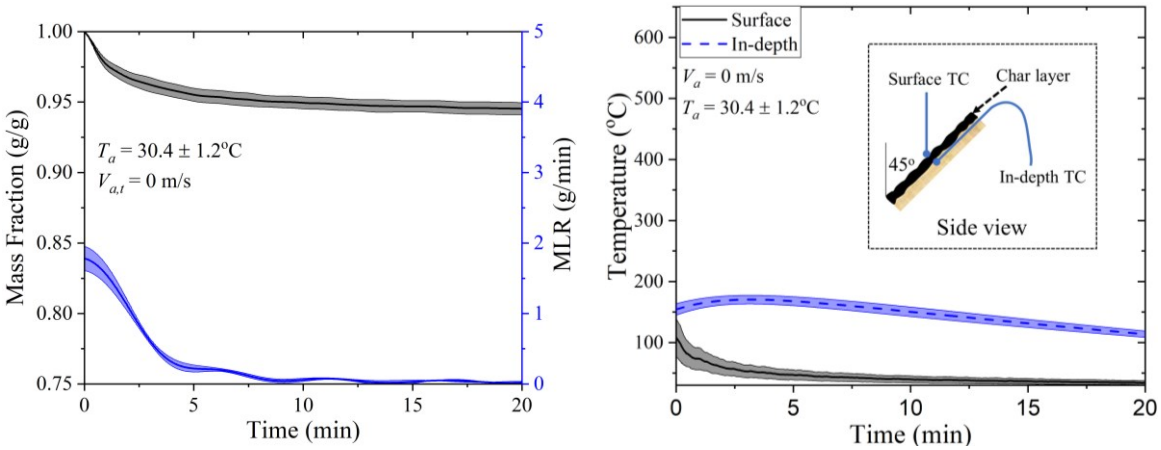

Figure 5.5. Experiment results with no wind exposure. (a) Average mass fraction (g/g) and MLR (g/min) of the sample, and (b) Surface and in-depth temperature of the sample. Clouds in these plots represent standard deviation from three experiments.

Table 5.1. Matrix and summary of the total number of experiments conducted in this study. The temperature of the wind was maintained at 30.5 ± 1.3°C.

Wind speed (m/s)	Continuous wind	Pulse wind	
	Number of experiments	Number of experiments	Range of wind exposure duration (min)
0	3	Smouldering was not self-sustained	
1.9±0.2	3		
2.6±0.1	3	7*	5 to 50
3.1±0.02	5	15	3 to 13
6±0.1	4	10	1.3 to 5
9.1±0.1	5	7	0.2 to 1
11.8±0.1	5	7	0.1 to 0.6

*Smouldering was weakly self-sustained and StF transition only occurred 1 out of 3 experiments in continuous wind experiments. The flaming from the StF transition was also not self-sustained and only lasted for ~4.5 min. In pulsed wind experiments, no StF transition was observed.

In pulse wind experiment series, the wind exposure was stopped at a specified time by closing the wind diversion plate (Figure 5.1). This experiment series was conducted to investigate whether a sudden wind stop contributes to StF transition. In case of continuous wind exposure, the wind may disperse the pyrolyzate gases causing the StF transition to be delayed to a point in which the pyrolyzate production rate overcome the dispersion effect from the wind advection. With pulse wind experiments, the time at which StF transition occurred if there

is no wind advection can be identified. The wind exposure duration was increased gradually until StF transition consistently occurred upon the closing of the plate. In example, at $V_{a,t}$ = 6 m/s, 10 experiments with different exposure duration (1.5 to 5 min) were conducted where StF transition consistently occurred with exposure duration more than 4 min. Table 5.1 shows the matrix of experiments conducted in this study.

5.3. Results and discussions

5.3.1. Continuous wind exposure

Figure 5.6 shows the mass fraction and mass loss rate (MLR) from continuous wind experiment series across six wind exposures. At $V_{a,t}$= 1.9 ± 0.2 m/s (Figure 5.6A), smouldering was not self-sustained and the MLR drastically decreased in the first 5 min followed by complete extinction at ~10 min. This implies that oxygen supplied by the wind at this speed was not sufficient to maintain char oxidation. At $V_{a,t}$= 2.6 ± 0.1 m/s (Figure 5.6B), smouldering weakly sustained and self-sustainability of the smouldering is uncertain. In all of the three experiments conducted at this wind speed, MLR in all experiments were drastically decreasing in the first 5 min to ~0.5 g/min followed by extinction at 23.1, 73.7, 133 min in each of the 3 experiments. StF transition occurred at 1 of the 3 experiments at this wind speed, when the smouldering sustained until 133 min. The flaming occurred at t = 18.9 min, but only last for 4.5 min despite continuous wind supply. Thus, at $V_{a,t}$= 2.6 ± 0.1 m/s, smouldering was weakly self-sustained and the StF transition occurrence was inconsistence.

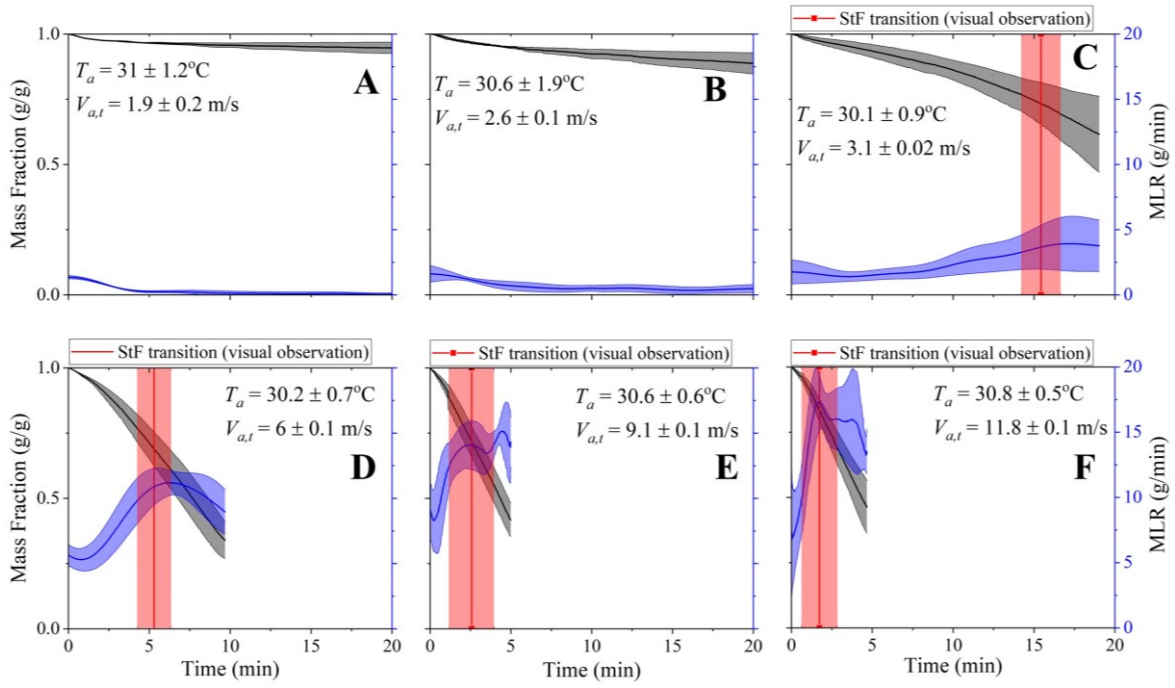

Figure 5.6. Mass fraction and mass loss rate from continuous wind experiment series showing StF transition consistently occurred from $V_{a,t}$= 3.1 ± 0.1 m/s. Clouds represent

standard deviation from experiment repetitions. (A) Experiments at $V_{a,t}$= 1.9 ± 0.2 m/s (2 repetitions). (B) Experiments at $V_{a,t}$= 2.6 ± 0.1 m/s (2 repetitions). StF transition occurred in 1 out of 3 experiments at t = 18.9 min (not shown here). (C) Experiments at $V_{a,t}$= 3.1 ± 0.02 m/s (4 repetitions). StF transition occurred in all 5 experiment at t = 15.4 ± 1.2 min. (D) Experiments at $V_{a,t}$= 6 ± 0.1 m/s (3 repetitions). StF transition occurred in all 4 experiment at t = 5.3 ± 1 min. (E) Experiments at $V_{a,t}$= 9.1 ± 0.1 m/s (4 repetitions). StF transition occurred in all 5 experiment at t = 2.6 ± 1.4 min. (F) Experiments at $V_{a,t}$= 11.8 ± 0.1 m/s (4 repetitions). StF transition occurred in all 5 experiment at t = 1.7 ± 1.1 min.

At higher wind speed, from $V_{a,t}$ = 3 to 12 m/s, StF transition occurrence was consistent (Figure 5.6C to F), occurring in all experiment repetitions. Figure 5.7 shows snapshots of experiments at 3, 6, 9, and 12 m/s, showing the sample surface underwent smouldering at the start of the experiment to the StF transition up to the time when sample almost fully consumed. During ignition, the sample underwent strong smouldering indicated by glowing surface. Upon removal from ignition all sample ceased to glow and the surface of all samples were charred. However, as has been previously discussed and shown in Figure 5.5, the smouldering char was not extinguished yet. The time gap between sample removal from the cone heater to the start of the experiment was ~40 to 50 s. After 1 min of wind exposure at 3 to 12 m/s (Figure 5.7A to D), all the sample underwent strong glowing smouldering again, with different intensity according to the wind speed. At 3 m/s, burning rate was 2.5 ± 1.4 g/min and glowing smouldering propagate slowly on the sample surface. The propagation started at patchy locations, indicating preferable locations for smouldering to sustained in low oxygen supply rate. The cause of these separate locations of the start of smouldering propagation is uncertain, which probably caused by several factors such as non-uniform wood composition across sample (cellulose, lignin, and hemicellulose), non-uniform density and MC, grain direction or might be related to cracking lines which were formed during char layer formation.

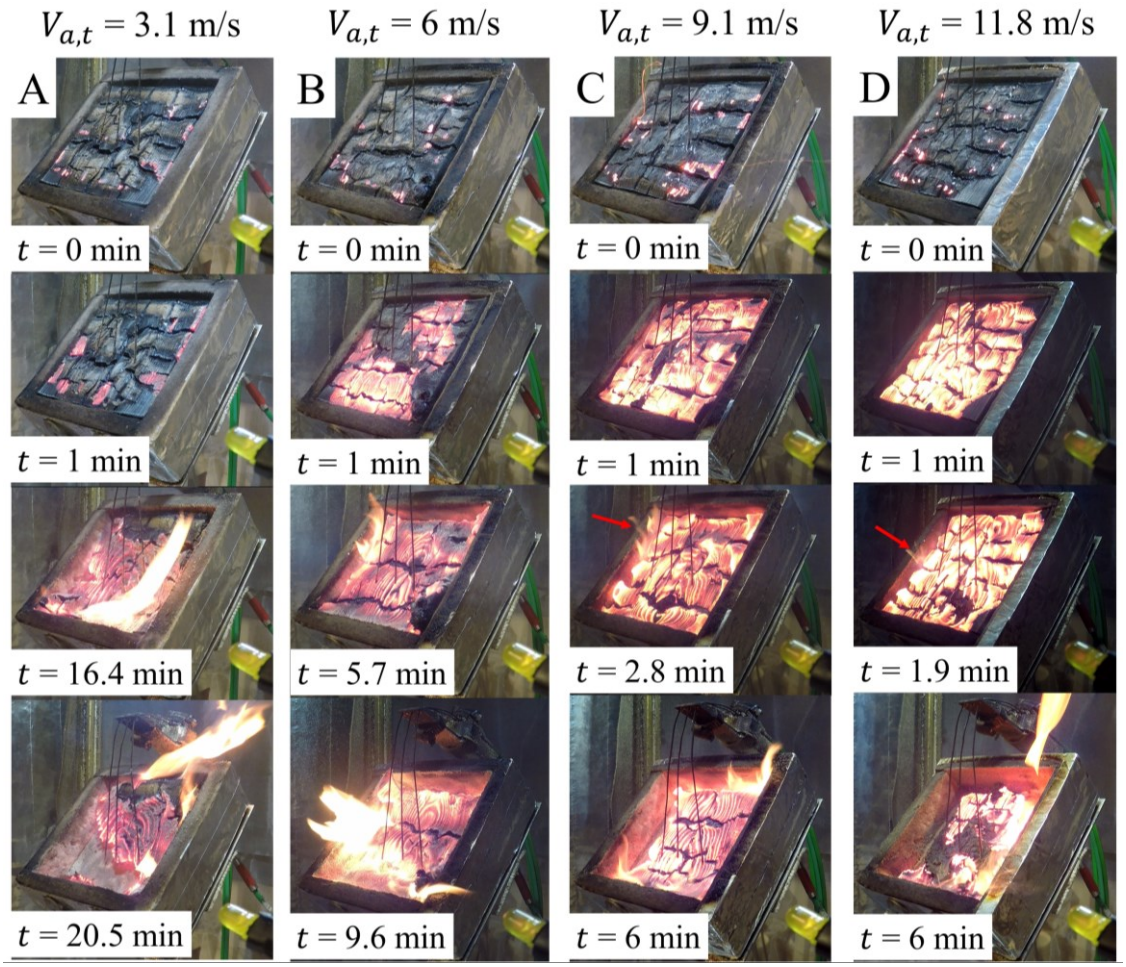

Figure 5.7. Snapshots of smouldering sample surface across different wind speed and time, from the start of the expertiment to the StF transition occurrence to the decay of the sample. (A) $V_{a,t}$ = 3.1 ± 0.02 m/s. (B) $V_{a,t}$ = 6 ± 0.1 m/s. (C) $V_{a,t}$ = 9.1 ± 0.1 m/s. (D) $V_{a,t}$ = 11.8 ± 0.1 m/s.

At higher wind speeds, i.e. 6 to 12 m/s, the burning rate increased and strong smouldering spread more uniform across the sample surface, indicated by more uniform glowing on the sample surface at 1 min of experiment. During continuous wind exposure, StF transition was mostly indicated by flaming appearance near the edge of the sample. This might be related to the relatively stagnant flow at the sample surface. With higher wind speed, the flames were less visible due to the advection effect from the wind. This will be discussed further in pulse wind experiment results in the next section.

Further investigation of Figure 5.6 reveals that even though StF transition time decreases drastically between 3 to 12 m/s, the mass fraction at which transition occurred was not much different (Figure 5.8A). Figure 5.8A shows that the mass fraction at which StF transition occurred was relatively constant at 0.7 ± 0.1, when about 30% of sample burnt. Comparing this constant mass fraction value with both time to StF transition and average MLR shows that the earlier StF transition occurrence was achieved due to higher burning rate because of the higher oxygen supply rate, simultaneously increasing pyrolyzate production rate.

Then StF transition occurred once sufficient pyrolyzate production rate obtained and forming sufficient concentration of pyrolyzate gases that fall within the flammability limit. Interestingly, this is also indicated by a constant mass fraction. This suggests two possible explanations. First, the sample became thermally thin at that thickness, or second, the reactor walls became sufficiently high relative to the sample ensuring sufficient pyrolyzates mixing. Figure 5.8B compares average MLR with the MLR value at the instance of StF transition, showing that the latter is a bit higher than the former. This trend agrees with Figure 5.6 that StF transition occurred while MLR close to its peak. Once StF transition occurred, MLR slowly decreases as sample started to burn out due to high burning rate because of the flaming. The lower average MLR than MLR at the instance of StF transition is because the former also includes the growing and decaying state of the smouldering sample.

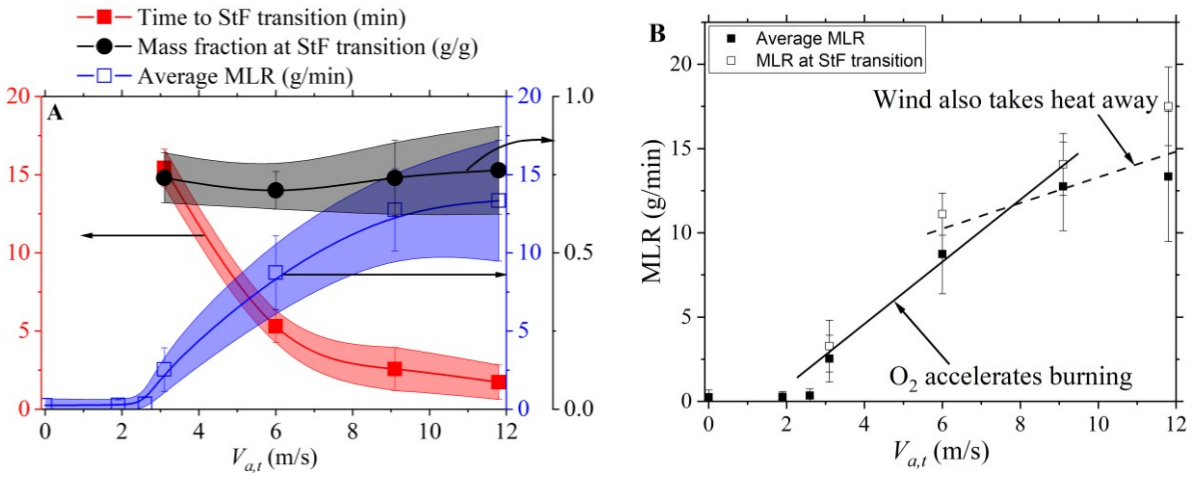

Figure 5.8. (A) Mass loss rate, StF transition time, and mass fraction at the instance of StF transition in continuous wind experiment series. (B) Comparison of the average MLR and MLR at StF transition showing that StF transition occurred when MLR (burning rate) was around its peak value, thus a bit higher than the average MLR.

Figure 5.8 also shows that the MLR increases drastically from ~0.4 to 12.8 g/min, at $V_{a,t}$ = 2.6 to 9.1 m/s. However, further increasing $V_{a,t}$ to 11.8 m/s only increases MLR to 13.3 g/min, indicating that MLR increase has reached a plateau. This is also indicated by the significant decrease of StF transition time from 15.4 to 1.7 min with $V_{a,t}$ increased from 3.1 to 9.1 m/s. A possible explanation for this is that at $V_{a,t}$ from 2.6 to 9.1 m/s the burning process is controlled by chemistry that the increase of oxygen supply significantly increases burning rate. At this stage, convective heat losses are insignificant to the burning process but gaining importance as can be seen by the plateauing trend of MLR as $V_{a,t}$ increases further. From 9.1 to 11.8 m/s, the further increase in oxygen supply does not increase the MLR. At this stage, heat loss controls the burning process.

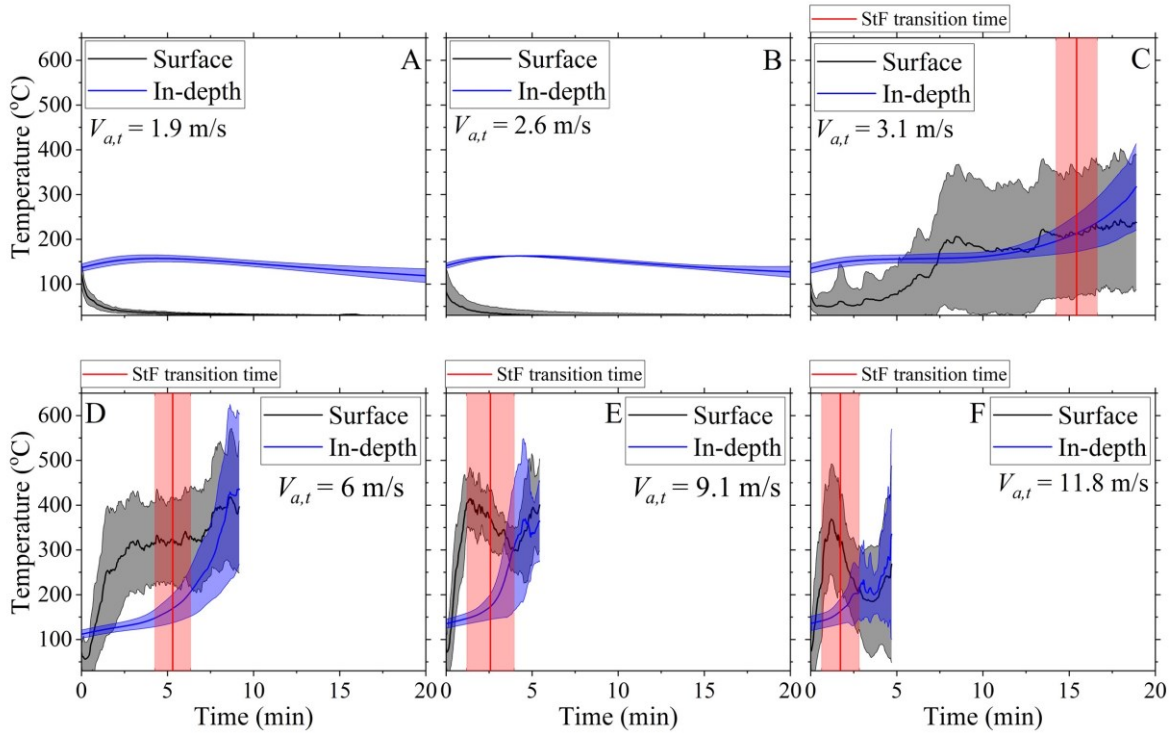

Figure 5.9. Surface and in-depth temperature from continuous wind experiment series. Wind temperature was maintained at 30.5 ± 1.3°C. Clouds represent standard deviation from experiment repetitions. (A) Experiments at $V_{a,t}$= 1.9 ± 0.2 m/s (2 repetitions). (B) Experiments at $V_{a,t}$= 2.6 ± 0.1 m/s (2 repetitions). StF transition occurred in 1 out of 3 experiments at t = 18.9 min (not shown here). (C) Experiments at $V_{a,t}$= 3.1 ± 0.02 m/s (4 repetitions). StF transition occurred in all 5 experiment at t = 15.4 ± 1.2 min. (D) Experiments at $V_{a,t}$= 6 ± 0.1 m/s (3 repetitions). StF transition occurred in all 4 experiment at t = 5.3 ± 1 min. (E) Experiments at $V_{a,t}$= 9.1 ± 0.1 m/s (4 repetitions). StF transition occurred in all 5 experiment at t = 2.6 ± 1.4 min. (F) Experiments at $V_{a,t}$= 11.8 ± 0.1 m/s (4 repetitions). StF transition occurred in all 5 experiment at t = 1.7 ± 1.1 min.

Surface and in-depth temperature of the sample are shown in Figure 5.9. Since surface temperature was only measured at three points on the sample surface and the uncertainty of strong smouldering propagation on the surface, error on surface temperature measurement is relatively wide (the clouds in Figure 5.9 represents standard deviation). However, it can still be seen that StF transition occurs when surface temperature was around its peak. The trend and uncertainty in in-depth spread are smoother and narrower than surface temperature, probably because no convective effect in the sample in-depth. The StF transition can be seen to occur when in-depth temperature started to increase, indicating the pyrolysis front getting closer to the in-depth location, i.e. 1.3 cm below the sample surface. Produced pyrolyzates then ignited by the strong smouldering on the sample surface with temperature 311 ± 49.8°C.

In-depth temperature indicates a relatively constant value at the instance of StF transition, at 190 ± 17.9°C (Figure 5.10), with a weak decrease between $V_{a,t}$ of 3.1 and 6 m/s. This decrease of in-depth temperature coincides with increasing

surface temperature, indicating a stronger smouldering causing pyrolysis production rate to increase and ignited by the hot smouldering surface. However, due to limited thermocouple resolution in this study, it is uncertain to conclude whether StF transition occurred with shallower pyrolysis front propagation with increasing wind speed. At this point, it is fair to conclude that pyrolysis front was located between the sample surface and 1.35 cm depth of the sample as the surface temperature was higher and in-depth temperature was lower than the lower range of wood pyrolysis temperature, i.e. ~277°C [226].

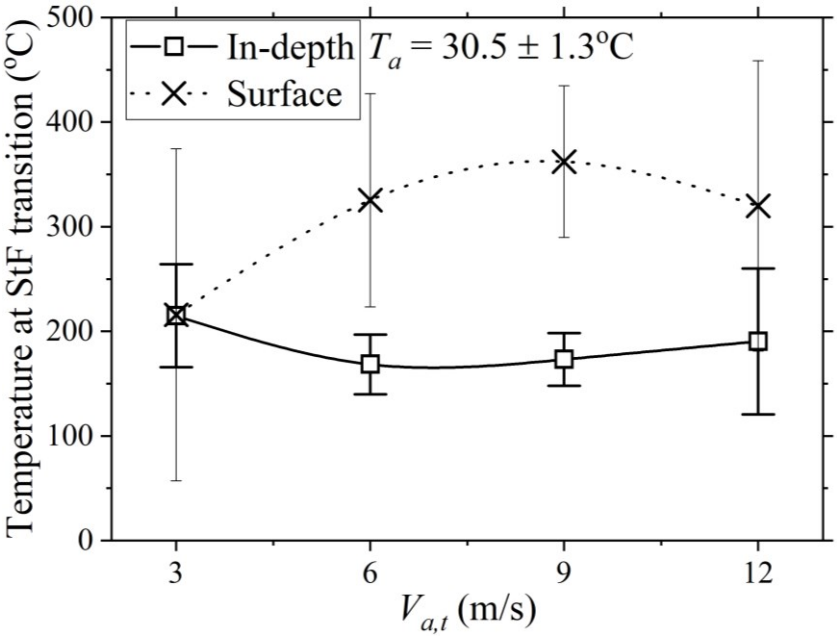

Figure 5.10. In-depth and surface temperature at the instance of StF transition occurrence. Surface temperature at each experiment is average of three thermocouple measurement points on the sample surface, while in-depth temperature from one thermocouple measurement point at 1.35 cm depth of the sample. Error bars are from experiment repetitions. There were 5, 4, 5, and 5 experiments conducted at $V_{a,t}$ of 3.1, 6, 9.1, 11.8 m/s, respectively.

5.3.2. Pulse wind

Figure 5.11 shows an experiment in pulse wind series at $V_{a,t}$ = 11.8 m/s when the wind diversion plate was closed at 35 s. During this experiment, 5 s before the wind plate was closed, intermittent appearances of flaming was identified at the sample edge. When the wind plate was closed, the flame sheet covered the whole surface area of the sample. This indicates that without wind advection, flaming can occur on the whole surface of the sample. There are two possible explanations on the effect of wind advection on flame sheet. First, the strong wind advection forced the flame to incline on the sample surface, or second, the pyrolyzate gases were diluted by the wind advection and then intermittently appeared at the edge of the sample due to eddies that might be formed when the flow interacted with the sample side-wall boundary. However, the wind advection can be too strong

that the dispersion of flammable pyrolyzate gases is not always followed by its ignition around the sample edge. Only after the wind stopped that the time at which sample produced flammable pyrolyzate gases can be identified. Figure 5.12 shows the sketch of area on the sample where flames were observed in both continuous and pulse wind. Continuous wind leads to transition at sample edges while pulse wind leads to transition all over the sample. The lack of edge effect means that transition with pulse wind is expected to depend less on sample size.

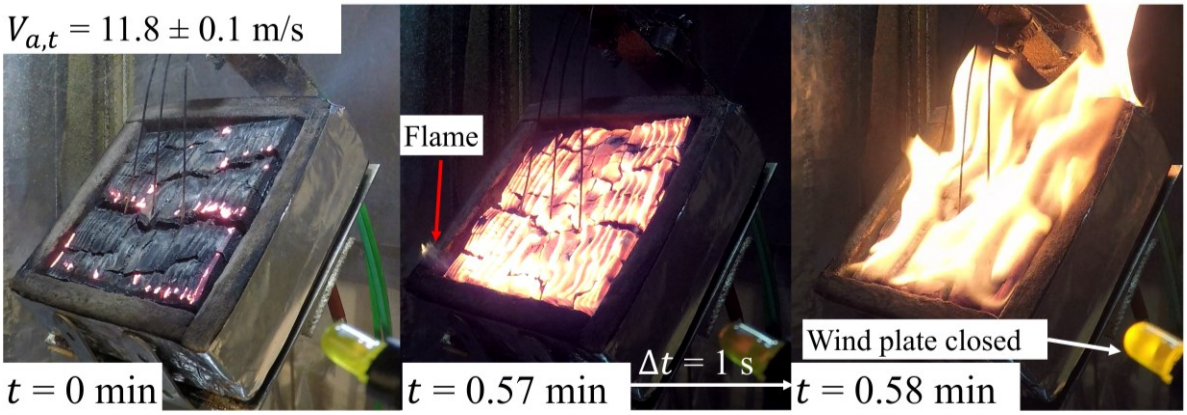

Figure 5.11. Snapshots of smouldering sample surface showing the intermittent flaming occurrences around the edge of the sample due to the dispersion of the pyrolyzate gases because of the wind advection. After the wind stopped, flaming sheet developed on the whole surface of the sample. Δt is time difference between middle to right figures.

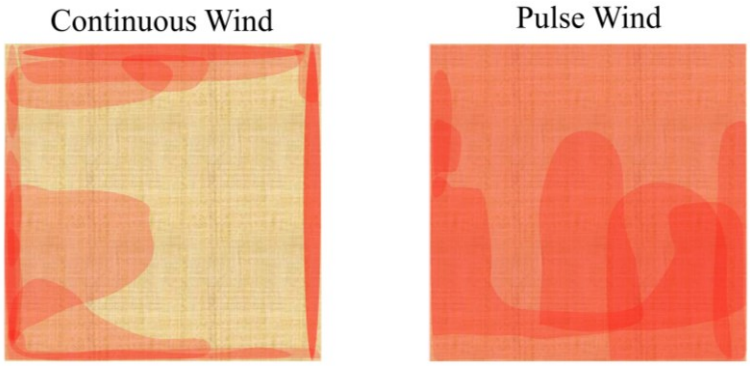

Figure 5.12. Sketch of transition location in both continuous and pulse wind experiment. Red represents the area where flames were observed, with darker colour represents area where flames were observed frequently.

In pulse wind experiments, StF transition is identified to be occurred earlier than with continuous wind (Figure 5.13a). The largest time gap between StF transition in pulse and continuous wind is at $V_{a,t}$ 3.1 m/s, at ~5 min. However, at this wind speed, the wind exposure time that can result in StF transition is uncertain (Figure 5.13b). Unlike at higher wind speed, the increasing of wind exposure time at $V_{a,t}$ 3.1 m/s is not followed by a sharp contrast of StF transition occurrence probability, as shown in Figure 5.13b. At $V_{a,t}$ of 6.0, 9.1, and 11.8 m/s,

StF transition occurrence based on wind exposure time is sharply identified, and with 50% probability at 4, 0.3, and 0.2 min, respectively. At $V_{a,t}$ of 3.1 m/s, however, the probability is more uncertain with p-value of 0.0605 (>0.05). Complete set of pulsed wind experiment data points are shown in Figure A 5.1 in Appendices.

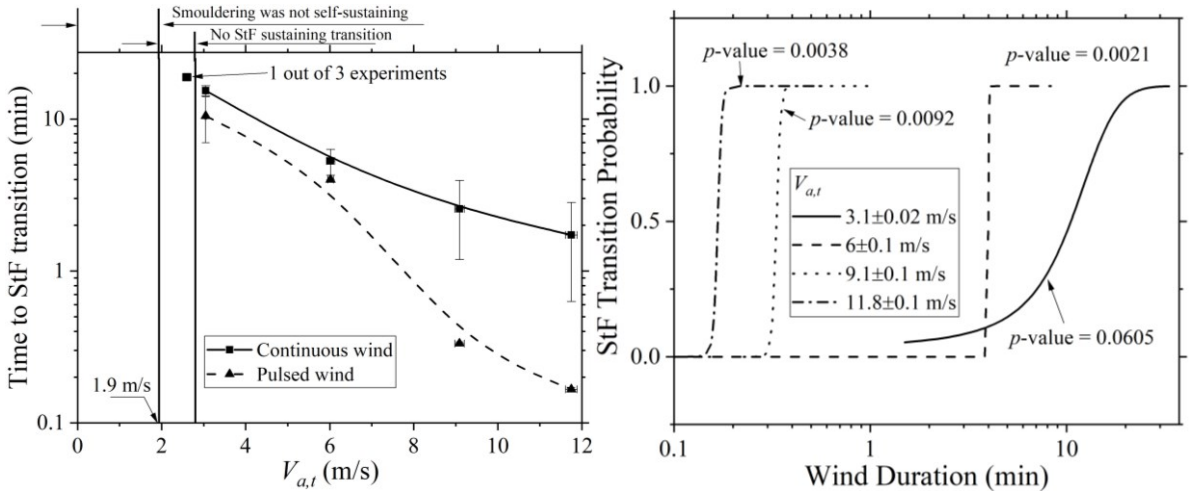

Figure 5.13. (a) Time to StF transition vs wind speed at two conditions, i.e. continuous and pulse wind supply. Pulse wind supply decreases StF transition time up to ~5 min. (b) The probability of StF transition time and occurrence, demonstrated to be more statistically certain with wind speed.

Figure 5.13 shows that wood may require a relatively high wind speed to certainly undergoes StF transition to flaming, about 6 to 12 m/s. However, the wind may be too strong for the flame to form and sustain, requiring pauses in wind to allow the accumulation of pyrolyzates. Pulse wind experimental method shows a mechanism of StF transition that has not yet been considered in literature, proving that continuous wind may make transition slightly more difficult because of wind advection. In natural environment, wind is unsteady accompanied by often strong gusts of wind. As shown by experimental data and repeatable measurements here, pulse wind provides the optimal conditions for StF transition.

Both heat loss and wind advection negatively affect StF transition time. The effect of wind advection in delaying StF transition time was more significant at low wind speed (3 m/s), thus at low oxygen supply, with delay time of ~5 min. As wind speed increasing, the effect of wind advection in delaying StF transition decreased to ~1.7 min in average across wind speed of 6 to 11.8 m/s, thus already started to be overcame by the effect of oxygen supply by increasing pyrolyzates production rate. Wind advection might have effect on the plateauing of the mass loss rate at wind speed above 9 m/s (Figure 5.8A). However, considering that wind speed has been started to be overcame by oxygen supply at wind speed lower than 9 m/s, the plateauing of the mass loss rate is suggested to be dominated by heat loss.

5.4. Conclusion

Smouldering-to-flaming (StF) transition experiments on wood samples have been conducted across varying wind speed, i.e. from 0 to 12 m/s. Within this range, three regimes were identified, below 1.9 m/s where smouldering was self-sustained, between 1.9 and 3.1 m/s where smouldering self-sustained but no StF transition identified, and about 3.1 m/s where StF transition consistently occurred. Results at wind speed above 3.1 m/s confirm that the time to StF transition significantly decreases with wind speed. This indicates a significant role of oxygen supply on the StF transition occurrence. At low wind speeds, smouldering spread rate increases with wind speed because additional oxygen supply overcomes the higher convective heat losses. The role of oxygen supply is also supported by the fact that the StF transition in this study is highly repeatable, especially with pulse wind exposure. The effect of convective heat loss from wind gain importance above 9 m/s, making the decreasing of transition time non-linear. Stronger char oxidation with wind speed is identified, acting both as a pilot and source of pyrolyzate to form flammability mixture.

Beside increasing oxygen and convective heat loss, wind advection also contributes to the dilution of pyrolyzate gases. The experiments with pulse wind identified the StF transition time when the dilution of pyrolyzate gases was stopped once the wind stopped, hence increasing flow time. Under pulse wind condition, StF transition can occur up to ~5 min earlier than under continuous wind. We conclude that pulse wind enhances the StF transition by first providing strong smouldering driven by oxygen supply, and then once wind stopped by increasing the flow time and the concentration of pyrolyzates. Both heat loss and wind advection negatively affect StF transition time. The effect of wind advection in delaying StF transition time was more significant at low wind speed and started to be overcame by the effect of oxygen supply at higher wind speed. Though wind advection might have effect, the plateauing of the mass loss rate at wind speed above 9 m/s is suggested to be dominated by heat loss. The results presented in this study reveals the mechanism in which StF transition occurs on burning wood in different wind speeds.

Chapter 6

Conclusion

Wildfires are the occurrence of uncontrolled combustion in the natural environment. The frequency and size of wildfires are projected to increase due to climate change and land-use change, and has taken into effects in various locations around the globe such as the smouldering peatland fires in southeast Asia and Arctic and flaming wildfire in USA, Europe, and Australia. Effective prevention and mitigation plans need to incorporate understanding on the fundamental process of wildfires. This thesis aims to provide novel understanding on the smouldering peat fire and its suppression, and on the fundamental understanding of smouldering-to-flaming transition, contributing to the better mitigation of smouldering wildfires (Figure 6.1).

Chapter 1 of this thesis provides a review of smouldering peatland fire, providing discussion of smouldering peat propagation and effects to the soil. The difficulty in the mitigation of smouldering wildfires is identified due to the persistent nature of this fire, suppression difficulty, and the current lack understanding of the transition from smouldering to flaming combustion that has been reported to might have contributed to reignition [214].

Chapter 2 of this thesis presents GAMBUT the largest to-date field experiments of peatland fires, conducted in Riau, Indonesia, in 2018. This study was conducted to fill the gap in the literature which has abundant experiments at lab-scale and forensic study at the field scale but lacks in systematic experiments in length scale comparable to real peat fire. The smouldering peat fire in this experiment, with a size of 0.2 × 0.5 m to 8 × 10 m area, persistently propagated across the whole duration of the experiment, up to 10 days, until controlled suppression attempts were conducted (Figure 6.2A). Slash-and-burn ignition resulted in strong ignition at shallow layer indicated by maximum temperature of 700^{o}C and smouldering residence time of 8.2 ± 7.8 h, while charcoal ignition resulted with strong ignition at deep layer with maximum temperature of 550^{o}C and residence time of 16.8 ± 12.2 h. The horizontal spread rate is 0.7 ± 0.1 cm/h and the depth of burn is 25 cm in average.

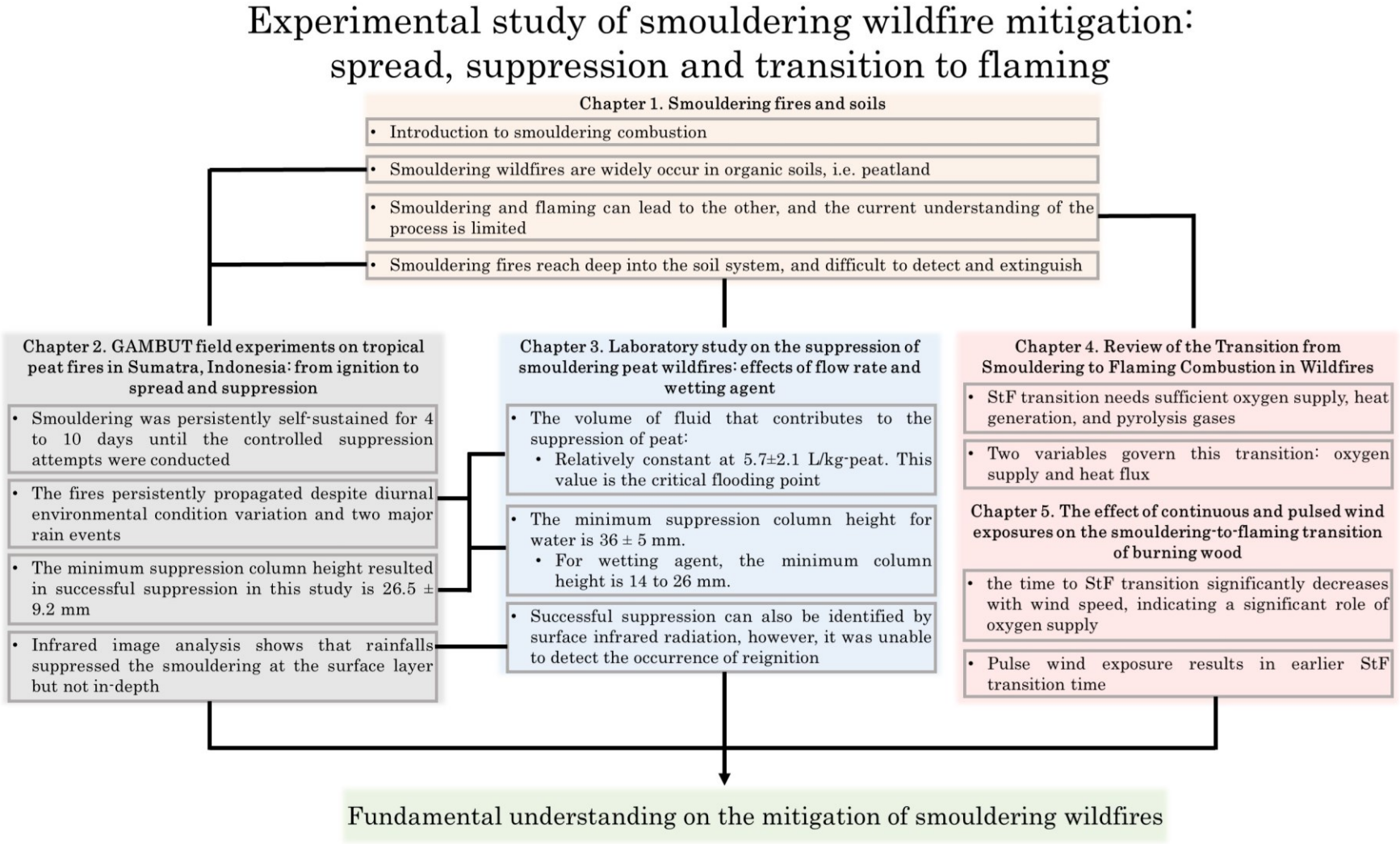

Figure 6.1. Diagram illustrating the connections between chapters in this thesis. The main output of this thesis is the fundamental understanding of the mitigation of smouldering wildfire through a better comprehension of peat fire suppression dynamics and transition to flaming in smouldering wildfires.

During GAMBUT, two rainfall events with column height of 4.8 and 2.5 mm occurred and failed to suppress the peat fires. Infrared image analysis, however, suggests that rainfall might have suppressed the smouldering peat at the surface but failed to reach smouldering at in-depth layer. Comparison of suppression column height between failed suppression from rainfall events to the controlled suppression attempts suggests that there is a critical suppression column height below which suppression is not possible. A suppression column height less than this minimum value results in the water not reaching the in-depth smouldering, thus only suppressing smouldering on the surface, such as the case of failed suppression by rainfalls. Suppression method by means of a lance injection resulted in a low efficiency, shown by a significant excess use of water but not much shorter suppression time than with spray method. However, the ability of the injection method to directly attack an in-depth smouldering hotspot might be proven to be effective during the mopping up stage of large-scale peat fire suppression, to avoid reignition and fire regrowth.

In Chapter 3, further systematic study of the smouldering peat fire suppression at lab-scale conducted across different suppression flow rate and wetting agent concentration is presented. This study further confirms the existence of a critical value of suppression column height mentioned in Chapter 2. Furthermore, it was found that suppression time decreases non-linearly with flow rate, and wetting agent concentration further decreases suppression time up to 26 to 39%. Demonstration of a simple upscaling of the results in the lab scale to a small peat fire in the field such as in the order 1 ha, shows about 50% decrease in the required volume of suppressant to successfully suppress peat fire can be achieved by using a wetting agent. The shorter suppression time by wetting agent is identified due to a better flooding of the peat sample. In order to be successfully suppressed, peat fire is required to be flooded to a rather constant level of 5.7±2.1 L/kg, or equivalent to increase the peat MC to 573±208% (in dry base) which is double the value of a pristine peatland MC (Figure 6.2B). This critical flooding point is constant despite the change in flow rate and wetting agent concentration. Comparison of run-off between water and wetting agent suppression suggests that run-off can occur through two mechanisms, i.e. channelling or uniform penetration. Because of the lower surface tension of the wetting agent, it can uniformly penetrate through the peat sample thus quickly flooding the peat fire to the critical flooding point, hence the shorter suppression time than water. In case of water, the higher surface tension than wetting agent causes the water to form a channel in peat sample. When this channel is formed, most of the water goes through this channel and is not contributing to the flooding of the peat, hence the higher run-off and longer suppression time of water than wetting agent. The surface tension of the wetting agent is ~2.5 times lower than water. Thus, a development of a suppressant agent that can decrease water surface tension can help in the

mitigation of smouldering peat fire in terms faster suppression and lower required suppression agent volume.

In wildfire, combustion can be driven by two fundamental processes, i.e. smouldering and flaming. Despite their different characteristics, smouldering can transition to flaming combustion, and vice versa. Smouldering-to-flaming (StF) transition, however, presents a sudden and drastic increase of fire hazards, such as faster spread and higher temperature. The literature review of StF transition in Chapter 4 reveals that transition is governed by two processes, i.e. chemistry and heat transfer. Specifically, wind speed has been identified to influence StF transition occurrence [43,170–172,178,185], and fundamentally has two competing effects on combustion process, i.e. oxygen supply and convective heat loss. Chapter 5 presents the systematic investigation of wind effects on StF transition by conducting series of experiments on a burning wood in a rig designed to control well the wind temperature and speed, thus controlling the effects of oxygen supply and convective heat loss. The results of these experiments show that StF transition time significantly decreases with wind speed, indicating an important role of oxygen supply (chemistry) (Figure 6.2C). As wind speed increases, the effect of heat transfer is gaining importance. This is indicated by a weak increase of mass loss rate (MLR) as wind increases above 9 m/s, below which MLR drastically increases. The occurrence of StF transition is also accompanied by a more uniform and vigorous char smouldering on the surface of the sample, indicating the important role of char oxidation to provide heat to support pyrolysis process and to act as a pilot ignition. Other than supplying oxygen and increasing convective heat loss, wind also contributes to the dispersion of the pyrolyzate gases due to wind advection. This is revealed by suddenly stopped the wind supply, thus pulse wind exposure, at which StF transition could occurred up to ~5 min earlier than when the wind is continuously supplied to the sample. With pulse wind, StF transition was also indicated to be less dependent on sample size. The results in this chapter could help in the mitigation and modelling of wildfire propagation through a better temporal observation of wind speed, and might contribute to estimate fire risk based on a likelihood of StF transition occurrence across different wind speed magnitude.

To summarize, this thesis provides results to fundamentally understand the effective mitigation of smouldering wildfire (Figure 6.1). Both field and lab-scale experiments of smouldering peat fires reported in this thesis reveal the critical flooding point, run-off mechanisms, and critical suppression column height. The investigation of smouldering-to-flaming transition reported in this thesis provide the fundamental understanding of this process by confirming the role of heat transfer and oxygen supply to the StF transition. Through understandings presented in this study (Figure 6.2), better prevention and mitigation strategies can be developed to be prepared against an increasingly warming earth in which wildfires have been projected to be larger.

Below are highlighted points that can be considered as prospective study to be conducted in the future:

- In term of field study, field-scale experiment on peatland with lower IC than the study presented in Chapter 2 will be beneficial to have a complete understanding of smouldering peat fire dynamics on both pristine and degraded peatland. Some measurement techniques can also be improved further, such as the use of drone attached with IR camera to collect a larger data set of surface spread rate measurements, both spatially and temporally
- In term of suppression, validation of findings in Chapter 3 regarding suppression dynamics with wetting agent by conducting field-scale experiment can also be done to fill the gap in the literature. In lab-scale, more suppression experiments can be done by further varying the MC and bulk density of the peat sample. Other techniques of suppression on peat fire can also be explored in lab-scale, such as injection method.
- In term of transition from smouldering to flaming, more experiments with the same setup as shown in Chapter 5 but with various wind temperature can further clarify the effects of heat loss, oxygen supply, and wind advection. StF transition experiments on fuel with different characteristics of permeability and consolidation are also prospective to validate the generality of the fundamental mechanism of StF transition in Chapter 5 across various types of fuel.

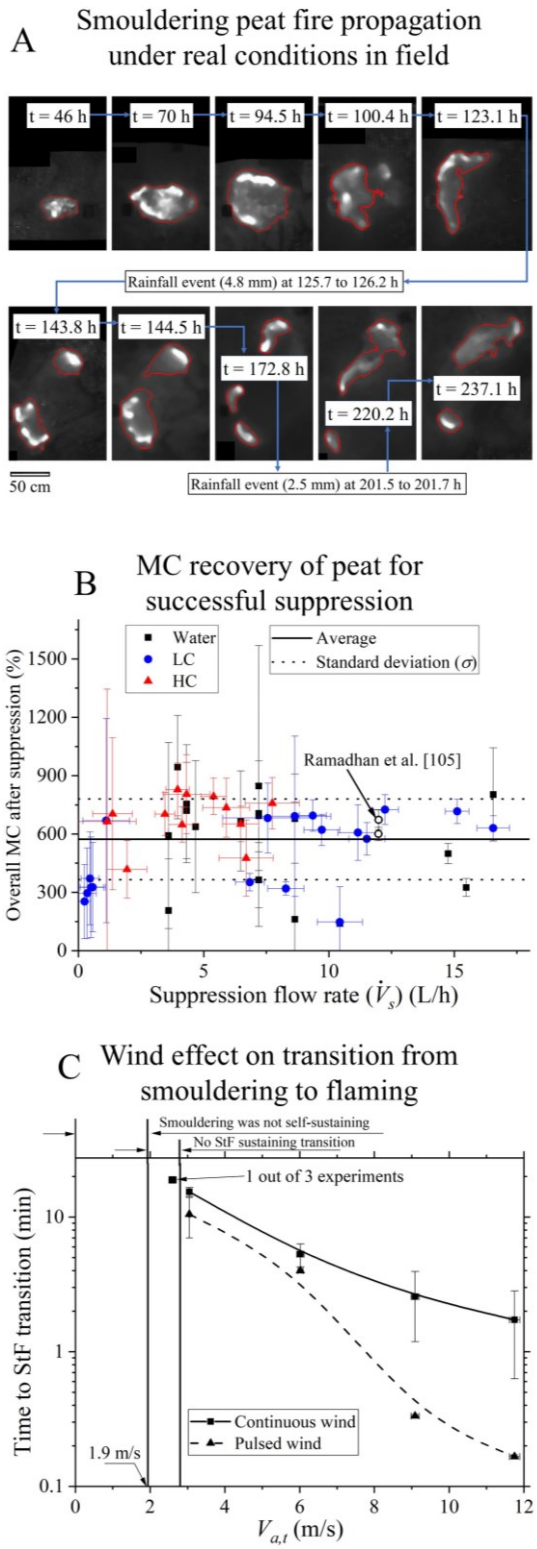

Figure 6.2. Main outputs of this thesis. (A) Propagation behaviour of smouldering peat fire under real conditions, persistently spread for 10 days during day and night, and despite two major rainfalls. This is presented in **Chapter 2**. (B) The level of MC of peat that needs to be recovered in order to successfully suppress peat fire is found to be constant at 573±208% (in dry base). This is presented in **Chapter 3**. (C). Smouldering-to-flaming (StF) transition time significantly decreased with wind speed and earlier with pulse wind, indicating the significant role of oxygen supply, presented in **Chapter 5**.

Reference

[1] Rein, G., 2016, "Smoldering Combustion," *SFPE Handbook of Fire Protection Engineering*, M.J. Hurley, D. Gottuk, J.R. Hall, K. Harada, E. Kuligowski, M. Puchovsky, J. Torero, J.M. Watts, and C. Wieczorek, eds., Springer New York, New York, NY, pp. 581–603.

[2] Davies, G. M., Gray, A., Rein, G., and Legg, C. J., 2013, "Peat Consumption and Carbon Loss Due to Smouldering Wildfire in a Temperate Peatland," For. Ecol. Manage., **308**, pp. 169–177.

[3] Huang, X., and Rein, G., 2017, "Downward Spread of Smouldering Peat Fire: The Role of Moisture, Density and Oxygen Supply," Int. J. Wildl. Fire, **26**(11), pp. 907–918.

[4] Ohlemiller, T., 2002, "Smoldering Combustion," *SFPE Handbook of Fire Protection Engineering*, P.J. DiNenno, D. Drysdale, C.L. Beyler, W.D. Walton, R.L.P. Custer, J.R. Hall Jr., and J.M. Watts Jr., eds., National Fire Protection Association, Boston, MA, pp. 200–209.

[5] NRCS, 1999, *Soil Taxonomy: A Basic System of Soil Classification for Making and Interpreting Soil Surveys*, Washington DC.

[6] Mokma, D. L., 2005, "ORGANIC SOILS," *Encyclopedia of Soils in the Environment*, D.B.T.-E. of S. in the E. Hillel, ed., Elsevier, Oxford, pp. 118–129.

[7] Huang, P.-T., Patel, M., Santagata, M. C., and Bobet, A., 2009, *Classification of Organic Soils*, West Lafayette, IN.

[8] Yu, Z. C., 2012, "Northern Peatland Carbon Stocks and Dynamics: A Review," Biogeosciences, **9**(10), pp. 4071–4085.

[9] Page, S. E., Rieley, J. O., and Banks, C. J., 2011, "Global and Regional Importance of the Tropical Peatland Carbon Pool," Glob. Chang. Biol., **17**(2), pp. 798–818.

[10] Turetsky, M. R., Benscoter, B., Page, S., Rein, G., van der Werf, G. R., and Watts, A., 2015, "Global Vulnerability of Peatlands to Fire and Carbon Loss," Nat. Geosci., **8**(1), pp. 11–14.

[11] Rein, G., Cleaver, N., Ashton, C., Pironi, P., and Torero, J. L., 2008, "The Severity of Smouldering Peat Fires and Damage to the Forest Soil," CATENA, **74**(3), pp. 304–309.

[12] Page, S. E., Siegert, F., Rieley, J. O., Boehm, H.-D. V, Jaya, A., and Limin, S., 2002, "The Amount of Carbon Released from Peat and Forest Fires in Indonesia during 1997," Nature, **420**(6911), pp. 61–65.

[13] Ballhorn, U., Siegert, F., Mason, M., and Limin, S., 2009, "Derivation of Burn Scar Depths and Estimation of Carbon Emissions with LIDAR in Indonesian Peatlands," Proc. Natl. Acad. Sci. U. S. A., **106**(50), pp. 21213–21218.

[14] Huijnen, V., Wooster, M. J., Kaiser, J. W., Gaveau, D. L. A., Flemming, J., Parrington, M., Inness, A., Murdiyarso, D., Main, B., and van Weele, M., 2016, "Fire Carbon Emissions over Maritime Southeast Asia in 2015 Largest since 1997," Sci. Rep., **6**(1), p. 26886.

[15] Koplitz, S. N., Mickley, L. J., Marlier, M. E., Buonocore, J. J., Kim, P. S., Liu, T., Sulprizio, M. P., DeFries, R. S., Jacob, D. J., Schwartz, J., Pongsiri, M., and Myers, S. S., 2016, "Public Health Impacts of the Severe Haze in Equatorial Asia in September–October 2015: Demonstration of a New Framework for Informing Fire Management Strategies to Reduce Downwind Smoke Exposure," Environ. Res. Lett., **11**(9), p. 94023.

[16] Stockwell, C. E., Jayarathne, T., Cochrane, M. A., Ryan, K. C., Putra, E. I., Saharjo, B. H., Nurhayati, A. D., Albar, I., Blake, D. R., Simpson, I. J., Stone, E.

A., and Yokelson, R. J., 2016, “Field Measurements of Trace Gases and Aerosols Emitted by Peat Fires in Central Kalimantan, Indonesia, during the 2015 El Niño,” Atmos. Chem. Phys., **16**(18), pp. 11711–11732.
[17] Byram, G. M., 1959, “Combustion of Forest Fuels,” *Forest Fire: Control and Use*, K.P. Davis, ed., McGraw-Hill, New York, NY, pp. 61–89.
[18] Laris, P., Jacobs, R., Koné, M., Dembélé, F., and Rodrigue, C. M., 2020, “Determinants of Fire Intensity in Working Landscapes of an African Savanna,” Fire Ecol., **16**(1), p. 27.
[19] Alexander, M. E., and Cruz, M. G., 2019, “Fireline Intensity,” Encycl. Wildfires Wildland-Urban Interface Fires.
[20] Johnston, J. M., Wooster, M. J., Paugam, R., Wang, X., Lynham, T. J., and Johnston, L. M., 2017, “Direct Estimation of Byram’s Fire Intensity from Infrared Remote Sensing Imagery,” Int. J. Wildl. Fire, **26**(8), pp. 668–684.
[21] Gorham, E., 1991, “Northern Peatlands: Role in the Carbon Cycle and Probable Responses to Climatic Warming,” Ecol. Appl., **1**(2), pp. 182–195.
[22] Flannigan, M. D., Krawchuk, M. A., de Groot, W. J., Wotton, B. M., and Gowman, L. M., 2009, “Implications of Changing Climate for Global Wildland Fire,” Int. J. Wildl. Fire, **18**(5), pp. 483–507.
[23] Wieder, R. K., Scott, K. D., Kamminga, K., Vile, M. A., Vitt, D. H., Bone, T., Xu, B. I. N., Benscoter, B. W., and Bhatti, J. S., 2009, “Postfire Carbon Balance in Boreal Bogs of Alberta, Canada,” Glob. Chang. Biol., **15**(1), pp. 63–81.
[24] Moreno, L., Jiménez, M.-E., Aguilera, H., Jiménez, P., and de la Losa, A., 2011, “The 2009 Smouldering Peat Fire in Las Tablas de Daimiel National Park (Spain),” Fire Technol., **47**(2), pp. 519–538.
[25] Rein, G., 2013, “Smouldering Fires and Natural Fuels,” Fire Phenom. Earth Syst., pp. 15–33.
[26] Tarnocai, C., Canadell, J. G., Schuur, E. A. G., Kuhry, P., Mazhitova, G., and Zimov, S., 2009, “Soil Organic Carbon Pools in the Northern Circumpolar Permafrost Region,” Global Biogeochem. Cycles, **23**(2).
[27] Hu, Y., Fernandez-Anez, N., Smith, T. E. L., and Rein, G., 2018, “Review of Emissions from Smouldering Peat Fires and Their Contribution to Regional Haze Episodes,” Int. J. Wildl. Fire, **27**(5), pp. 293–312.
[28] Emmanuel, S. C., 2000, “Impact to Lung Health of Haze from Forest Fires: The Singapore Experience,” Respirology, **5**(2), pp. 175–182.
[29] Harrison, R. M., and Yin, J., 2000, “Particulate Matter in the Atmosphere: Which Particle Properties Are Important for Its Effects on Health?,” Sci. Total Environ., **249**(1), pp. 85–101.
[30] Kunii, O., Kanagawa, S., Yajima, I., Hisamatsu, Y., Yamamura, S., Amagai, T., and Ismail, I. T. S., 2002, “The 1997 Haze Disaster in Indonesia: Its Air Quality and Health Effects,” Arch. Environ. Heal. An Int. J., **57**(1), pp. 16–22.
[31] Harden, J. W., Trumbore, S. E., Stocks, B. J., Hirsch, A., Gower, S. T., O’neill, K. P., and Kasischke, E. S., 2000, “The Role of Fire in the Boreal Carbon Budget,” Glob. Chang. Biol., **6**(S1), pp. 174–184.
[32] Li, W., Dickinson, R. E., Fu, R., Niu, G.-Y., Yang, Z.-L., and Canadell, J. G., 2007, “Future Precipitation Changes and Their Implications for Tropical Peatlands,” Geophys. Res. Lett., **34**(1).
[33] BALSHI, M. S., McGUIRE, A. D., DUFFY, P., FLANNIGAN, M., WALSH, J., and MELILLO, J., 2009, “Assessing the Response of Area Burned to Changing Climate in Western Boreal North America Using a Multivariate Adaptive Regression Splines (MARS) Approach,” Glob. Chang. Biol., **15**(3), pp. 578–600.
[34] Albertson, K., Aylen, J., Cavan, G., and McMorrow, J., 2010, “Climate Change and the Future Occurrence of Moorland Wildfires in the Peak District of the UK ,”

Clim. Res., **45**, pp. 105–118.
[35] Héon, J., Arseneault, D., and Parisien, M.-A., 2014, "Resistance of the Boreal Forest to High Burn Rates," Proc. Natl. Acad. Sci., p. 201409316.
[36] Ohlemiller, T. J., 1985, "Modeling of Smoldering Combustion Propagation," Prog. Energy Combust. Sci., **11**(4), pp. 277–310.
[37] Bertschi, I., Yokelson, R. J., Ward, D. E., Babbitt, R. E., Susott, R. A., Goode, J. G., and Hao, W. M., 2003, "Trace Gas and Particle Emissions from Fires in Large Diameter and Belowground Biomass Fuels," J. Geophys. Res. Atmos., **108**(D13).
[38] Hadden, R., Alkatib, A., Rein, G., and Torero, J. L., 2014, "Radiant Ignition of Polyurethane Foam: The Effect of Sample Size," Fire Technol., **50**(3), pp. 673–691.
[39] Tse, S. D., Carlo, A., Nde-Pello, F., and Miyasaka, K., 1996, "Controlling Mechanisms in the Transition from Smoldering to Flaming of Flexible Polyurethane Foam," Symp. Combust., **26**(1), pp. 1505–1513.
[40] Fernandez-Pello, A. C., 2017, "Wildland Fire Spot Ignition by Sparks and Firebrands," Fire Saf. J., **91**, pp. 2–10.
[41] Manzello, S., Shields, J., Hayashi, Y., and Nii, D., 2008, "Investigating the Vulnerabilities of Structures to Ignition From a Firebrand Attack," Fire Saf. Sci., **9**, pp. 143–154.
[42] Suzuki, S., Manzello, S. L., Kagiya, K., Suzuki, J., and Hayashi, Y., 2015, "Ignition of Mulch Beds Exposed to Continuous Wind-Driven Firebrand Showers," Fire Technol., **51**(4), pp. 905–922.
[43] Wang, S., Huang, X., Chen, H., and Liu, N., 2017, "Interaction between Flaming and Smouldering in Hot-Particle Ignition of Forest Fuels and Effects of Moisture and Wind," Int. J. Wildl. Fire, **26**(1), pp. 71–81.
[44] Hakes, R. S. P., Salehizadeh, H., Weston-Dawkes, M. J., and Gollner, M. J., 2019, "Thermal Characterization of Firebrand Piles," Fire Saf. J., **104**, pp. 34–42.
[45] Wagner, C. E. Van, 1972, "Duff Consumption by Fire in Eastern Pine Stands," Can. J. For. Res., **2**(1), pp. 34–39.
[46] Wein, R. W., 1983, "Fire Behaviour and Ecological Effects in Organic Terrain," *The Role of Fire in Northern Circumpolar Ecosystems*, R.W. Wein, and D.A. MacLean, eds., John Wiley & Sons, Ltd, pp. 81–95.
[47] Frandsen, W. H., 1987, "The Influence of Moisture and Mineral Soil on the Combustion Limits of Smoldering Forest Duff," Can. J. For. Res., **17**(12), pp. 1540–1544.
[48] Huang, X., Rein, G., and Chen, H., 2015, "Computational Smoldering Combustion: Predicting the Roles of Moisture and Inert Contents in Peat Wildfires," Proc. Combust. Inst., **35**(3), pp. 2673–2681.
[49] Frandsen, W., 1997, "Ignition Probability of Organic Soils," Can. J. For. Res., **27**, pp. 1471–1477.
[50] Huang, X., and Rein, G., 2014, "Smouldering Combustion of Peat in Wildfires: Inverse Modelling of the Drying and the Thermal and Oxidative Decomposition Kinetics," Combust. Flame, **161**, pp. 1633–1644.
[51] Usup, A., Hashimoto, Y., Takahashi, H., and Hayasaka, H., 2004, "Combustion and Thermal Characteristic of Peat Fire in Tropical Peatland in Central Kalimantan, Indonesia," Tropics, **14**, pp. 1–19.
[52] Watts, A. C., 2013, "Organic Soil Combustion in Cypress Swamps: Moisture Effects and Landscape Implications for Carbon Release," For. Ecol. Manage., **294**, pp. 178–187.
[53] Huang, X., Restuccia, F., Gramola, M., and Rein, G., 2016, "Experimental Study of the Formation and Collapse of an Overhang in the Lateral Spread of Smouldering Peat Fires," Combust. Flame, **168**, pp. 393–402.
[54] Rieley, J., and Page, S., 2016, "Tropical Peatland of the World," *Tropical Peatland*

Ecosystems, M. Osaki, and N. Tsuji, eds., Springer, Tokyo, Japan, pp. 3–32.
[55] Cazaly, E., 2012, "Laboratory Study of Smouldering Peat Fires Using Infra-Red Imaging.," The University of Edinburgh, UK.
[56] Prat-Guitart, N., Rein, G., Hadden, R. M., Belcher, C. M., and Yearsley, J. M., 2016, "Propagation Probability and Spread Rates of Self-Sustained Smouldering Fires under Controlled Moisture Content and Bulk Density Conditions," Int. J. Wildl. Fire, **25**(4), pp. 456–465.
[57] Shetler, G., Turetsky, M. R., Kane, E., and Kasischke, E., 2008, "Sphagnum Mosses Limit Total Carbon Consumption during Fire in Alaskan Black Spruce Forests," Can. J. For. Res., **38**(8), pp. 2328–2336.
[58] Hudspith, V. A., Belcher, C. M., and Yearsley, J. M., 2014, "Charring Temperatures Are Driven by the Fuel Types Burned in a Peatland Wildfire ," Front. Plant Sci. , **5**, p. 714.
[59] Prat-Guitart, N., Belcher, C. M., Thompson, D. K., Burns, P., and Yearsley, J. M., 2017, "Fine-Scale Distribution of Moisture in the Surface of a Degraded Blanket Bog and Its Effects on the Potential Spread of Smouldering Fire," Ecohydrology, **10**(8), p. e1898.
[60] Miyanishi, K., and Johnson, E. A., 2002, "Process and Patterns of Duff Consumption in the Mixedwood Boreal Forest," Can. J. For. Res., **32**(7), pp. 1285–1295.
[61] Hille, M. G., and Stephens, S. L., 2005, "Mixed Conifer Forest Duff Consumption during Prescribed Fires: Tree Crown Impacts," For. Sci., **51**(5), pp. 417–424.
[62] Reddy, A. D., Hawbaker, T. J., Wurster, F., Zhu, Z., Ward, S., Newcomb, D., and Murray, R., 2015, "Quantifying Soil Carbon Loss and Uncertainty from a Peatland Wildfire Using Multi-Temporal LiDAR," Remote Sens. Environ., **170**, pp. 306–316.
[63] Hartford, R. A., and Frandsen, W. H., 1992, "When It's Hot, It's Hot... Or Maybe It's Not! (Surface Flaming May Not Portend Extensive Soil Heating)," Int. J. Wildl. Fire, **2**(3), pp. 139–144.
[64] Doerr, S. H., and Shakesby, R. A., 2013, "Fire and the Land Surface," Fire Phenom. Earth Syst., pp. 135–155.
[65] Pereira, P., Úbeda, X., and Francos, M., 2019, "Laboratory Fire Simulations: Plant Litter and Soils," *Fire Effects on Soil Properties*, P. Pereira, J. Mataix-Solera, X. Ubeda, G. Rein, and A. Cerdà, eds., CSIRO Publishing, pp. 15–38.
[66] Pereira, P., Brevik, E., Bogunovic, I., and Estebaranz-Sánchez, F., 2019, "Ash and Soils: A Close Relationship in Fire-Affected Areas," *Fire Effects on Soil Properties*, P. Pereira, J. Mataix-Solera, X. Ubeda, G. Rein, and A. Cerdà, eds., CSIRO Publishing, pp. 39–68.
[67] Badía, D., and Martí, C., 2019, "Texture, Mineralogy and Structure," *Fire Effects on Soil Properties*, P. Pereira, J. Mataix-Solera, X. Ubeda, G. Rein, and A. Cerdà, eds., CSIRO Publishing, pp. 69–80.
[68] Arcenegui, V., Jiménez-Morillo, N. T., and Jiménez-Pinilla, P., 2019, "Soil Water Repellency," *Fire Effects on Soil Properties*, P. Pereira, J. Mataix-Solera, X. Ubeda, G. Rein, and A. Cerdà, eds., CSIRO Publishing, pp. 81–88.
[69] Sheridan, G., Lane, P., and Nyman, P., 2019, "Erosion," *Fire Effects on Soil Properties*, P. Pereira, J. Mataix-Solera, X. Ubeda, G. Rein, and A. Cerdà, eds., CSIRO Publishing, pp. 89–114.
[70] Santín, C., and Doerr, S., 2019, "Carbon," *Fire Effects on Soil Properties*, P. Pereira, J. Mataix-Solera, X. Ubeda, G. Rein, and A. Cerdà, eds., CSIRO Publishing, pp. 115–128.
[71] Muñoz-Rojas, M., and Bárcenas-Moreno, G., 2019, "Microbiology," *Fire Effects on Soil Properties*, P. Pereira, J. Mataix-Solera, X. Ubeda, G. Rein, and A. Cerdà, eds., CSIRO Publishing, pp. 157–174.

[72] Wittenberg, L., and Tessler, N., 2019, "Recurrent Fires," *Fire Effects on Soil Properties*, P. Pereira, J. Mataix-Solera, X. Ubeda, G. Rein, and A. Cerdà, eds., CSIRO Publishing, pp. 185–202.
[73] Stoof, C. R., 2019, "Soil Heating," *Fire Effects on Soil Properties*, P. Pereira, J. Mataix-Solera, X. Ubeda, G. Rein, and A. Cerdà, eds., CSIRO Publishing, pp. 229–240.
[74] Mack, M. C., Bret-Harte, M. S., Hollingsworth, T. N., Jandt, R. R., Schuur, E. A. G., Shaver, G. R., and Verbyla, D. L., 2011, "Carbon Loss from an Unprecedented Arctic Tundra Wildfire," Nature, **475**(7357), pp. 489–492.
[75] Turetsky, M. R., Kane, E. S., Harden, J. W., Ottmar, R. D., Manies, K. L., Hoy, E., and Kasischke, E. S., 2011, "Recent Acceleration of Biomass Burning and Carbon Losses in Alaskan Forests and Peatlands," Nat. Geosci., **4**(1), pp. 27–31.
[76] Turetsky, M., Wieder, K., Halsey, L., and Vitt, D., 2002, "Current Disturbance and the Diminishing Peatland Carbon Sink," Geophys. Res. Lett., **29**(11), pp. 21–24.
[77] Kasischke, E. S., and Bruhwiler, L. P., 2002, "Emissions of Carbon Dioxide, Carbon Monoxide, and Methane from Boreal Forest Fires in 1998," J. Geophys. Res. Atmos., **107**(D1), p. FFR 2-1-FFR 2-14.
[78] Turetsky, M. R., and Wieder, R. K., 2001, "A Direct Approach to Quantifying Organic Matter Lost as a Result of Peatland Wildfire," Can. J. For. Res., **31**(2), pp. 363–366.
[79] Turetsky, M. R., Donahue, W. F., and Benscoter, B. W., 2011, "Experimental Drying Intensifies Burning and Carbon Losses in a Northern Peatland," Nat. Commun., **2**(1), p. 514.
[80] Lukenbach, M. C., Hokanson, K. J., Moore, P. A., Devito, K. J., Kettridge, N., Thompson, D. K., Wotton, B. M., Petrone, R. M., and Waddington, J. M., 2015, "Hydrological Controls on Deep Burning in a Northern Forested Peatland," Hydrol. Process., **29**(18), pp. 4114–4124.
[81] Benscoter, B. W., Thompson, D. K., Waddington, J. M., Flannigan, M. D., Wotton, B. M., de Groot, W. J., and Turetsky, M. R., 2011, "Interactive Effects of Vegetation, Soil Moisture and Bulk Density on Depth of Burning of Thick Organic Soils," Int. J. Wildl. Fire, **20**(3), pp. 418–429.
[82] Poulter, B., Christensen Jr., N. L., and Halpin, P. N., 2006, "Carbon Emissions from a Temperate Peat Fire and Its Relevance to Interannual Variability of Trace Atmospheric Greenhouse Gases," J. Geophys. Res. Atmos., **111**(D6).
[83] van der Werf, G. R., Dempewolf, J., Trigg, S. N., Randerson, J. T., Kasibhatla, P. S., Giglio, L., Murdiyarso, D., Peters, W., Morton, D. C., Collatz, G. J., Dolman, A. J., and DeFries, R. S., 2008, "Climate Regulation of Fire Emissions and Deforestation in Equatorial Asia," Proc. Natl. Acad. Sci., p. pnas.0803375105.
[84] Konecny, K., Ballhorn, U., Navratil, P., Jubanski, J., Page, S. E., Tansey, K., Hooijer, A., Vernimmen, R., and Siegert, F., 2016, "Variable Carbon Losses from Recurrent Fires in Drained Tropical Peatlands," Glob. Chang. Biol., **22**(4), pp. 1469–1480.
[85] Simpson, J. E., Wooster, M. J., Smith, T. E. L., Trivedi, M., Vernimmen, R. R. E., Dedi, R., Shakti, M., and Dinata, Y., 2016, "Tropical Peatland Burn Depth and Combustion Heterogeneity Assessed Using UAV Photogrammetry and Airborne LiDAR," Remote Sens. , **8**(12).
[86] DeBano, L., Neary, D., and Ffolliott, P., 1998, *Fire Effects on Ecosystems*, John Wiley & Sons, Ltd, Chichester, UK.
[87] Certini, G., 2005, "Effects of Fire on Properties of Forest Soils: A Review," Oecologia, **143**(1), pp. 1–10.
[88] Hooijer, A., Page, S., Jauhiainen, J., Lee, W. A., Lu, X. X., Idris, A., and Anshari,

G., 2012, “Subsidence and Carbon Loss in Drained Tropical Peatlands,” Biogeosciences, **9**(3), pp. 1053–1071.
[89] Chistjakov, V., Kuprijanov, A., Gorshkov, V., Artsybashev, E., Wein, R., and Maclean, D., 1983, “Measures for Fire-Prevention on Peat Deposits,” *The Role of Fire in Northern Circumpolar Ecosystems*, R. Wein, and D. MacLean, eds., John Wiley & Sons, Ltd, Chichester, UK, pp. 259–271.
[90] Wösten, J. H. M., Clymans, E., Page, S. E., Rieley, J. O., and Limin, S. H., 2008, “Peat–Water Interrelationships in a Tropical Peatland Ecosystem in Southeast Asia,” CATENA, **73**(2), pp. 212–224.
[91] Dikici, H., and Yilmaz, C. H., 2006, “Peat Fire Effects on Some Properties of an Artificially Drained Peatland,” J. Environ. Qual., **35**(3), pp. 866–870.
[92] Smith, S. M., Newman, S., Garrett, P. B., and Leeds, J. A., 2001, “Differential Effects of Surface and Peat Fire on Soil Constituents in a Degraded Wetland of the Northern Florida Everglades,” J. Environ. Qual., **30**(6), pp. 1998–2005.
[93] Choromanska, U., and DeLuca, T. H., 2001, “Prescribed Fire Alters the Impact of Wildfire on Soil Biochemical Properties in a Ponderosa Pine Forest,” Soil Sci. Soc. Am. J., **65**(1), pp. 232–238.
[94] Benscoter, B. W., and Vitt, D. H., 2008, “Spatial Patterns and Temporal Trajectories of the Bog Ground Layer Along a Post-Fire Chronosequence,” Ecosystems, **11**(7), pp. 1054–1064.
[95] Christensen, E., Y., H., Restuccia, F., Sontoso, M. A., Huang, X., and Rein, G., 2019, “Experimental Methods and Scales in Smouldering Wildfires,” *Fire Effects on Soil Properties*, P.M.-S. Pereira Jorge Ubeda, Xavier Rein, Guillermo Cerdà, Artemi, ed., CSIRO Publishing, pp. 267–280.
[96] Pastor, E., Oliveras, I., Urquiaga-Flores, E., Quintano-Loayza, J. A., Manta, M. I., and Planas, E., 2017, “A New Method for Performing Smouldering Combustion Field Experiments in Peatlands and Rich-Organic Soils,” Int. J. Wildl. Fire, **26**(12), pp. 1040–1052.
[97] Chen, H., Zhao, W., and Liu, N., 2011, “Thermal Analysis and Decomposition Kinetics of Chinese Forest Peat under Nitrogen and Air Atmospheres,” Energy & Fuels, **25**(2), pp. 797–803.
[98] Cancellieri, D., Leroy-Cancellieri, V., Leoni, E., Simeoni, A., Kuzin, A. Y., Filkov, A. I., and Rein, G., 2012, “Kinetic Investigation on the Smouldering Combustion of Boreal Peat,” Fuel, **93**, pp. 479–485.
[99] Christensen, E. G., Fernandez-Anez, N., and Rein, G., 2020, “Influence of Soil Conditions on the Multidimensional Spread of Smouldering Combustion in Shallow Layers,” Combust. Flame, **214**, pp. 361–370.
[100] Huang, X., and Rein, G., 2019, “Upward-and-Downward Spread of Smoldering Peat Fire,” Proc. Combust. Inst., **37**(3), pp. 4025–4033.
[101] Prat-Guitart, N., Rein, G., Hadden, R. M., Belcher, C. M., and Yearsley, J. M., 2016, “Effects of Spatial Heterogeneity in Moisture Content on the Horizontal Spread of Peat Fires,” Sci. Total Environ., **572**.
[102] Hu, Y., Cui, W., and Rein, G., 2020, “Haze Emissions from Smouldering Peat: The Roles of Inorganic Content and Bulk Density,” Fire Saf. J., **113**, p. 102940.
[103] Hu, Y., Christensen, E., Restuccia, F., and Rein, G., 2019, “Transient Gas and Particle Emissions from Smouldering Combustion of Peat,” Proc. Combust. Inst., **37**(3), pp. 4035–4042.
[104] Hu, Y., Christensen, E. G., Amin, H. M. F., Smith, T. E. L., and Rein, G., 2019, “Experimental Study of Moisture Content Effects on the Transient Gas and Particle Emissions from Peat Fires,” Combust. Flame, **209**, pp. 408–417.
[105] Ramadhan, M. L., Palamba, P., Imran, F. A., Kosasih, E. A., and Nugroho, Y. S., 2017, “Experimental Study of the Effect of Water Spray on the Spread of

Smoldering in Indonesian Peat Fires," Fire Saf. J., **91**, pp. 671–679.
[106] Lin, S., Cheung, Y. K., Xiao, Y., and Huang, X., 2020, "Can Rain Suppress Smoldering Peat Fire?," Sci. Total Environ., p. 138468.
[107] Smith, T. E. L., Evers, S., Yule, C. M., and Gan, J. Y., 2018, "In Situ Tropical Peatland Fire Emission Factors and Their Variability, as Determined by Field Measurements in Peninsula Malaysia," Global Biogeochem. Cycles, **32**(1), pp. 18–31.
[108] See, S. W., Balasubramanian, R., Rianawati, E., Karthikeyan, S., and Streets, D. G., 2007, "Characterization and Source Apportionment of Particulate Matter ≤ 2.5 Mm in Sumatra, Indonesia, during a Recent Peat Fire Episode," Environ. Sci. Technol., **41**(10), pp. 3488–3494.
[109] Hoyt, A. M., Chaussard, E., Seppalainen, S. S., and Harvey, C. F., 2020, "Widespread Subsidence and Carbon Emissions across Southeast Asian Peatlands," Nat. Geosci., **13**(6), pp. 435–440.
[110] Iriana, W., Tonokura, K., Inoue, G., Kawasaki, M., Kozan, O., Fujimoto, K., Ohashi, M., Morino, I., Someya, Y., Imasu, R., Rahman, M. A., and Gunawan, D., 2018, "Ground-Based Measurements of Column-Averaged Carbon Dioxide Molar Mixing Ratios in a Peatland Fire-Prone Area of Central Kalimantan, Indonesia," Sci. Rep., **8**(1), p. 8437.
[111] Gaveau, D. L. A., Salim, M. A., Hergoualc'h, K., Locatelli, B., Sloan, S., Wooster, M., Marlier, M. E., Molidena, E., Yaen, H., DeFries, R., Verchot, L., Murdiyarso, D., Nasi, R., Holmgren, P., and Sheil, D., 2014, "Major Atmospheric Emissions from Peat Fires in Southeast Asia during Non-Drought Years: Evidence from the 2013 Sumatran Fires," Sci. Rep., **4**(1), p. 6112.
[112] Tacconi, L., 2016, "Preventing Fires and Haze in Southeast Asia," Nat. Clim. Chang., **6**(7), pp. 640–643.
[113] Satianpakiranakorn, P., Khunnamwong, P., and Limtong, S., 2020, "Yeast Communities of Secondary Peat Swamp Forests in Thailand and Their Antagonistic Activities against Fungal Pathogens Cause of Plant and Postharvest Fruit Diseases," PLoS One, **15**(3), p. e0230269.
[114] Lupascu, M., Akhtar, H., Smith, T. E. L., and Sukri, R. S., 2020, "Post-Fire Carbon Dynamics in the Tropical Peat Swamp Forests of Brunei Reveal Long-Term Elevated CH4 Flux," Glob. Chang. Biol., **26**(9), pp. 5125–5145.
[115] Hooijer, A., Page, S., Canadell, J. G., Silvius, M., Kwadijk, J., Wösten, H., and Jauhiainen, J., 2010, "Current and Future CO_2 Emissions from Drained Peatlands in Southeast Asia," Biogeosciences, **7**(5), pp. 1505–1514.
[116] 2015, *Rata-Rata Curah Hujan Di Kabupaten Rokan Hilir (Mm) 2013-2015*.
[117] BMKG, 2020, "Indonesia Online Climate Database," http://dataonline.bmkg.go.id/data_iklim.
[118] Santoso, M. A., Huang, X., Prat-Guitart, N., Christensen, E., Hu, Y., and Rein, G., 2019, "Smouldering Fires and Soils," *Fire Effects on Soil Properties*, P. Pereira, J. Mataix-Solera, X. Ubeda, G. Rein, and A. Cerdà, eds., CSIRO Publishing, Melbourne, pp. 203–216.
[119] Könönen, M., Jauhiainen, J., Laiho, R., Kusin, K., and Vasander, H., 2015, "Physical and Chemical Properties of Tropical Peat under Stabilised Land Uses," Mires Peat, **16**, pp. 1–13.
[120] Cowan, D. A., Page, W. G., Butler, B. W., and Blunck, D. L., 2020, "Effects of Fuel Characteristics on Horizontal Spread Rate and Ground Surface Temperatures of Smouldering Duff," Int. J. Wildl. Fire, **29**(9), pp. 820–831.
[121] Christensen, E. G., Fernandez-Anez, N., and Rein, G., 2020, "Influence of Soil Conditions on the Multidimensional Spread of Smouldering Combustion in Shallow Layers," Combust. Flame, **214**, pp. 361–370.

[122] Hadden, R., and Rein, G., 2011, “Burning and Water Suppression of Smoldering Coal Fires in Small-Scale Laboratory Experiments,” Coal Peat Fires A Glob. Perspect., pp. 317–326.
[123] Santoso, M. A., Cui, W., Amin, H. M. F., Christensen, E. G., Nugroho, Y. S., and Rein, G., 2021, “Laboratory Study on the Suppression of Smouldering Peat Wildfires: Effects of Flow Rate and Wetting Agent,” Int. J. Wildl. Fire.
[124] McCaffrey, S. M., and Rhodes, A., 2009, “Public Response to Wildfire: Is the Australian ‘Stay and Defend or Leave Early’ Approach an Option for Wildfire Management in the United States?,” J. For., **107**(1), pp. 9–15.
[125] Gibbons, P., van Bommel, L., Gill, A. M., Cary, G. J., Driscoll, D. A., Bradstock, R. A., Knight, E., Moritz, M. A., Stephens, S. L., and Lindenmayer, D. B., 2012, “Land Management Practices Associated with House Loss in Wildfires,” PLoS One, **7**(1), p. e29212.
[126] Plucinski, M. P., 2019, “Fighting Flames and Forging Firelines: Wildfire Suppression Effectiveness at the Fire Edge,” Curr. For. Reports, **5**(1), pp. 1–19.
[127] Neal, M., 2018, “Peat Fires Burning in South-West Victoria since Mid-March Appear to Be Out” [Online]. Available: https://www.abc.net.au/news/2018-05-07/peat-fires-south-west-victoria-appear-to-be-out/9734054. [Accessed: 19-Jul-2020].
[128] Pumps Journalist, 2018, “Fighting the Cobrico Peat Fire” [Online]. Available: https://www.pumpindustry.com.au/fighting-the-cobrico-peat-fire. [Accessed: 14-May-2020].
[129] Mikalsen, R. F., Hagen, B. C., Steen-Hansen, A., Krause, U., and Frette, V., 2019, “Extinguishing Smoldering Fires in Wood Pellets with Water Cooling: An Experimental Study,” Fire Technol., **55**(1), pp. 257–284.
[130] Shukla, J. B., Misra, A. K., Naresh, R., and Chandra, P., 2010, “How Artificial Rain Can Be Produced? A Mathematical Model,” Nonlinear Anal. Real World Appl., **11**(4), pp. 2659–2668.
[131] Sutikno, S., Amalia, I. R., Sandhyavitri, A., Syahza, A., Widodo, H., and Seto, T. H., 2020, “Application of Weather Modification Technology for Peatlands Fires Mitigation in Riau, Indonesia,” AIP Conf. Proc., **2227**(1), p. 30007.
[132] Bill, 2008, “NC: Evans Road Fire Update” [Online]. Available: https://wildfiretoday.com/2008/06/17/nc-evans-road-fire-update/. [Accessed: 13-Nov-2020].
[133] North Carolina Division of Air Quality, 2009, *N.C. EXCEPTIONAL EVENT (JUNE, 2008)*.
[134] U.S. Fish & Wildlife Service, 2009, “Largest Refuge Fire of 2008 Declared Out” [Online]. Available: https://www.fws.gov/fire/news/nc/evans_road.shtml. [Accessed: 19-Jul-2020].
[135] Mickler, R. A., Welch, D. P., and Bailey, A. D., 2017, “Carbon Emissions during Wildland Fire on a North American Temperate Peatland,” Fire Ecol., **13**(1), pp. 34–57.
[136] Bourgault, M.-A., Larocque, M., and Garneau, M., 2019, “How Do Hydrogeological Setting and Meteorological Conditions Influence Water Table Depth and Fluctuations in Ombrotrophic Peatlands?,” J. Hydrol. X, **4**, p. 100032.
[137] Kennedy, M. J., Conroy, M. W., Dougherty, J. A., Otto, N., Williams, B. A., Ananth, R., and Fleming, J. W., 2015, “Bubble Coarsening Dynamics in Fluorinated and Non-Fluorinated Firefighting Foams,” Colloids Surfaces A Physicochem. Eng. Asp., **470**, pp. 268–279.
[138] Hinnant, K. M., Giles, S. L., and Ananth, R., 2017, “Measuring Fuel Transport through Fluorocarbon and Fluorine-Free Firefighting Foams,” Fire Saf. J., **91**, pp. 653–661.

[139] Rakowska, J., Szczygieł, R., Kwiatkowski, M., Porycka, B., Radwan, K., and Prochaska, K., 2017, "Application Tests of New Wetting Compositions for Wildland Firefighting," Fire Technol., **53**(3), pp. 1379–1398.
[140] Hinnant, K. M., Giles, S. L., Smith, E. P., Snow, A. W., and Ananth, R., 2019, "Characterizing the Role of Fluorocarbon and Hydrocarbon Surfactants in Firefighting-Foam Formulations for Fire-Suppression," Fire Technol.
[141] Rivai, M., Hambali, E., Suryani, A., Pramuhadi, G., and Subekti, P., 2020, "Performance Improvement of Palm Oil Foaming Agent Concentrates as Fire Extinguishment Materials in Peatlands," IOP Conf. Ser. Earth Environ. Sci., **460**, p. 12026.
[142] Subekti, P., Hambali, E., Suryani, A., Suryadarma, P., Saharjo, B. H., and Rivai, M., 2020, "The Effects of Magnesium Sulphate Addition into Foaming Agents Resulted from Palm Oil Fatty Acid Saponification in the Performance of Peat Fire Suppression," IOP Conf. Ser. Earth Environ. Sci., **460**, p. 12028.
[143] Ratnasari, N. G., Dianti, A., Palamba, P., Ramadhan, M. L., Prayogo, G., Pamitran, A. S., and Nugroho, Y. S., 2018, "Laboratory Scale Experimental Study of Foam Suppression on Smouldering Combustion of a Tropical Peat," J. Phys. Conf. Ser., **1107**, p. 52003.
[144] Giesy, J. P., and Kannan, K., 2001, "Global Distribution of Perfluorooctane Sulfonate in Wildlife," Environ. Sci. Technol., **35**(7), pp. 1339–1342.
[145] U.S. Environmental Protection Agency USEPA, 2012, *Emerging Contaminants-Perfluorooctane Sulfonate (PFOS) and Perflu-Orooctanoic Acid (PFOA). Emerging Contaminants Fact Sheet–PFOS and PFOA.*
[146] (OECD) Organisation for Economic Co-operation and Development, 2013, "Synthesis Paper on Per-and Polyfluorinated Chemicals (PFCs)."
[147] Ruan, T., and Jiang, G., 2017, "Analytical Methodology for Identification of Novel Per- and Polyfluoroalkyl Substances in the Environment," TrAC Trends Anal. Chem., **95**, pp. 122–131.
[148] de Voogt, P., Zurano, L., Serné, P., and Haftka, J. J. H., 2012, "Experimental Hydrophobicity Parameters of Perfluorinated Alkylated Substances from Reversed-Phase High-Performance Liquid Chromatography," Environ. Chem.
[149] Perdana, L., Ratnasari, N., Ramadhan, M., Palamba, P., Nasruddin, N., and Nugroho, Y., 2018, "Hydrophilic and Hydrophobic Characteristics of Dry Peat," IOP Conf. Ser. Earth Environ. Sci., **105**, p. 12083.
[150] Hao, T., 2005, "Chapter 1 - Colloidal Suspensions and Electrorheological Fluids," *Electrorheological Fluids*, T. Hao, ed., Elsevier, pp. 1–17.
[151] Firefreeze, 2019, *ColdFire: The Next Generation in FireFighting*, FireFreeze Worldwide, Inc.
[152] Nikitas, P., and Pappa-Louisi, A., 1990, "Thermodynamic and Modelistic Study of Surface Solution: Aqueous Solutions Containing 2-Butanol," J. Phys. Chem., **94**, pp. 361–370.
[153] Gerhart, P. M., Gerhart, A. L., and Hochstein, J. I., 2016, *Munson, Young and Okiishi's Fundamentals of Fluid Mechanics, 8th Edition*, Wiley.
[154] World Health Organization, 2006, *Air Quality Guidelines: Global Update 2005: Particulate Matter, Ozone, Nitrogen Dioxide, and Sulfur Dioxide*, Copenhagen.
[155] Caton, S. E., Hakes, R. S. P., Gorham, D. J., Zhou, A., and Gollner, M. J., 2017, "Review of Pathways for Building Fire Spread in the Wildland Urban Interface Part I: Exposure Conditions," Fire Technol., **53**(2), pp. 429–473.
[156] NWCG, 2012, *Glossary of Wildland Fire Terminology*.
[157] Mell, W. E., Manzello, S. L., Maranghides, A., Butry, D., and Rehm, R. G., 2010, "The Wildland-Urban Interface Fire Problem Current Approaches and Research Needs," Int. J. Wildl. Fire, **19**(2), pp. 238–251.

[158] Manzello, S. L., Park, S.-H., and Cleary, T. G., 2009, "Investigation on the Ability of Glowing Firebrands Deposited within Crevices to Ignite Common Building Materials," Fire Saf. J., **44**(6), pp. 894–900.
[159] Manzello, S. L., Suzuki, S., and Hayashi, Y., 2012, "Enabling the Study of Structure Vulnerabilities to Ignition from Wind Driven Firebrand Showers: A Summary of Experimental Results," Fire Saf. J., **54**, pp. 181–196.
[160] Manzello, S. L., Suzuki, S., and Nii, D., 2017, "Full-Scale Experimental Investigation to Quantify Building Component Ignition Vulnerability from Mulch Beds Attacked by Firebrand Showers," Fire Technol., **53**(2), pp. 535–551.
[161] Manzello, S. L., 2014, "Enabling the Investigation of Structure Vulnerabilities to Wind- Driven Firebrand Showers in Wildland-Urban Interface (WUI) Fires," Fire Saf. Sci., **11**, pp. 83–96.
[162] Manzello, S. L., and Suzuki, S., 2014, "Exposing Decking Assemblies to Continuous Wind-Driven Firebrand Showers," Fire Saf. Sci., **11**, pp. 1339–1352.
[163] Manzello, S. L., and Suzuki, S., 2017, "Experimental Investigation of Wood Decking Assemblies Exposed to Firebrand Showers," Fire Saf. J., **92**, pp. 122–131.
[164] Zhou, K., Suzuki, S., and Manzello, S. L., 2015, "Experimental Study of Firebrand Transport," Fire Technol., **51**(4), pp. 785–799.
[165] Manzello, S. L., and Quarles, S. L., 2017, "Special Section on Structure Ignition in Wildland-Urban Interface (WUI) Fires," Fire Technol., **53**(2), pp. 425–427.
[166] Manzello, S. L., Almand, K., Guillaume, E., Vallerent, S., Hameury, S., and Hakkarainen, T., 2018, "FORUM Position Paper: The Growing Global Wildland Urban Interface (WUI) Fire Dilemma: Priority Needs for Research," Fire Saf. J., **100**, pp. 64–66.
[167] Palmer, K. N., 1957, "Smouldering Combustion in Dusts and Fibrous Materials," Combust. Flame, **1**(2), pp. 129–154.
[168] Rein, G., Carlos Fernandez-Pello, A., and Urban, D. L., 2007, "Computational Model of Forward and Opposed Smoldering Combustion in Microgravity," Proc. Combust. Inst., **31**(2), pp. 2677–2684.
[169] Rein, G., 2009, "Smouldering Combustion Phenomena in Science and Technology," Int. Rev. Chem. Eng., **1**, pp. 3–18.
[170] Chen, Y., Kauffman, C. W., Sichel, M., Fangrat, J., and Guo, Y., 1990, "The Transition from Smoldering to Glowing to Flaming Combustion," Chem. Phys. Process. Combust., **68**, pp. 1–4.
[171] Ohlemiller, T. J., 1990, "Forced Smolder Propagation and the Transition to Flaming in Cellulosic Insulation," Combust. Flame, **81**(3), pp. 354–365.
[172] Ohlemiller, T. J., 1991, "Smoldering Combustion Propagation On Solid Wood," Fire Saf. Sci., **3**, pp. 565–574.
[173] Aldushin, A. P., Bayliss, A., and Matkowsky, B. J., 2009, "Is There a Transition to Flaming in Reverse Smolder Waves?," Combust. Flame, **156**(12), pp. 2231–2251.
[174] Ortiz-Molina, M. G., Toong, T.-Y., Moussa, N. A., and Tesoro, G. C., 1979, "Smoldering Combustion of Flexible Polyurethane Foams and Its Transition to Flaming or Extinguishment," Symp. Combust., **17**(1), pp. 1191–1200.
[175] Torero, J. L., and Fernandez-Pello, A. C., 1995, "Natural Convection Smolder of Polyurethane Foam, Upward Propagation," Fire Saf. J., **24**(1), pp. 35–52.
[176] Sato, K., and Sega, S., 1991, "Mode of Burning Zone Spread in an Opposed Gas Flow," Combust. Flame, **83**(1), pp. 146–154.
[177] Bilbao, R., Mastral, J. F., Aldea, M. E., Ceamanos, J., Betrán, M., and Lana, J. A., 2001, "Experimental and Theoretical Study of the Ignition and Smoldering of Wood Including Convective Effects," Combust. Flame, **126**(1), pp. 1363–1372.
[178] Bar-Ilan, A., Putzeys, O. M., Rein, G., Fernandez-Pello, A. C., and Urban, D. L., 2005, "Transition from Forward Smoldering to Flaming in Small Polyurethane

Foam Samples," Proc. Combust. Inst., **30**(2), pp. 2295–2302.
[179] Putzeys, O. M., Carlos Fernandez-Pello, A., and Urban, D. L., 2006, "Ignition of Combustion Modified Polyurethane Foam," J. ASTM Int., **3**(3), pp. 1–11.
[180] Putzeys, O., Bar-Ilan, A., Rein, G., Fernandez-Pello, A. C., and Urban, D. L., 2007, "The Role of Secondary Char Oxidation in the Transition from Smoldering to Flaming," Proc. Combust. Inst., **31**(2), pp. 2669–2676.
[181] Putzeys, O. M., Fernandez-Pello, A. C., Rein, G., and Urban, D. L., 2008, "The Piloted Transition to Flaming in Smoldering Fire Retarded and Non-Fire Retarded Polyurethane Foam," Fire Mater., **32**(8), pp. 485–499.
[182] Chao, C. Y. H., and Wang, J. H., 2001, "Transition from Smoldering to Flaming Combustion of Horizontally Oriented Flexible Polyurethane Foam with Natural Convection," Combust. Flame, **127**(4), pp. 2252–2264.
[183] Manzello, S. L., Cleary, T. G., Shields, J. R., and Yang, J. C., 2006, "Ignition of Mulch and Grasses by Firebrands in Wildlandurban Interface Fires<xref Ref-Type="fn" Rid="fn1"/>," Int. J. Wildl. Fire, **15**(3), pp. 427–431.
[184] Manzello, S. L., Cleary, T. G., Shields, J. R., and Yang, J. C., 2006, "On the Ignition of Fuel Beds by Firebrands," Fire Mater., **30**(1), pp. 77–87.
[185] Valdivieso, J. P., and Rivera, J. de D., 2014, "Effect of Wind on Smoldering Combustion Limits of Moist Pine Needle Beds," Fire Technol., **50**(6), pp. 1589–1605.
[186] Alexopoulos, S., and Drysdale, D. D., 1988, "The Transition from Smouldering to Flaming Combustion," Fire Mater., **13**(1), pp. 37–44.
[187] Chang, L., Die, M., Rongkun, P., Bei, P., and Minggao, Y., 2011, "The Effect of Sample Size on Smoldering and the Transition to Flaming Combustion," *2011 Third International Conference on Measuring Technology and Mechatronics Automation*, pp. 793–797.
[188] Stoliarov, S. I., Zeller, O., Morgan, A. B., and Levchik, S., 2018, "An Experimental Setup for Observation of Smoldering-to-Flaming Transition on Flexible Foam/Fabric Assemblies," Fire Mater., **42**(1), pp. 128–133.
[189] Tse, S. D., and Fernandez-Pello, A. C., 1995, "Some Observations of Two-Dimensional Smoldering and the Transition to Flaming," *Eighth International Symposium on Transport Phenomena in Combustion. Vol. 1*, pp. 689–700.
[190] Babrauskas, V., and Krasny, J. F., 1985, *Fire Behavior of Upholstered Furniture*, Washington, DC.
[191] Babrauskas, V., and Krasny, J., 1997, "Upholstered Furniture Transition from Smoldering to Flaming," J. Forensic Sci., **42**(6), pp. 1029–1031.
[192] Ogle, R. A., and Schumacher, J. L., 1998, "Fire Patterns on Upholstered Furniture: Smoldering versus Flaming Combustion," Fire Technol., **34**(3), pp. 247–265.
[193] Hagen, B. C., Frette, V., Kleppe, G., and Arntzen, B. J., 2015, "Transition from Smoldering to Flaming Fire in Short Cotton Samples with Asymmetrical Boundary Conditions," Fire Saf. J., **71**, pp. 69–78.
[194] Clarke, F., and Ottoson, J., 1976, "Fire Death Scenarios and Fire Safety Planning," Fire J., **70**, pp. 20–22.
[195] Bukowski, R. W., Christian, W. J., and Waterman, T. E., 1977, *Detector Sensitivity and Siting Requirements for Dwellings*, Boston.
[196] Harpe, S. W., Waterman, T. E., and Christian, W. J., 1977, *Detector Sensitivity and Siting Requirements for Dwellings, Phase 2*, Boston.
[197] Bukowski, R. W., 1979, *Investigation of the Effects of Heating and Air Conditioning on the Performance of Smoke Detectors in Mobile Homes*, Washington, DC.
[198] Dodd, A. B., Lautenberger, C., and Fernandez-Pello, C., 2012, "Computational

Modeling of Smolder Combustion and Spontaneous Transition to Flaming," Combust. Flame, **159**(1), pp. 448–461.
[199] Yang, J., Liu, N., Chen, H., and Gao, W., 2019, "Smoldering and Spontaneous Transition to Flaming over Horizontal Cellulosic Insulation," Proc. Combust. Inst., **37**(3), pp. 4073–4081.
[200] Lin, S., Sun, P., and Huang, X., 2019, "Can Peat Soil Support a Flaming Wildfire?," Int. J. Wildl. Fire, **28**(8), pp. 601–613.
[201] Wang, F., Jiao, L., Lian, P., and Zeng, J., 2019, "Apparent Gas Permeability, Intrinsic Permeability and Liquid Permeability of Fractal Porous Media: Carbonate Rock Study with Experiments and Mathematical Modelling," J. Pet. Sci. Eng., **173**, pp. 1304–1315.
[202] Soulsby, R., 1997, *Dynamics of Marine Sands: AManual for Practical Applications*, Thomas Telford, London.
[203] Song, Z., Huang, X., Luo, M., Gong, J., and Pan, X., 2017, "Experimental Study on the Diffusion–Kinetics Interaction in Heterogeneous Reaction of Coal," J. Therm. Anal. Calorim., **129**(3), pp. 1625–1637.
[204] Pagni, P. J., 1993, "Causes of the 20 October 1991 Oakland Hills Conflagration," Fire Saf. J., **21**(4), pp. 331–339.
[205] Butler, B. W., Bartlette, R. A., Bradshaw, L. S., Cohen, J. D., Andrews, P. L., Putnam, T., and Mangan, R. J., 1998, *Fire Behavior Associated With the 1994 South Canyon Fire on Storm King Mountain, Colorado*, Ogden, UT.
[206] Babrauskas, V., 2003, *Ignition Handbook: Principles and Applications to Fire Safety Engineering, Fire Investigation, Risk Management and Forensic Science*, Fire Science Pub, Issaquah,WA.
[207] Maranghides, A., and Mell, W., 2009, *A Case Study of a Community Affected by the Witch and Guejito Fires. NIST Technical Note 1635*, Gaithersburg, MD.
[208] Bell, A., 1985, "How Bushfires Set Houses Alight—Lessons from Ash Wednesday," Ecos 43, pp. 3–7.
[209] Hadden, R. M., Scott, S., Lautenberger, C., and Fernandez-Pello, A. C., 2011, "Ignition of Combustible Fuel Beds by Hot Particles: An Experimental and Theoretical Study," Fire Technol., **47**(2), pp. 341–355.
[210] Urban, J. L., Zak, C. D., Song, J., and Fernandez-Pello, C., 2017, "Smoldering Spot Ignition of Natural Fuels by a Hot Metal Particle," Proc. Combust. Inst., **36**(2), pp. 3211–3218.
[211] Pacheco, A. P., Claro, J., and Oliveira, T., 2012, "Rekindle Dynamics: Validating the Pressure on Wildland Fire Suppression Resources and Implications for Fire Management in Portugal," *Modelling, Monitoring, and Management of Forest Fires III*, C.A. Brebbia, and G. Perona, eds., WIT Press, Southampton, pp. 225–236.
[212] Schwebke, S., 2017, "Canyon Fire 2, Which Torched 9,200-plus Acres and Destroyed Homes, Ignited by Embers from Previous Fire," Orange Cty. Regist. [Online]. Available: https://www.ocregister.com/2017/11/06/canyon-fire-2-which-torched-9000-plus-acres-and-destroyed-homes-ignited-by-embers-from-previous-fire/. [Accessed: 02-Nov-2020].
[213] Gabbert, B., 2018, "Overwintering Fires Are a Concern in Northern Rockies," Wildfire Today [Online]. Available: https://wildfiretoday.com/2018/05/12/overwintering-fires-are-a-concern-in-northern-rockies/. [Accessed: 02-Nov-2020].
[214] Gunning, M., 2019, "Managing the Complexities and Consequences of Peat Fires around Communities," *Proceedings for the 6th International Fire Behavior and Fuels Conference*, International Association of Wildland Fire, Missoula, MT.
[215] Mortsch, L. D., 2006, "Impact of Climate Change on Agriculture, Forestry and

Wetlands," *Climate Change and Managed Ecosystems*, J. Bhatti, R. Lal, M. Apps, and M. Price, eds., Taylor & Francis; CRC Press, Boca Raton, FL, pp. 45–67.
[216] Hammer, R. B., Radeloff, V. C., Fried, J. S., and Stewart, S. I., 2007, "Wildland Urban Interface Housing Growth during the 1990s in California, Oregon, and Washington," Int. J. Wildl. Fire, **16**(3), pp. 255–265.
[217] Simeoni, A., 2016, "Wildland Fires," *SFPE Handbook of Fire Protection Engineering*, M.J. Hurley, D. Gottuk, J.R. Hall, K. Harada, E. Kuligowski, M. Puchovsky, J. Torero, J.M. Watts, and C. Wieczorek, eds., Springer New York, New York, NY, pp. 3283–3302.
[218] Bartlett, A. I., Hadden, R. M., and Bisby, L. A., 2019, "A Review of Factors Affecting the Burning Behaviour of Wood for Application to Tall Timber Construction," Fire Technol., **55**(1), pp. 1–49.
[219] McAllister, S., 2013, "Critical Mass Flux for Flaming Ignition of Wet Wood," Fire Saf. J., **61**, pp. 200–206.
[220] Smith, C., Hatchett, B. J., and Kaplan, M., 2018, "A Surface Observation Based Climatology of Diablo-Like Winds in California's Wine Country and Western Sierra Nevada," Fire, **1**(2).
[221] Boonmee, N., and Quintiere, J. G., 2002, "Glowing and Flaming Autoignition of Wood," Proc. Combust. Inst., **29**(1), pp. 289–296.
[222] Spearpoint, M. J., and Quintiere, J. G., 2001, "Predicting the Piloted Ignition of Wood in the Cone Calorimeter Using an Integral Model — Effect of Species, Grain Orientation and Heat Flux," Fire Saf. J., **36**(4), pp. 391–415.
[223] Morrisset, D., Hadden, R. M., Bartlett, A. I., Law, A., and Emberley, R., 2020, "Time Dependent Contribution of Char Oxidation and Flame Heat Feedback on the Mass Loss Rate of Timber," Fire Saf. J., p. 103058.
[224] Ohlemiller, T. J., Kashiwagi, T., and Werner, K., 1987, "Wood Gasification at Fire Level Heat Fluxes," Combust. Flame, **69**(2), pp. 155–170.
[225] Vermesi, I., DiDomizio, M. J., Richter, F., Weckman, E. J., and Rein, G., 2017, "Pyrolysis and Spontaneous Ignition of Wood under Transient Irradiation: Experiments and a-Priori Predictions," Fire Saf. J., **91**, pp. 218–225.
[226] Di Blasi, C., and Branca, C., 2001, "Kinetics of Primary Product Formation from Wood Pyrolysis," Ind. Eng. Chem. Res., **40**(23), pp. 5547–5556.

Appendices

Appendices (Chapter 2)

Local survey on the plot topography were conducted by taking the distance from a predetermined height to the surface of the plots (Figure A 2.1A). Figure A 2.1B to D show the topography of the experimental plots showing a significant elevation difference of ~1 m between south and north sides. This topography difference influences the decision on pre-experiment sampling location to investigate the peat properties and on the location of ignition (Figure 2.2A and Figure 2.3).

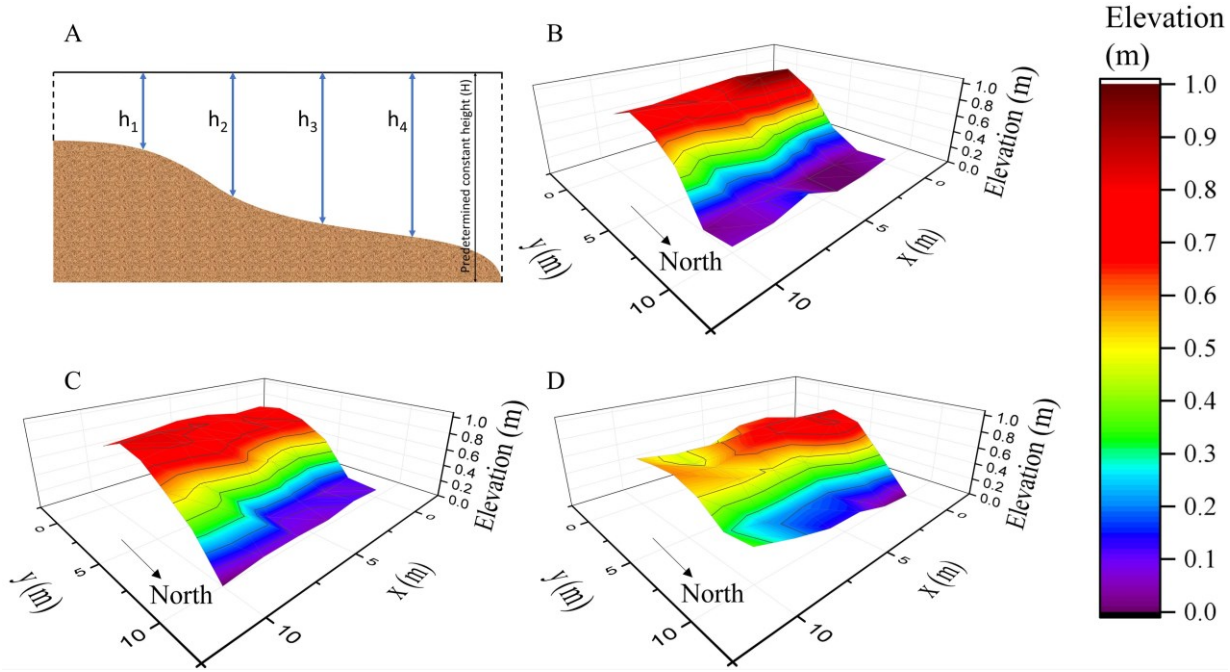

Figure A 2.1. Plot topography measurement. (A) Schematic of the in-situ measurement. Topography of (B) plot 1 (C) plot 2 (D) plot 3

At each point, thermocouples were inserted at an angle using a thermocouple inserter (Figure A 2.2). This insertion method assumes that smouldering propagation is coming from the right-hand side of Figure A 2.2A. This insertion angle facilitates the thermocouple junctions to be at the predetermined depths, i.e. 10 cm and 30 cm, and records temperature while keeping the thermocouple wire away from the heat and prevents it from melting.

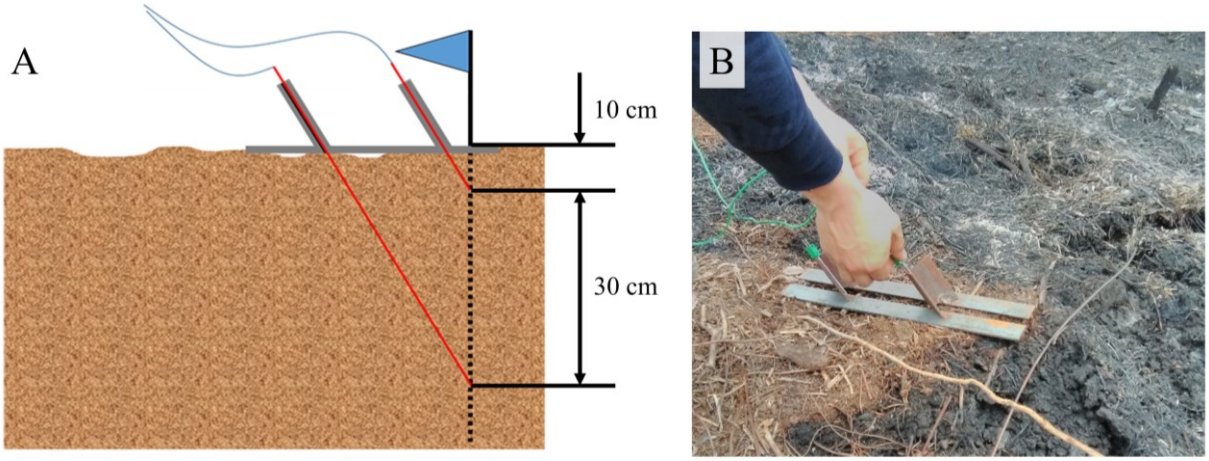

Figure A 2.2. Thermocouple placement (A) Illustration of the insertion of the thermocouples at an angle. Blue flag represents the thermocouple point. (B) thermocouples being inserted during the experiments.

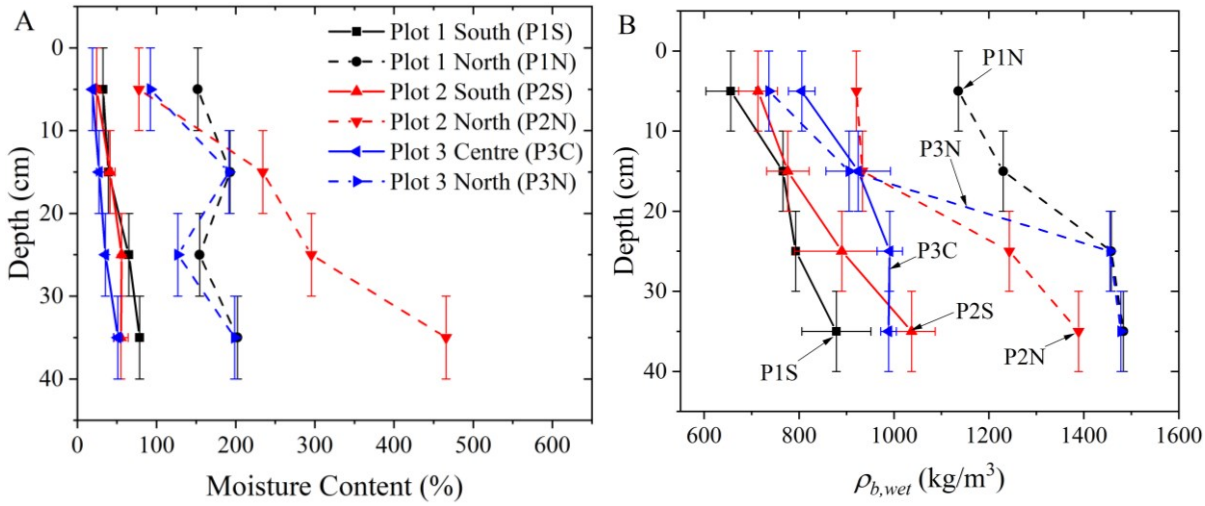

Figure A 2.3. MC and bulk density of peat in this study (A) dry-mass-based moisture content (MC) (%). (B) Peat wet bulk density ($\rho_{b,wet}$) (kg/m^3)

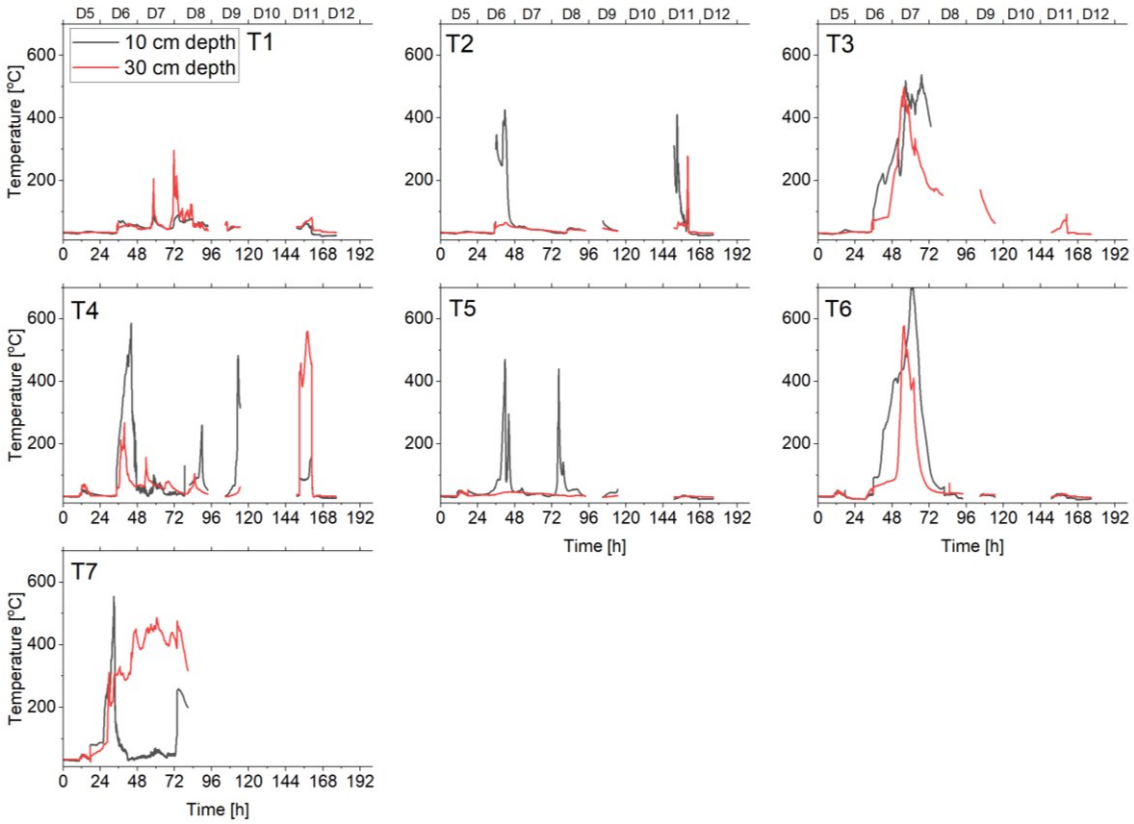

Figure A 2.4. Temperature profiles in P1N fire showing all temperature measurement points as shown in Figure 2.11A. Time at 0 h indicates 00:00:00 am in D5. Slash-and-burn ignition was conducted in D5 at ~11:27:00.

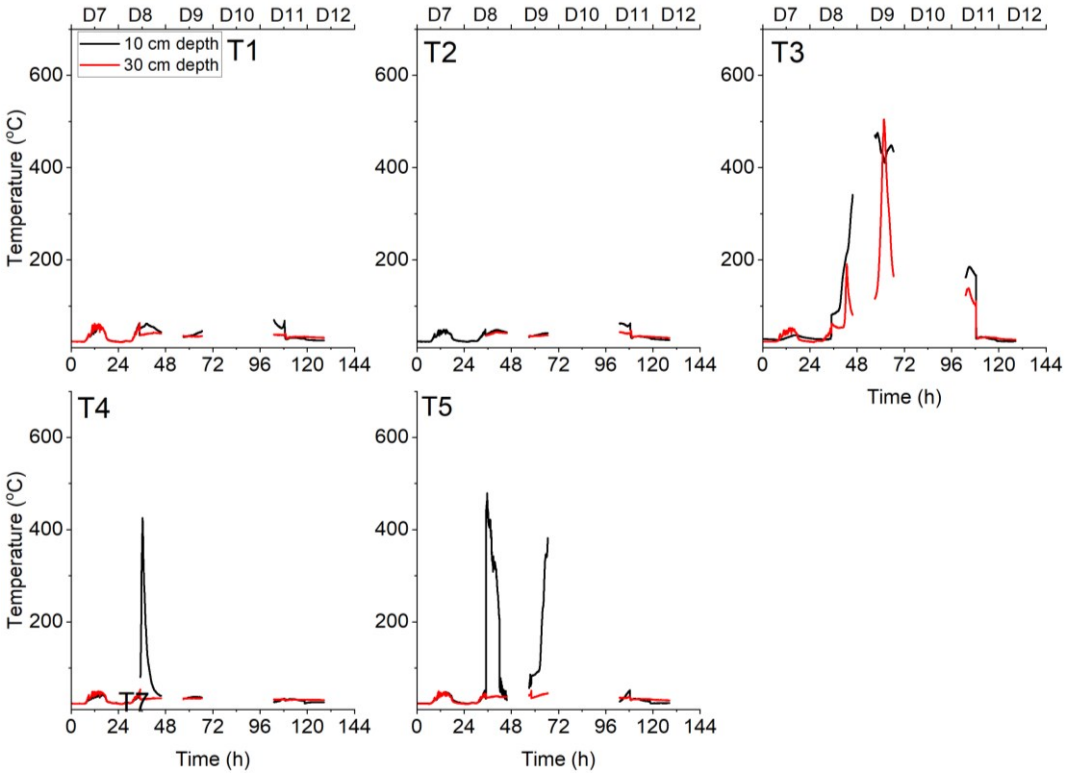

Figure A 2.5. Temperature profiles in P2N fire showing all temperature measurement points as shown in Figure 2.11B. Time at 0 h indicates 00:00:00 am in D7. Slash-and-burn ignition was conducted in D7 at ~12:40:00.

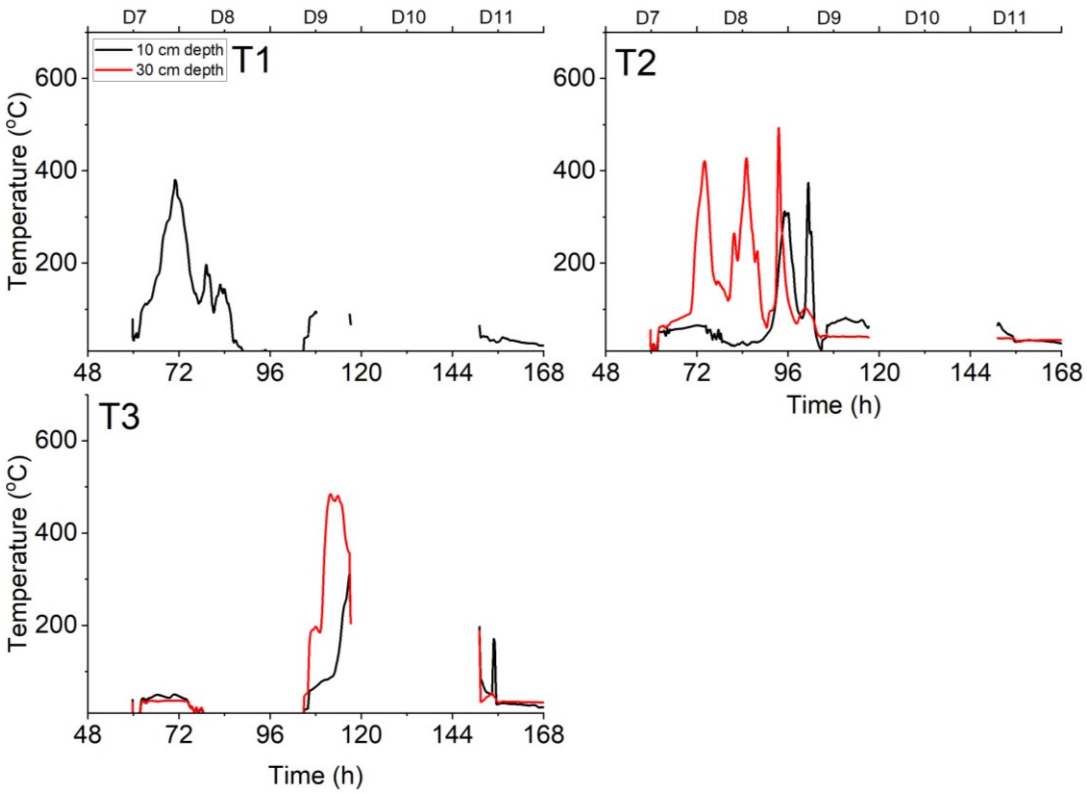

Figure A 2.6. Temperature profiles in P3N fire showing all temperature measurement points as shown in Figure 2.11C. Time at 0 h indicates 00:00:00 am in D7. Slash-and-burn ignition was conducted in D5 at ~16:12:00.

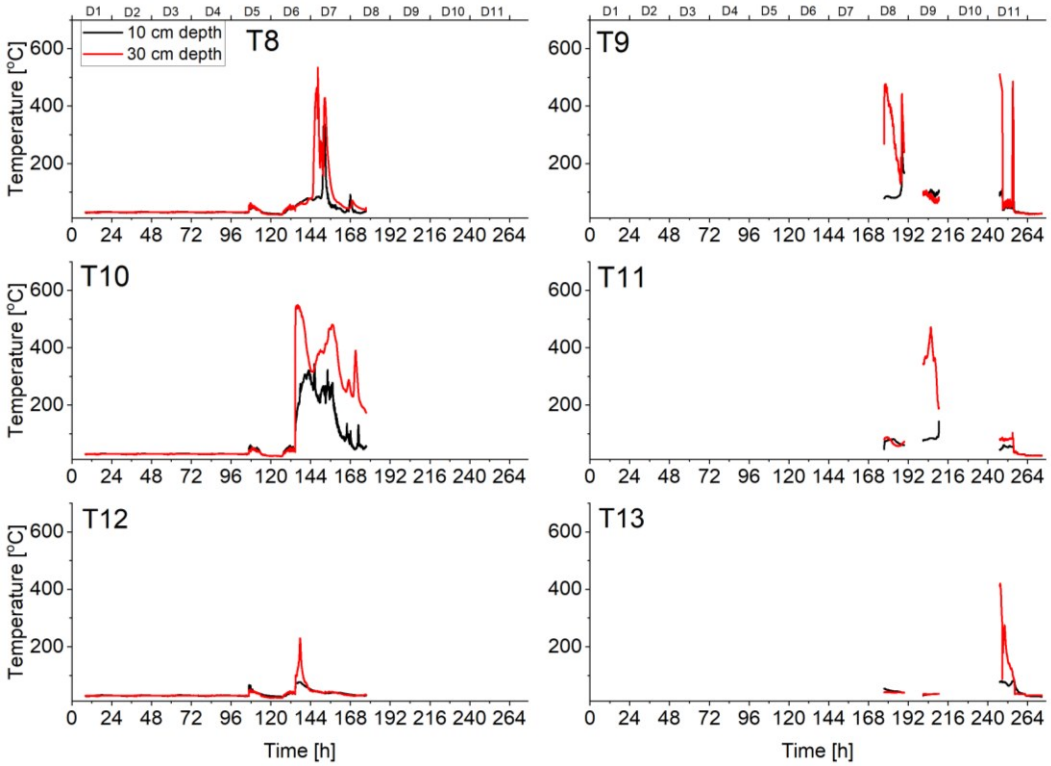

Figure A 2.7. Temperature profiles in P1S fire showing all temperature measurement points as shown in Figure 2.11A. Time at 0 h indicates 00:00:00 am in D1. Charcoal ignition was conducted in D1 at ~12:00:00.

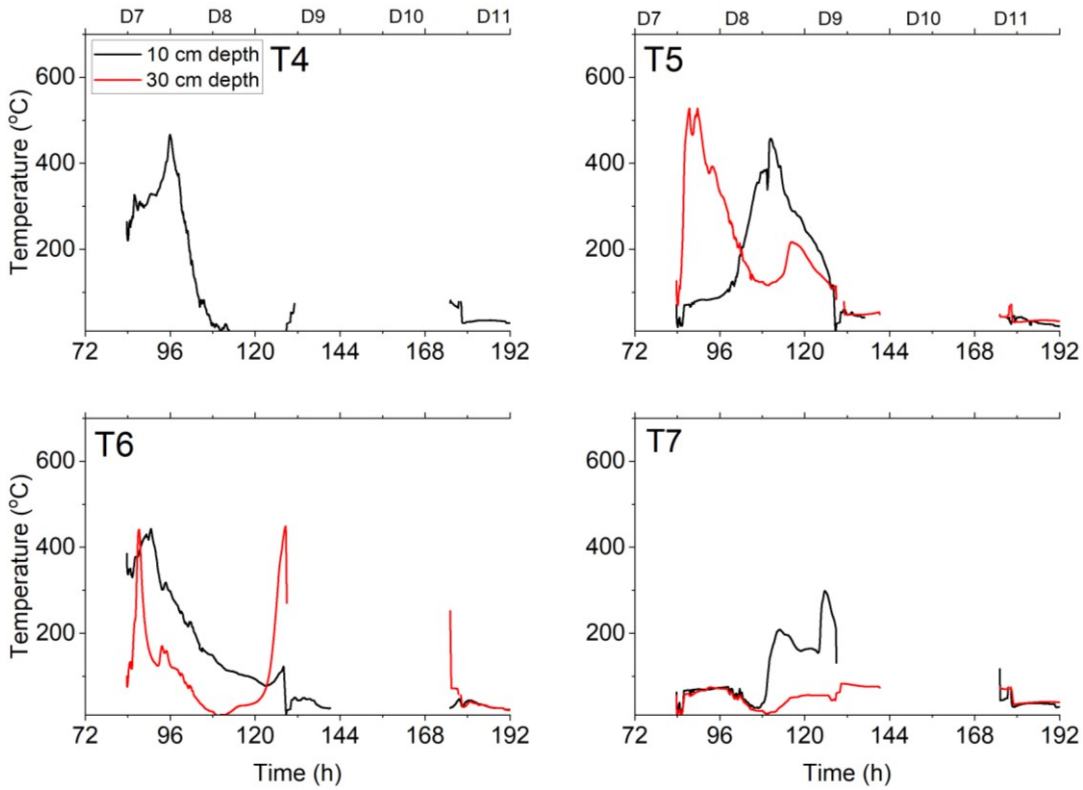

Figure A 2.8. Temperature profiles in P3C fire showing all temperature measurement points as shown in Figure 2.11C. Time at 0 h indicates 00:00:00 am in D7. Charcoal ignition was conducted in D4 at ~09:27:00.

Figure A 2.9A shows a typical overhang observed in this study. As smouldering continues to propagate deep below the surface, the surface vegetation was intact up to the point that it loses its stability and the burning peat in this overhang collapse onto the soil around the TCs, represented by abrupt temperature increase such as can be seen at T7 at 10 cm depth at noon of D8 in Figure A 2.4. Before the abrupt increase, temperature at T7 (10 cm depth) increased up to ~600°C for a short time and then followed by a rapid decay, probably represents either the smouldering propagation well passed this point or the part of the smouldering peat at this depth collapsed since the deeper 30 cm deep layer underwent strong smouldering. This occurrence left the thermocouple at T7 at 10 cm deep free-hanging as can be seen by the rapid temperature fluctuation after this rapid decay, demonstrating convective effect from the ambient air. The later rapid increase at ~72 h or ~00:00 am of D8 shows that the part of surface overhang above this TC was still intact from D6 to D8, before collapsing and causing rapid increase at T7 (10 cm deep).

Few transitions from smouldering to flaming were observed in this field experiment (Figure A 2.9B). The occurrence was close to the overhang location and occurred once overhang started to crack and collapse. The sudden flux of pyrolyzate from deep layer might have been ignited and act as a pilot to ignite surface litter vegetations at the surface layer.

(A) (B)

Figure A 2.9. (A) Overang formation and collapse in this study. In addition to the different spread rate between surface and in-depth layers, the surface vegetation layer provided temporary stability support for overhang formation due to the fibrous structure. (B) Transition from smouldering to flaming encountered during these field experiments (photograph by Wuquan Cui).

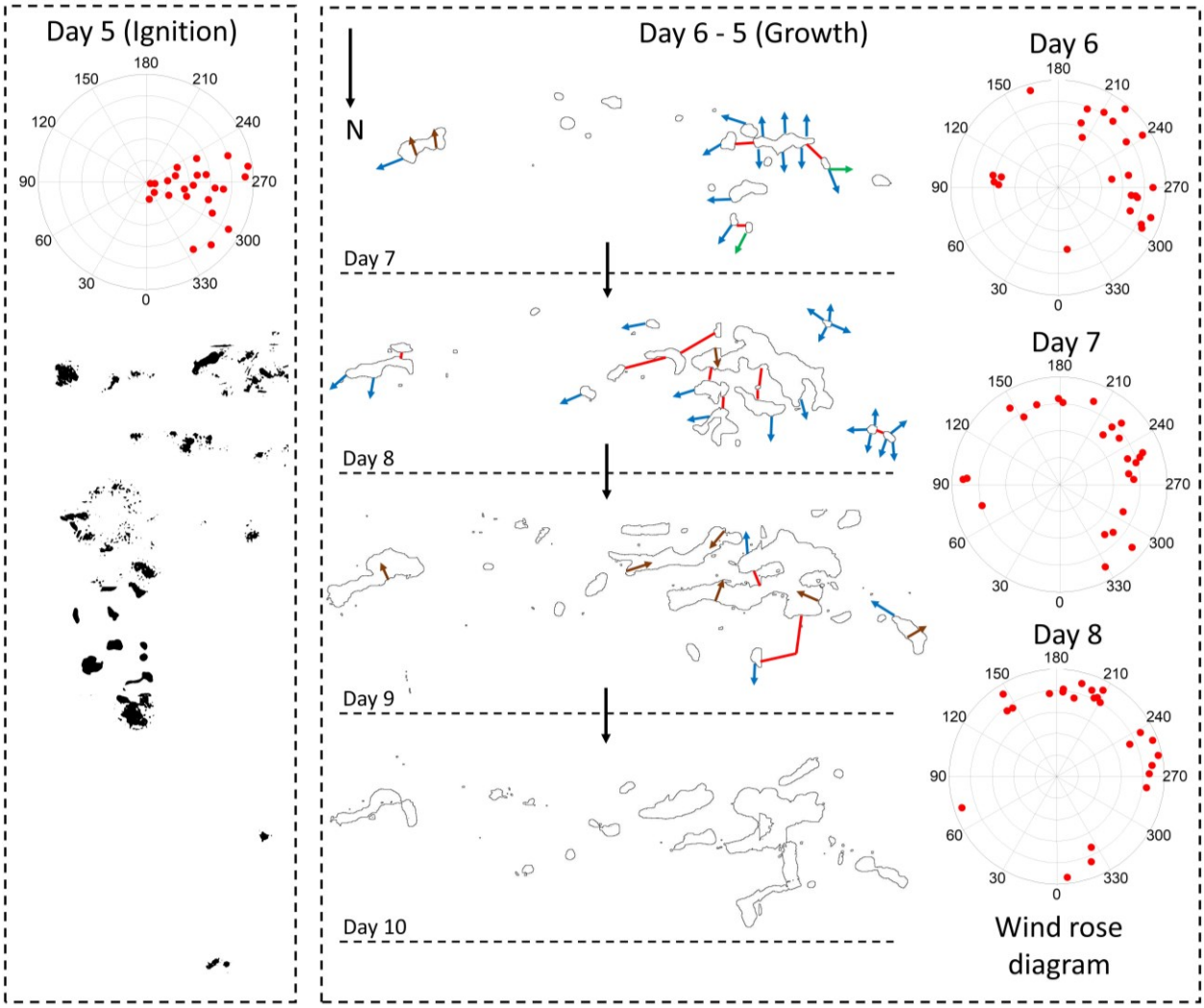

Figure A 2.10. Smouldering propagation in P1N analyzed from infrared images showing separate surface smouldering hotspots after slash-and-burn was conducted in D5 at ~11:27:00. The outside perimeter of the wind rose diagram represents average wind speed of 2.4 m/s. Different colour of the arrows approximately indicate spread rate, with blue to brown to red correspond to slowest to fastest spread rate.

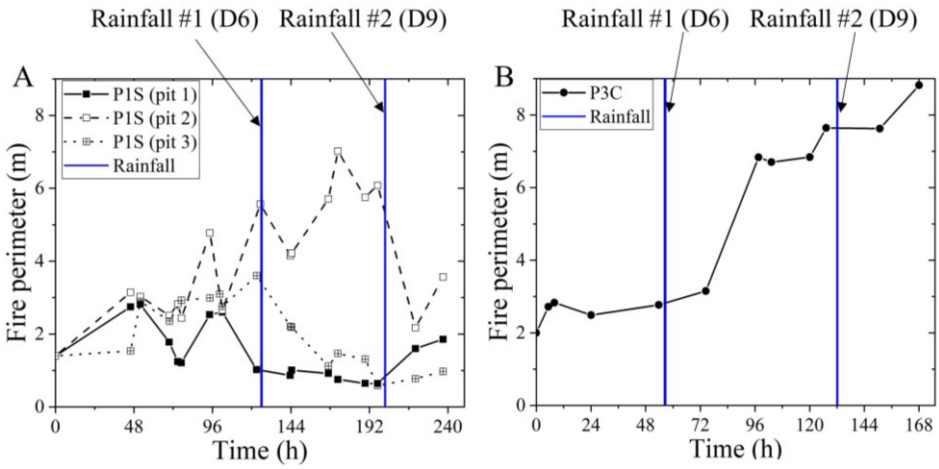

Figure A 2.11. Smouldering perimeter in P1S and P3C from infrared image analysis. The x-axis scale in time between P1S and P3C are different due to different time of ignition (Figure 2.4). Time at 0 h in each plots represent the time of ignition and the last data point represent infrared measurement before controlled suppression in D11 was conducted.

Table A 2.1. Suppression method, flow rate ($\dot{V}_s$ (L/h)), fire area (A_f (m^2)), and suppression time (Δt_s (h)) during the controlled suppression attempts conducted in D11.

Fire location	Suppression method	$\dot{V}_s$ (L/h)	A_f (m^2)	A_s (m^2)	Δt_s (h)
P1N	Water spray	3024 ± 18	~80	30 ± 0.3	0.7 ± 0.2
P2N	Water spray	3024 ± 18	~20	30 ± 0.3	0.3 ± 0.03
P3C	Water spray	4878 ± 120	0.8	54 ± 1.5	0.4 ± 0.2
Pit 2 of P1S	Lance injection	1669	0.5	Point location	15 ± 1
Pit 3 of P1S	Lance injection	1669	0.3	Point location	13 ± 1

Appendices (Chapter 3)

Figure A 3.1 shows visual images of an experiment where smouldering spread up to 366 min, a minute before suppression. The side-view schematic of smouldering front at the start of suppression is sketched in Figure 3.7.

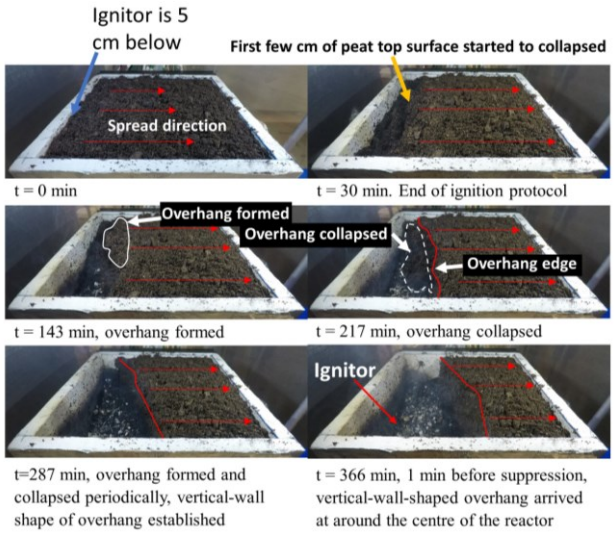

Figure A 3.1. Visual images of 100% MC peat showing smouldering ~8 cm below top surface forming a step in the sample due to overhang. Red arrow indicates spread direction.

Indication of successful suppression can be identified by surface infrared radiation (Figure A 3.2). However, surface infrared was unable to detect the occurrence of persistent smouldering at a later stage of suppression. Image F in Figure A 3.3 shows a very low surface infrared radiation despite in-depth temperature reached the peak of reignition temperature at 220°C, even though the distance between the surface and the in-depth temperature is ~1 cm. The absence of indication of the persistent smouldering by surface infrared radiation can be caused by the surface MC. In this case, the surface MC was too high for surface infrared to indicate any in-depth temperature increase since the persistent smouldering occurred late after suppression started, i.e. at 25 min. As in the first early persistent smouldering (image B to D), the surface MC was not too wet for surface infrared to indicate an in-depth temperature increase.

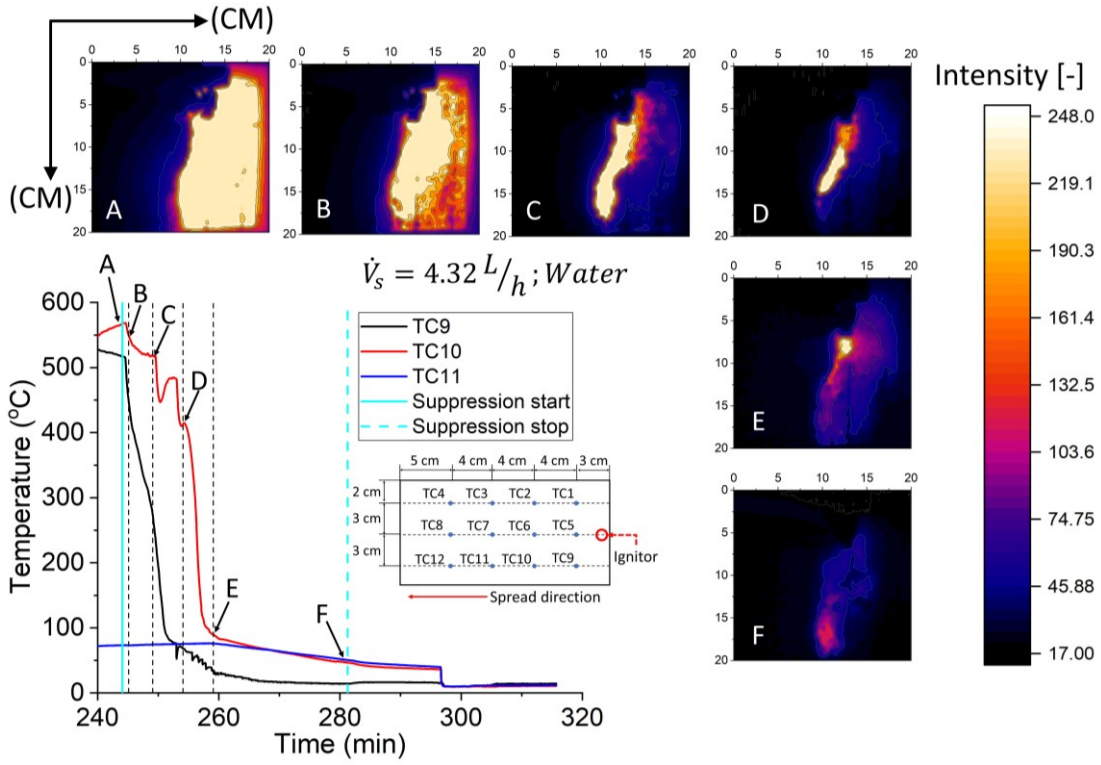

Figure A 3.2. Surface infrared radiation vs. in-depth temperature in an experiment with 4.32 L/h flow rate of water suppression. The intensity unit is the grayscale pixel intensity, i.e. 0 to 255, represents surface infrared radiation flux.

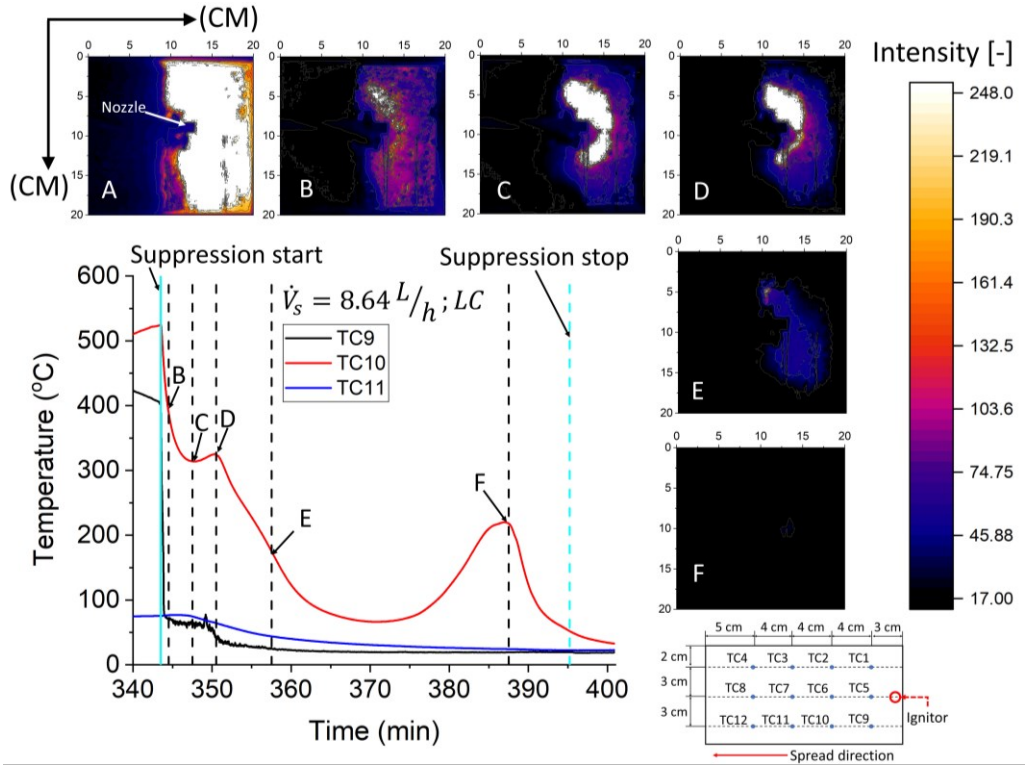

Figure A 3.3. Surface infrared radiation vs. in-depth temperature in an experiment with 8.64 L/h flow rate of LC suppression. The intensity unit is the grayscale pixel intensity, i.e. 0 to 255, represents surface infrared radiation flux

Appendices (Chapter 5)

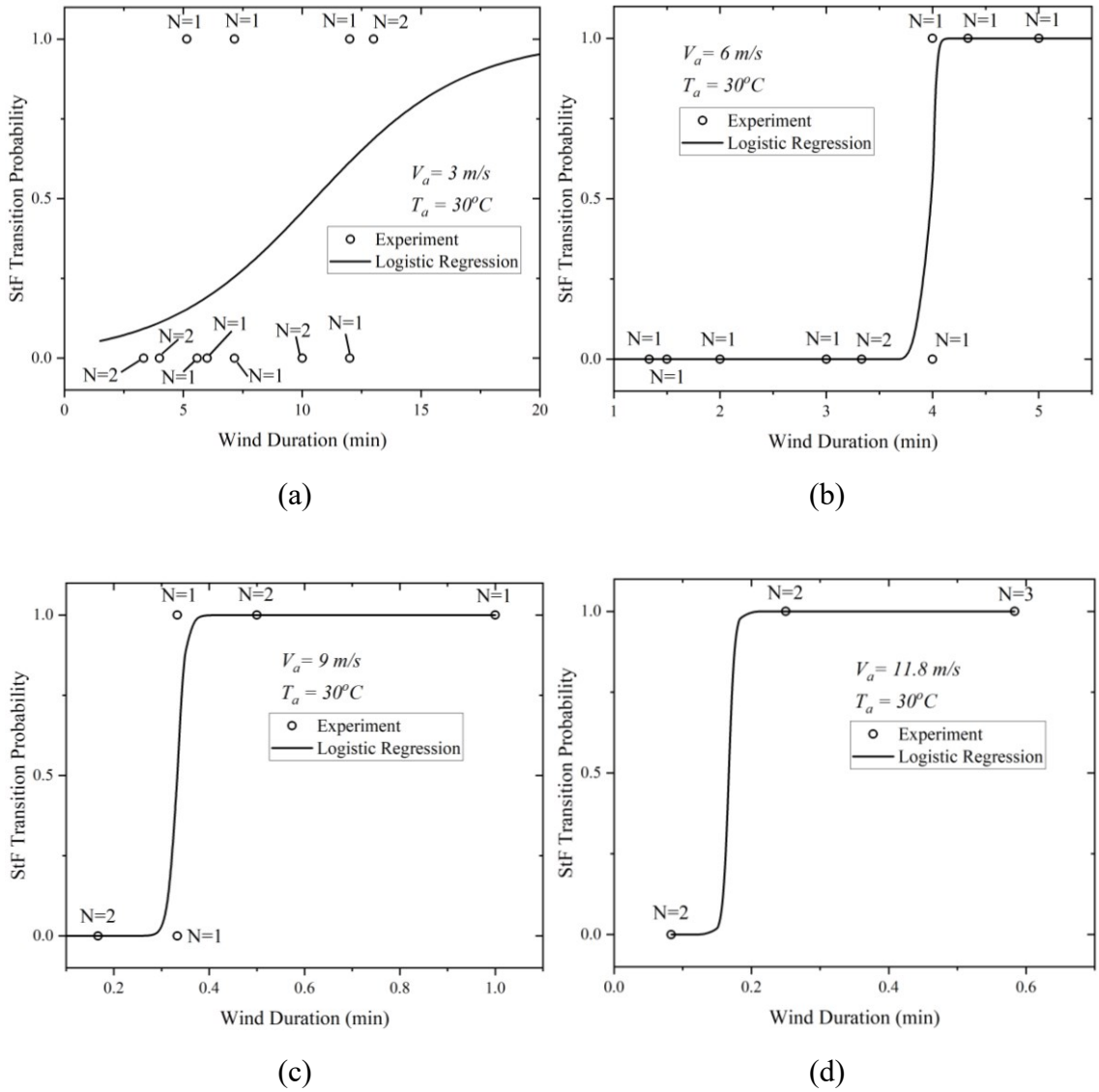

Figure A 5.1. Experiment data points from pulsed wind experiment series at wind speed of (a) 3 m/s, (b) 6 m/s, (c) 9 m/s, and (d) 11.8 m/s. Experiment result of 1 means that StF transition was observed at that data point and 0 means StF transition was not observed, where N is the number of experiments at each specified wind speed and duration.